

Study of Viscous Flow during Thin Film
Polymer Coating and Drawing of a Continuum

by

Suraiya Akter, *BSc. Eng, M.Sc. Eng*

Ph.D.

1997

Study of Viscous Flow during Thin Film Polymer Coating and Drawing of Continuum

by

Suraiya Akter, *BSc Eng, M Sc Eng*

This thesis is submitted to Dublin City University as the fulfilment of the
requirement for the award of Degree of

Doctor of Philosophy

Supervisor. Professor M.S.J. Hashmi, *D Sc*

*School of Mechanical and Manufacturing Engineering
Dublin City University*

January 1997

Dedicated to my Parents, Husband and Son Orowa

DECLARATION

I hereby certify that this material, which I now submit for assessment on the programme of study leading to the award of *Doctor of Philosophy*, is my own work and has not been taken from the work of others save and to the extent that such work has been cited and acknowledged within the text of my work.

Signed -----

I D No 93700342

Date *10th* February, 1997

CONTENTS

	Page
CHAPTER ONE	
Introduction	
1 1 Hydrodynamic phenomenon	1
1 2 Development of wire drawing and coating processes	2
1 3 Historical background of hydrodynamic lubrication	2
1 4 Background of polymer melt as a lubricant	3
1 5 Objective of the present studies and relation with previous work	5
Figures 1 1-1 4	7-9
CHAPTER TWO	
Rheology of polymer	
2 1 Introduction	10
2 2 Effect of temperature	10
2 3 Effect of pressure	11
2 4 Stress-strain dependent viscosity	13
2 5 Effect of polymer flow characterisation	15
Figures 2 1-2 6	16-19
2 6 Boundary layer behaviour of polymer melt in melt chamber	20
2 6 1 Boundary layer analytical solution	20
Figure 2 7	21
Figure 2 8	22
2 6 2 Boundary layer numerical solution	29
2 6 3 Comparison between analytical and numerical solution	32
Figure 2 9-2 22	33-39
2 6 4 Formation and remelting of solid polymer layer	40
Figure 2 23	41
Figures 2 24-2 27	47-48
CHAPTER THREE	
Experimental equipments, materials and test procedure	
3 1 Design of the drawing bench	49
3 2 Modification of the rig	49
3 3 Brief description of some instruments	51
3 4 Test preparation	51
3 5 Test procedure	53
Plates 3 1-3 5	54-57
CHAPTER FOUR	
Plasto-hydrodynamic analysis using stepped bore unit	
4 1 Introduction	58

4 2 Non-Newtonian plasto-hydrodynamic pressure analysis for wire coating in a stepped parallel bore unit	59
Figure 4 1	59
Figures 4 2-4 9	70-73
4 3 Analysis for continuum drawing in stepped parallel bore unit	74
4 3 1 Analysis for wire drawing	74
Figures 4 10-4 18	83-87
4 3 2 Analysis for tube sinking process	88
Figures 4 19-4 27	96-101
4 5 Analysis for strip drawing	102
Figures 4 28-4 36	109-114

CHAPTER FIVE

Plasto-hydrodynamic analysis using converging tapered, parabolic and exponential geometry unit

5 1 Introduction	115
5 2 Plasto-hydrodynamic non-Newtonian pressure analysis for wire coating in a tapered unit	115
Figure 5 1	116
Figures 5 2-5 9	122-125
5 3 Analysis for wire drawing in tapered unit	126
Figures 5 10-5 14	131-133
5 4 Finite element temperature and pressure analysis for wire coating in a tapered bore unit	134
Figures 5 15-5 19	137-139
5 5 Plasto-hydrodynamic pressure analysis in converging parabolic and exponential unit	140
Figures 5 20-5 25	146-148

CHAPTER SIX

Plasto-hydrodynamic analysis using combined geometry unit

6 1 Introduction	149
6 2 Non-Newtonian pressure analysis for wire coating	149
Figure 6 1	150
Figures 6 2-6 9	159-162
6 3 Wire drawing in a combined unit	163
Figures 6 10-6 15	172-175
6 4 Finite element temperature and pressure simulation for wire coating in combined parallel and tapered unit	176
Figures 6 16-6 20	178-180

CHAPTER SEVEN

Experimental results

7 1 Introduction	181
------------------	-----

7 2 Experimental procedure and equipment	182
7 3 Experimental results and discussions	183
Figures 7 1-7 30	191-205

CHAPTER EIGHT

Conclusions and suggestions for future works

8 1 Introduction	210
8 2 Statement of the tasks	210
8 3 Summery of theoretical and experimental investigations	211
8 4 General conclusions	211
8 5 Thesis contribution	212
8 6 Recommendation for future work	213

REFERENCES	214
------------	-----

Appendix I Program to calculate boundary layer thickness for velocity gradient and coefficient of friction factor by analytical metod

Appendix II Program to calculate pressure distribution in a stepped parallel bore unit

Appendix III Program to calculate percentage reduction in diameter in a tube

Appendix IV Program to calculate pressure distribution in a tapered unit

Appendix V Program to calculate pressure distribution in a combined unit

Appendix VI Program to calculate the mesh generation for temperature distribution within hydrodynamic unit

Appendix VII Program to calculate the temperature distribution by two dimensional finite element simulation

Appendix VII List of publications

ACKNOWLEDGEMENTS

The author would like to express her thanks and gratitude to Professor M S J Hashmi for his kind supervision, guidance and advice to carry out this work. His encouragement and inspiring suggestions were always an ingredient to this work. The author also likes to thank him for offering the opportunity and providing the financial support to her.

The author would also like to express her sincere thanks to Martin Johnson and Liam Domican for their help in manufacturing and installing the rig. Their practical ideas and assistance during experimentation are highly appreciated.

She also would like to express her appreciation to Dr Lisa Looney, Ms Lesley Lawlor, Mr Tommy Walsh and all others for their valuable support at various stages of this work.

The author would also like to acknowledge the collaboration with Printing Wire Supplies Ltd, Ireland on the project.

The author was on study leave from Bangladesh Chemical Industries Corporation (BCIC) during the period of this work. She thanks BCIC for the study leave.

The author would like to offer her thanks to all Bangladeshi families and friends for their friendly support through these years. Special thanks goes to Mrs Ainunnahar Begum for her loving care to my son during the initial year of the study.

The author also acknowledges her parents especially of her mother who always cared and encouraged her from the childhood to advance her knowledge.

Finally, special thanks goes to her husband for his support, encouragement and patience during the period of completion her work.

Study of Viscous Flow during Thin Film Polymer Coating and Drawing of Continuum

Suraiya Akter, BSc. Eng, M.Sc Eng.

ABSTRACT

This study involves both theoretical and experimental thin polymer coating on wire as well as drawing of wire by hydrodynamic pressure technique. Hydrodynamic pressure technique is a relatively new and innovative technique for wire drawing and thin polymer coating. The wire submerged in polymer melt inside the pressure unit of different geometry, when pulled developed hydrodynamic pressure in the melt. This pressure is largely responsible for wire drawing or coating.

Most of the theoretical works carried out to date on this new process have considered that the viscosity of the polymer remains unchanged during the process. Change in shear stress was also not accounted for in those studies. Also the pressure in the fluid film was considered to be constant across the film thickness. It is felt that any analysis of the process addressing the above shortcoming would give a more thorough understanding of the process. With this aim in view, several numerical and analytical models were developed for the process. These models help to predict the pressure, temperature and deformation profiles for different die geometries. Finite difference and finite element technique were used to obtain the solutions. Theoretical results from these models were compared with previous experimental and theoretical results. All models predict closer or marginally closer results to the experimental results than the previous.

As the wire is first pulled through the polymer melt chamber before the hydrodynamic pressure unit, the first interaction between the wire and the polymer melt plays an important role for subsequent process in the pressure unit. Theoretical study of the effect of the melt chamber condition on the whole process was so far been overlooked. In this project some theoretical models were developed to study the temperature and velocity gradient boundary layer thickness as well as the melting profile of the solid polymer layer within the polymer melt chamber.

Finally, most experimental works on the process concentrated on wire or other continuum drawing. Works on good thin polymer coating by the process had mixed success. The maximum wire speed attained in these works was 0.6 m/s which is considered to be rather low for industrial scale production. The experimental work in this project was mainly focused to attain at 15 to 20 times higher than the best previous achievement. To this end, the work bench, wire feed mechanism, polymer feed system and hydrodynamic pressure units were either modified or designed and manufactured a new. With this new set up it was possible to produce quality coating at as high as 12 m/s speed of the wire at different temperatures and back pressures of the polymer melt.

NOMENCLATURE

B	temperature-pressure coefficient, slope of the deformation line
b, B	factor determining theoretical deformation profile for thickness
b*, B*	factor determining theoretical deformation profile for width
C	temperature-length coefficient
C _f	friction factor
C _p	specific heat
DP	change in hydrodynamic pressure
DX	increment in length
h	radial gap in the unit and the wire
h	heat transfer coefficient
K	thermal conductivity for fluid, non-Newtonian factor
K ₀	strain hardening constant
k	viscosity coefficient for power law fluid
l, L	length of section
n	power law index, strain hardening constant
Nu	Nusselt number
Pr	Prandtl number
PRA	percentage reduction in area
PRT	percentage reduction in thickness
PRW	percentage reduction in width
Q	flow of polymer
q	heat flux
Re	Reynolds number
V	wire velocity
P'	pressure gradient
T	temperature
t	constant wall thickness of tube, thickness of strip
U	velocity of polymer
V	wire velocity
W	width of strip

x	length passed by continuous wire in the melt chamber
x_1	yielding point
Y_0	initial yield stress
Y	yield stress of the wire material
α	thermal diffusivity, semi-angle of the effective die
δ, δ_t	thickness of velocity and thermal boundary layer respectively
ρ	density
τ	shear stress
μ	viscosity
τ_c	shear stress at wall
γ	shear rate
σ_x	axial stress
σ_r	radial stress
σ_θ	Hoop stress

Subscripts

0	free stream, reference
1	first section of the unit
2	second section of the unit
i	at the increment of length in first unit
j	at the increment of length in the second unit
m	maximum (step)
w	wire surface
x	local

CHAPTER ONE

INTRODUCTION

1.1 Hydrodynamic phenomenon

When a viscous fluid is present between a fixed surface and a moving surface then, depending on the geometrical features of the pair of surfaces, a convergent wedge may occur. It is the convergence, coupled with the speed and viscosity that generates the fluid pressure film.

The mechanics of fluid pressure formation can be explained as follows. The moving surface drags the fluid into the gap formed between it and the fixed surface and the relative motion between the moving surface and the fluid gives rise to the pressure which acts on the surfaces.

This pressure is termed as hydrodynamic pressure and depends on the viscosity of the fluid, the geometrical configuration of the confined passage and the relative speed between the moving and fixed surfaces.

If the fluid is oil type then the generated pressure is not so high. But if it is of polymer solution type then the generated pressure is many times higher. This is why for plastic processing industry the pressure generation due to hydrodynamic phenomenon could be a significant design factor for the processing equipment and pipe works.

This high pressure should be advantageous for drawing and coating processes of wires, strips and tubes, the magnitude of this pressure being dependent upon the geometrical configuration and other factors mentioned above. In a drawing process where reduction in cross section of the moving continuum is needed, the higher the hydrodynamic pressure the greater would be the reduction. But for a coating process the pressure needs only to be sufficient to produce uniform thickness and continuous coating.

1.2 Development of wire drawing and coating processes

Traditionally the wire drawing process involves the drawing of a circular wire

through a continuously varying tapered die, the main purpose of the wire drawing process being to reduce the wire diameter to a specified size and to obtain the required metallurgical properties, including surface finish and a high degree of repeatability

In general in the wire drawing process, metal to metal contact takes place causing friction which leads to the reduction in die life due to wear, and to the increase in the drawing load. Due to this reason, lubrication is essential. Two main types of lubrication are used at present "wet drawing" and "dry drawing". In wet drawing, the wire and the drawing apparatus are submerged in a bath of lubricant. This method produces a high quality surface finish and it is usually used for drawing fine wires of less than 0.5 mm diameter. In dry drawing, the wire passes through a soap powder container before entering the die. This method is used when the surface finish is not so critical or when the presence of lubricant is desirable for further processing.

For both the "wet" and "dry" drawing, friction between the wire and the die is of the boundary type, i.e., metal to metal contact occurs even though lubricant is present. To reduce the die wear and to obtain a good surface finish, the hydrodynamic lubrication method is employed where a high pressure is developed by the viscous action between the wire and the lubricant in the tube through which the wire passes.

1.3 Historical background of hydrodynamic lubrication

With the progress of wire drawing research, lubrication was proved necessary to promote efficiency, surface finish, quality, heat dissipation and reduce production time. This may be summarized as

- 1 Reduced drawing time
- 2 Elimination of pre-drawing time
- 3 Reduction of number of interpass heat treatment
- 4 Reducing machine maintenance time required due to excessive die wear

Christoperson and Naylor[1] first investigated hydrodynamic lubrication. They employed a long tube, with very close tolerances, attached to the front end of a

conventional die as shown in Figure 1.1. As the wire was pulled through the die, it pressurized the lubricant (oil) by viscous action and fed into the inlet of the die. This pressurized lubricant then completely separated the wire from the die, preventing metal to metal contact. Christoperson and Naylor experimentally showed that deformation of wire commences in the tube before the die entrance. Though hydrodynamic lubrication was achieved under the designed conditions, the pressure nozzle had to be placed in a vertical position and was of such a length that the wire industry found it too inconvenient to put it into practice.

Following all these findings, Wistreich[2] carried out experimental work on the forced lubrication based on a pressure tube system. Dry soap was used for lubrication in a short nozzle as it is a very good boundary lubricant. Experimental results showed that the speed, temperature and the tube gap had a direct effect on the property of the film thickness produced. He also noted that oil produced a thicker film than soap. Schematic diagram of the unit used by Wistreich is shown in Figure 1.2.

Orlov et al[3] developed a double die arrangement using externally pressurised oil as shown in Figure 1.3. The lubricant was transported into the chamber formed by the exit cone of the pressure die and the entry part of the drawing die, where the pressurised lubricant provides the hydrodynamic lubrication during drawing. Though better result was claimed for reduced die wear and reduced power consumption, however there was a lack of substantial evidence to support this claim.

1.4 Background of polymer melt as a lubricant

Polymer melts have recently been used as lubricants in drawing processes. Because of their very different characteristics from the conventional oil based lubricants such as high viscosity at higher temperatures, Symmons and Thompson[4] first suggested polymer melt as a lubricant in wire drawing. They investigated the adherence of the polymer coat on to the drawn wire. Subsequently Stevens[5] conducted experimental work which showed that polymer coating of wire was possible. Crampton[6] carried out a study of the wire drawing using a unit similar to the one adopted by Stevens[5]. The apparatus Crampton and Stevens used consisted of a pressure tube connected to the forward end of a conventional die. The polymer melt was dragged

into the tube by the motion of the wire generating high pressures which resulted in hydrodynamic lubrication and coating of the wire. The experiments they conducted reduced the cross-sectional area of the wire. They noted that the polymer coating of the wire is affected by the temperature of the polymer melt, viscosity of the polymer and the drawing speed of the wire. They also observed that with the increase in wire speed, the coating thickness decreased. A schematic diagram of this unit is shown in Figure 1.4. Further works carried out by different researchers with different geometries of the reduction units with polymer melt are briefly described here.

1.4.1 Stepped parallel bore unit

The stepped bore pressure unit consists of two parallel bore sections. Parvinmehr et al [7-11] showed that reduction of the wire diameter is possible using a polymer melt in conjunction with a stepped parallel bore unit which eliminates the need for a conventional reduction die. The least diameter of the stepped or tapered bore reduction unit was greater than the nominal wire diameter before deformation. Then a new concept in wire drawing was investigated and patented as "Plasto-hydrodynamic Die-less drawing". In this novel technique, the wire, tube or strip is pulled through a melt chamber filled with polymer melt and then passed through a stepped, tapered, combined or any other geometry bore reduction unit. Motion of the continuously moving wire or other continuum drags the polymer melt and causes the gap between the moving surface and the inner surface of the unit to be filled with the polymer melt which results in hydrodynamic lubrication and under certain conditions, coating as well as deformation of the wire. Following the work of Parvinmehr, Panwher et al [12-16] carried out work on the die-less tube sinking process and analyzed the system taking account of Newtonian and non-Newtonian characteristics of the polymer melt. Symmons et al [17-20] developed a microcomputer-based control system for the die-less wire drawing process. For the deformation of strip using a stepped parallel bore unit, Memon et al [21-25] also published theoretical and experimental works.

1.4.2 Tapered bore unit

Hashmi and Symmons [26-27] first presented analytical and numerical solutions for a solid continuum pulled through a tapered bore unit filled with a viscous fluid.

Parvinmehr [11] also carried out some experimental work for the wire drawing using a tapered bore hydrodynamic unit. Later, Nwir and Hashmi [28-30] developed the model for a wire considering the polymer as a non-Newtonian fluid. They also carried out experiments to observe the pressure profile within the unit.

1.4.3 Combined parallel and tapered bore unit

Investigation was also carried out by Al-Natour and Hashmi [31-32] using a combined parallel and tapered bore pressure unit in conjunction with a polymer melt. They developed a theoretical analysis assuming Newtonian pressure medium. Nwir and Hashmi [33] then published the pressure model considering the polymer as a non-Newtonian fluid. Experiments were carried out to obtain the pressure profile for different geometry of the combined unit.

In all these three cases the smallest bore size is greater than the cross-section of the wire, tube or strip so that metal to metal contact should never take place.

1.5 Objective of the present studies and relation with previous work

The aforementioned three types of chambers have been used by a number of researchers to explore and study the die-less drawing process. However, some limitations were observed in those studies. The viscosity of the polymer melt was considered to remain unchanged during the drawing and coating process. Also the change in shear stress was not taken into account while analysing the process. In stepped parallel bore unit the pressure could be found only in the step of the unit. In combined parallel and tapered bore unit pressure could be calculated only in the tapered part of the unit. No attempt was taken to predict any difference in the pressure through the fluid film thickness. In all studies the pressure was considered to be constant.

As the solid continuum (wire, tube or strip) is first pulled through the polymer melt chamber before the plasto-hydrodynamic die-less unit, the melt chamber plays an important role for the drawing and coating of the wire. The fluid flow and temperature characteristics developing in the melt chamber were also not investigated in previous studies.

As regards good quality polymer coating by hydrodynamic process, the maximum wire speed attained in previous studies was only 0.6 m/s. This speed is considered

to be rather low for industrial scale production

Keeping the above mentioned shortcomings and inadequacies, the broad objectives of the present work are to carry out new theoretical analysis of the process incorporating more realistic behaviour of the process parameters and to experimentally explore the possibility of coating at higher speed of the wire. The specific objectives of the project are listed below

The objective of this present project are:

- 1 Development of a theoretical model for the velocity and temperature gradient boundary layer thickness for the continuous drawing of a wire through a polymer melt chamber located before hydrodynamic unit
- 2 Developing a model of the melting profile for the solid polymer layer produced on the wire in the melt chamber
- 3 To develop new mathematical models for different types of pressure units (combined parallel and tapered unit, tapered unit, converging exponential and parabolic) for the prediction of hydrodynamic pressure as well as deformation in the continuum
- 4 To modify some previous mathematical models in relation to pressure and deformation (for stepped parallel bore unit in association with wire, strip and tube) and compare these solutions with experimental results reported elsewhere
- 5 To simulate the hydrodynamic process for different types of pressure unit (tapered, combined, converging exponential and parabolic) by finite element method where the pressure and temperature can be calculated both in the direction of the fluid film thickness and along the wire velocity direction
- 6 To carry out experiments to obtain continuous and concentric coating on wire upto wire speed of 12 m/s using different types of plasto-hydrodynamic pressure unit

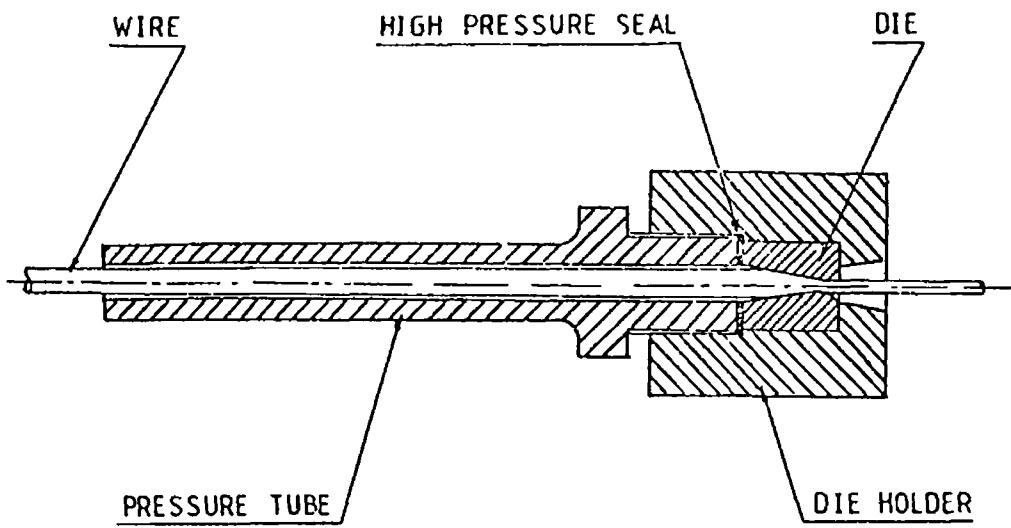


Figure 1 1 Typical pressure tube and die

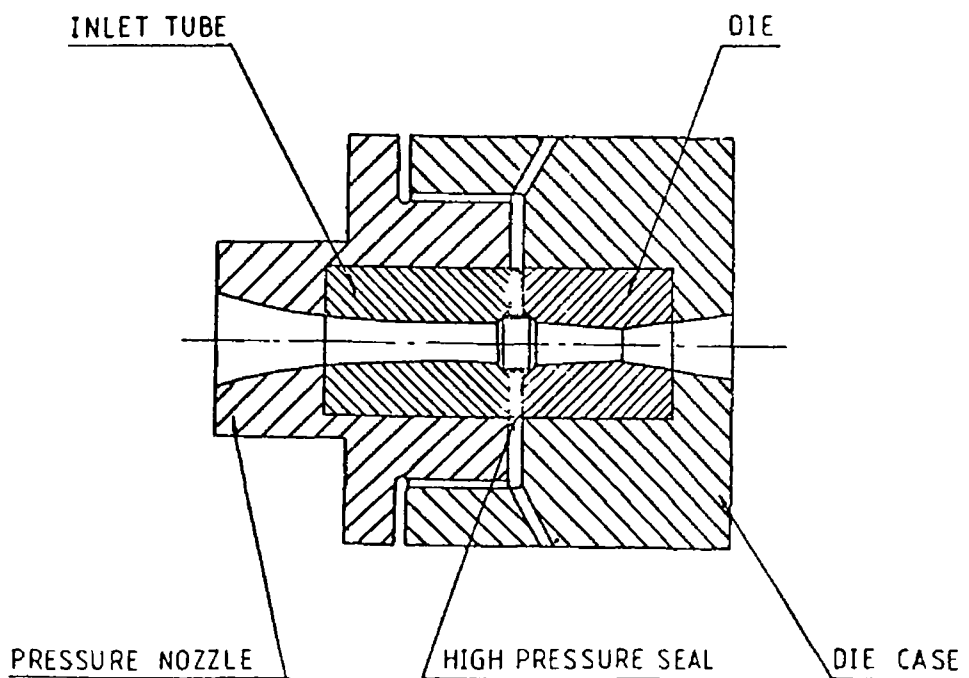


Figure 1 2 Nozzle-die unit (BISRA)

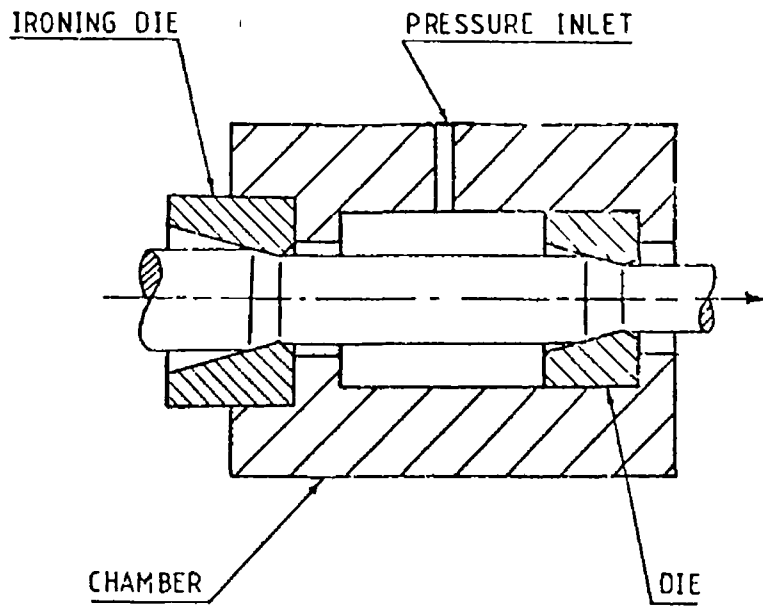


Figure 1 3 Pressurized chamber

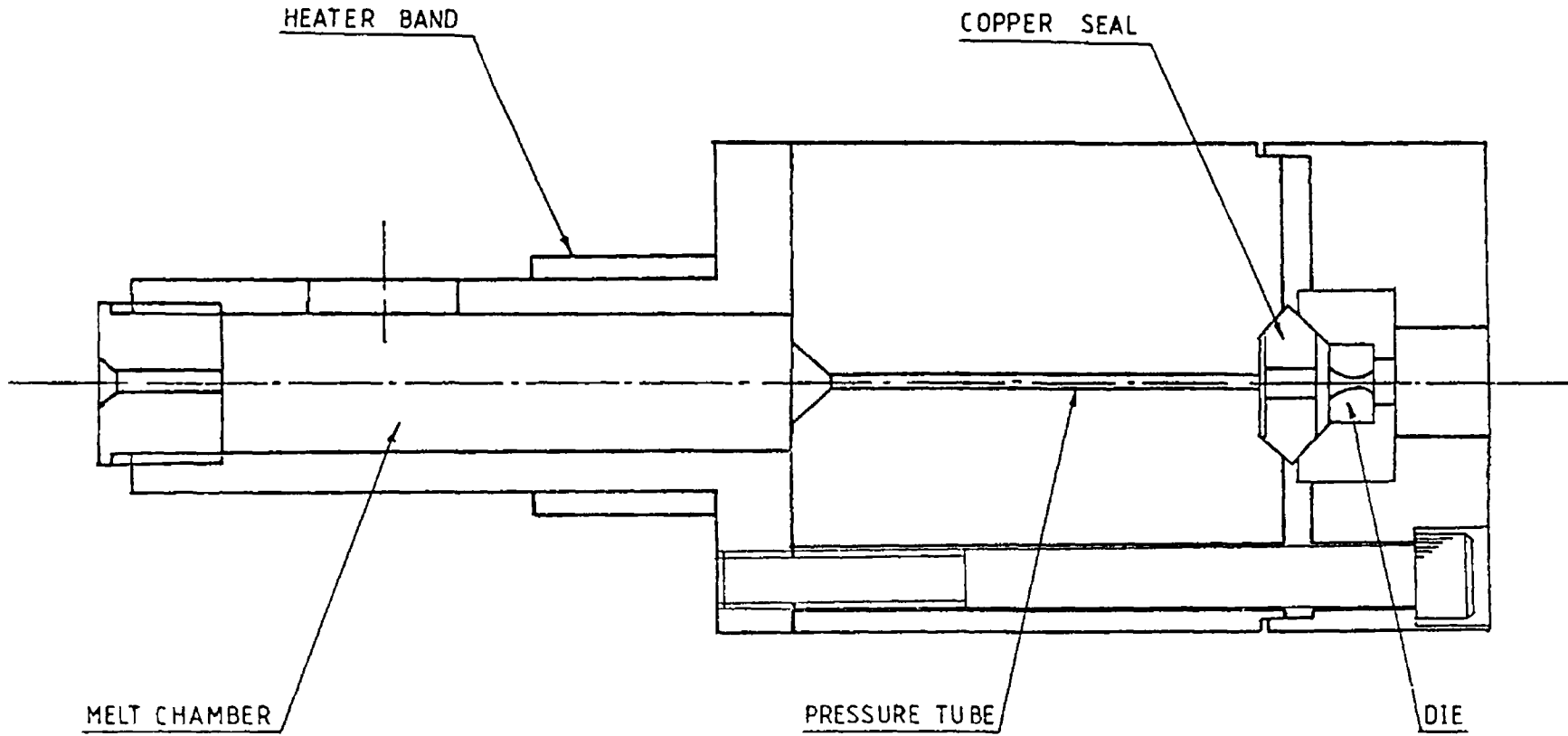


Figure 1 4 Pressure tube-die arrangement

CHAPTER 2

RHEOLOGY OF POLYMER MELT

2.1 Introduction

Flow of polymer melt occurs when the molecules slide past each other. Ease of flow depends on the mobility of the molecular chains and the forces holding the molecules together. The flow characteristics of the polymer melts are influenced by many factors which are described in this chapter in relation to the present work.

2.2 Effect of temperature

For Newtonian fluids the relation between the viscosity and temperature may be related expressed by an Arrhenius type equation

$$\mu = Ae^{E/RT} \quad (2.1)$$

where A is a constant, E is the activation energy. This equation permits calculation of the coefficient of viscosity for an absolute temperature T, R being the universal gas constant.

The polymer melt exhibits non-Newtonian behaviour except for very low shear rates[34]. Another form of equation is often used,

$$\mu = ae^{-bT} \quad (2.2)$$

where both a and b are constants.

A number of attempts have been made to obtain a fundamental explanation of the difference in temperature dependence of viscosity between different polymers. The most successful is the application of "free volume theory"[34].

This theory suggests that at some temperature T_0 (which appears to be about 52°C below the measured glass transition temperature, T_g) there is no "free volume" between the molecules. This free volume, f , is postulated to increase linearly with temperature so that at T_g the fractional free volume has a value f_g . The expansion

coefficient α_f is defined by the equation

$$f = f_g + \alpha_f (T - T_g) \quad (2.3)$$

where f_g has the universal value of 0.025 and α_f a universal value of 4.8×10^{-4} . William et al [35] have argued from this that the viscosity μ of a polymer at temperature T may be related to its viscosity μ_a at an arbitrary reference temperature T_a by the equation

$$\log \frac{\mu}{\mu_a} = - \frac{C_1^a (T - T_a)}{C_2^a + T - T_a} \quad (2.4)$$

If the arbitrary temperature is taken as T_g then equation (2.4) becomes

$$\log \frac{\mu}{\mu_g} = - \frac{C_1^g (T - T_g)}{C_2^g + T - T_g} \quad (2.5)$$

In this case

$$C_1^g = \frac{1}{2.303 f_g} = 17.44$$

and

$$C_2^g = \frac{1}{2.303 C_1^g \alpha_f} = 51.6$$

were proposed as universal constants. These equations are known as the WLF equations.

2.3 Effect Of Pressure

The influence of pressure on the polymer melt was first checked by Westover [36], developing a suggestion by Maxwell and Jung [37], by the use of a double piston rheometer. The rheometer consists of two barrels in series separated by a die. Two pistons acting in opposite directions, are used to apply pressure evenly to each barrel.

and the pistons are locked in position This causes the melt to flow through the die There is consequently a pressure drop between the reservoirs, from which, with a knowledge of the capillary dimensions, the shear rate and shear stress may be calculated Westover's experiments yielded results that exposed what Cogswell [38] later described as the "convenient heresy that liquids are incompressible" A further capillary-based device for measuring the effect of pressure was developed by Choi[39] This treated the barrel/die assembly as two capillaries in series All the above capillary techniques suffer from the disadvantage that the shear stress is determined by the same force as that which gives rise to pressure However this disadvantage was overcome with the "pressurised Couette-Hatschek viscometer" originally used by Semjonov[40] and later by Cogswell[38] This apparatus consists of two concentric cylinders, the gap between which is filled by the melt at a controlled pressure The inner cylinder remains stationary while the outer cylinder rotates causing the melt to shear The resultant viscous drag produces a torque on the inner cylinder and this is interpreted as the shear stress Using a lower ram the system could be pressurised ranging from atmospheric to $1.7 \times 10^8 \text{ Nm}^2$

Cogswell observed that the flow curves for a given material obtained at various temperatures and pressures were, within the range of practical interest, usually superimposable by a shift at constant stress Assuming the change in $\log(\text{viscosity})$ to be linearly proportional to the temperature or pressure change an adequate approximation was possible This followed that the effect of the temperature on the viscosity could be related to the effect of the pressure on viscosity through a coefficient The coefficient was found not to vary greatly with polymer type (Table 2.1) Hence the polymers whose viscosity is sensitive to changes in temperature are similarly sensitive to changes in pressure

2.4 Stress-Strain Dependent Viscosity

For a Newtonian fluid there is a linear relation between the stress and shear rate when it is under shear stress conditions The slope of the line represents the viscosity of the fluid which is constant For a non-Newtonian shear-thinning fluid, i.e. pseudoplastic fluid, the viscosity decreases with the increase of the shear rate Polymer solutions exhibit such behaviour Another non-Newtonian fluid, shear-

thickening, shows the opposite rheological effect to shear-thinning and is termed as dilatant fluid

Two different equations are generally used to express the stress vs shear rate relation for a polymer solution. The first is a power law equation given by

$$\tau = k \left(\frac{dU}{dy} \right)^n \quad (2.6)$$

This equation is applicable for any type of fluid. Here n is the power law index which equals 1 for a Newtonian fluid, greater than 1 for a dilatant fluid and less than 1 for a pseudoplastic fluid. In this equation τ is the shear stress, k is the viscosity coefficient for power law fluid and (dU/dy) is the shear rate.

Table 2.1 Temperature-Pressure Coefficients at Constant Viscosity, Entropy and Volume ($^{\circ}\text{C}/\text{Nm}^2$) (after Cogswell [38])

Polymer	$-(\Delta T/\Delta P)_{\mu}$	$(\delta T/\delta P)_s$	$(\delta T/\delta P)_v$
PVC	3.1×10^7	1.1×10^7	16.0×10^7
Nylon	3.2	1.2	11.0
Poly(methyl-methacrylate)	3.3	1.2	13.0
Polystyrene	4.0	1.5	13.0
Polyethylene (high-density)	4.2	1.5	13.0
Acetal-copolymer	5.1	1.4	14.0
Polyethylene (low-density)	5.3	1.6	16.0
Silicone-polymer	6.7	1.9	9.0
Polypropylene	8.6	2.2	19.0

The second is an empirical equation relating shear stress and shear rate of polymer melts suggested by Rabinowitch [41] in the form

$$\tau + K\tau^3 = \mu \left(\frac{dU}{dy} \right) \quad (2.7)$$

Here K is the non-Newtonian factor, μ is the viscosity of the polymer melt, τ and (dU/dy) are the shear stress and shear rate respectively

Figures 2.1 and 2.2 show the effect of the shear rate on the viscosity in which the influence of the temperature may be noticed. These curves were produced by extruding polymer melts (Alkathene WVG23 and Polypropylene KM61) through an extrusion rheometer[11]. The viscosity of the polymer may be calculated at any known shear rate by measuring the slope of the curve. Figures 2.3 and 2.4 show the viscosity vs shear rate curves [11] of Alkathene WVG23 and Polypropylene KM61. Figures 2.5 and 2.6 show the viscosity vs shear rate curves of Borosiloxane[42] and Nylon 6 (Durethan B 31 F)[43] respectively.

2.4.1 Critical Shear Stress

The critical shear stress is the stress at which the uniformity of the polymer melt flow ceases to exist. This phenomenon was investigated by several workers[44-49] and they showed that certain flow defects are associated with the polymer melts at the critical shear stress. Irregularities of flow were shown to take the form of Ripple, Bamboo, Spiral, ZigZag or Helix for different types of polymers. The terms "Melt fracture", "Elastic turbulence" and "Flow distortion" have been used to describe this effect. However, there is a general agreement on the following points:

- 1 The Critical Shear Stress(CSS) has values in the region of 0.01 to 1.0 MN/m² for most polymers
- 2 The CSS is independent of the die length and diameter
- 3 The CSS does not vary widely with temperature
- 4 The flow defect always takes place when non-Newtonian fluids were involved
- 5 A discontinuity in the viscosity shear stress curves occurred
- 6 The CSS was shown by a cinematography method to take place in the die

2.4.2 Sharkskin

The surface irregularity known as sharkskin is characterised by a series of ridges perpendicular to the flow direction. In milder form it is known as mattness where

the extrudate has a lack of surface gloss Sharkskin has usually been distinguished from elastic turbulence for the following reasons (Howells and Benbow[48])

- (a) Sharkskin has a perpendicular distortion whereas elastic turbulence often gives a helical or irregular pattern
- (b) Sharkskin can occur at lower extrusion rates than elastic turbulence and appears to be a function of the linear output rate as opposed to the critical apparent wall shear rate for elastic turbulence
- (c) Sharkskin is very dependent on temperature, being considerably delayed by increase in temperature
- (d) Sharkskin appears to be unaffected by die entry angle, length to diameter ratio and the material of construction of the die

2.5 Effect of Polymer Flow Characteristics

In a plasto-hydrodynamic pressure unit the polymer melt is subjected to very high shear rates and pressures, much greater than those capable of being investigated in any extrusion rheometer. The presence of critical shear stress at low shear rate decreases the coating thickness, as concluded by Crampton[6]. However it is also believed that the poor performance of the units at higher drawing speeds is related to a combination of factors such as shear rate, melt flow instability, partial crystallization, compressibility etc and not just by the critical shear stress. The high pressure generation is believed to have the effect of increasing the melt viscosity in the unit. Crampton maintained the temperature at a steady value when the tests were conducted thus minimising the effects inherent with changing temperature. However to understand these effects fully further investigation is needed. In the present work some theoretical studies have been done in relation to the fluid flow and temperature distribution inside the melt chamber which are given in the following section

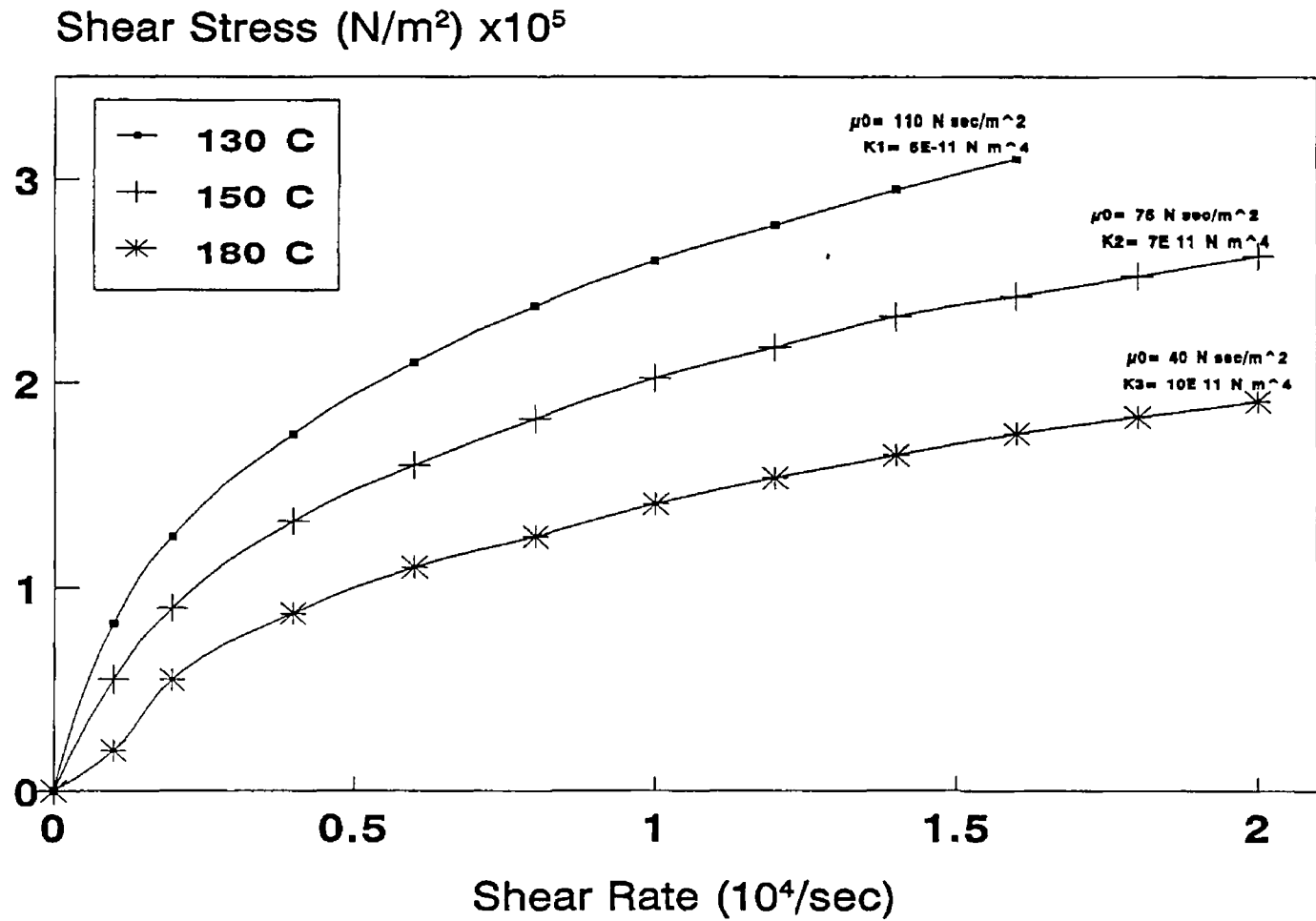


Figure 2 1 Flow curves for Alkathane WVG 23

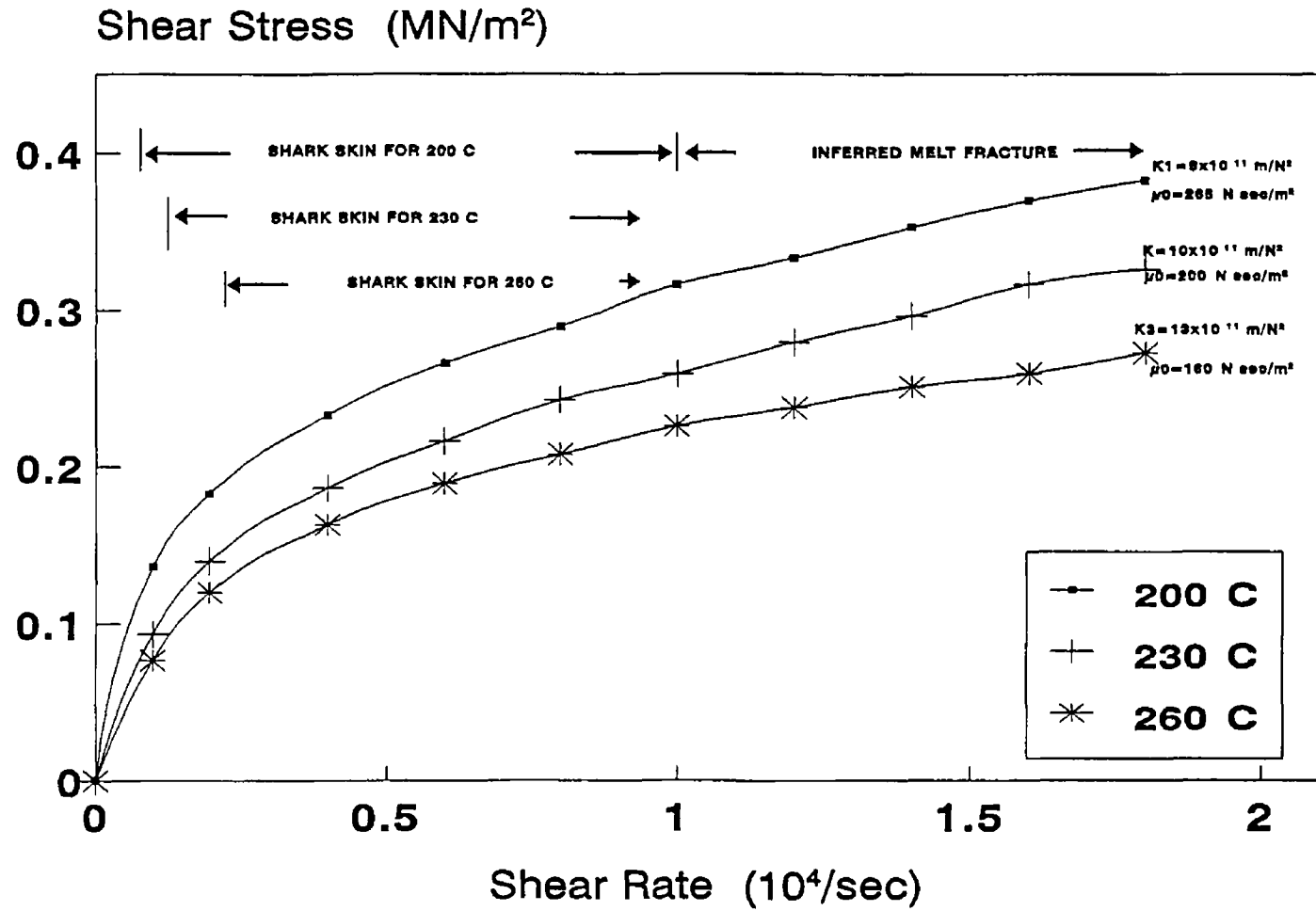


Figure 2 2 Flow curves for Polypropylene KM 61

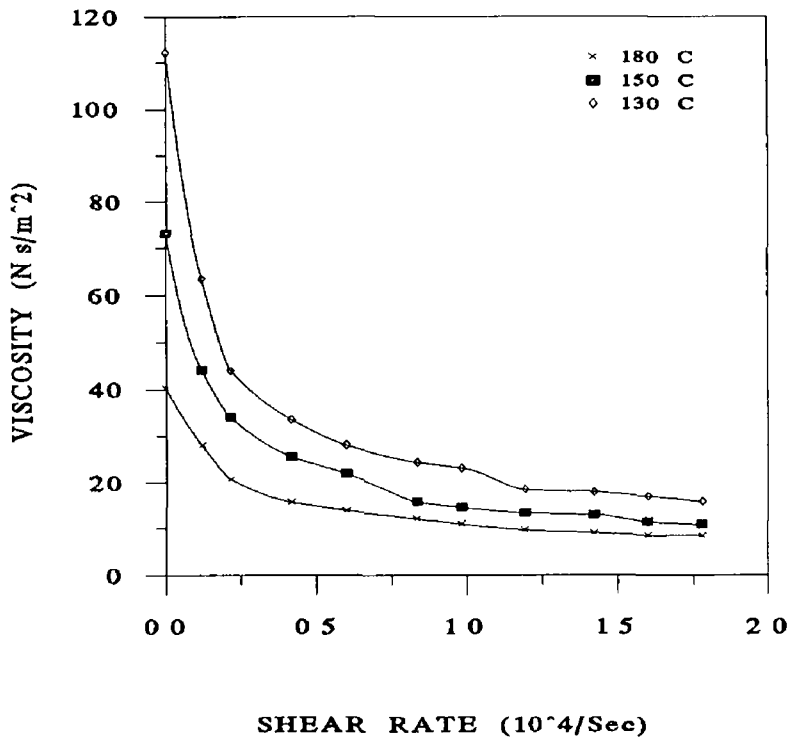


Figure 2.3 Effect of temperature on viscosity/shear rate for Alkathane WVG23

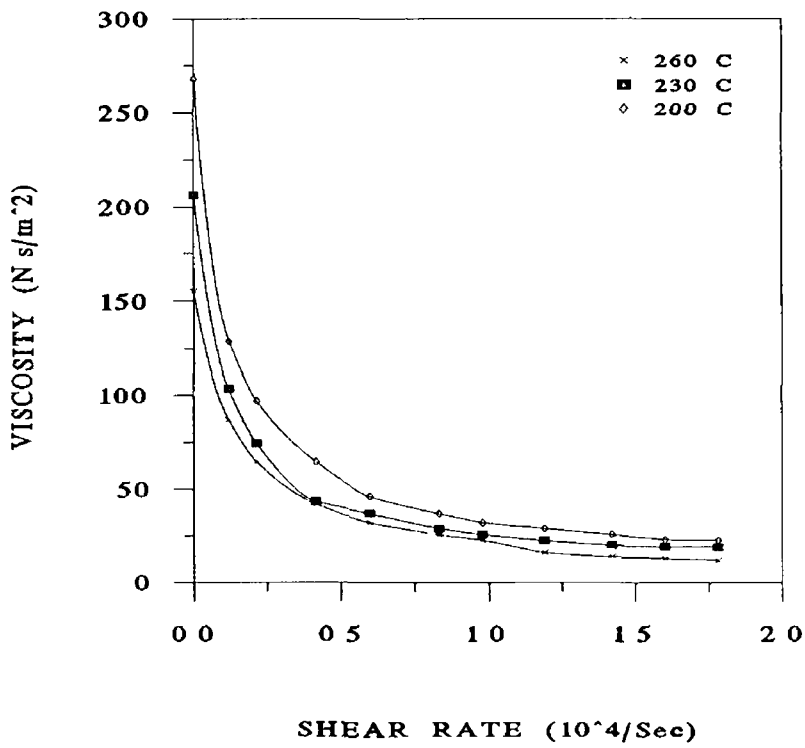


Figure 2.4 Effect of temperature on viscosity/shear rate for Polypropylene KM61

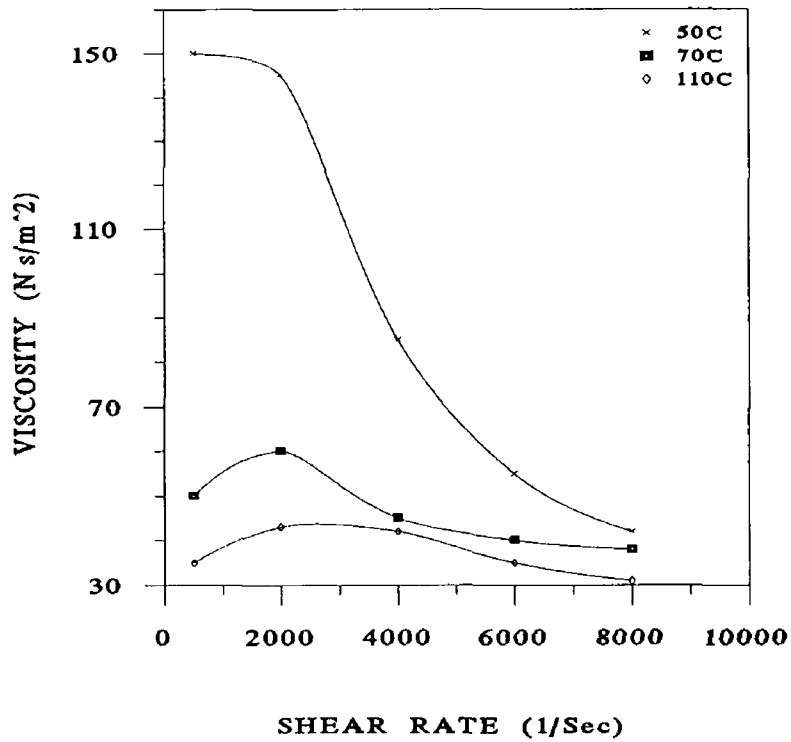


Figure 2 5 Effect of temperature on viscosity/shear rate for Borosiloxane

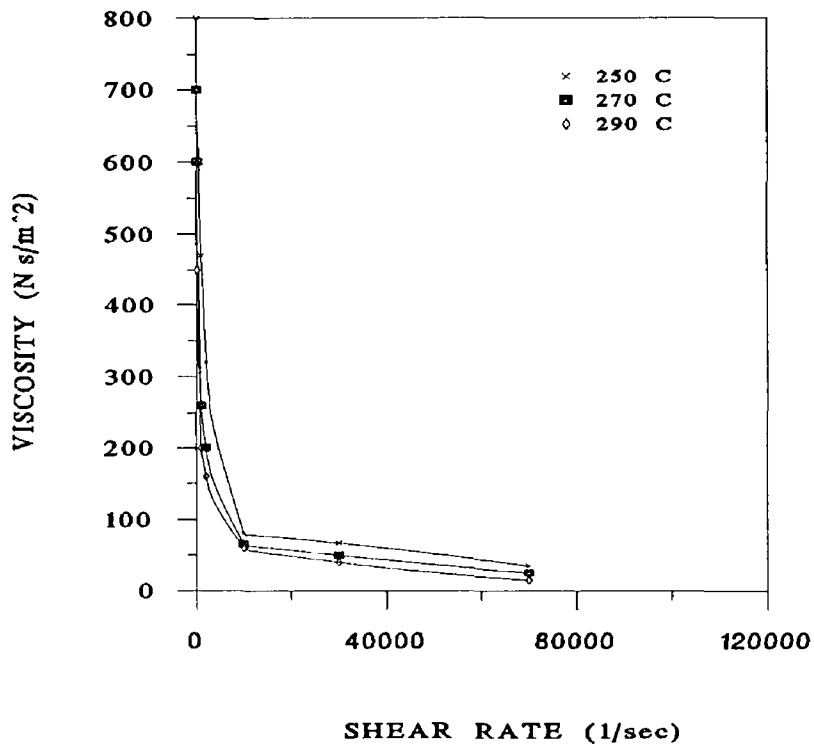


Figure 2 6 Effect of temperature on viscosity/shear rate for Nylon 6 (Durethan B 35 F 9000/0 KYY Resin)

2.6 Boundary layer behaviour of polymer melt in melt chamber

In the plasto-hydrodynamic drawing or coating process (Figure 2.7) the continuous surface (wire, strip or tube) passes through a melt chamber positioned before the plasto-hydrodynamic pressure chamber unit. The polymer in the melt chamber is a non-Newtonian fluid. Discussions for laminar boundary layer heat transfer to power law fluid have been published by others in references [50-51]. The following analysis has already been published which was given as reference [52]. In this analysis the wire and the fluid are assumed to move in the same direction. Here the velocity of wire V is greater than the free stream velocity V_0 .

2.6.1 Boundary layer analytical solution

The governing equation for the velocity boundary layer in the case of Figure 2.8, neglecting external body forces is [53]

$$-\tau_w - \frac{dp}{dx} \delta = -\rho \frac{d}{dx} \int_0^\delta (V_0 - U) U dy + \frac{dV_0}{dx} \int_0^\delta \rho U dy \quad (2.8)$$

This is the integral momentum equation for boundary layer. Considering the pressure to be constant throughout the flow,

$$\frac{dp}{dx} = 0 = -\rho V_0 \frac{dV_0}{dx} \quad (2.9)$$

As for the wall shear stress

$$\tau_w = k \left(\frac{dU}{dy} \right)_{y=0}^n \quad (2.10)$$

and making use of equation (2.9) and combining equations (2.8) and (2.10), the integral boundary-layer equation is obtained as

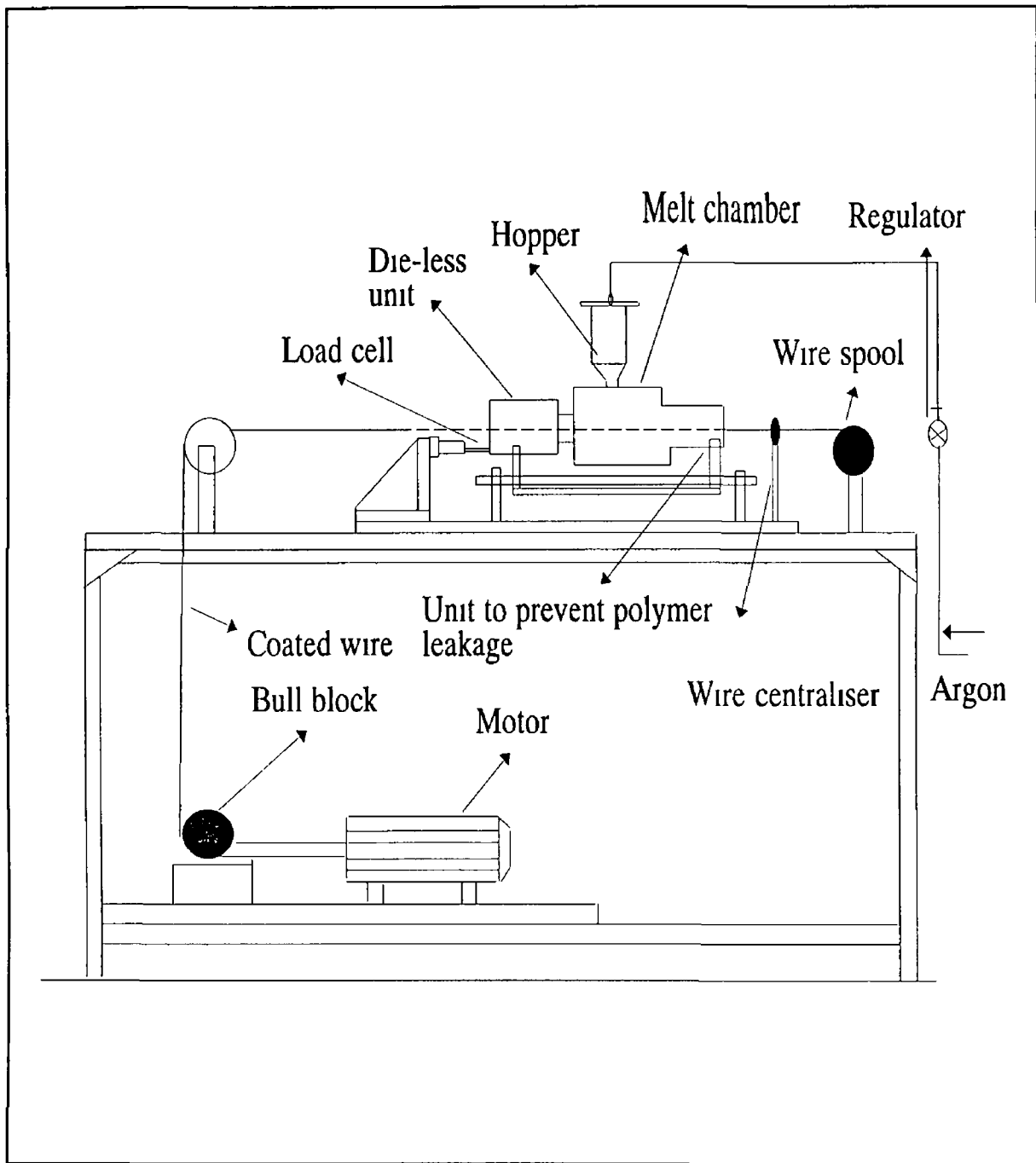


Figure 2 7 Schematic diagram of the plasto-hydrodynamic wire coating process

$$\rho \frac{d}{dx} \int_0^{\delta} (V_0 - U) U dy = \tau_w = K \left(\frac{dU}{dy} \right)_{y=0}^n \quad (2.11)$$

For approximate analysis boundary conditions are given, which are satisfied by velocity functions

- (a) $U=V$ at $y=0$, (b) $U=V_0$ at $y=\delta$, (c) $(dU/dy)=0$ at $y=\delta$

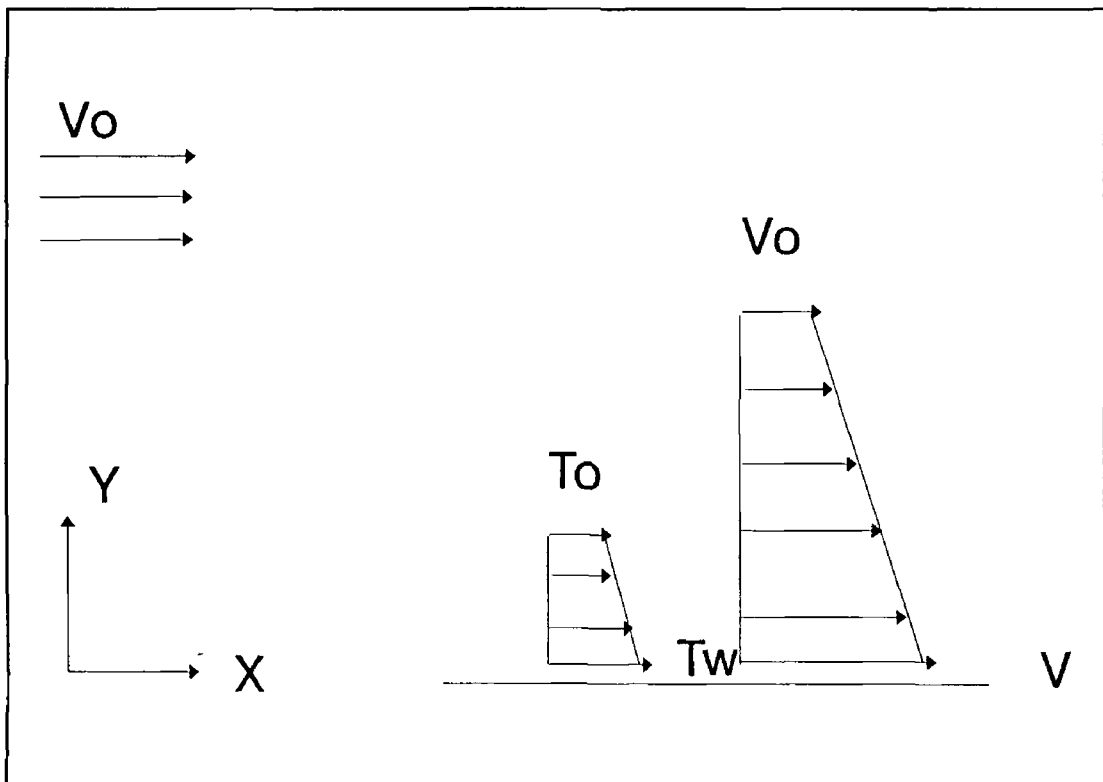


Figure 2.8 Schematic diagram of the flow model

and for constant pressure condition, (d) $(d^2U/dy^2) = 0$ at $y=0$

It is assumed that the velocity profile at different x is the same which should satisfy the above conditions. There are four conditions to satisfy. The simplest function that satisfies these conditions is a polynomial with four arbitrary constants. Therefore,

$$U=C_1+C_2y+C_3y^2+C_4y^3 \quad (2.12)$$

Solution of this equation with the above four conditions gives the velocity profile which is

$$U=V-\frac{3}{2}(V-V_0)\left(\frac{y}{\delta}\right)+\frac{1}{2}(V-V_0)\left(\frac{y}{\delta}\right)^3 \quad (2.13)$$

Therefore, from equation (2.10) and (2.13) it gives,

$$\tau_w=K\left(-\frac{3}{2}\frac{(V-V_0)}{\delta}\right)^n \quad (2.14)$$

Substituting the expressions for U from (2.13) in equation (2.11) and after integration it yields

$$\left(\rho V^{2-n}\frac{x^n}{K}\right)\left(\frac{\delta}{x}\right)^{n+1}=\frac{\left(\frac{3}{2}\right)^n\left(1-\frac{V_0}{V}\right)^n(n+1)}{\left(\frac{33}{140}+\frac{39}{280}\frac{V_0}{V}\right)\left(1-\frac{V_0}{V}\right)} \quad (2.15)$$

which upon rearrangement gives,

$$\delta=\frac{\left(\frac{3}{2}\right)^{\frac{n}{n+1}}(n+1)^{\frac{1}{n+1}}\left(1-\frac{V_0}{V}\right)^{\frac{n-1}{n+1}}}{Re_x^{\frac{1}{n+1}}\left(\frac{33}{140}+\frac{39}{280}\frac{V_0}{V}\right)^{\frac{1}{n+1}}}x \quad (2.16)$$

where the modified Reynolds number for the non-Newtonian fluid is $Re_x=\rho v^{2n}x^n/K$

Also, the friction factor may be expressed as

$$C_{fx}=\frac{\tau_w}{\left(\frac{\rho V^2}{2}\right)} \quad (2.17)$$

Combining equations (2 14), (2 16) and (2 17) the expression for the local friction factor becomes

$$C_{fx} = (-1)^n (2) \left(\frac{3}{2}\right)^{\frac{n}{n+1}} \left(1 - \frac{V_0}{V}\right)^{\frac{2n}{n+1}} \left(\frac{\left(\frac{33}{140} + \frac{39}{280} \frac{V_0}{V}\right)}{(n+1)}\right)^{\frac{n}{n+1}} (Re_x)^{-\frac{1}{n+1}} \quad (2 18)$$

Thermal boundary layer thickness

The governing equation for the thermal boundary layer [53] may be expressed as,

$$\frac{d}{dx} \left(\int_0^{\delta_t} (T_0 - T) U dy \right) = \alpha \left(\frac{dT}{dy} \right)_{y=0} \quad (2 19)$$

The boundary conditions are

(e) $T = T_w$ at $y = 0$, (f) $T = T_0$ at $y = \delta_t$, (g) $(dT/dy) = 0$ at $y = \delta_t$ and (h) at $y = 0$ viscous dissipated heat generation is zero, so that $(d^2T/dy^2) = 0$ at $y = 0$

These conditions may be fitted to a cubic polynomial as in the case of the velocity profile, so that,

$$T = T_w + \frac{3}{2} (T_0 - T_w) \left(\frac{y}{\delta_t}\right) - \frac{1}{2} (T_0 - T_w) \left(\frac{y}{\delta_t}\right)^3 \quad (2 20)$$

Substituting the expression of T in equation (2 19) and after integration it gives

$$V(T_0 - T_w) \frac{d}{dx} \left(\frac{3}{8} \delta_t - \frac{3}{20} \frac{\delta_t^2}{\delta} \left(1 - \frac{V_0}{V}\right) + \frac{3}{280} \frac{\delta_t^4}{\delta^3} \left(1 - \frac{V_0}{V}\right) \right) = \frac{3}{2\delta_t} \alpha (T_0 - T_w) \quad (2 21)$$

As $\delta_t \ll \delta$ then (δ_t^4/δ^3) is small compared with other terms Therefore this term can

be neglected and the above equation becomes,

$$\frac{d}{dx} \left(\frac{3}{8} \delta_t - \frac{3}{20} \frac{\delta_t^2}{\delta} \left(1 - \frac{V_0}{V} \right) \right) = \frac{3}{2} \frac{\alpha}{V \delta_t} \quad (2.22)$$

Let $Z = \delta_t / \delta$ so that the above equation may be written as,

$$Z \delta \frac{d}{dx} \delta \left(\frac{3}{8} Z - \frac{3}{20} Z^2 \left(1 - \frac{V_0}{V} \right) \right) = \frac{3}{2} \frac{\alpha}{V} \quad (2.23)$$

In order to solve this equation it may be assumed that

$$Z = \sum_{i=0}^{\infty} \left(1 - \frac{V_0}{V} \right)^i Z_i = Z_0 + \left(1 - \frac{V_0}{V} \right) Z_1 + \dots \quad (2.24)$$

From equation (2.23) and (2.24) the following expressions can be obtained by equating the coefficients of like powers of $(1 - V_0/V)$

$$Z_0 \delta \frac{d}{dx} \delta \left(\delta \frac{3}{8} Z_0 \right) = \frac{3}{2} \frac{\alpha}{V} \quad (2.25)$$

and

$$Z_0 \delta \frac{d}{dx} \delta (\delta Z_1) + Z_1 \delta \frac{d}{dx} \delta \left(\delta \frac{3}{8} Z_0 \right) + Z_0 \delta \frac{d}{dx} \delta \left(-\frac{3}{20} Z_0^2 \right) = 0 \quad (2.26)$$

Combining equation (2.25) and (2.26) gives

$$Z_0^2 = \frac{8\alpha}{xV} \left(\frac{x}{\delta} \right)^2 \quad (2.27)$$

which upon substitution for δ becomes,

$$Z_0^2 = \frac{8}{Pr} \left(\frac{\left(\frac{3}{2}\right)^n (n+1) \left(1 - \frac{V_0}{V}\right)^{(n-1)}}{\left(\frac{33}{140} + \frac{39}{280} \frac{V_0}{V}\right)} \right)^{-\frac{2}{n+1}} \quad (2.28)$$

where the generalized Prandtl number Pr for a non-Newtonian fluid is, $Pr = Vx/\alpha(\text{Re}^{2/n+1})$ and,

$$Z_1 = \frac{6}{55} Z_0^2 \quad (2.29)$$

Now

$$Z = \frac{\delta_t}{\delta} = Z_0 + \left(1 - \frac{V_0}{V}\right) Z_1 \quad (2.30)$$

gives the expression for the temperature boundary layer thickness δ_t as well as the local Nusselt number,

$$Nu_x = \left(\frac{h_x}{k_f}\right) = \left(\left(\frac{dT}{dy}\right)_{y=0}\right) / \left(\left(T_0 - T_w\right)/x\right) = \frac{3x}{2\delta_t} \quad (2.31)$$

In the case of plasto-hydrodynamic wire drawing or coating, the wire is passed through a polymer melt chamber positioned before the plasto hydrodynamic pressure unit. Here, the polymer melt at δ is almost stagnant. Therefore, V_0 may be considered to be zero. Then the analytical expressions for the velocity boundary layer thickness, coefficient of friction factor, temperature boundary layer thickness and the Nusselt number become,

$$\delta = \frac{\left(\frac{3}{2}\right)^{\frac{n}{n+1}} (n+1)^{\frac{1}{n+1}}}{\left(\frac{33}{140} Re_x\right)^{\frac{1}{n+1}}} x \quad (2.32)$$

$$C_{fx} = (-1)^n (2) \left(\frac{3}{2}\right)^{\frac{n}{n+1}} \left(\frac{33}{140}\right)^{\frac{n}{n+1}} (Re_x)^{-\frac{1}{n+1}} \quad (2.33)$$

$$\delta_t = \delta \left(\sqrt{\frac{8}{Pr}} \left(\frac{3}{2}\right)^{\frac{n(n+1)}{n+1}} \left(\frac{33}{140}\right)^{-\frac{1}{n+1}} + \frac{6}{55} \left(\frac{8}{Pr}\right)^{\frac{1}{2}} \left(\frac{3}{2}\right)^{\frac{n(n+1)}{n+1}} \left(\frac{33}{140}\right)^{-\frac{2}{n+1}} \right) \quad (2.34)$$

$$Nu_x = \frac{3}{2} Re_x^{\frac{1}{n+1}} \frac{1}{(Z_0 + Z_1)} \left(\frac{3}{2}\right)^{\frac{n(n+1)}{n+1}} \left(\frac{33}{140}\right)^{-\frac{1}{n+1}} \quad (2.35)$$

Results have been calculated on the basis of equations derived in the theoretical analysis. In order to calculate the theoretical results, the following values of the parameters were used

Length of the melt chamber, $x = 40$ mm

Table 2 2 Polymer data used in theoretical analysis[54-55]

Polymer	Power law index(n)	Molten polymer temperature($^{\circ}$ C)	Viscosity (N s/m ²)	Density(kg/m ³)
PA6	0 7	280	63	969
HDPE	0 5	240	63	960
LDPE	0 35	220	39	780
PP	0 35	240	148	914
PS	0 25	200	137	1100
PMMA	0 3	250	97	1000

Figure 2 9 displays velocity boundary layer thickness versus wire velocity for different polymer melts This thickness decreases with the decrease in the power law index n (as shown in Table 2 2) and increase in the wire velocity With the increase in the velocity gradient boundary layer thickness, the surface friction factor also increases as shown in Figure 2 10 As the temperature gradient boundary layer depends on the velocity gradient boundary layer, it behaves in a similar way with the power law index and the wire velocity (Figure 2 11) A thinner thermal boundary layer promotes sharper surface gradients for the temperature and thus enhances the Nusselt number (Figure 2 12)

As the wire velocity increases for a certain polymer the velocity gradient thickness as well as the temperature gradient boundary layer thickness decrease With the decrease in thickness the possibility of solidification of polymer on the wire in the melt chamber decreases Polymer solidification on the wire in the melt chamber may lead to sharkskin in the polymer coating produced by hydrodynamic pressure inside the plasto-hydrodynamic pressure unit Experiments showed that sharkskin[11] was formed on Copper wire coating for speeds upto 1 5m/s with Alkathane WVG ($n=0 4$) and 1m/s with Polypropylene KM61($n=0 35$) This sharkskin disappeared above these velocities

The appearance of sharkskin is dependent on the temperature, being considerably delayed by the increase in the surface temperature [48] Preheating of the wire is a way to make the temperature distribution less sharp in the temperature gradient boundary layer thickness Figure 2 13 (at wire velocity 2 m/s) shows preheating of wire makes the temperature distribution in the temperature gradient boundary layer thickness flatter, which discourages the solidification of polymer on the wire in the melt chamber thereby avoiding sharkskin formation in the polymer coating

Figure 2 14 shows the temperature boundary layer thickness with different length of melt chamber at wire velocity of 2 m/s From 40 mm to 70 mm length of the melt chamber the temperature boundary layer thickness increases linearly After that, the thickness increases at a slower rate Thus it may be said that from the point from which the increase in temperature gradient boundary layer thickness starts at a slower rate, remelting of the polymer solid layer starts

2.6.2. Numerical analysis for boundary layer

Substituting for U from (2 13) in equation (2 11) yields .

$$\left(\rho \frac{V^{2-n}}{k}\right) \left(\delta^n \frac{d\delta}{dx}\right) = \frac{\left(\frac{3}{2}\right)^n \left(1 - \frac{V_0}{V}\right)^n}{\left(\frac{33}{140} + \frac{39}{280} \frac{V_0}{V}\right) \left(1 - \frac{V_0}{V}\right)} \quad (2 36)$$

which upon rearrangement in finite difference term gives,

$$\left(\rho \frac{V^{2-n}}{K}\right) \left(\frac{\delta_1^n (\delta_1 - \delta_{1-1})}{x_1 - x_{1-1}}\right) = \frac{\left(\frac{3}{2}\right)^n \left(1 - \frac{V_0}{V}\right)^n}{\left(\frac{33}{140} + \frac{39}{280} \frac{V_0}{V}\right) \left(1 - \frac{V_0}{V}\right)} \quad (2 37)$$

Therefore,

$$\delta_{1}^{n+1} - \delta_{1}^n \delta_{1-1} - \left(\frac{3}{2}\right)^n \frac{(x_1 - x_{1-1}) \left(1 - \frac{V_0}{V}\right)^{n-1}}{\left(\frac{\rho V^{2-n}}{K}\right) \left(\frac{33}{140} + \frac{39}{280} \frac{V_0}{V}\right)} = 0 \quad (2.38)$$

The solution of equation (2.38) gives the numerical value of the velocity boundary layer thickness

The friction factor is given by equation (2.17) as

$$C_{fx} = \frac{\tau_w}{\left(\frac{\rho V^2}{2}\right)}$$

Substituting for τ_w from equation (2.14) the expression for the local numerical friction factor becomes

$$C_{f_{x(1)}} = \frac{K \left(-\frac{3}{2} \left(\frac{V-V_0}{\delta_1}\right)\right)}{\frac{(\rho V^2)}{2}} \quad (2.39)$$

Equation (2.22) may be written as,

$$\frac{3}{8} \frac{(\delta_{t(i)} - \delta_{t(i-1)})}{(x_1 - x_{1-1})} - \frac{3}{20} \frac{\frac{(\delta_{t(i)} - \delta_{t(i-1)})^2 \left(1 - \frac{V_0}{V}\right)}{(\delta_1 - \delta_{1-1})}}{(x_1 - x_{1-1})} = \frac{3}{2\alpha V \delta_{t(i)}}$$

which after rearrangement becomes

$$2 \left(1 - \frac{V_0}{V}\right) \delta_{t(i)}^3 - (4\delta_{t(i-1)} \left(1 - \frac{V_0}{V}\right) + 5(\delta_1 - \delta_{1-1})) \delta_{t(i)}^2 + (2\delta_{t(i-1)}^2 \left(1 - \frac{V_0}{V}\right) + 5\delta_{t(i-1)} (\delta_1 - \delta_{1-1})) \delta_{t(i)} + \frac{20\alpha}{V} (x_1 - x_{1-1}) (\delta_1 - \delta_{1-1}) = 0 \quad (2.40)$$

This is a cubic equation, the solution of which gives the numerical value of the

thermal boundary layer thickness

The expression for Nusselt number is

$$Nu_x = \left(\frac{h_x}{k_f} \right) = \left(\left(\frac{dT}{dy} \right)_{y=0} \right) / \left((T_0 - T_w) / x \right) = \frac{3x}{2\delta_t} \quad (2.41)$$

In numerical form this becomes

$$Nu_{x(i)} = \frac{3x_i}{2\delta_{t(i)}} \quad (2.42)$$

For the plasto-hydrodynamic wire drawing or coating process, the wire is passed through the polymer melt chamber positioned before the plasto-hydrodynamic pressure unit. The polymer melt at δ is almost stagnant. Therefore, V_0 may be considered to be zero. Then the numerical expressions for the velocity boundary layer thickness and temperature boundary layer thickness can be obtained from the following equations

$$\delta_{i-1}^{n+1} - \delta_i^n \delta_{i-1} - \frac{\left(\frac{3}{2} \right)^n (x_i - x_{i-1})}{\left(\frac{\rho V^{2-n}}{k} \right) \left(\frac{33}{140} \right)} = 0 \quad (2.43)$$

$$2\delta_{t(i)}^3 - (4\delta_{t(i-1)} + 5(\delta_i - \delta_{i-1}))\delta_{t(i)}^2 + (2\delta_{t(i-1)}^2 + 5\delta_{t(i-1)}(\delta_i - \delta_{i-1}))\delta_{t(i)} + \frac{20\alpha}{V}(x_i - x_{i-1})(\delta_i - \delta_{i-1}) = 0 \quad (2.44)$$

The expressions for coefficient of friction factor and Nusselt number are same as equations (2.39) and (2.42)

To calculate the theoretical results, the polymer melt was taken as Nylon 6 or PA6 (property from Table 2 1)

Increment in length = $x_1 - x_{1,1} = 1\text{mm}$

Figure 2 15 displays the velocity boundary layer thickness at different location of the polymer melt chamber for Nylon 6 at different wire velocities. It can be seen that the thickness grows exponentially along the length of the melt chamber. The growth rate is different for different velocity. Also the thickness decreases with increasing velocity. With the increase in the wire velocity, the surface friction factor decreases as shown in Figure 2 16. This friction factor decreases exponentially along the length. As the temperature gradient boundary layer thickness depends on the velocity gradient boundary layer thickness, the former behaves in a similar manner as in Figure 2 16. This is evident in Figure 2 17. With the increase in the wire velocity the thermal boundary layer thickness becomes thinner and it promotes sharper surface gradients for the temperature and thus enhances the Nusselt number. Figure 2 18 shows the variation of Nusselt number along the length for different wire velocities.

2.6.3 Comparison between analytical and numerical boundary value solution results

Results have been calculated based on the analysis of section 2 6 1 and 2 6 2. The polymer melt was PA6 and the wire velocity 2 m/s.

Figure 2 19 displays comparisons of the velocity boundary layer thickness for both the analytical and the numerical solutions. The velocity gradient boundary layer thickness obtained from the analytical solution is slightly higher than that of the numerical solution. The coefficient of friction factor obtained by both the analytical and the numerical solutions are almost the same (Figure 2 20). The temperature gradient boundary layer thickness by the analytical method is slightly higher than that of the numerical method (Figure 2 21). The Nusselt number (Figure 2 22) is same at initial lengths for both the analytical and the numerical solutions but as the length increases the numerical values tend to be slightly diverging from the analytical values. However the difference is not very significant.

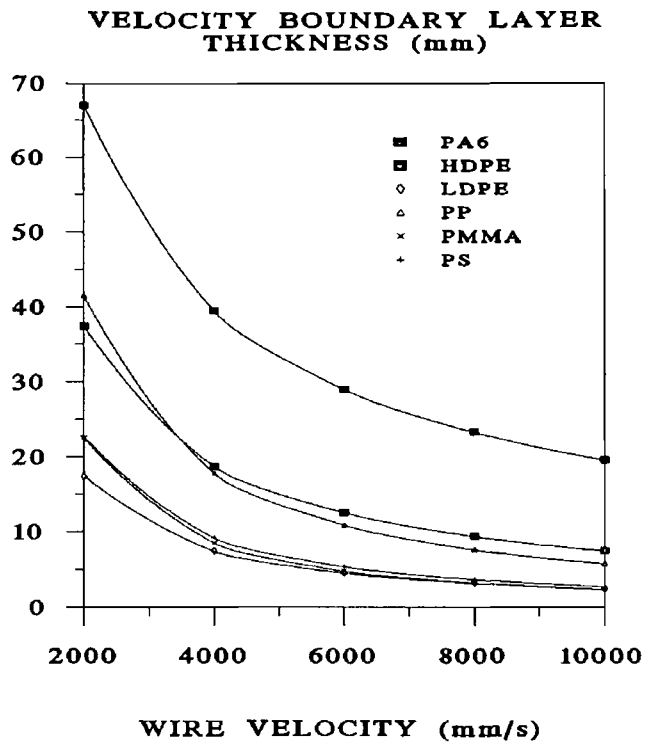


Figure 2.9 Velocity gradient boundary layer thickness by analytical method

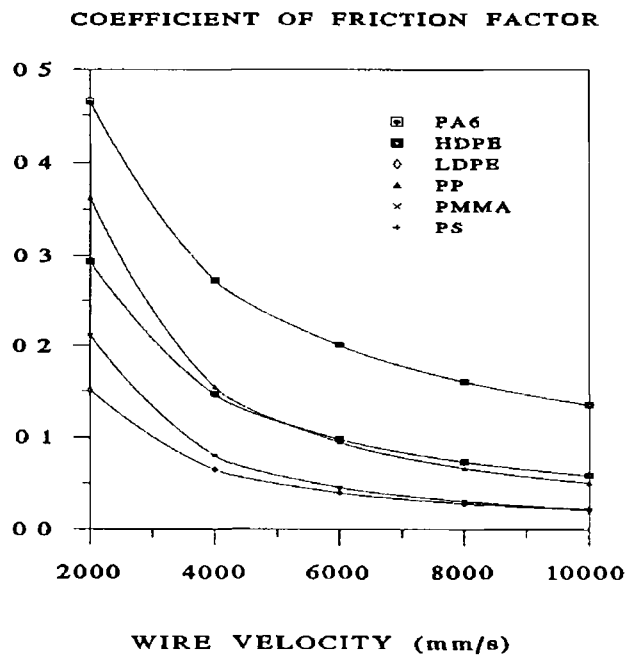


Figure 2.10 Analytical coefficient of friction

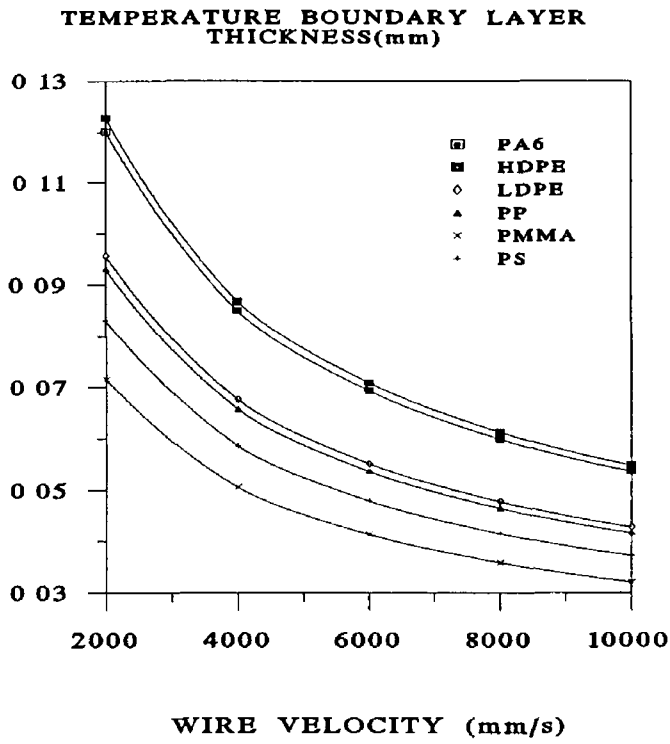


Figure 2 11 Analytical temperature gradient boundary layer thickness

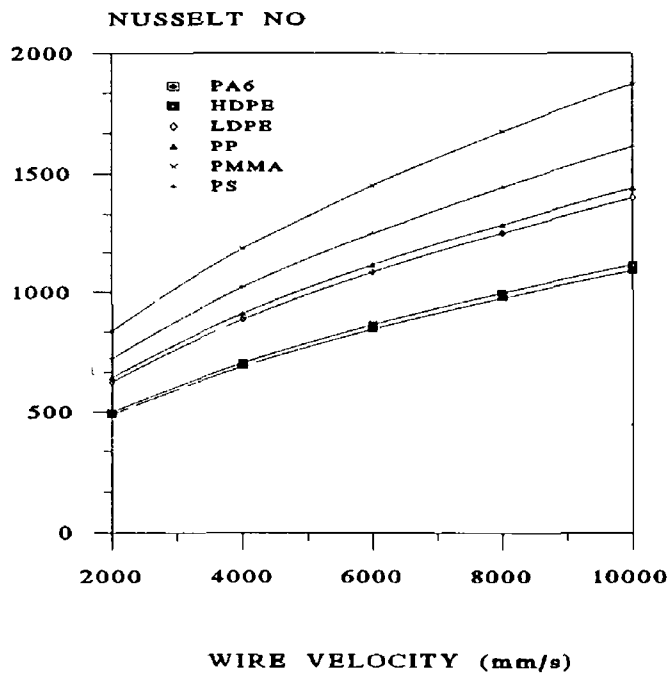


Figure 2 12 Nusselt number by analytical method

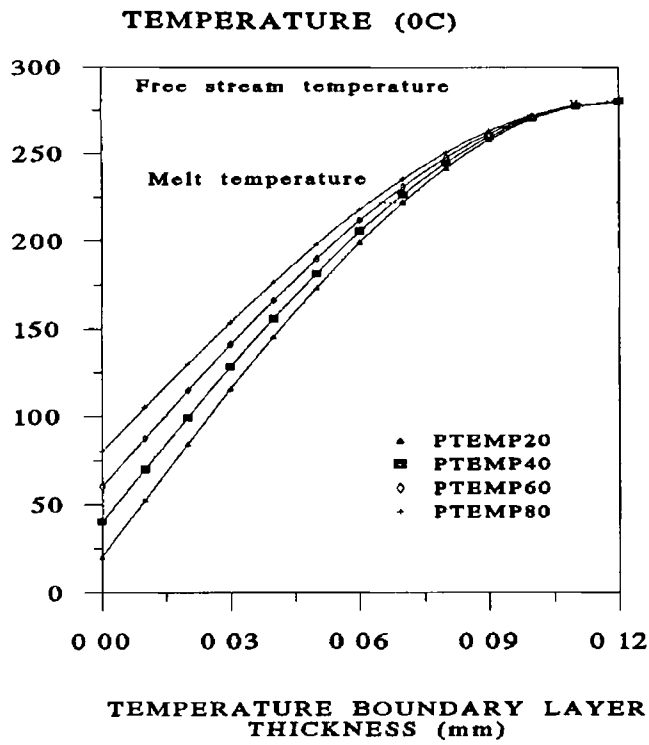


Figure 2 13 Distribution of temperature within temperature gradient boundary layer thickness for different wire preheating temperature

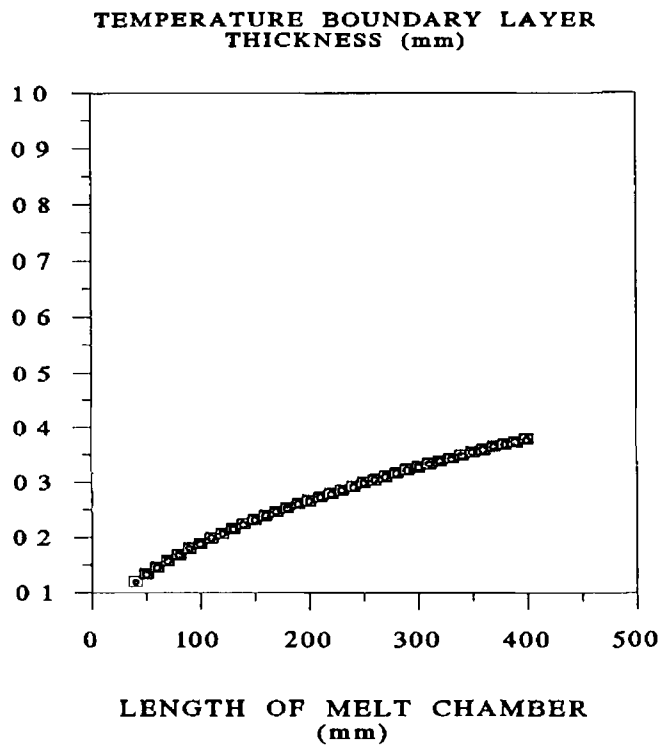


Figure 2 14 Temperature gradient layer thickness for different length of melt chamber

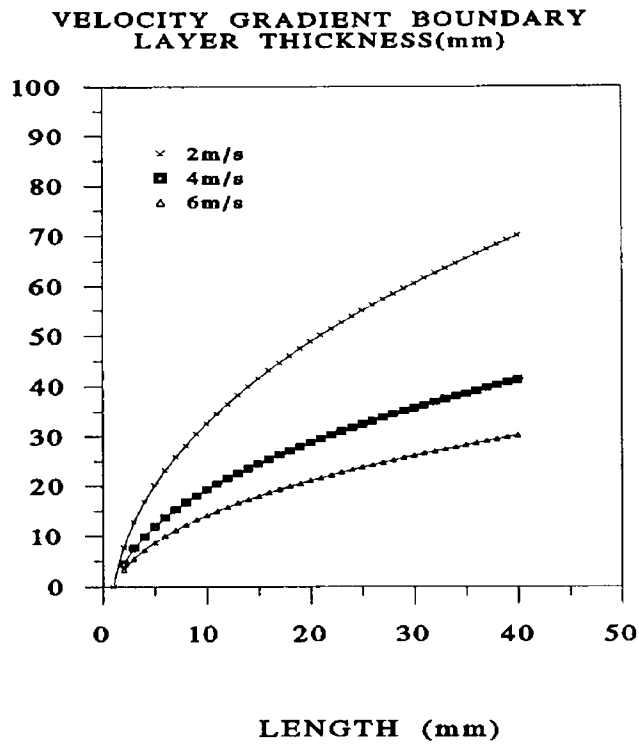


Figure 2 15 Velocity boundary gradient layer thickness by numerical method (polymer- PA6)

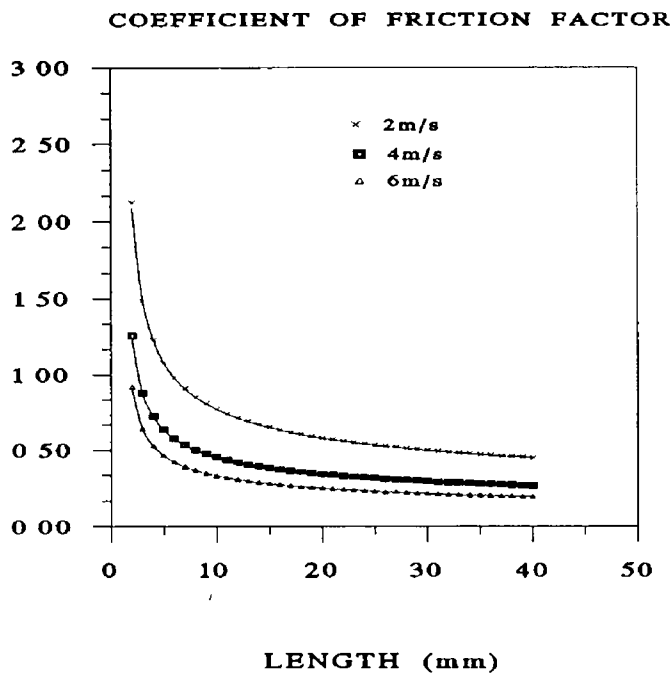


Figure 2 16 Coefficient of friction factor by numerical method (polymer- PA6)

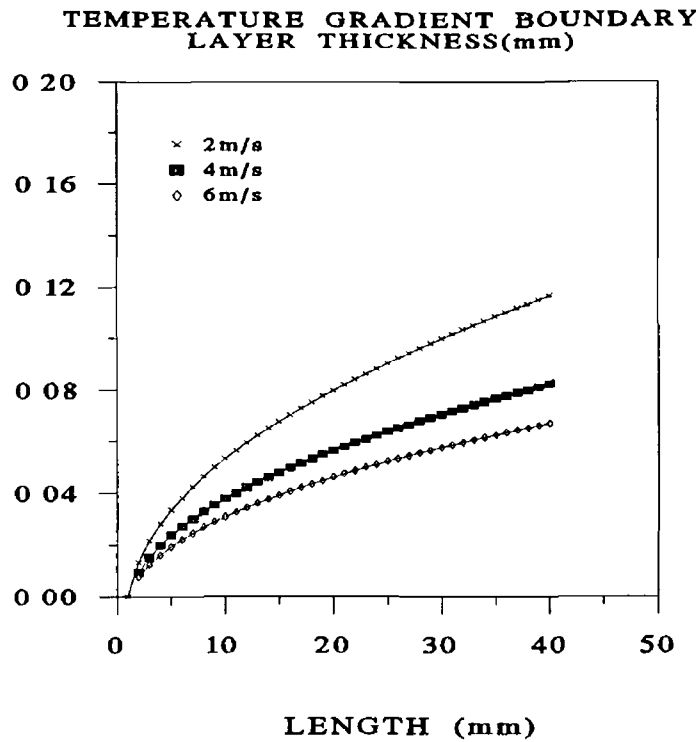


Figure 2 17 Temperature gradient boundary layer thickness by numerical method (polymer- PA6)

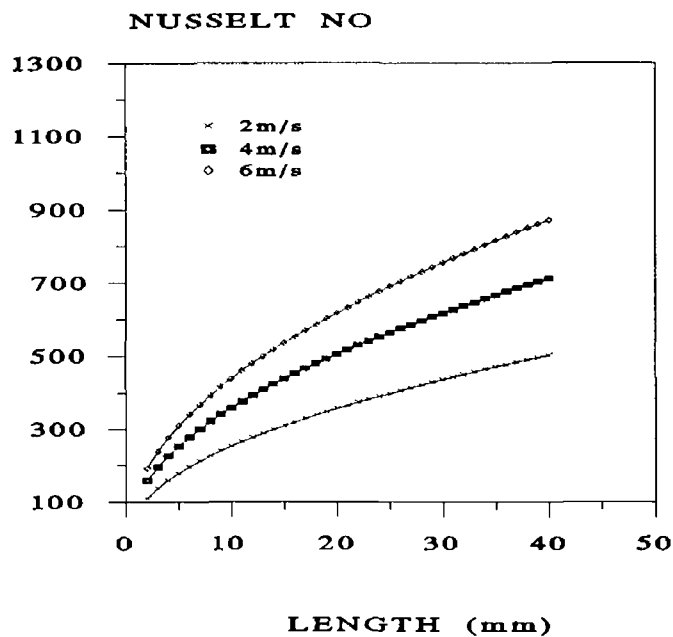


Figure 2 18 Nusselt number by numerical method (polymer-PA6)

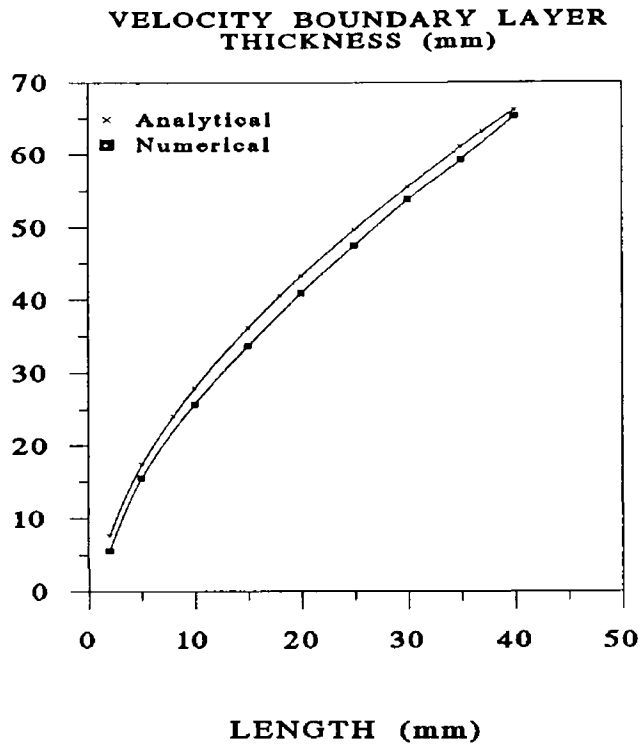


Figure 2 19 Comparison of velocity gradient boundary layer thickness for analytical and numerical method (polymer-PA6)

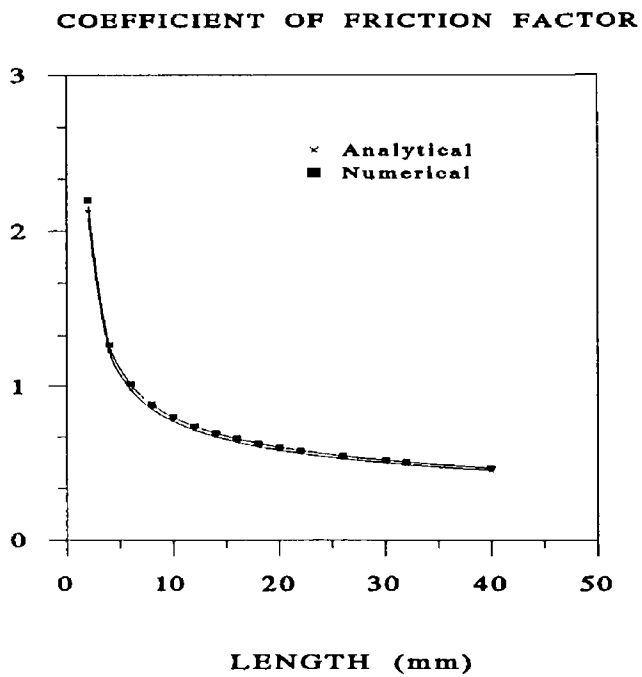


Figure 2 20 Comparison of coefficient of friction factor for analytical and numerical method (polymer-PA6)

TEMPERATURE GRADIENT BOUNDARY
LAYER THICKNESS (mm)

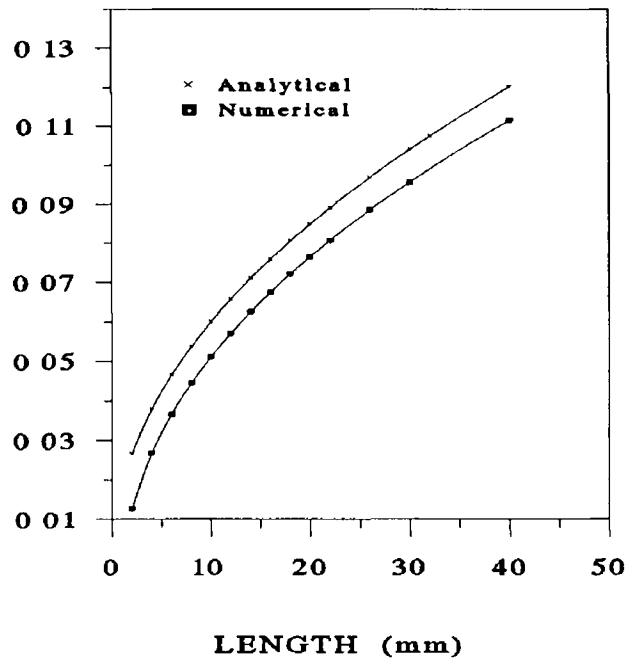


Figure 2 21 Comparison of temperature gradient boundary layer thickness for analytical and numerical method (polymer-PA6)

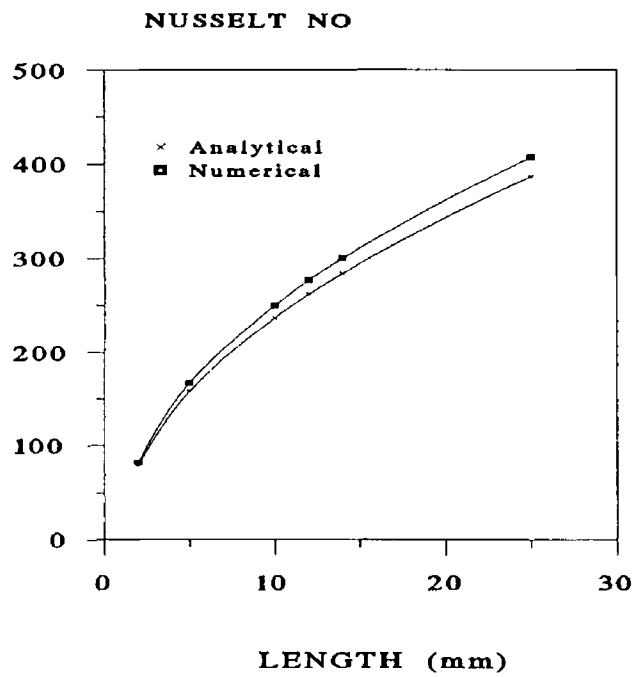


Figure 2 22 Comparison of Nusselt number for analytical and numerical method (polymer-PA6)

2.6.3 Formation and remelting of solid polymer layer

In plasto-hydrodynamic drawing or coating when the wire is drawn through the melt chamber a temperature gradient boundary layer thickness forms due to the difference in temperature in the wire and the polymer melt. As a result a solid layer of the polymer forms at the adjacent layer of the continuous surface. For a thin temperature gradient boundary layer, the thickness of the solid layer is very small and dissolves very quickly before the surface reaches the plasto-hydrodynamic unit. But for a thick boundary layer it takes time to dissolve the solid layer. Here, the expression is given to explain how the solid layer becomes molten as well as the distribution of temperature at different time instants. Also the effect of preheating the wire is given on the rate at which the solid layer melts [56]

Mathematical formulation

As the wire passes along the x coordinate the temperature gradient boundary layer thickness and the temperature distribution can be expressed by equation (2.34) and (2.20) respectively. Different phases are formed within this temperature gradient boundary layer thickness (Figure 2.23). At the cold wire surface, there is a solid layer which is followed by a mushy or semi-solid layer. After the semi-solid layer the melt layer starts which extends from melt temperature T_m to T_0 .

The energy balance equation for this case becomes [57]

$$\rho C \frac{dT}{dt} + \rho C (U \frac{dT}{dx}) = k_x \frac{d^2T}{dx^2} + k_y \frac{d^2T}{dy^2} + \tau_{xy} \left(\frac{dU}{dy} \right) \quad (2.45)$$

The temperature profile in the melt film can be determined from the velocity profile in the melt film. To derive the temperature profile in the melt film, it is assumed [54] that

- a) the convective heat transfer term is negligible
- b) the conductive heat transfer happens only in the direction normal to the interface
- c) the process is steady state

With these assumptions equation (2 45) becomes

$$k_m \frac{d^2 T}{dy^2} + \tau_{xy} \left(\frac{dU}{dy} \right) = 0 \quad (2 46)$$

where k_y is replaced by k_m

If the melt flow is considered to be laminar, there is no slip at the wire and the polymer interface and no pressure gradient towards y axis in the wire surface then

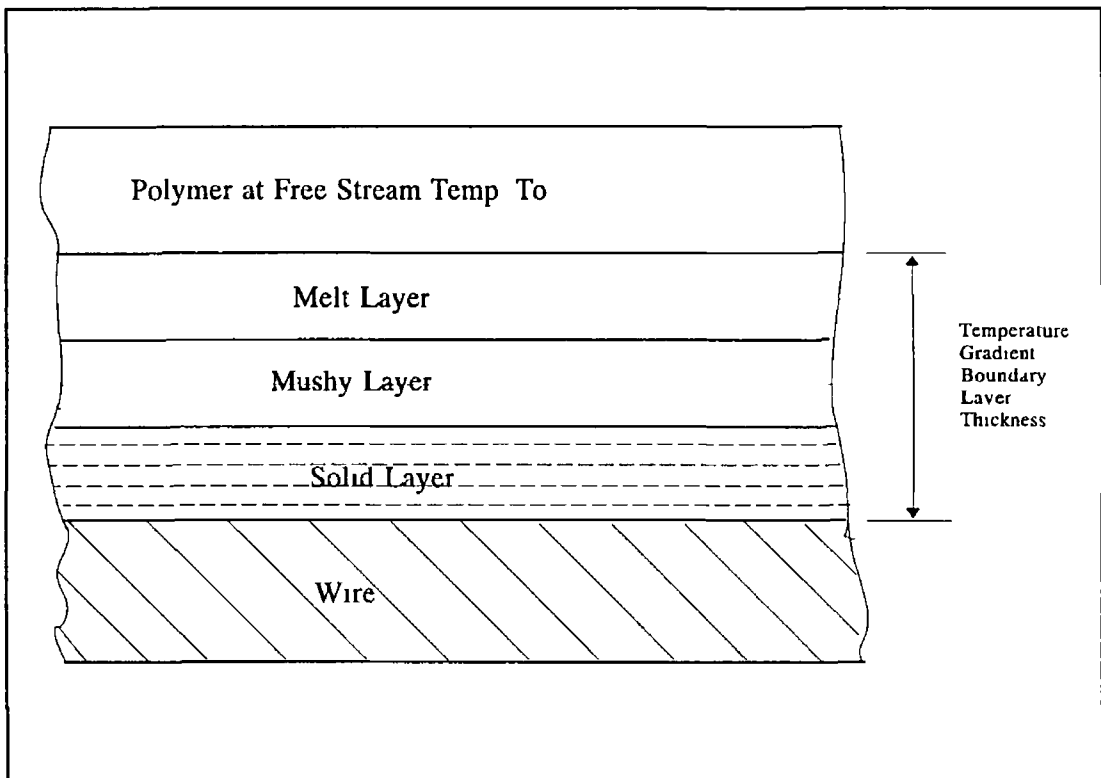


Figure 2 23 Different phases formed within the temperature gradient boundary layer thickness

$$\frac{d\tau_{xy}}{dy} = 0 \quad (2 47)$$

Let the polymer melt behave as a Newtonian fluid, then

$$\frac{d^2U}{dy^2}=0 \quad (2.48)$$

The boundary condition that at the melt solid interface $U(0)=0$ and at the end of the temperature gradient layer $U(Y_m)=V_r$, where V_r is the relative velocity between this two points

Applying the boundary conditions equation (2.48) gives the velocity profile

$$U = \frac{y}{Y_m} V_r \quad (2.49)$$

Also for Newtonian fluid,

$$\tau_{xy} = \mu \left(\frac{dU}{dy} \right) \quad (2.50)$$

Combining equations (2.49) and (2.50), equation (2.46) becomes

$$k_m \frac{d^2T}{dy^2} + \mu \left(\frac{V_r}{Y_m} \right)^2 = 0 \quad (2.51)$$

The boundary conditions are $T(0)=T_m$ and $T(Y_m)=T_o$

Integrating equation (2.51) twice the above two boundary condition the temperature profile becomes

$$T(y) = \left(\frac{-\mu V_r^2}{2k_m Y_m^2} \right) y^2 + \left(\frac{2k_m \Delta T_o + \mu V_r^2}{2k_m Y_m^2} \right) y + T_m \quad (2.52)$$

where $\Delta T_o = T_o - T_m$

The heat flow into the interface Q_i per unit area can now be determined from the

Fourier law

$$-q_m = -\frac{Q_1}{A} = K_m \frac{dT(0)}{dy} = \left(\frac{2k_m \Delta T_o + \mu V_f^2}{2k_m Y_m^2} \right) \quad (2.53)$$

Also considering steady state condition the temperature profile in the solid layer can be termed as

$$\rho_s C_s V_{sm} \left(\frac{dT}{dy} \right) = k_s \frac{d^2 T}{dy^2} \quad (2.54)$$

Here, V_{sm} is termed as the velocity at which the solid layer melts

For simplicity the pure solid layer and the semi-solid layer are considered as solid layer. Taking the temperature at the melt layer as $T(0) = T_m$ and at the average solid layer which can be considered far from the interface $T(-\infty) = T_{sav}$, the temperature profile in the solid layer becomes

$$T(y) = \Delta T_s \exp\left(\frac{y V_{sm}}{\alpha_s}\right) + T_{sav} \quad (2.55)$$

where, $\Delta T_s = T_m - T_{sav}$

The heat flux from the interface into the solid layer may be expressed as

$$-q_{out} = -\frac{Q_{out}}{A} = K_s \frac{dT(0)}{dy} = \rho_s C_s V_{sm} \Delta T_s \quad (2.56)$$

The solid layer melt velocity can be determined taking the heat balance in the interface. The heat flux into the interface minus the heat flux out of the interface is used to melt the polymer at the interface. Therefore,

$$V_{sm}\rho_s\Delta H_f = \left(\frac{2k_m\Delta T_o + \mu V_r^2}{2Y_m} \right) - V_{sm}\rho_s C_s \Delta T_s \quad (2 57)$$

Now the solid layer melt rate is

$$V_{sm} = \left(\frac{2k_m\Delta T_o + \mu V_r^2}{2\rho_s Y_m \Delta H} \right) \quad (2 58)$$

where $\Delta H = \Delta H_f + C_s \Delta T_s$

From the melt velocity and the total solid thickness, the time of melting of the solid can be determined Therefore for each time step there is an increase in temperature in each layer including the wire

For the wire

$$\rho_w C_w \frac{dT_w}{dt} = k_w \frac{d^2 T_w}{dy_w^2} \quad (2 59)$$

For the solid layer

$$\rho_s C_s \frac{dT_s}{dt} = k_s \frac{d^2 T_s}{dy_s^2} \quad (2 60)$$

For the semy-solid or mushy layer

$$\rho_T C_T \frac{dT_T}{dt} = k_T \frac{d^2 T_T}{dy_T^2} \quad (2 61)$$

Each property in the semy-solid layer is considered to be the average of the solid and the molten polymer

For the molten layer

$$\rho_m C_m \frac{dT_m}{dt} = k_m \frac{d^2 T_m}{dy_m^2} \quad (2.62)$$

For each unit time step the temperature added to the solid layer is- $(T_m - T_{s1})/(t_m)$ where, t_m is the total time needed to melt the solid layer

The boundary conditions are

at the interface of the wire and the solid polymer

$$T_w(\text{final}) = T_s(\text{initial})$$

at the interface of the solid polymer and the semy-solid layer

$$T_s(\text{final}) = T_T(\text{initial})$$

at the interface of the semy-solid layer and the melt polymer

$$T_T(\text{final}) = T_m(\text{initial})$$

With the increase in time the semy-solid layer becomes molten and the solid layer becomes at first semy-solid and then molten. The properties of the polymer also change with this change of phases.

Theoretical results were calculated on the basis of equations derived in the analysis. In order to calculate the theoretical results, the following values of the parameters were used [54,58] which can produce a thick temperature gradient boundary layer thickness so that the melt front of the solid layer can be explained clearly.

Polymer = stiff grade Nylon 6 (n=0.7) with viscosity 260 N s/m² at 280°C

Heat of fusion of solid stiff grade Nylon 6 = 650 kJ/kg

Specific heat of this solid polymer = 14.84 kJ/kg°C

Density of this solid polymer = 1100 kg/m³

Polymer melt temperature = 220°C

Semy-solid temperature = 175°C

Initial wire temperature = 20°C

Diameter of wire = 2 mm

Wire velocity = 0.5 m/s

Length of melt bath = 40 mm

With these conditions the velocity gradient boundary layer thickness becomes 100 mm and the corresponding temperature gradient boundary layer thickness 1.52 mm. Within this thickness, the thickness of the solid, mushy and liquid layer is 0.65 mm, 0.24 mm and 0.63 mm respectively. The relative velocity between the layer is 0.06 mm/s. It takes 3 seconds to melt this solid layer.

The heat is transferred from the polymer melt to the temperature gradient boundary layer thickness and then to the wire. With the increase in time, the temperature of the temperature gradient layer thickness as well as of the wire increase. Then a time arises when the solid layer becomes molten.

This phenomena is illustrated in Figures 2.24 to 2.26. The first 1mm thickness presents the wire thickness from its centre and the remaining 1.52mm is for the temperature gradient boundary layer thickness. In Fig 2.24, after 1 second the wire surface temperature increases but the core temperature remains the same. Also there is a rise in temperature in the solid, semi-solid and liquid layers.

After 2 seconds, in Figure 2.25, the wire core temperature is about 85°C and a fraction of the solid has been transformed to semi-solid state. Also some fraction of the semi-solid layer is now in liquid state. Most of the liquid part has achieved the free stream temperature of the melt chamber.

In Figure 2.26, after 3 seconds the wire core temperature is now 152°C and the surface temperature is about 220°C which is the melt temperature of the polymer. The whole temperature gradient boundary layer thickness is now in the melt state.

Figure 2.27 shows the contribution of preheating the wire in the solid melt velocity. With the increase in wire temperature the solid melt velocity increases and then the total time needed to melt the solid layer is less than that of without preheating of the wire. This solid polymer on wire may lead to sharkskin in the polymer coating produced by hydrodynamic pressure in the plasto-hydrodynamic pressure unit. As sharkskin is dependent on the temperature, being considerably delayed by increase in surface temperature [48], preheating the wire is a way to avoid formation of sharkskin which makes the solid melt velocity faster and the temperature distribution in the temperature gradient boundary layer thickness less sharp.

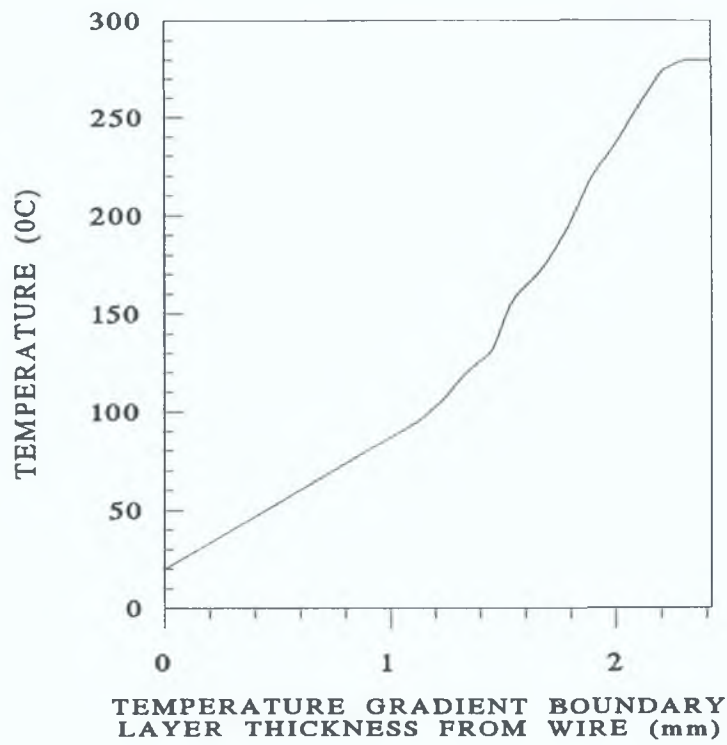


Figure 2.24. Temperature distribution in temperature gradient boundary layer thickness after 1 second

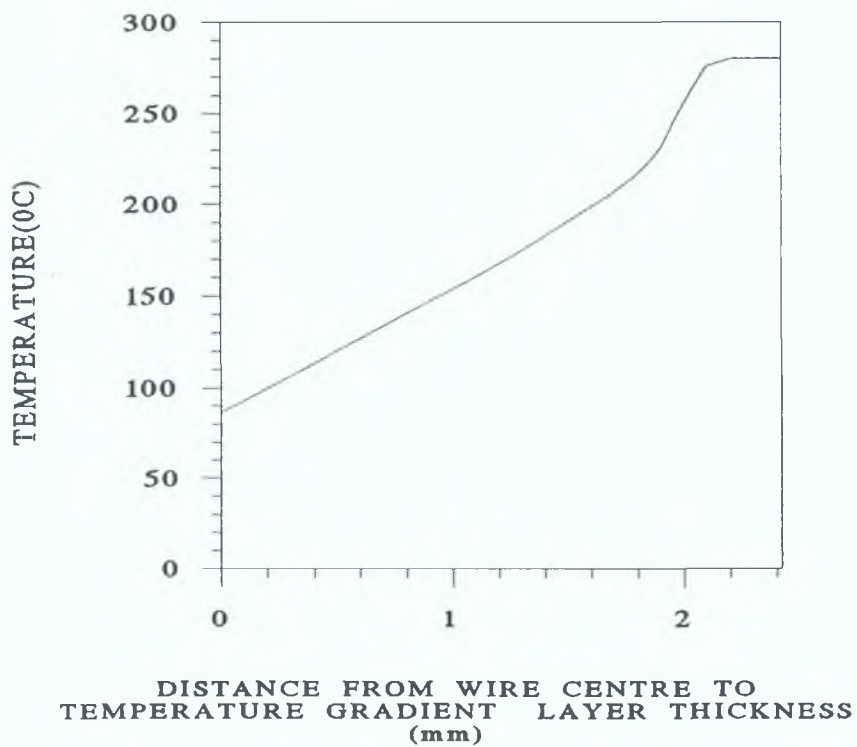


Figure 2.25. Temperature distribution in wire and temperature gradient boundary layer thickness after 2 second

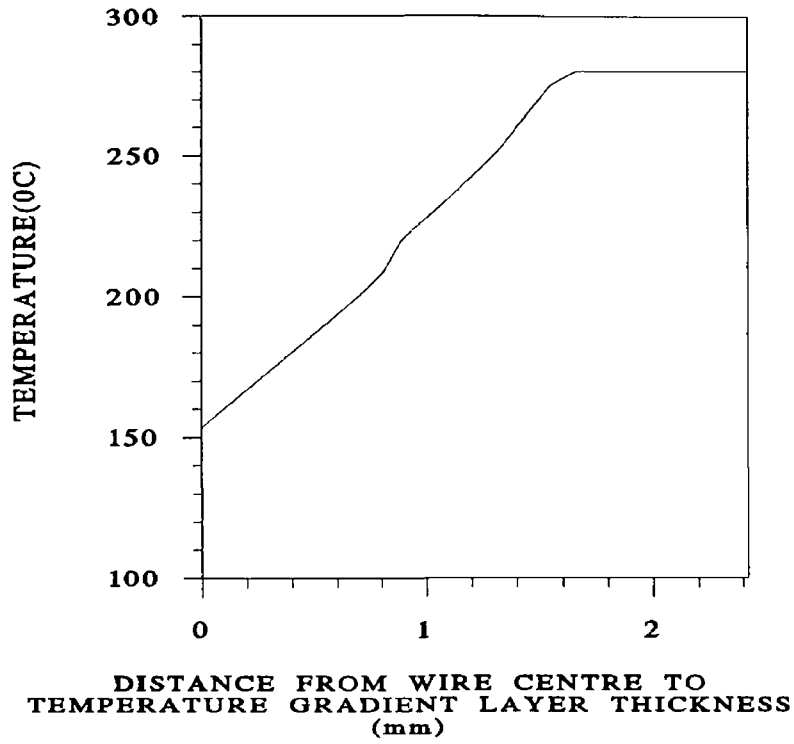


Figure 2 26 Temperature distribution in wire and temperature gradient boundary layer thickness after 3 second

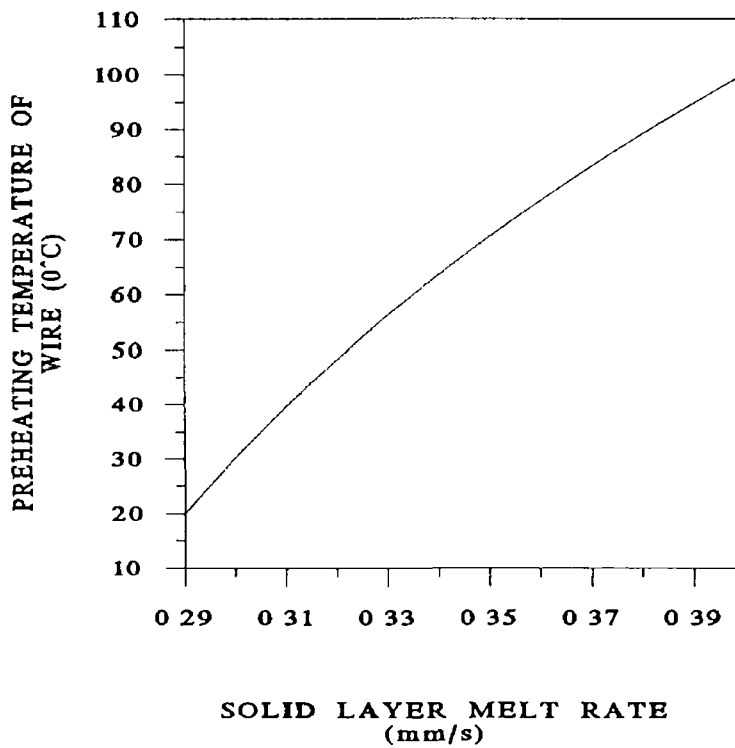


Figure 2 27 Solid layer melt rate for different preheating temperature of wire

CHAPTER- THREE

EXPERIMENTAL EQUIPMENTS, MATERIALS AND TEST PROCEDURES

3.1 Design of the drawing bench:

The drawing bench was designed to be a multi-purpose, multi-user facility. The general view of the drawing bench is shown in plate (3 1) and in Figure 2 7

The electrics for the bench were designed to allow multi-user facilities with associated interlocks so that equipment cannot be turned on without its control sensor to monitor the process(plate 3 2). The polymer was heated by means of an electric heater band and the temperature was controlled thermostatically to within $\pm 5^{\circ}\text{C}$ of the pre-set temperature using a temperature regulator. The temperature was monitored continuously by means of thermo-couples. The drawing force was measured by using a piezo-electric load cell located at the exit end of the pressure unit.

The motor for the drawing bench enables the wire to be drawn at any speed between 0.05 to 20 m/s. The drive system is made up with an electric motor (squirrel cage 3 kw, 380 volt, 3 phase power supply) and a small bull block (shown in plate 3 3). The motor speed was governed by a frequency controller which was preset on a hand held operator. The motor in turn drives the bull block. The motor speed in RPM was obtained using a remote hand held digital tachometer- SHIMPO type DT-205 which measures the speed of a rotating mark on the motor output shaft. The drawing bench supported all electrical and mechanical equipment and ensured that the drive system was rigid. It contains a flat surface area on which experiments can be mounted.

3.2 Modification of the rig

Most of the parts of the rig were designed and fabricated a new. Only the temperature control unit and the variable speed motor were used from the existing rig. Here the description is given for the newly designed units.

Design of the wire feed mechanism

The wire feed mechanism involved pulling the wire off the spool along its

longitudinal axis. The path of the wire through the pressure assembly was as follows. It entered the melt chamber from the reel through a centralising unit. From the melt chamber the wire is passed through the plasto-hydrodynamic pressure unit where it was coated by polymer melt through plasto hydrodynamic pressure action. The coated wire is then passed over a pulley and wound onto the bull block. The first attempt was to produce a unit which was able to coat four wires at a time. For this purpose a polymer melt bath was fabricated which stored the polymer melt provided by an injection moulding machine at high back pressure. The problem was that the heat generation in that bath was not controllable and hence was not suitable for the purpose.

The second attempt was to produce another unit for single wire coating. An injection moulding machine was used to supply the polymer melt. Some test runs were made and it was found that the coating on the wire was not continuous.

The injection moulding machine was very old and by this time it was not able to produce sufficient back pressure. The working polymer, Nylon 6, absorbs moisture quickly. Hence day by day it absorbs an increasing amount of moisture. So when the polymer melts, a prominent amount of steam is produced. The back pressure problem in the injection moulding machine and the presence of the moisture in polymer seems to be responsible for the discontinuous coating.

There was a leakage of polymer melt from the melt chamber from the side where the wire entered the unit. This leakage of polymer melt and the high pressure steam evaporating from the polymer combined to make a hazardous atmosphere in the laboratory.

To eliminate the moisture problem a drying oven was purchased. Before the experiment the polymer was dried in the oven to eliminate the moisture. Another unit was then manufactured with a melt chamber connected with a hopper, not with the injection moulding machine. This melt chamber was designed in such way that the temperature gradient boundary layer thickness is very thin with high speed wire and the solid layer on the wire melts down before it reaches the hydrodynamic unit. The hopper supplied polymer for multiple tests. First the hopper was not large enough to store a sufficient amount of polymer to complete a series of tests. Then it was modified to carry out enough tests with the stored polymer in it. The hopper

was heated by an electric heater band and the temperature of the polymer was controlled thermostatically at the set temperature equal to that of the melt chamber. For the back pressure in the polymer, the hopper was connected to a pressurized bottle argon gas supply of 3000 psi (20.4 MPa) via a 2-way servo valve. To avoid the polymer leakage problem a narrow unit was then added before the melt chamber. This unit also acted as a preheating unit for the wire. A bull block and a wire spool holder were designed and fabricated so that they prevent the wire from unwinding at the time of experiments at high speed. For this purpose also a tensioner was attached with the wire spool. A "cropping" device was incorporated before the pulley so that it was possible to cut the coated wire instantaneously while being drawn to obtain samples at any drawing speed.

3.3 Brief description of some instruments

3.3.1 Load cell

The load cell was a RDP type. This transducer was a strain gauged compression load cell. It gives a proportional electrical output corresponding to the force which is generated during the pulling action. Maximum capacity of the load cell was 440N.

3.3.2 Amplifier

This is a mains-operated transducer indicator, (type RDP E308). It amplifies the millivolt signal output from the load cell. This output is proportional to the applied load.

3.3.3 A/D convertor

The analog to digital converter received a signal from the transducer via the amplifier. A computer digitized the signal through a programme written in basic language and displayed the magnitude of the force through a printer output.

3.3.4 Heater bands

Hollow cartridge heater bands were used to heat the hopper, pressure unit, and the melt chamber. The dimensions and specifications are given below.

The Hopper Heater band

Type	I D (mm)	Length (mm)	Volts(V)	Watts(W)
41536/1	66	190	240	1000

The Melt chamber and Pressure unit Heater band

Type	I D (mm)	Length (mm)	Volts(V)	Watts(W)
Fast heat BM0 20890	32	77	240	300

3.3.5 Temperature Controller

An electronic ON-OFF temperature relay "Type West 3300" was used to control the pre-set temperature. The controller was designed to be used with thermo-couples type (J, K, and T) to monitor the temperature. A relay change over contact within the controller operates at a pre-determined temperature previously set by a panel mounted digital temperature indicator model "RS 258-186". The operating temperature range for type J thermo-couple is -25°C to $+625^{\circ}\text{C}$.

3.3.6 Thermo-couples

To monitor the temperature continuously, J type thermo-couples "fibre glass insulated with 2 mm insulation diameter" were used to carry out the experiments. The working temperature range was 0 to $+450^{\circ}\text{C}$.

3.4 Melt chamber, hopper and the pressure unit

The hopper was made to store sufficient quantity of polymer melt for a full set of tests. The hopper was attached to the melt chamber (Plate 3 4). The pressure unit (plate 3 5) was attached with the end of the melt chamber. The hopper and the melt chamber were fabricated using the school workshop facilities. The pressure units were small in length (22 mm) and the other geometries were complex shaped and of smaller dimensions. Therefore, the different pressure units (stepped parallel bore, tapered bore and combined bore) were fabricated by computer aided manufacturing process. Heater bands were used for heating the melt chamber, hopper and pressure units. The temperature of polymer melt in these units was controlled by a thermostat sensed controller.

3.5 Test preparation

In order to conduct testing the following procedure was maintained

- (1) First the polymer granules were dried up in an oven for three hours at 85°C, so that they were free from moisture
- (2) The granules were poured into the hopper and the argon line was connected to provide back pressure (the argon line was connected only when the experiment was carried out with back pressure in the polymer melt)
- (3) The heater bands on the hopper, the melt chamber and the plasto-hydrodynamic pressure unit were switched on and controlled thermostatically to maintain the temperature at a preset level
- (4) When the polymer was in melt state the wire from the infeed spool was threaded through the centraliser, the leakage control unit, the melt chamber and the plasto-hydrodynamic pressure unit. After exiting the plasto-hydrodynamic unit, the wire was passed through a cropping tool (Plate 3.6) and then attached to the bull block. A load cell was used to obtain the drawing load due to the pulling action of the wire in the plasto-hydrodynamic wire coating system.

3.6 Test procedure

- (1) The diameter of the bull block was measured and the motor was set at a certain speed by the accelerator set on the frequency inverter to obtain the wire coating at the desired speed.
- (2) The wire was attached to the bull block and when a reasonable length of the wire was drawn the computer was operated to obtain the drawing load and then the coated wire was "chopped off" before the pulley to get a proper coated wire sample at that velocity.
- (3) The sample length between the pressure unit and the cropping device, was collected and put into marked envelopes. Each sample was later measured by a micrometer at five different places to obtain initial measurement of the wire coating thickness. A small portion of the wire was cold mounted and polished. An optical microscope was then used to assess more accurate coating thickness and the concentricity of the coating on the wire.



Plate 3.1. General view of the drawing bench

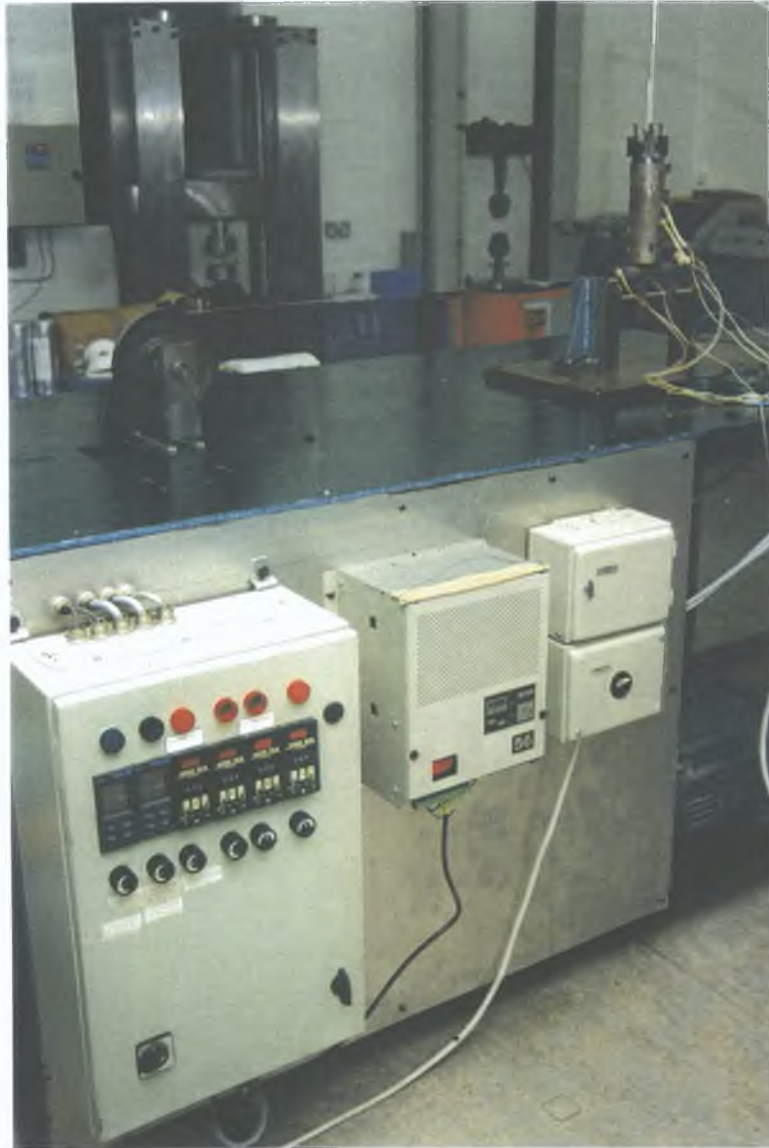


Plate 3.2. View of the control instruments

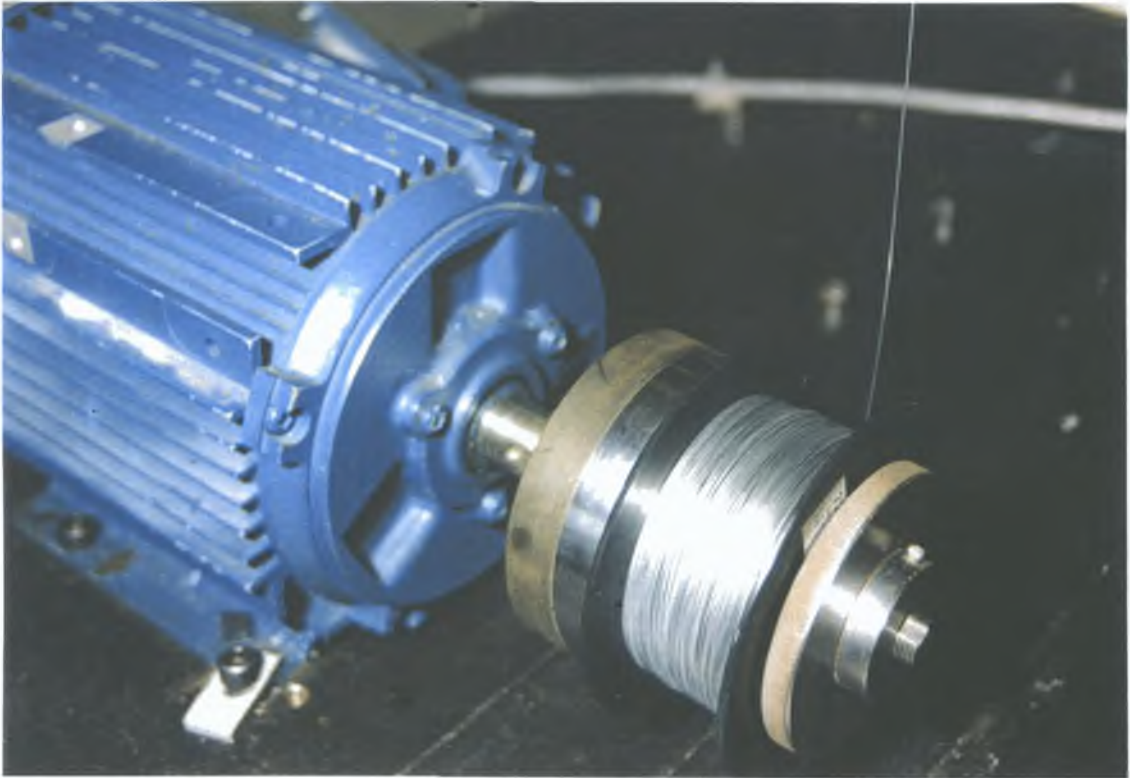


Plate 3.3. Bull block and the motor



Plate 3.4. Melt chamber with leakage control and pressure unit (inside the heater band) and load cell



Plate 3.5. A plasto-hydrodynamic pressure unit



Plate 3.6. The cropping unit

CHAPTER FOUR

PLASTO-HYDRODYNAMIC ANALYSIS USING THE STEPPED PARALLEL BORE UNIT

4.1 Introduction

A stepped parallel bore pressure unit consists of two parallel bore sections. The clearance between the moving continuum and the first section or part of the unit is greater than that in the second section. The bore size in the second section is just slightly greater than the cross section of the incoming continuum so that metal to metal contact can be totally avoided.

The initial tests with the stepped parallel bore pressure unit showed [7-11] higher deformations during the drawing process and also proved to be analytically simpler than the tapered bore reduction unit. Extensive experimental tests were conducted using this unit as- wire drawing, tube sinking, strip drawing, wire coating [7-25, 58] etc.

In relation to plasto-hydrodynamic die-less wire drawing and coating, theoretical model for pressure distribution has been presented in the previous publications [7] and [9]. The pressure media was non-Newtonian fluid (polymer melt). However, in this model the viscosity of the polymer melt was considered to remain unchanged during the drawing and coating process. But in reality the viscosity changes due to the variations in temperature and pressure within the unit.

In this chapter first a mathematical model has been developed for the pressure distribution within a stepped parallel bore unit taking account of the changes in the viscosity of the polymer melt during the coating process. The model is the same for any kind of continuum of uniform cross section, whether it is wire, tube or strip. The analysis predicts the pressure distribution in the unit, drawing load and stress in the continuum for coating or drawing process. The model is extended to predict plastic yielding and reduction in the cross-section and has been presented for wire, tube and strip drawing.

4.2 Pressure analysis for plasto-hydrodynamic coating in a stepped parallel bore unit

This is a non-Newtonian analysis of the coating process which has been reported in [59]. Figure 4.1 shows a schematic diagram of a stepped parallel bore hydrodynamic pressure unit. The analysis was done on the basis of the following assumptions:

- i) flow of polymer melt is laminar
- ii) flow of polymer melt is axial
- iii) thickness of the polymer layer is small compared to the dimensions of the pressure unit

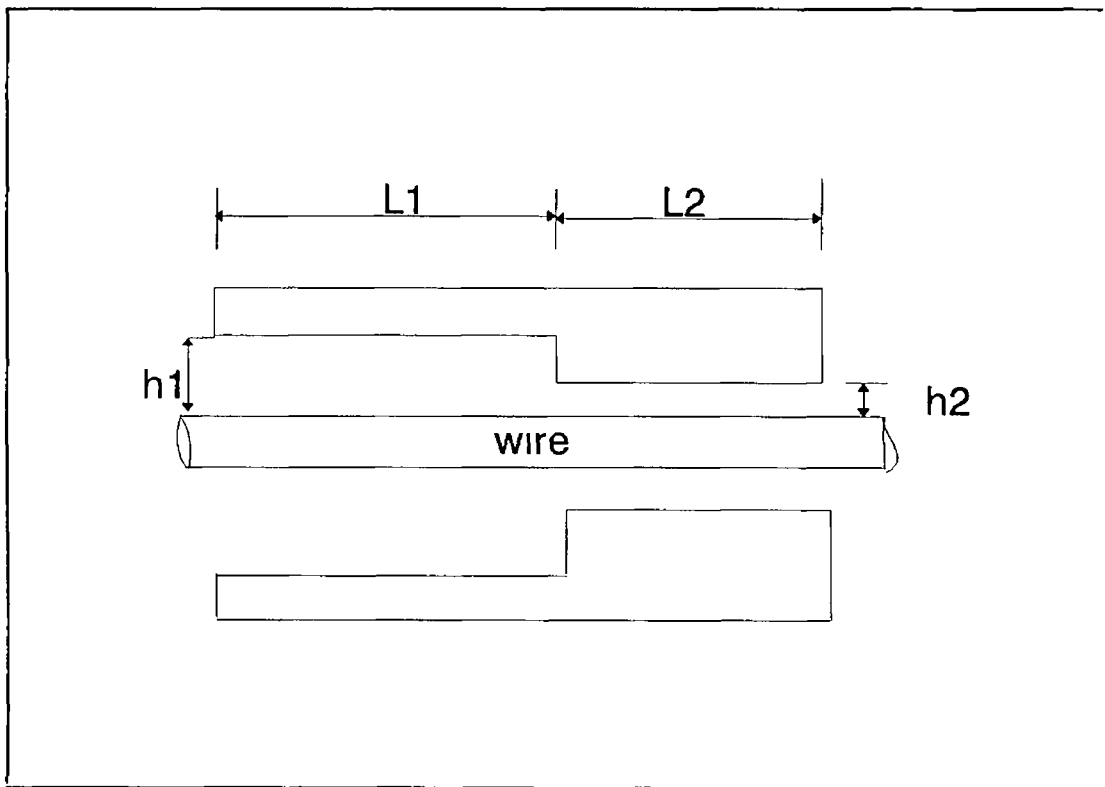


Figure 4.1 Schematic diagram of a stepped parallel bore pressure unit

The relationship between the pressure and shear stress gradient in the first part of

the unit is given by

$$\left(\frac{dp}{dx}\right)_1 = \left(\frac{d\tau}{dy}\right)_1 \quad (4.1)$$

According to Rabinowitsch [41] the equation for the polymer melt relating shear stress and shear rate is

$$\tau + K\tau^3 = \mu \left(\frac{dU}{dy}\right) = \mu \dot{\gamma} \quad (4.2)$$

Integration of equation (4.1) gives

$$\tau_1 = P'_1 y + \tau_{c1} \quad (4.3)$$

where τ_{c1} is the shear stress at $y=0$ and $P'_1 = (dP/dx)_1$ is assumed to be independent of y

Substituting for τ_1 into equation (4.2) gives

$$\mu \left(\frac{dU}{dy}\right)_1 = P'_1 y + \tau_{c1} + K(P_1'^3 y^3 + \tau_{c1}^3 + 3P_1'^2 y^2 \tau_{c1} + 3\tau_{c1}^2 P_1' y) \quad (4.4)$$

which after integration becomes

$$U_1 = \frac{P_1' y^2}{2\mu} + \frac{\tau_{c1} y}{\mu} + \frac{K}{\mu} \left(\frac{P_1'^3 y^4}{4} + \tau_{c1}^3 y + P_1'^2 y^3 \tau_{c1} + \frac{3}{2} \tau_{c1}^2 P_1' y^2 \right) + C \quad (4.5)$$

where C is the constant of integration

The boundary conditions are,

(a) at $y = 0$, $U_1 = V$

(b) at $y = h_1$, $U_1 = 0$

Applying condition (a) in equation (4.5) $C=V$ and hence

$$U_1 = \frac{P_1' y^2}{2\mu} + \frac{\tau_{C_1} y}{\mu} + \frac{K}{\mu} \left(\frac{P_1'^3 y^4}{4} + \tau_{C_1}^3 y + P_1'^2 y^3 \tau_{C_1} + \frac{3}{2} \tau_{C_1}^2 P_1' y^2 \right) + V \quad (4.6)$$

Also substituting condition (b) in equation (4.6) and rearranging gives

$$\tau_{C_1}^3 + \frac{3}{2} (P_1' h_1) \tau_{C_1}^2 + \left(\frac{1}{K} + P_1'^2 h_1^2 \right) \tau_{C_1} + \left(\frac{\mu V}{K h_1} + \frac{P_1' h_1}{2K} + \frac{P_1'^3 h_1^3}{4} \right) = 0$$

The real root of this equation is -

$$\tau_{C_1} = \left(-\frac{\mu V}{2K h_1} + \left(\frac{\mu^2 V^2}{4K^2 h_1^2} + \frac{1}{27} \left(\frac{1}{K} + \frac{1}{4} P_1'^2 h_1^2 \right)^3 \right)^{1/2} \right)^{1/3} + \left(-\frac{\mu V}{2K h_1} - \left(\frac{\mu^2 V^2}{4K^2 h_1^2} + \frac{1}{27} \left(\frac{1}{K} + \frac{1}{4} P_1'^2 h_1^2 \right)^3 \right)^{1/2} \right)^{1/3} - \frac{1}{2} P_1' h_1 \quad (4.7)$$

The flow of the polymer melt in the first part of the unit is given by,

$$Q_1 = \int_0^{h_1} U_1 dy \quad (4.8)$$

Substituting for U_1 from equation (4.6) into the above equation and integrating gives,

$$Q_1 = \frac{P_1' h_1^3}{6\mu} + \frac{\tau_{c_1} h_1^2}{2\mu} + \frac{K}{\mu} \left(\frac{P_1'^3 h_1^5}{20} + \frac{\tau_{c_1}^3 h_1^2}{2} + \frac{P_1'^2 h_1^4 \tau_{c_1}}{4} + \frac{\tau_{c_1}^2 P_1' h_1^3}{2} \right) + v h_1 \quad (4.9)$$

For continuous flow operation,

$$Q_1 = Q_2 \quad (4.10)$$

Hence establishment of the flow equation in the second section is necessary

The pressure gradient in the second section under steady state condition gives,

$$\left(\frac{dp}{dx} \right)_2 = - \left(\frac{d\tau_2}{dy} \right)_2 \quad (4.11)$$

Integration gives

$$\tau_2 = -P_2' y + \tau_{c_2}$$

where τ_{c_2} is the shear stress at $y=0$ and $P_2' = (dP/dx)_2$

Substituting for τ_2 into Rabinowitsch equation gives

$$\mu \left(\frac{dU}{dy} \right)_2 = -P_2' y + \tau_{c_2} + K \left(-P_2'^3 y^3 + \tau_{c_2}^3 + 3P_2'^2 y^2 \tau_{c_2} - 3\tau_{c_2}^2 P_2' y \right) \quad (4.12)$$

which after integration becomes

$$U_2 = -\frac{P_2' y^2}{2\mu} + \frac{\tau C_2 y}{\mu} + \frac{K}{\mu} \left(\frac{-P_2'^3 y^4}{4} + \tau C_2^3 y + P_2'^2 y^3 \tau C_2 - \frac{3}{2} \tau C_2^2 P_2' y^2 \right) + E$$

where E is the constant of integration

The boundary conditions are,

(c) at $y = 0$, $U_2 = V$

(d) at $y = h_2$, $U_2 = 0$

Since at $y=0$, $U_2=V$ hence $E=V$ Applying condition (c)

$$U_2 = -\frac{P_2' y^2}{2\mu} + \frac{\tau C_2 y}{\mu} + \frac{K}{\mu} \left(\frac{-P_2'^3 y^4}{4} + \tau C_2^3 y + P_2'^2 y^3 \tau C_2 - \frac{3}{2} \tau C_2^2 P_2' y^2 \right) + V \quad (4\ 13)$$

Applying (d) and rearrangement power of τC_2 equation (4 13) becomes

$$\tau C_2^3 + \left(-\frac{3}{2} P_2' h_2\right) \tau C_2^2 + \left(\frac{1}{K} + P_2'^2 h_2^2\right) \tau C_2 + \left(\frac{\mu V}{K h_2} - \frac{P_2' h_2}{2K} - \frac{P_2'^3 h_2^3}{4}\right) = 0$$

The real root of this equation is

$$\tau C_2 = \left(-\frac{\mu V}{2K h_2} + \left(\frac{\mu^2 V^2}{4K^2 h_2^2} + \frac{1}{27} \left(\frac{1}{K} + \frac{1}{4} P_2'^2 h_2^2\right)^3\right)^{1/2}\right)^{1/3} + \left(-\frac{\mu V}{2K h_2} - \left(\frac{\mu^2 V^2}{4K^2 h_2^2} + \frac{1}{27} \left(\frac{1}{K} + \frac{1}{4} P_2'^2 h_2^2\right)^3\right)^{1/2}\right)^{1/3} + \frac{1}{2} P_2' h_2 \quad (4\ 14)$$

The flow of the polymer melt in the second part of the unit is given by,

$$Q_2 = \int_0^{h_2} U_2 dy$$

Substituting for U_2 from equation (4 13) into the above equation and integrating gives,

$$Q_2 = -\frac{P_2' h_2^3}{6\mu} + \frac{\tau C_2 h_2^2}{2\mu} + \frac{K}{\mu} \left(\frac{-P_2'^3 h_2^5}{20} + \frac{\tau C_2^3 h_2^2}{2} + \frac{P_2'^2 h_2^4 \tau C_2}{4} - \frac{\tau C_2^2 P_2' h_2^3}{2} \right) + V h_2 \quad (4 15)$$

Introduction of viscosity in the pressure distribution:

Increase in hydrodynamic pressure has an effect on viscosity which is equivalent to reduction in temperature and vice versa[38] Also with the decrease in temperature the viscosity increases and with the increase in temperature it has a reverse effect For the ease of calculation it was assumed that temperature decreases only in the X direction Within the plasto-hydrodynamic pressure unit the effect of the change in hydrodynamic pressure on viscosity for every increment of length can be transformed into the effect of change in temperature on the viscosity The viscosity can be expressed arbitrarily as,

$$\mu (x) = \mu (x-1) e^{(-\alpha (T(x) - B DP - T(x-1)))} \quad (4 16)$$

Due to conduction and convection the temperature of the unit decreases starting from the entry to the exit To avoid the complication let the temperature decrease linearly towards the x axis, which can be written as

$$T(i) = T(i-1) - C \, DX \quad (4 \, 17)$$

Solution procedure

Equations(4 7), (4 9), (4 14), (4 15) may be solved simultaneously Numerical values of P_m (maximum step pressure) and hence P_1' and P_2' may be substituted into above equations An iteration technique is used for the solution until the condition $Q_1=Q_2$ is satisfied Shear stresses on the wire and volumetric flow rate can be determined from the solution

To determine the developed hydrodynamic pressure at each small increment of length of the first unit then equation (4 9) can be written in the following way

$$Q_2=Q_1 = \frac{P_1' h_1^3}{6\mu(i-1)} + \frac{\tau c_1 h_1^2}{2\mu(i-1)} + \frac{K}{\mu(i-1)} \left(\frac{P_1'^3 h_1^5}{20} + \frac{\tau c_1^3 h_1^2}{2} + \frac{P_1'^2 h_1^4 \tau c_1}{4} + \frac{\tau c_1^2 P_1' h_1^3}{2} \right) + V h_1 \quad (4 \, 18)$$

This equation is a cubic equation, where each term is known (viscosity can be determined from equation(4 16)) except P_1' Solution of this equation gives this term Now,

$$P_1' = (P_1(i) - P_1(i-1))/DX$$

$$\text{and } P_1(i) = P_1(i-1) + P_1' \, DX$$

$$\text{also } DP = P_1(i) - P_1(i-1)$$

The initial values are,

$$P_1(1)=0, T(1)=\text{Polymer melt temperature, } \mu(1)= \text{viscosity at } T(1)$$

Similarly, hydrodynamic pressure at the second unit can be obtained by rearranging equation(4 15) as

$$Q_2 = - \frac{P_2' h_2^3}{6\mu(j-1)} + \frac{\tau c_2 h_2^2}{2\mu(j-1)} + \frac{K}{\mu(j-1)} \left(- \frac{P_2'^3 h_2^5}{20} + \frac{\tau c_2^3 h_2^2}{2} + \frac{P_2'^2 h_2^4 \tau c_2}{4} - \frac{\tau c_2^2 P_2' h_2^3}{2} \right) + V h_2 \quad (4 \, 19)$$

The viscosity can be determined from equation(4 16) rearranging as

$$\mu (J) = \mu (J-1) e^{(-\alpha (T(J) - B DP - T(J-1)))} \quad (4 20)$$

where,

$$T(J) = T(J-1) - C DX \quad (4 21)$$

Equation (4 19) is also a cubic polynomial equation , solution of which gives P_j'

Here $P_j' = (P_2(j-1) - P_2(j)) / DX$,

so, $P_2(j) = P_2(j-1) - P_j' DX$

and $DP = P_2(j) - P_2(j-1)$

The initial values are,

$P_2(1) = P_1(L_1)$, $T(1) = T(L_1)$, $\mu(1) =$ viscosity at $T(L_1)$

It can be mentioned here that this non-Newtonian analysis is not valid for Newtonian fluid (substituting the value of k for zero)

Newtonian model

Here the polymer has been considered as a Newtonian fluid For Newtonian fluid the relation between shear stress, viscosity and shear rate is

$$\tau = \mu \left(\frac{dU}{dy} \right) \quad (4 22)$$

The step pressure is [60]

$$P_m = \frac{6 \mu V (h_1 - h_2)}{\frac{h_1^3}{L_1} + \frac{h_2^3}{L_2}} \quad (4 23)$$

The pressures at the entrance of the first unit and at the end of the second unit are zero

The drag force may be given by ,

$$F_d = \int_{x=0}^{x=L} \pi D \tau_x dx \quad (4.24)$$

The drawing stress is given by,

$$\sigma_x = \frac{4x\tau_x}{D} \quad (4.25)$$

where D is the equivalent diameter

For only coating but no drawing or reduction in cross sectional area, h_1 , h_2 , L_1 and L_2 should be selected in such way that according to the Tresca yield criterion

$$P + \sigma_x \leq Y \quad (4.26)$$

where Y is the flow stress of wire material

On the basis of this analysis theoretical results were calculated for two set of parameters. The parameters for the first set are

Polymer-Durethan B31F (Nylon-6)[38, 43 and 55]

$B = 3.2 \times 10^{-1} \text{ } ^\circ\text{C}/\text{Nmm}^{-2}$, $C = 0.1 \text{ } ^\circ\text{C}/\text{mm}$, $\alpha = 0.0114 \text{ } ^\circ\text{C}$, $DX = 1 \text{ mm}$, $h_1 = 0.5 \text{ mm}$, $h_2 = 0.05 \text{ mm}$, $K = 1.1 \times 10^{11} \text{ m}^4/\text{N}^2$, $L_1 = 25 \text{ mm}$, $L_2 = 10 \text{ mm}$, initial polymer temperature at the first unit = 280°C , initial polymer viscosity = 63 N s/m^2

Figure 4.2 shows, the theoretical change in viscosity of polymer from the entrance of the plasto-hydrodynamic unit. The temperature in the plasto-hydrodynamic unit decreases slowly, mainly due to conduction and convection. In the first section of the unit the hydrodynamic pressure increases from zero to a maximum pressure and in the second section of the unit it decreases from maximum pressure to zero. Viscosity is a function of temperature and pressure and increases with the decrease in the temperature and increase in the pressure. The combined effect of the decrease in temperature and increase in the pressure increases the viscosity of the polymer.

in the first section of the unit. In the second section, the pressure as well as the temperature decreases. Their combined effect decreases the viscosity in the second section of the unit. The viscosity increases with the increase in the wire velocity. Figures 4.3, 4.4 and 4.5 illustrate the theoretical hydrodynamic pressure distribution within the unit for wire velocities of 4 m/s, 8 m/s and 12 m/s respectively. In these figures the present solution in which the change in the viscosity has been included are compared with the results from the previous solution [7] where the viscosity of the polymer is assumed to be constant. In the present solution, the theoretical pressure has been generated for each small increment of length in the plasto-hydrodynamic pressure unit, whereas in the previous method the theoretical pressure can be found only in the interface of the two sections of the unit. The initial pressure in the first section of the unit and final pressure in the second section of the unit are zero. Two straight lines have been drawn by these three points. One from zero to step pressure for the first section of the unit. Another from step pressure to zero for the second section of the unit. In the previous solution the pressure increases in the first section and then decreases in the second section linearly. For the present solution the pressure in the first section increases linearly, in the second section it decreases linearly but near the end of the second section there is a sharp drop of pressure. The step pressure obtained by the previous method and the present method is different according to these three figures.

Figure 4.6 shows the theoretical maximum pressure generation with velocity for different geometry of the unit. The ratio of gap between the wire and the first and the second section of the unit has been considered as the geometry of the unit. As the gap ratio decreases the pressure generation increases. With the increase in velocity the pressure also increases.

The parameters for the second set are [30,42]

Polymer- Borosiloxane

$B=4.2 \times 10^{-1} \text{ } ^\circ\text{C}/\text{Nmm}^2$, $C=0.1 \text{ } ^\circ\text{C}/\text{mm}$, $\alpha=0.016 \text{ } ^\circ\text{C}$, $DX=1 \text{ mm}$, $h_1=1.5 \text{ mm}$, $h_2=0.075 \text{ mm}$, $K=5.6 \times 10^{13} \text{ m}^4/\text{N}^2$, $L_1=145 \text{ mm}$, $L_2=35 \text{ mm}$, initial polymer temperature at the first unit = 100°C , initial polymer viscosity = 50 N s/m^2

Figures 4.7, 4.8 and 4.9 illustrate the theoretical hydrodynamic pressure within the

unit for wire velocities of 0.094 m/s, 0.11 m/s and 0.24 m/s respectively. In these figures the present solution in which the change in viscosity has been included are compared with the results from the previous Newtonian[60] and non-Newtonian[7] solution where the viscosity of the polymer was assumed to be constant. Also the pressure profile from experiment[30] has been compared with those solutions. For the previous Newtonian and non-Newtonian solutions there is a linear rise in pressure in the first section and linear fall in pressure in the second section of the unit. For the present solution the pressure in the first section increases linearly, in the second section it also decreases linearly but near the end of the second section there is a sharp drop of pressure. Also from those figures it can be found that there is a pressure drop near the end of the second section for the experimental pressure profiles. The pressure profile obtained by the present non-Newtonian solution is closer to the experimental results than the previous Newtonian and non-Newtonian solutions.

This above analysis in this section has been done for plasto-hydrodynamic coating only where there is no deformation in the continuum. For deformation more analysis is required, which are given in the following sections.

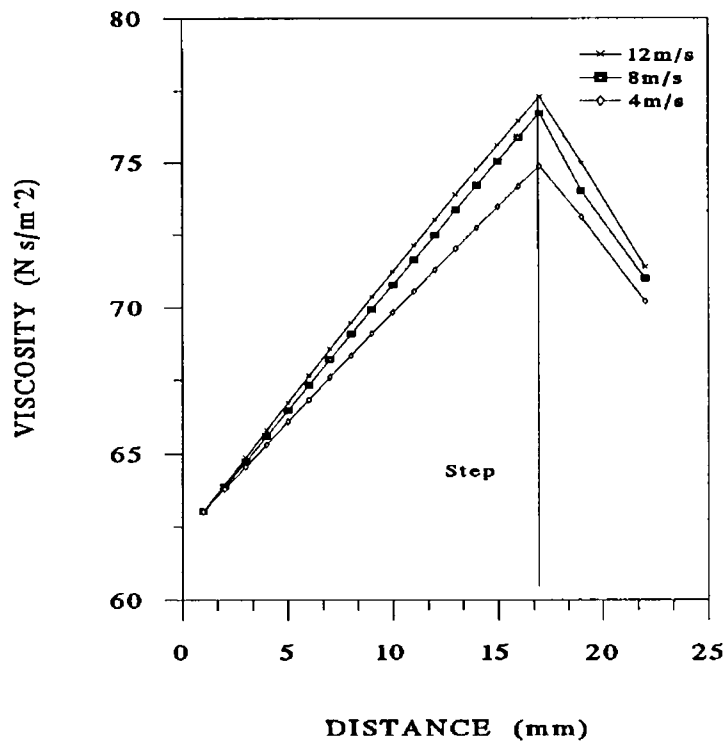


Figure 4 2 Viscosity distribution within stepped parallel bore unit for different wire velocities (Polymer-Durethan B31F)

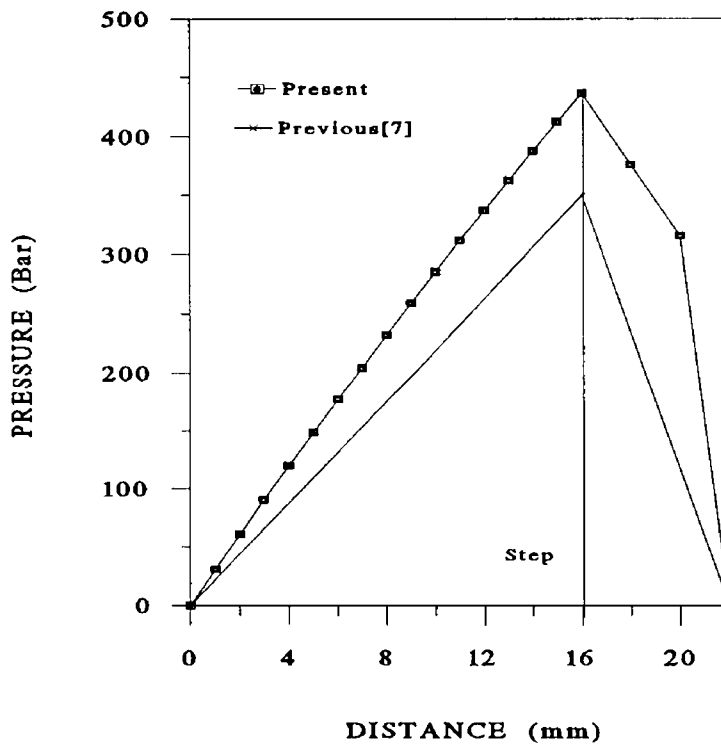


Figure 4 3 Pressure distribution within stepped parallel bore unit for wire velocity 4m/s (Polymer-Durethan B31F)

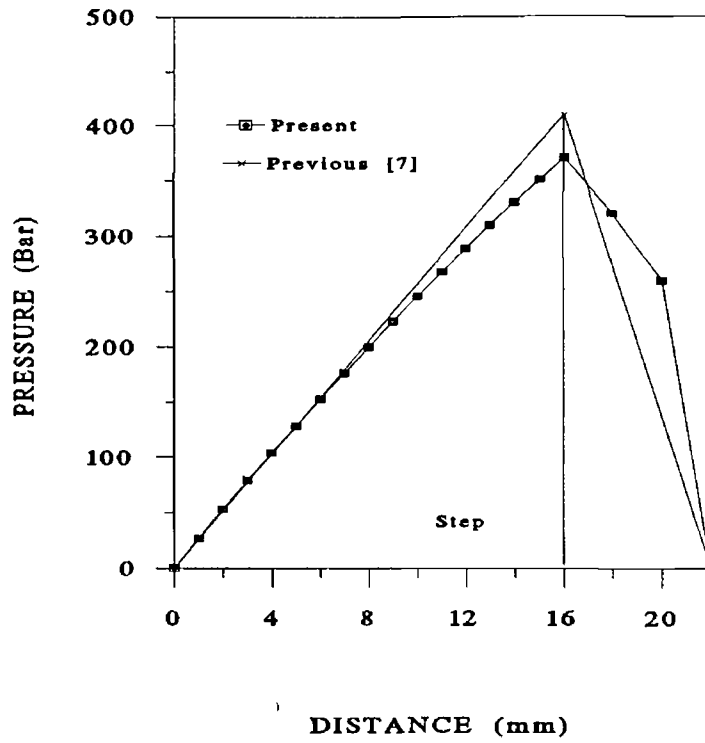


Figure 4 4 Pressure distribution within stepped parallel bore unit for wire velocity 8m/s (Polymer-Durethan B31F)

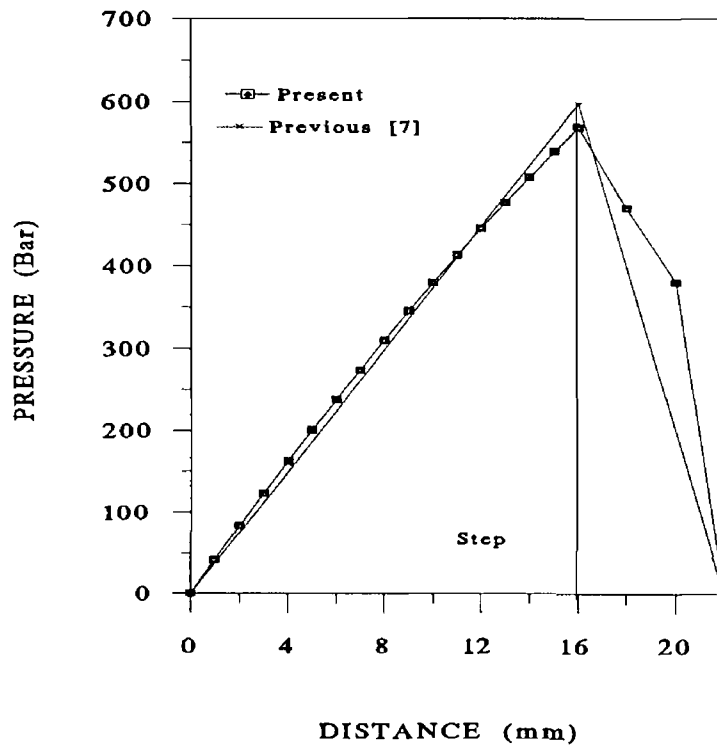


Figure 4 5 Pressure distribution within stepped parallel bore unit for wire velocity 12m/s (Polymer-Durethan B31F)

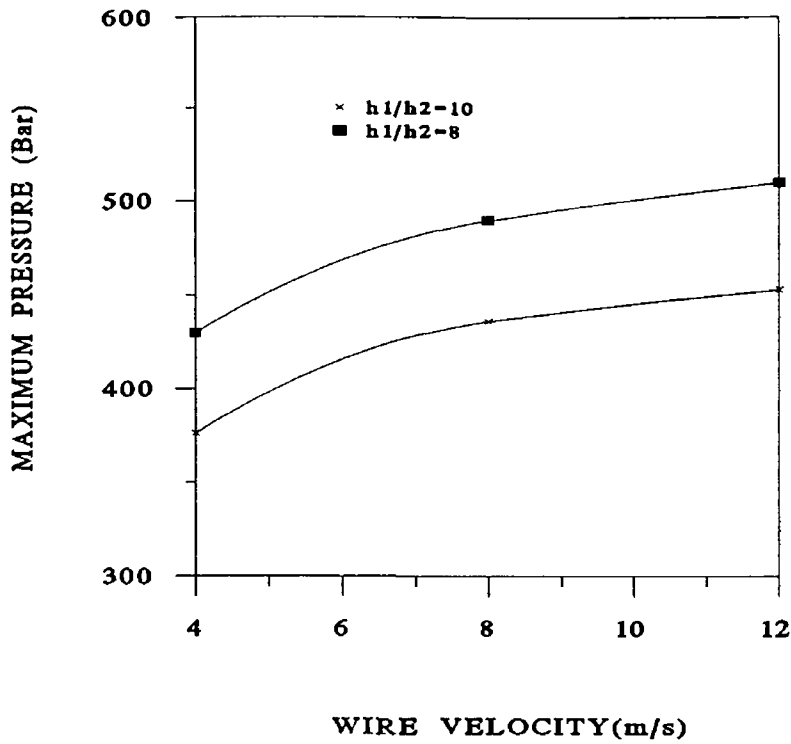


Figure 4 6 maximum pressure within stepped parallel bore unit for different unit geometry and wire velocities (Polymer-Durethan B31F)

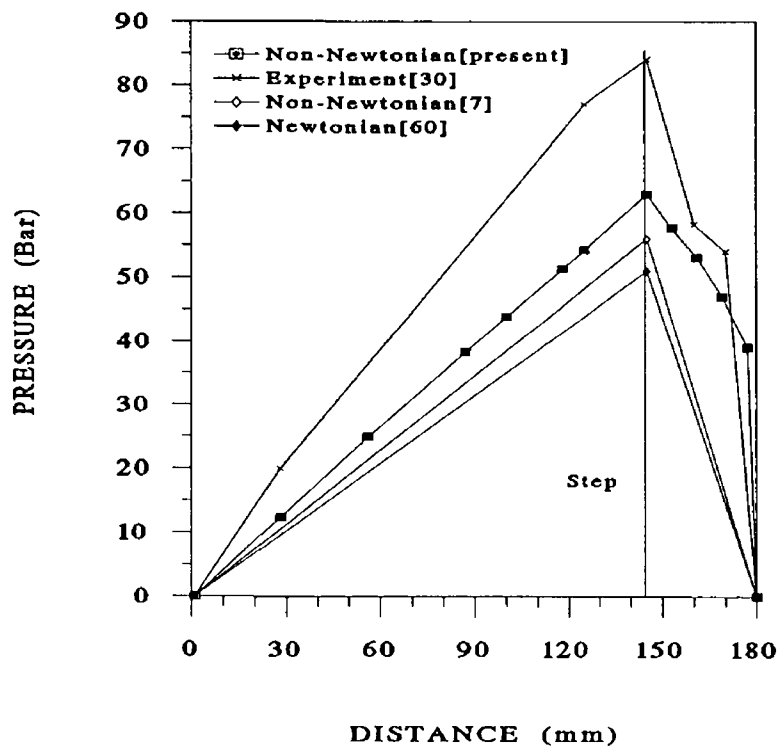


Figure 4 7 Pressure distribution within stepped parallel bore unit for wire velocity 0.094 m/s (Polymer-Borosiloxane)

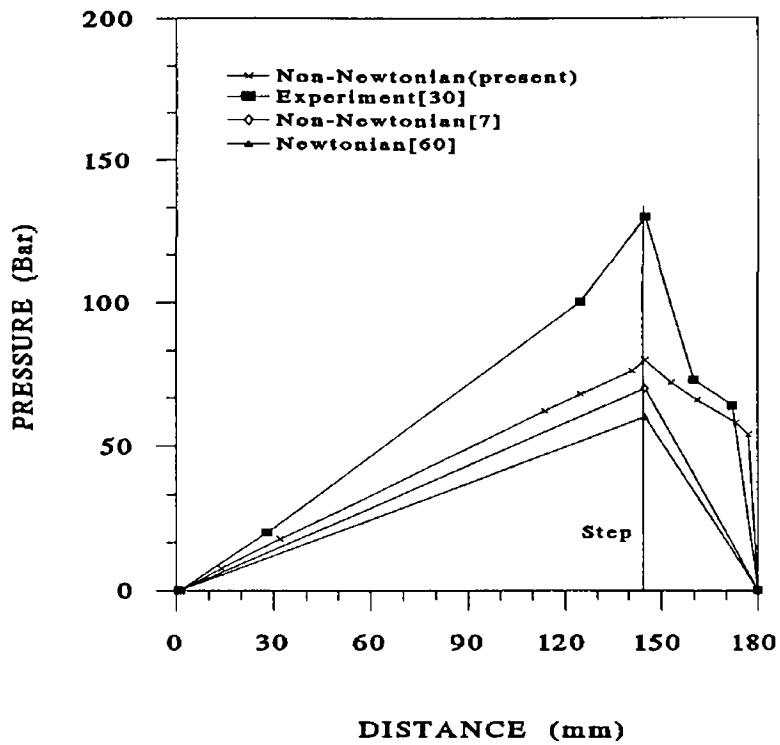


Figure 4 8 Pressure distribution within stepped parallel bore unit for wire velocity 0 11m/s (Polymer-Borosiloxane)

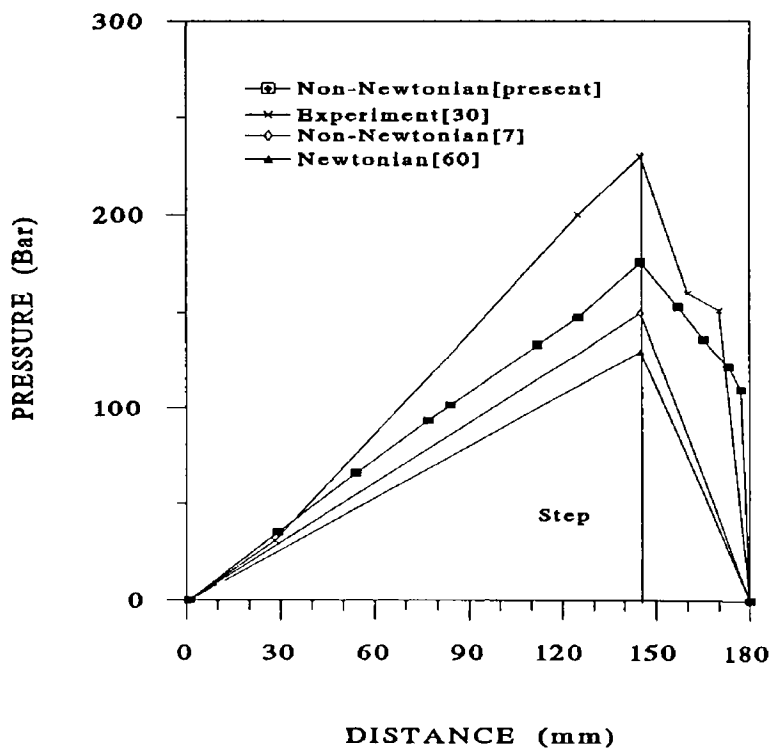


Figure 4 9 Pressure distribution within stepped parallel bore unit for wire velocity 0 24m/s (Polymer-Borosiloxane)

4.3 Analysis of continuum drawing in stepped parallel bore pressure unit :

In the previous section, non-Newtonian pressure analysis was carried out for the hydrodynamic coating process in a stepped parallel bore unit which is the same for any type of continuous surface as- wire, strip or tube. But the deformation profile is different for wire, tube and strip. In this section the deformation profile is given for wire, tube and strip respectively when their cross sections are reduced under the action of plasto-hydrodynamic pressure.

4.3.1 Analysis for wire drawing

For the stepped parallel bore plasto-hydrodynamic die-less wire drawing process a theoretical model for wire reduction has been presented in the previous publications [7-11]. The pressure medium was non-Newtonian fluid (polymer melt). The viscosity of polymer melt is influenced by the temperature as well as the hydrodynamic pressure. In that model this property of viscosity was not taken into consideration. Also the change in shear stress was not shown due to the change in the viscosity and reduction of wire diameter. In the following section a mathematical model has been developed for the wire drawing within a stepped parallel bore unit taking account of the changes in the viscosity of the polymer melt during the drawing process. Theoretical results are obtained for different wire speeds in terms of the changes in viscosity, shear stress, percentage reduction in area, coating thickness and pressure distributions within the unit. These results are compared with the experimental results from reference [7-11].

The yielding of the wire inside the dieless unit

As the hydrodynamic pressure increases in the first section from zero to a maximum value it is considered that the reduction also starts in the first section.

Consider a distance x_1 from the entry point of the unit where yielding of wire has just commenced [see Figure 4.10 a]. The principal stresses acting on the wire are $\sigma_1 = \sigma_{x_1}$ and $\sigma_2 = \sigma_3 = -P_1$,

where σ_{x_1} is the axial stress and P_1 is the radial pressure at point x_1 .

The stress- strain characteristics of the wire are assumed to be of the form

$$Y = Y_0 + K_0 \epsilon^n \quad (4.27)$$

where Y is the flow stress of the wire material and Y_0 is the yield stress
 Therefore, yielding commence when the condition $Y = Y_0$ is satisfied
 Using the Tresca or von-Mises theory of yielding gives,

$$P_1 + \sigma_x = Y \quad (4\ 28)$$

Equilibrium of forces on the wire in x direction gives

$$\sigma_{x1} \left(\frac{1}{4} \pi D_1^2 \right) = (\pi D_1 x_1) \tau_{c1}$$

hence,

$$\sigma_{x1} = \frac{4 x_1 \tau_{c1}}{D_1} \quad (4\ 29)$$

The pressure at x_1 is given as

$$P_1 = \frac{P_m x_1}{L_1} \quad (4\ 30)$$

as the pressure in the section builds up linearly along its length

Substituting equation (4 27), (4 29) and (4 30) into equation (4 28) and rearranging,
 the position of yield in the wire x_1 may be expressed as

$$x_1 = \frac{Y_0}{\frac{4 \tau_{c1}}{D_1} + \frac{P_m}{L_1}} \quad (4\ 31)$$

This equation enables the prediction of the position where the wire starts to yield

plastically within the first part of the unit. As soon as yielding occurs, plastic deformation will continue as long as equation (4.28) is satisfied.

Deformation zone

Consider a section of the unit within which the wire is plastically deformed as shown in Figure (4.10 b). Since the deformation of the wire is not pre-defined as a function of x , the equations containing this variable cannot be solved analytically. Hence a finite-difference technique is adopted to solve these equations governing the deformation zone assuming that between any two points of small distance dx apart on the deforming wire, the deformation takes place linearly, therefore,

$$\frac{dD}{2 dx} = B$$

Expressing this equation in finite-difference form yields,

$$D_1 = D_{1-1} - 2B_1 \Delta x \quad (4.32)$$

and similarly the variation in the gap, dh is given by

$$dh = \frac{dD}{2}$$

hence

$$h_1 = h_{1-1} + B_1 \Delta x \quad (4.33)$$

where B_1 is the slope of the deformation profile within distance Δx . Considering a small section of the wire, the radial equilibrium of forces gives,

$$\sigma_r (\pi D dx) = -P \left(\frac{\pi D dx}{\cos \alpha} \right) \cos \alpha + \tau_c \left(\frac{\pi D dx}{\cos \alpha} \right) \sin \alpha$$

hence

$$\sigma_r = -P \left(1 - \frac{\tau_c}{P} \tan \alpha \right) \quad (4.34)$$

The value of τ_c/P has been shown to be very small and since α is also very small, the term $\tau_c \tan \alpha / P$ can be ignored. The principal stresses acting on the wire are, $\sigma = \sigma_x$ and $\sigma_2 = \sigma_3 = -P$, where σ_x is the axial stress and P is the radial pressure at point x . Hence from the yield criteria, $P + \sigma_x = Y$.

Equilibrium of forces in x direction gives

$$-\sigma_x \left(\frac{1}{4} \pi D^2 \right) + (\sigma_x + d\sigma_x) \left(\frac{\pi}{4} (D + dD)^2 \right) + P \left(\frac{\pi D dx}{\cos \alpha} \right) \sin \alpha + \tau_c \left(\frac{\pi D dx}{\cos \alpha} \right) \cos \alpha = 0$$

Rearranging and ignoring powers of dD

$$2dD\sigma_x + Dd\sigma_x + 4P dx \tan \alpha + 4dx\tau_c = 0$$

but $\tan \alpha = dD/2dx$ hence

$$2dD(P + \sigma_x) + Dd\sigma_x + 4dx\tau_c = 0$$

Substituting for $(P + \sigma_x = Y)$ and rearranging gives

$$d\sigma_x = -\frac{2dDY}{D} - \frac{4\tau_c dx}{D}$$

This is the governing differential equation in the deformation zone for the axial stress in the wire. Rewriting this equation in finite-difference form gives,

$$\sigma_{x1} = \frac{2(D_{1-1} - D_1) Y_1}{D_1} + \frac{4\tau_{c1} dx}{D_1} + \sigma_{x1-1} \quad (4.35)$$

This equation is a function of shear stress on the wire and it must be determined independently. The equation for the wall shear stress in the first part of the unit may be written as (section 4.2),

$$\begin{aligned} \tau_{c1} = & \left(-\frac{\mu(1-1)V_1}{2Kh_1} + \left(\frac{\mu(1-1)^2 V_1^2}{4K^2 h_1^2} + \frac{1}{27} \left(\frac{1}{K} + \right. \right. \right. \\ & \left. \left. \frac{1}{4} P_1' h_1^2 \right)^3 \right)^{1/2} \left. \right)^{1/3} + \left(-\frac{\mu(1-1)V_1}{2Kh_1} - \left(\frac{\mu(1-1)^2 V_1^2}{4K^2 h_1^2} \right. \right. \\ & \left. \left. + \frac{1}{27} \left(\frac{1}{K} + \frac{1}{4} P_1' h_1^2 \right)^3 \right)^{1/2} \right)^{1/3} - \frac{1}{2} P_1' h_1 \end{aligned} \quad (4.36)$$

This equation contains the pressure gradient and variation of the wire velocity in the deformation zone and they must be determined separately. The flow of the polymer melt in this region may be expressed as (section 4.2),

$$\begin{aligned} Q_2 = Q_1 = & \frac{P_1' h_1^3}{6\mu(1-1)} + \frac{\tau_{c1} h_1^2}{2\mu(1-1)} + \frac{K}{\mu(1-1)} \left(\frac{P_1' h_1^5}{20} + \frac{\tau_{c1}^3 h_1^2}{2} + \right. \\ & \left. \frac{P_1' h_1^4 \tau_{c1}}{4} + \frac{\tau_{c1}^2 P_1' h_1^3}{2} \right) + Vh_1 \end{aligned} \quad (4.37)$$

Equations (4.36) and (4.37) may be solved simultaneously in order to determine P_1' and τ_{c1} by iterating P_1' at point 1 in the deformation zone.

Therefore,

$$P_1(1) = P_1(1-1) + P_1' \Delta x \quad (4.38)$$

The variation of speed of the wire in the deformation zone may be also included in the analysis. The continuity of flow of metal through the element [Figure 4.10c] gives

$$(V+dV) \frac{\pi}{4} (D+dD)^2 = \frac{\pi}{4} VD^2$$

Ignoring higher order terms of dD gives

$$\frac{dV}{V} = -\frac{2dD}{(D+2dD)}$$

Rewriting this equation in finite difference form gives

$$V_1 = \frac{V_{1-1}}{1 - \frac{2(D_{1-1} - D_1)}{2D_{1-1} - D_1}} \quad (4.39)$$

The true strain-stress relationship of the wire in the deformation zone may be shown as

$$Y_1 = Y_0 + K_0 \epsilon_1^n \quad (4.40)$$

where $\epsilon_1 = 2 \ln(D_1/D_0)$

Therefore,

$$Y_1 = Y_0 + K_0 \left(2 \ln \left(\frac{D_1}{D_0} \right) \right)^n \quad (4.41)$$

Substituting for Y_1 in equation (4.35) gives

$$\sigma_{x1} = 2 \left(\frac{D_{1-1} - D_1}{D_1} \right) \left(Y_0 + K_0 \left(2 \ln \left(\frac{D_1}{D_0} \right) \right)^n \right) + \frac{4\tau_{c1} dx}{D_1} + \sigma_{x1-1} \quad (4.42)$$

The new shear stress within the zone where deformation of wire has been observed is then given by,

$$\tau (i) = P'_i h_i + \tau_{ci} \quad (4.43)$$

At any point i in the deformation zone, D_i , h_i , and V_i may be calculated from equation (4.32), (4.33) and (4.39) respectively for an arbitrary value of B_i . By substituting the values of D_i and V_i into equations (4.41) the yield stress Y_i may be calculated. Also by substituting for V_i and h_i into equations (4.36) and (4.37) gives P'_i and τ_{ci} and simultaneously iterating for P''_i until equation (4.37) is satisfied. Hence equation (4.38) gives $P_i(i)$. Similarly τ_{ci} and D_i may be substituted into equation (4.42) to evaluate σ_{xi} . This $P_i(i)$, τ_{ci} and h_i gives the shear stress within the deformation zone. Other variables in the above equations are known physical properties. Having calculated σ_{xi} , P_i and Y_i the values of B_i may be iterated in the above equations until equation $\sigma_{xi} + P_i = Y_i$ is satisfied. The drawing speed, final wire diameter and the coating thickness are given by,

$$\text{drawing speed} = V_s = V_i$$

$$\text{final wire diameter} = D_s = D_i$$

$$\text{coat thickness } h_3 = h_i - h_1 + h_2$$

respectively. This analysis thus enables the prediction of the pressure in the melt, shear stress on the wire and the profile of the effective die in the deformation zone.

Condition of slip

It is known that polymers have a critical shear stress at which slip occurs. This has been confirmed by many researchers [47-49] and the magnitude of this shear stress is shown to be between 0.1 and 1 MN m⁻² for different polymer melts. Evidence of slip for polypropylene KM61 polymer was observed at a shear stress of about 0.32 MN m⁻². Therefore in the present analysis an average shear stress of 0.5 MN m⁻² is assumed for the slip. It is also assumed that slip only takes place at the wire-polymer interface and not at the unit wall-polymer interface. When the condition of slip is developed, ie. when the shear stress reaches the assumed value, the flow of polymer as well as the hydrodynamic pressure is considered to remain constant.

To obtain the results following values of the parameters were used based on references [7-11].

$$B = 5.6 \times 10^{-1} \text{ } ^\circ\text{C}/\text{Nmm}^{-2}, \quad C = 0.1 \text{ } ^\circ\text{C}/\text{mm}, \quad \alpha = 0.017 \text{ } ^\circ\text{C}, \quad DX = 1\text{mm}, \quad h_1 = 0.2 \text{ mm},$$

$h_2=0.05$ mm, $K=5.0 \times 10^{11}$ m⁴/N², $L_1=50$ mm, $L_2=20$ mm, initial polymer temperature at the first unit=130°C, initial polymer viscosity =110 N s/m², $y_0=50$ MNm², $K_0=440$ MNm², $n=0.52$, $D_1=1.6$ mm

The polymer was Alkathane WVG23 and the wire material was Copper

Figure 4.11 shows the theoretical change in the viscosity of the polymer from the entrance of the plasto-hydrodynamic unit. The combined effects of the decrease in the temperature and the increase in the pressure increase the viscosity of the polymer in the first part of the unit. In the second part of the unit, the viscosity decreases upto a certain value. Figure 4.12 shows the theoretical magnitude of change in the shear stress within the unit due to the change in the shear rate and viscosity. In the first part, before the deformation there is no change in shear stress as there is no change in the gap, after the yielding point it increases linearly upto the step where the deformation of the wire stops. The change in shear stress within the deformation zone increases with the increase in the wire velocity.

Figures 4.13 and 4.14 illustrate the theoretical hydrodynamic pressure within the unit for the wire velocity of 1m/s and 2m/s respectively. In these figures the pressure profile from the present solution in which the change in the viscosity has been included are compared with experimental and theoretical pressure profiles[11]. The initial pressure in the first section of the unit and final pressure in the second section of the unit is zero. For the present solution, the pressure in the first section increases linearly before the deformation zone. After that zone, it also increases linearly but at a different rate. In the second section of the unit the pressure decreases linearly but near the end of the second section there is a sharp drop of pressure. With the increase in the wire velocity the pressure also increases. From the Figures (4.13 and 4.14) it can be seen that the present theoretical pressure rises at the same way as the experimental pressure. But the magnitude of the present theoretical pressure is marginally closer to that of the experimental pressure than that theoretically predicted by Parvinmehr et al [7-11]. It may be mentioned here that the viscosity and pressure profile obtained by the drawing and coating process is different from the coating process only.

Figure 4.15 shows comparisons of the percentage reduction in area for different speeds of the wire both theoretically and experimentally. Theoretically, these

reductions increase with the increase in wire velocities. After the wire velocity of about 2.7 m/s they become almost constant as the wall shear stress reaches the critical value. The reduction obtained by the present solution is less than that obtained theoretically by Parvinmehr et al [7-11]. From the experimental curve it appears that the reduction is maximum at a wire velocity of 0.5 m/s. After that velocity it decreases gradually. And at velocity 2.4 m/s it becomes almost constant. However, the present theoretical prediction of the reduction compares fairly with the experimental curve at higher velocities. Figure 4.16 shows comparisons of the coating thickness for different speeds of the wire both theoretically and experimentally. Also in this case it can be observed that the theoretical coating thickness matches with the experimental thickness at higher velocities. However, the experimental works done by Xie[17] show that the percentage reduction in area of wire increases with the increase in the wire speed. He carried out the experiment with the same Alkathane WVG 23 as other experimental works. The wire diameter was 0.46 mm. Figure 4.17 and 4.18 show the comparisons of this experimental percentage reduction in area with the present theoretical prediction which are quite closer. The geometry of the unit was the same as Parvinmehr[11] for Figure 4.18. However, the h_1/h_2 ratio was different from that of Parvinmehr in the case of Figure 4.17.

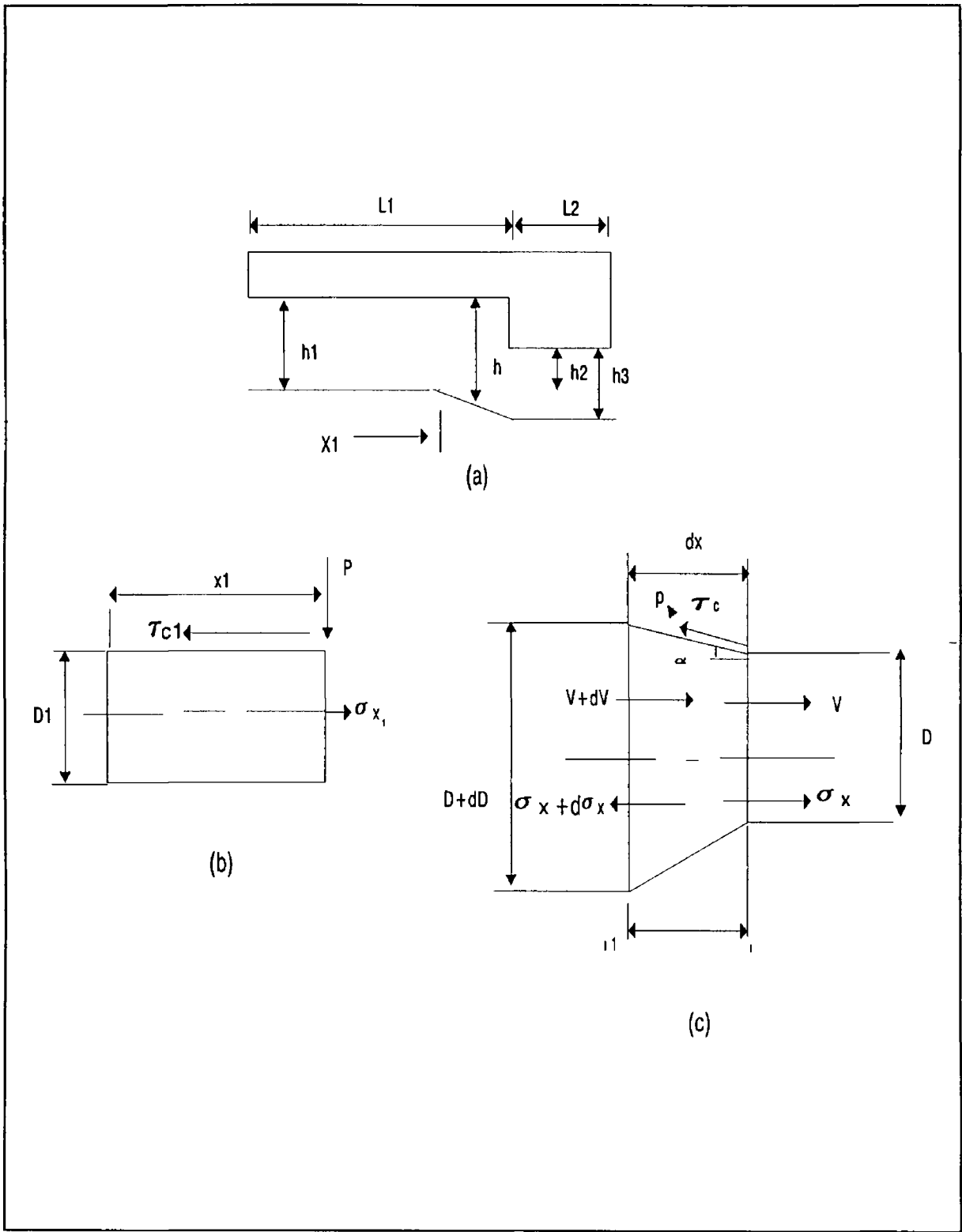


Figure 4 10 Geometry used in the wire drawing analysis in case of stepped parallel bore unit

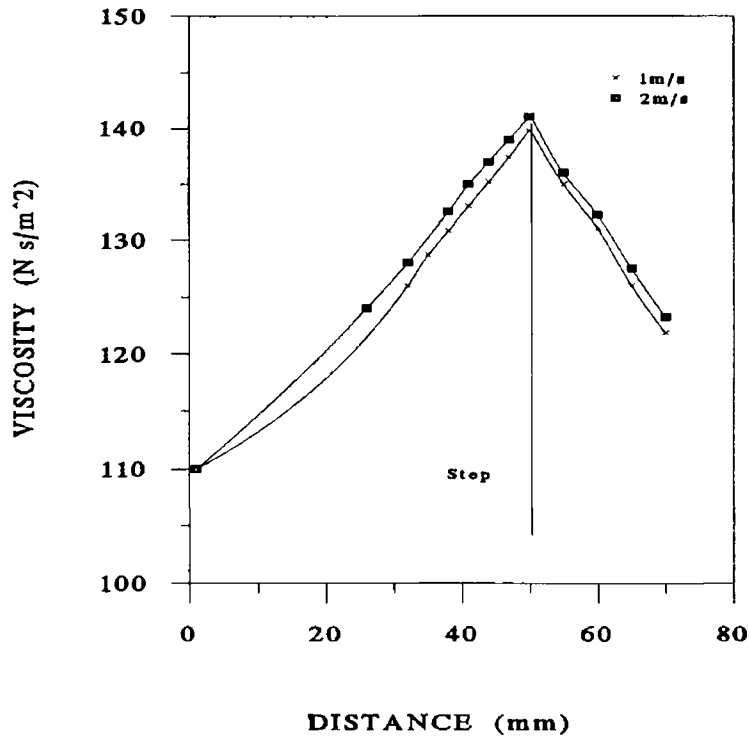


Figure 4 11 Theoretical change in viscosity of polymer along the unit during wire drawing (Polymer-Alkathane WVG23)

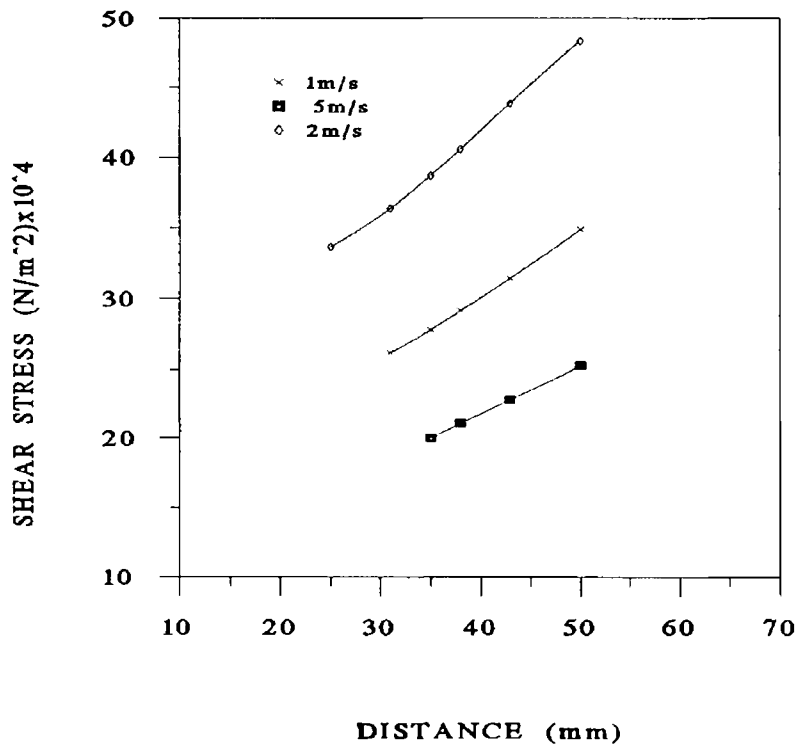


Figure 4 12 Theoretical change in shear stress of polymer within deformation zone during wire drawing (Polymer-Alkathane WVG23)

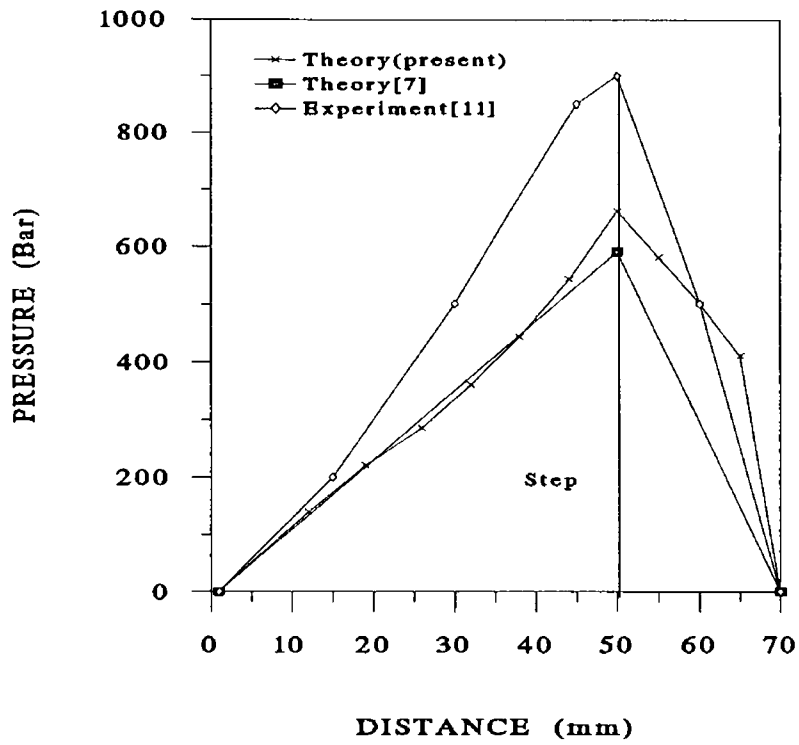


Figure 4 13 Pressure distribution within the unit during wire drawing velocity 1m/s (Polymer-Alkathane WVG23)

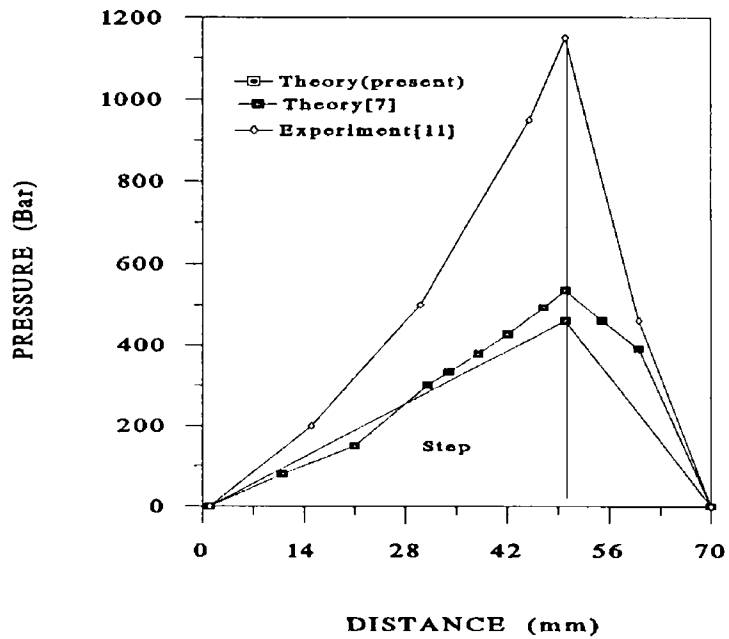


Figure 4 14 Pressure distribution within the unit during wire drawing velocity 2m/s (Polymer-Alkathane WVG23)

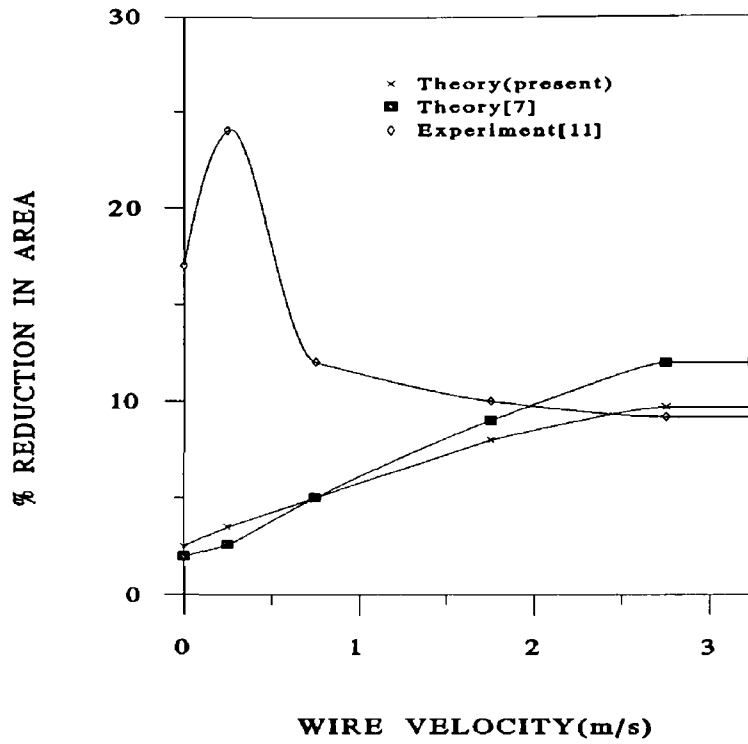


Figure 4 15 Percentage reduction in area during wire drawing at different velocities (D1 = 1.6 mm, L1/L2=2.5, h1/h2=4, Polymer-Alkathane WVG23)

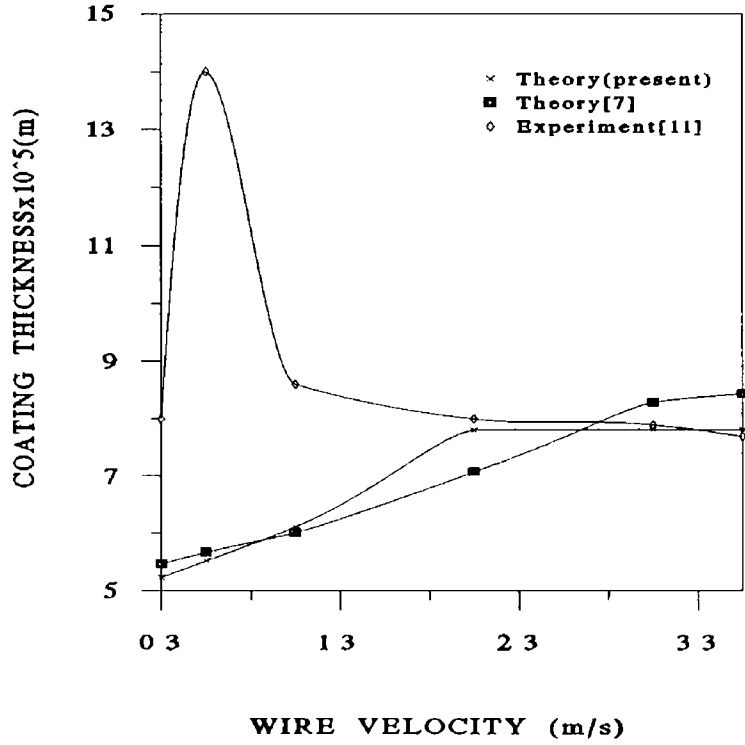


Figure 4 16 Coating thickness during wire drawing at different velocities (D1 = 1.6mm, L1/L2=2.5, h1/h2=4, Polymer-Alkathane WVG23)

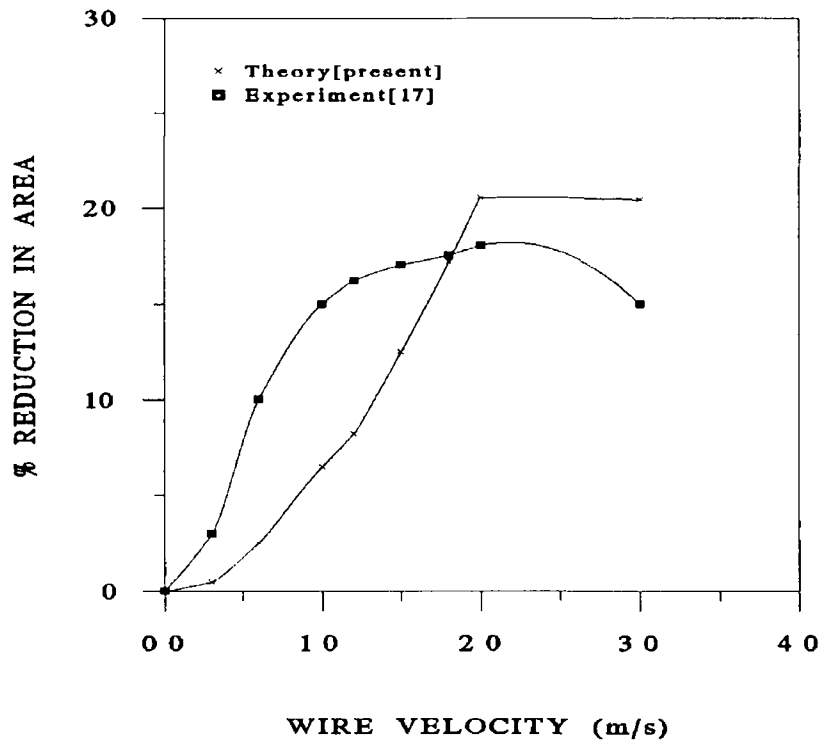


Figure 4 17 Percentage reduction in area during wire drawing at different velocities ($D_1=0.46$ mm, $L_1/L_2=2.5$, $h_1/h_2=1.5$, Polymer-Alkathane WVG23)

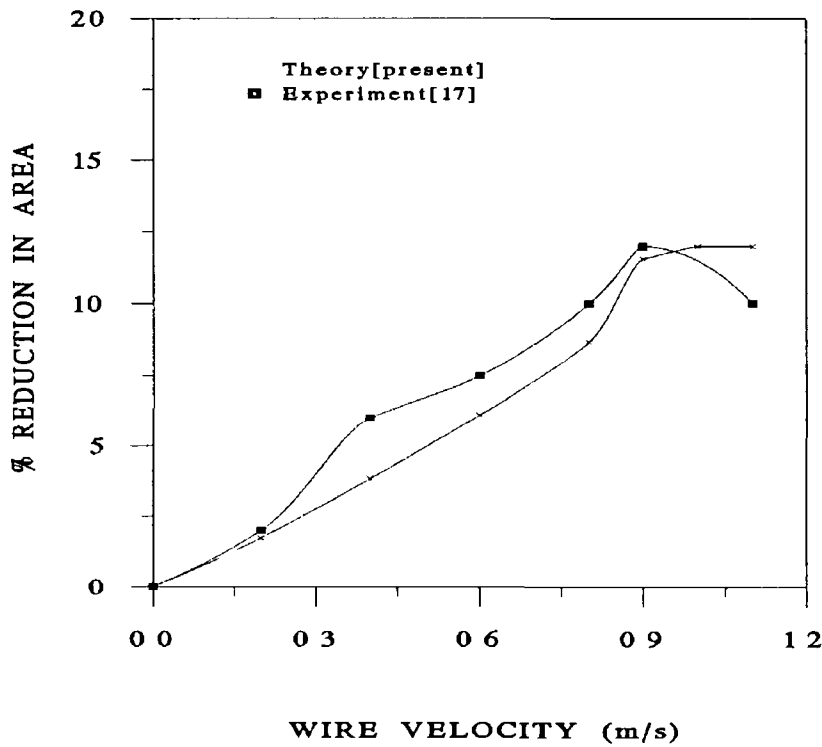


Figure 4 18 Percentage reduction in area during wire drawing at different velocities ($D_1=0.46$ mm, $L_1/L_2=2.5$, $h_1/h_2=4$, Polymer-Alkathane WVG23)

4.3.2 Plasto-hydrodynamic tube sinking process

In the conventional tube sinking process the diameter of the tube is reduced to a specific size whilst pulling it through a trumpet-shaped die. For the plasto-hydrodynamic tube sinking process, the tube is pulled through an orifice of stepped parallel or tapered bore unit which is filled with polymer melt.

Results of plasto-hydrodynamic die-less tube sinking have been presented in reference [12-16, 61]. But the pressure medium, polymer, was considered to remain unchanged during the sinking process. Also the change in shear stress was not shown due to the change in viscosity and reduction of the tube diameter. Raising the hydrodynamic pressure makes the polymer melt viscosity rise by a certain factor [38] and a number of degree decrease in temperature increase the viscosity by a certain factor [35]. In this section a mathematical model has been developed for the pressure distribution within a stepped parallel bore unit taking account of the changes in the viscosity of the polymer melt during the drawing process. The change in the shear stress was also shown during the sinking process.

The yielding position of the tube inside the dieless unit .

Consider a point at a distance x_1 from entry of the unit, where yielding of tube has just commenced [see Figure 4 19 a]. Principal stresses acting on the tube are $\sigma_1 = \sigma_x$ and $\sigma_3 = -\sigma_\theta$.

The equilibrium of forces in longitudinal direction (Figure 4 19 b and 4 19 c)

$$2\pi r t d\sigma_x - 2\pi r dx \tau_{c1} = 0$$

so that $d\sigma_x = (\tau_{c1}/t) dx$, which after integration and substituting boundary conditions at $x=0$, $\sigma_x=0$ becomes

$$\sigma_x = \tau_{c1} x / t \quad (4 44)$$

Equilibrium of radial force gives

$$Pr \, d\theta \, dx = 2\sigma_\theta \, dx \, t \sin(d\theta/2)$$

which for a small angle, $d\theta$, becomes

$$\sigma_\theta = Pr/t$$

where σ_θ is the hoop stress and P is the pressure ($\sigma_x \ll P \ll \sigma_\theta$)

For plastic deformation to commence the yield criterion according to the Tresca theory of yielding gives

$$\sigma_x + \sigma_\theta = Y_0 \quad (4.45)$$

Let x_1 be the distance from the entry to step where plastic deformation commences, so that $\sigma_x = (\tau_{c1} x_1 / t)$ and $\sigma_\theta = Pr_1 / t = P_m x_1 r_1 / L_1 t$ (considering linear pressure build-up along the length of the unit)

Equation (4.45) thus becomes

$$(\tau_{c1} x_1 / t) + P_1 x_1 r_1 / L_1 t = Y_0$$

So that,

$$x_1 = Y_0 / ((\tau_{c1} / t) + P_1 r_1 / L_1 t) \quad (4.46)$$

The plastic deformation continues after the yielding starts. The yield characteristics of the tube are assumed to be

$$Y = Y_0 + K_0 \epsilon^n \quad (4.47)$$

Therefore yielding occurs as soon as $Y = Y_0$

Deformation zone

Consider a section of the unit within which the tube is plastically deformed as shown in Figure (4.20). It is assumed that the tube diameter reduces linearly in the first section of the unit, from the point of first yielding to the end of the section. Also

any relation involving the variables in the deformation zone cannot be resolved analytically. Hence a finite-difference technique is adopted to solve the different equations governing the deformation zone. As assumed, the change of radius between two points at dx distance apart on the deforming tube can be given as

$$\frac{dr}{dx} = \text{constant} = \tan \alpha = B$$

Expressing this equation in finite-difference form gives

$$r_i = r_{i-1} + B_i \Delta x \quad (4.48)$$

and similarly the variation in gap

$$dh = dr$$

hence

$$h_i = h_{i-1} + B_i \Delta x \quad (4.49)$$

where B_i is the slope of the deformation profile within distance Δx . Considering a small section of the tube (Figure 4.21) where the deformation takes place at an angle α , the radial equilibrium of forces gives

$$P \left(r d\theta \frac{dr}{\sin \alpha} \right) - \sigma_\theta \left(t \frac{dr}{\sin \alpha} \right) d\theta \cos \alpha = 0$$

which after simplification gives

$$P = \sigma_\theta \left(\frac{t}{r} \right) \cos \alpha \quad (4.50)$$

Equilibrium of forces in the x direction gives

$$(\sigma_x + d\sigma_x)(r + dr) \Delta\theta (t + dt) - \sigma_x t r \Delta\theta + \sigma_\theta \left(t \frac{dr}{\sin\alpha} \right) \Delta\theta \sin\alpha + \tau_c \left(r \Delta\theta \frac{dr}{\sin\alpha} \right) = 0$$

which after simplification, neglecting second-order smaller quantities and division by dr , becomes

$$\frac{d}{dr} (\sigma_x r t) + \sigma_\theta t + \tau_c \left(\frac{r}{\sin\alpha} \right) = 0 \quad (4.51)$$

Let the wall thickness of the tube remain unaltered during the deformation, so that the above equation becomes

$$\frac{d}{dr} (\sigma_x r) + \sigma_\theta + \tau_c \left(\frac{r}{t \sin\alpha} \right) = 0$$

or

$$r \frac{d\sigma_x}{dr} + \sigma_x + \sigma_\theta + \tau_c \left(\frac{r}{t \sin\alpha} \right) = 0 \quad (4.52)$$

Substituting for $(\sigma_x + \sigma_\theta)$ from equation (4.45) in equation (4.52) and rearranging gives

$$r \frac{d\sigma_x}{dr} + Y + \tau_c \left(\frac{r}{t \sin\alpha} \right) = 0$$

or

$$d\sigma_x = -Y \frac{dr}{r} - \tau_c \left(\frac{dr}{t \sin\alpha} \right) \quad (4.53)$$

where $\sin\alpha = dr/\sqrt{(dr^2 + dx^2)}$

This is the governing differential equation in the deformation zone for the axial stress in the tube. Rewriting this equation in finite-difference form gives

$$\sigma_{x_1} = \frac{(r_{1-1} - r_1) Y_1}{r_1} + \frac{\tau_{c1}}{t} \sqrt{(r_{1-1} - r_1)^2 + (x_1 - x_{1-1})^2} + \sigma_{x_{1-1}} \quad (4.54)$$

This equation is a function of the shear stress on the tube and it must be determined independently, the wall shear stress within deformation zone of section one may be rewritten as (from section 4.2)

$$\begin{aligned} \tau_{c1} = & \left(-\frac{\mu(1-1)V_1}{2Kh_1} + \left(\frac{\mu(1-1)^2 V_1^2}{4K^2 h_1^2} + \frac{1}{27} \left(\frac{1}{K} + \right. \right. \right. \\ & \left. \left. \frac{1}{4} P_1' h_1^2 \right)^3 \right)^{1/2} \right)^{1/3} + \left(-\frac{\mu(1-1)V_1}{2Kh_1} - \left(\frac{\mu(1-1)^2 V_1^2}{4K^2 h_1^2} \right. \right. \\ & \left. \left. + \frac{1}{27} \left(\frac{1}{K} + \frac{1}{4} P_1' h_1^2 \right)^3 \right)^{1/2} \right)^{1/3} - \frac{1}{2} P_1' h_1 \end{aligned} \quad (4.55)$$

This equation contains the pressure gradient and variation of the tube velocity in the deformation zone and they must be determined separately. Hence the flow of the polymer melt in this region may be expressed as

$$\begin{aligned} Q_1 = Q_1 = & \frac{P_1' h_1^3}{6\mu(1-1)} + \frac{\tau_{c1} h_1^2}{2\mu(1-1)} + \frac{K}{\mu(1-1)} \left(\frac{P_1' h_1^5}{20} + \frac{\tau_{c1}^3 h_1^2}{2} + \right. \\ & \left. \frac{P_1' h_1^4 \tau_{c1}}{4} + \frac{\tau_{c1}^2 P_1' h_1^3}{2} \right) + V h_1 \end{aligned} \quad (4.56)$$

Equations (4.55) and (4.56) may be solved simultaneously in order to determine P_1' and τ_{c1} by iterating P_1' at point 1 in the deformation zone.

Therefore

$$P_1(1) = P_1(1-1) + P_1' \Delta x \quad (4.57)$$

Variation of speed of the tube in the deformation zone may also be included in the analysis. The continuity of flow of metal through the element gives

$$(V+dV) \Delta\theta (t+dt) (r+dr) = Vrt\Delta\theta$$

Ignoring second order smaller quantities gives

$$\frac{dV}{V} = -\frac{dr}{(r+dr)}$$

Rewriting this equation in finite difference form gives

$$V_1 = \frac{V_{1-1}}{\left(1 - \frac{r_{1-1} - r_1}{r_{1-1}}\right)} \quad (4\ 58)$$

The hoop stress in the deformation zone may be rewritten as

$$\sigma_{\theta 1} = \frac{P_1 r_1 \sqrt{(r_{1-1} - r_1)^2 + (x_1 - x_{1-1})^2}}{t (x_1 - x_{1-1})} \quad (4\ 59)$$

The true strain-stress relationship of the tube material in the deformation zone may be shown as

$$Y_1 = Y_0 + K_0 \epsilon_1^n$$

where $\epsilon_1 = \ln (r_1 / r_i)$

Therefore,

$$Y_1 = Y_0 + K_0 \left(\ln \left(\frac{r_1}{r_i} \right) \right)^n \quad (4\ 60)$$

The new shear stress within the zone where deformation of tube has been observed is then given by,

$$\tau (z) = P'_1 h_z + \tau_{c1} \quad (4.61)$$

The parameters to calculate the theoretical results are taken from reference [12-16]. These are $h_1=0.5$ mm, $h_2=0.01$ mm, $L_1=160$ mm, $L_2=30$ mm, $y_0=50$ MNm², $K_0=700$ MNm², $n=0.18$, $D_1=13.52$ mm, $t=2.5$ mm

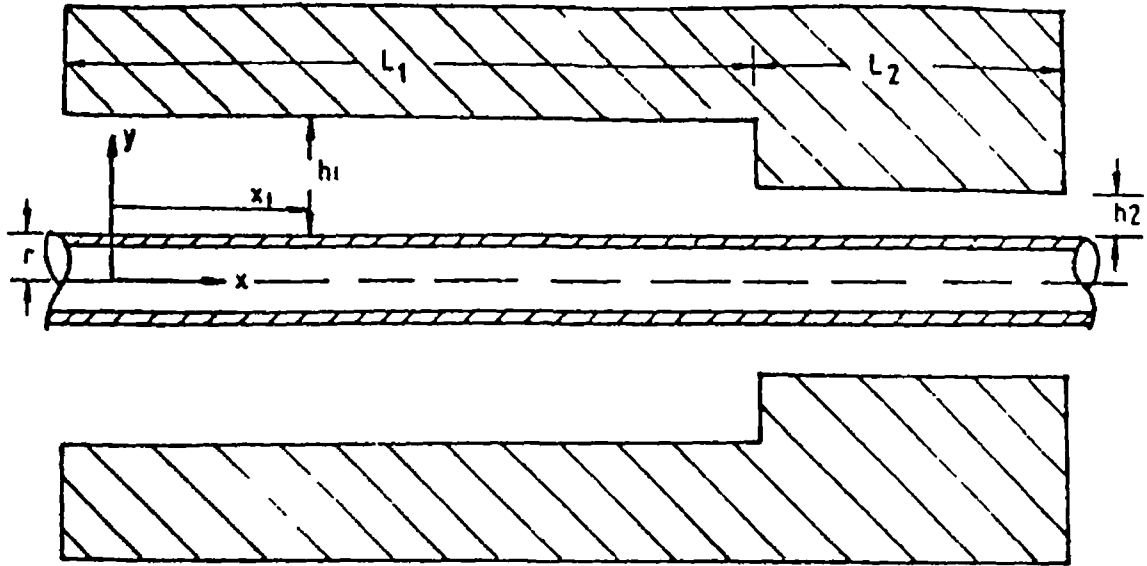
The polymer was Alkathane WVG23 at 130°C and the tube material was Copper. Figure 4.22 shows the theoretical change in the viscosity of polymer from the entrance of the plasto-hydrodynamic unit. The viscosity of the polymer increases in the first part of the unit. In the second part, the viscosity decreases upto a certain value. It is also seen that the viscosity increases with the increase in the tube velocity.

Figure 4.23 shows the magnitude of change in the shear stress within the deformation zone in the unit for different velocity of tube. The deformation increases and then decreases gradually upto the step. The change is sharper at higher velocity than at lower velocity.

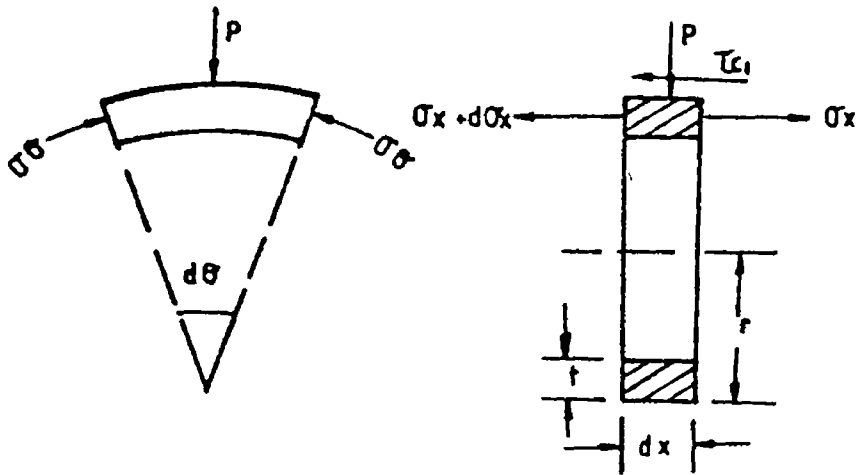
Figures 4.24 and 4.25 illustrate the theoretical hydrodynamic pressure within the unit for tube velocity of 0.3 m/s and 0.5 m/s respectively. In these figures the present solution in which the change in viscosity has been included are compared with the pressure profile from experiment [16] and with the theoretical pressure predicted in reference [12-16]. The initial pressure in the first part of the unit and final pressure in the second part of the unit are zero. For the present solution, the pressure in the first part increases in somewhat non-linear manner. In the second part of the unit the pressure decreases linearly but near the end of the second part there is a large drop of pressure. As evident from Figures 4.24 and 4.25 with the increase in the tube

velocity the pressure also increases. In the theoretical solution of Panwher et al [12-16] pressure only can be obtained within the deformation zone of the unit. From the Figures (4 24 and 4 25) it can be seen that the present theoretical pressure profiles are closer to that of the experimental profiles in the first part of the unit than the theoretical profile by Panwher et al [12-16]. There was no experimental data available at any intermediate position of the second section of the unit from reference [12-16]. As a result no comparison could be made.

Figure 4 26 shows comparisons of the percentage reduction in diameter for different speeds of the tube both theoretically and experimentally. Theoretically, these reductions increase with the increase in velocities. After a tube velocity of 0.4 m/s they become almost constant as wall shear stress reaches the critical value. The reduction obtained by present solution is different than that by Panwher et al [12-16]. From the experimental curve it appears that the reductions do not vary much with the tube velocity as predicted by theory. However, the present theoretical prediction of reduction is marginally closer to the experimental results [16] than the previous prediction at higher tube velocity. Figure 4 27 displays the coating thickness on tube due to the hydrodynamic action. The experimental and theoretical thickness profile are the same as Figure 4 26.



(a)



(b)

(c)

Figure 4.19 (a) Geometrical configuration of the stepped bore reduction unit and the tube

(b) Stresses acting on a small element of the tube

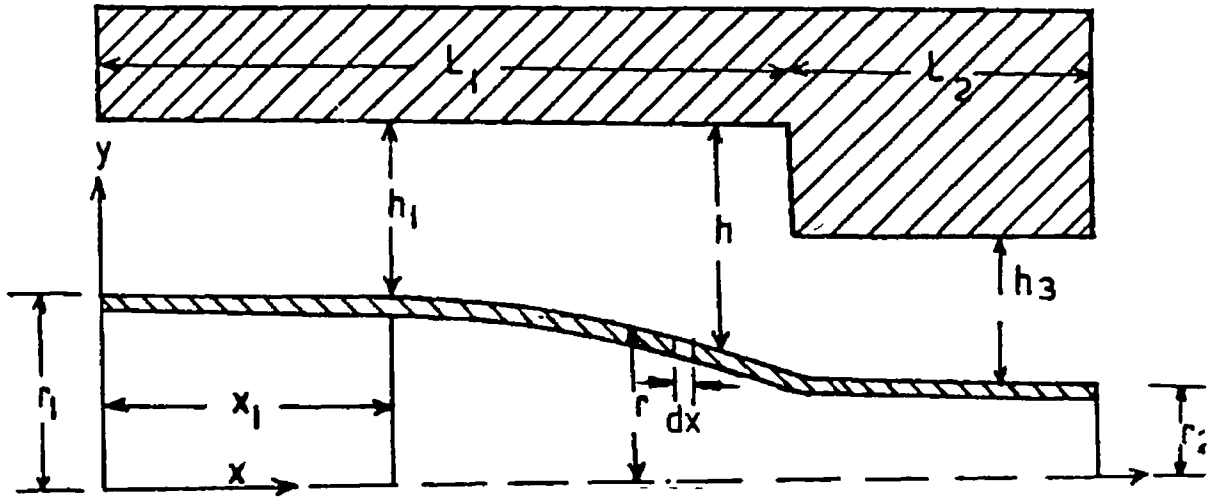


Figure 4.20. Geometry used in the analysis

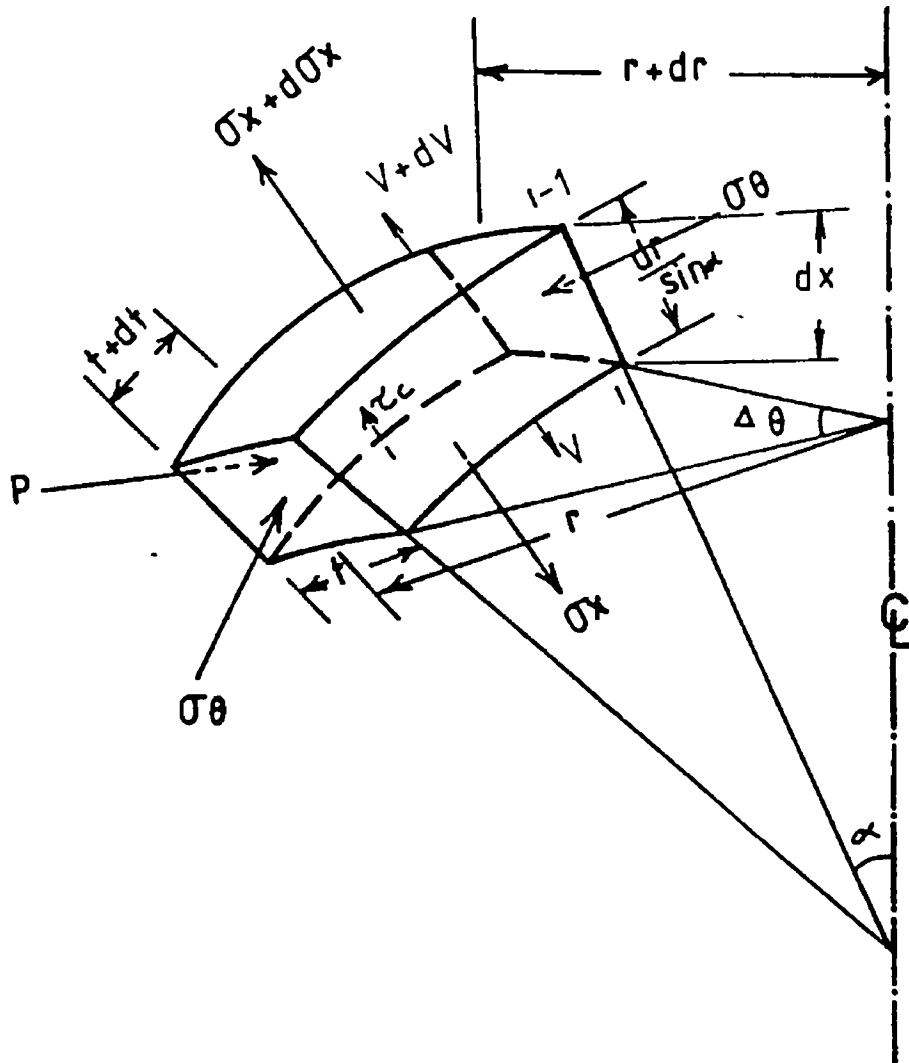


Figure 4.21. Stresses acting on a small element of the tube

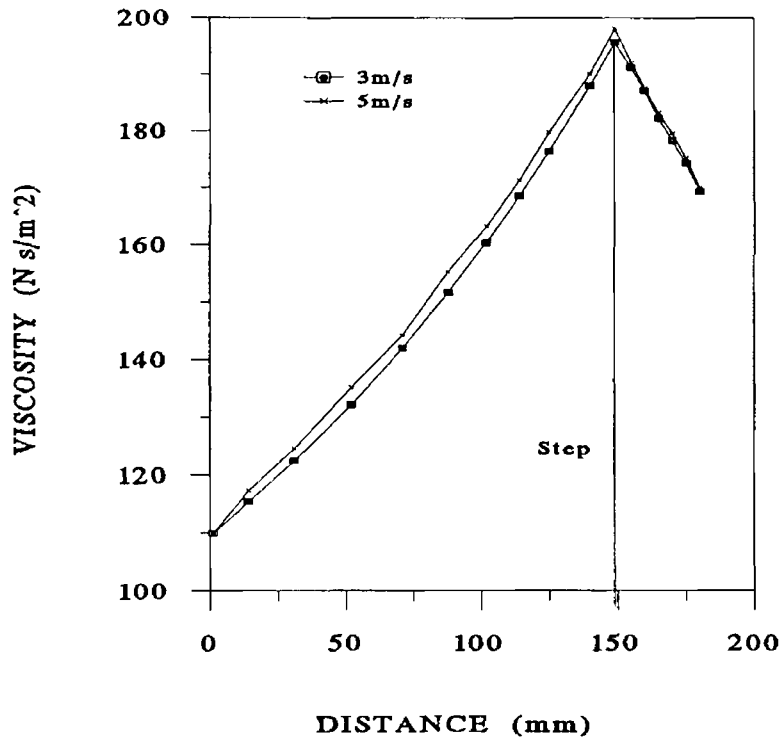


Figure 4 22 Theoretical change in viscosity along the unit during tube sinking

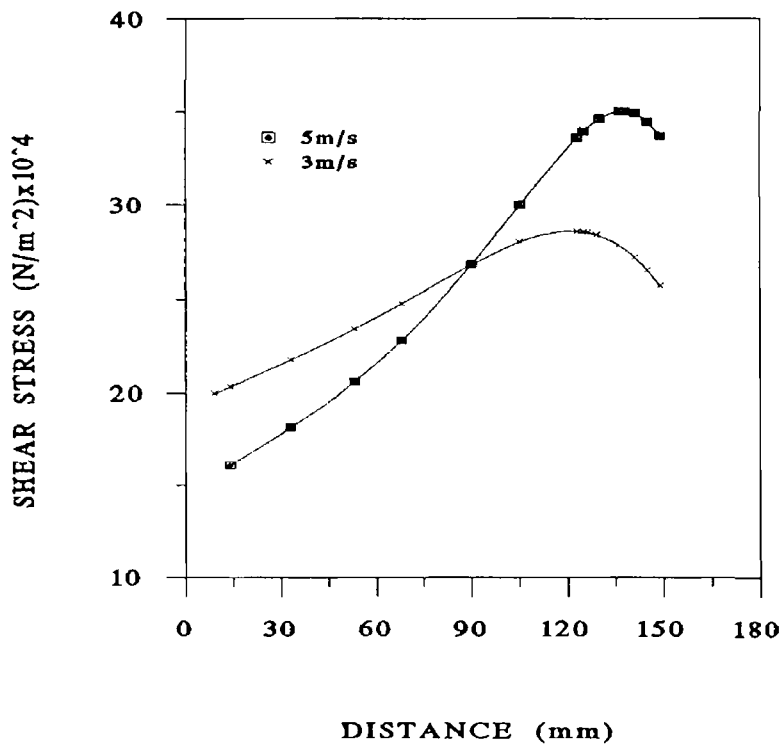


Figure 4 23 Theoretical change in shear stress along the unit within the deformation zone during tube sinking process

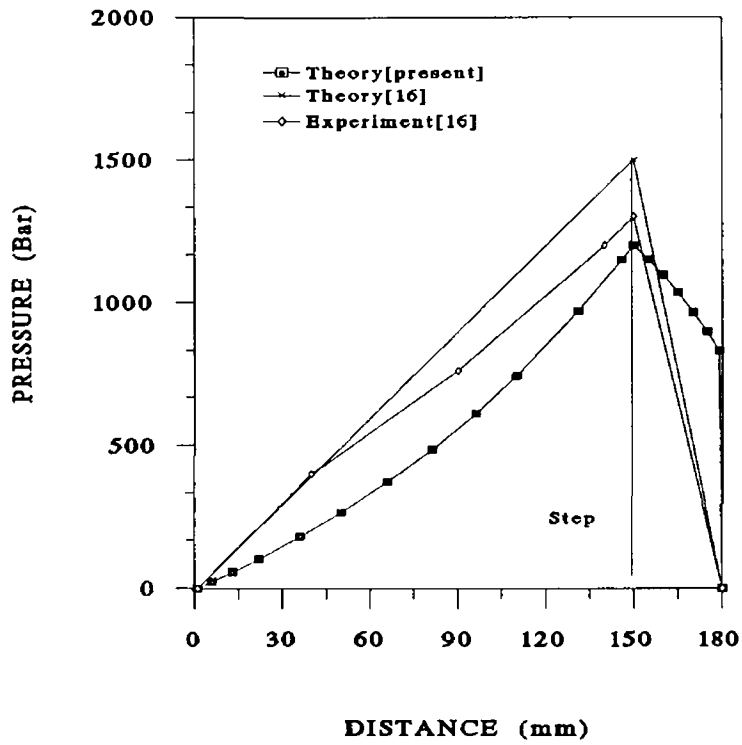


Figure 4 24 Pressure distribution within the unit during tube sinking velocity 0.3m/s

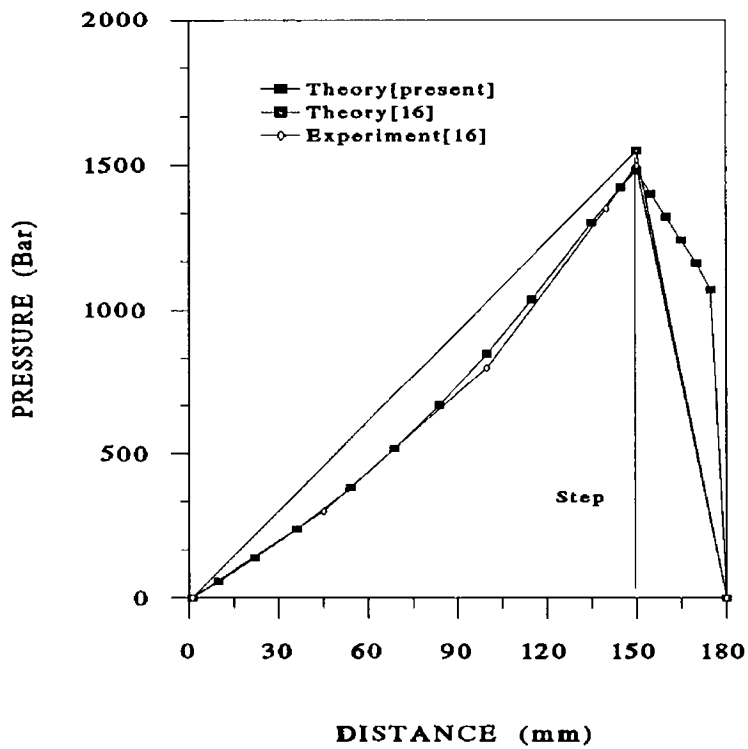


Figure 4 25 Pressure distribution within the unit during tube sinking velocity 0.5m/s

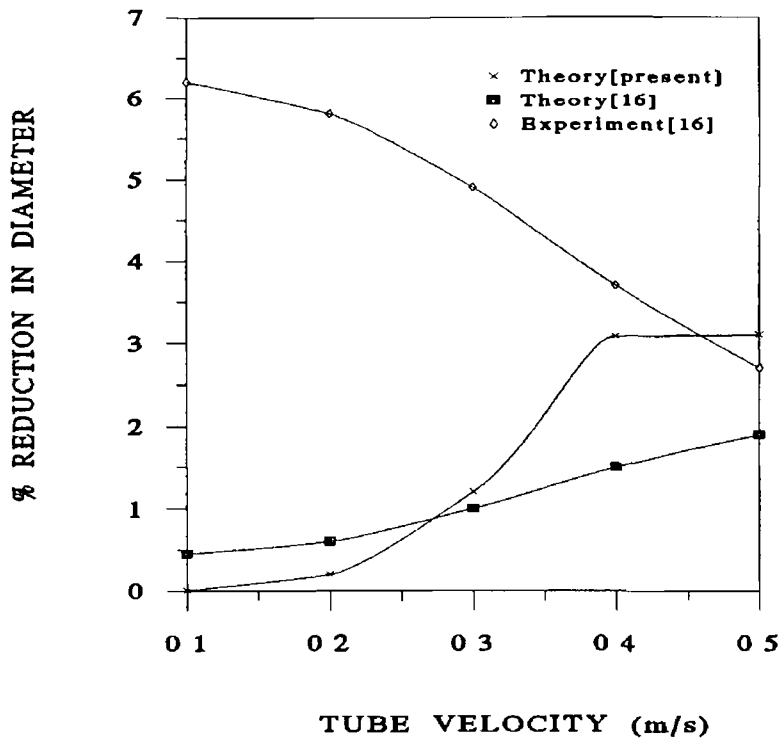


Figure 4 26 Percentage reduction in diameter during tube sinking process

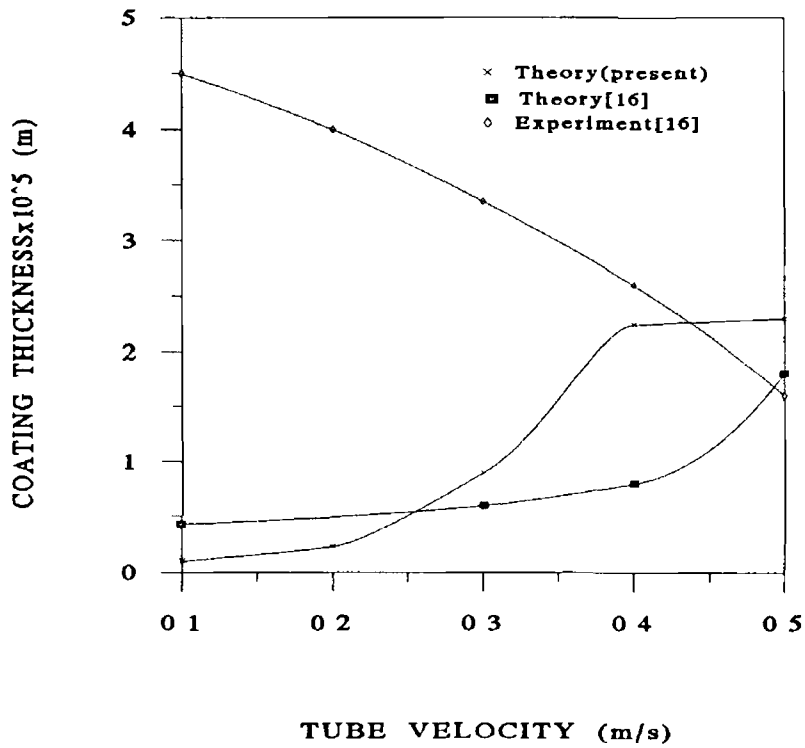


Figure 4 27 Coating thickness developed on tube surface during tube sinking process

4.3.3 Analysis for strip drawing

In the plasto-hydrodynamic strip drawing process, a strip is pulled through a rectangular orifice of stepped bore which is filled with polymer melt. Analytical results have been presented in references [20-25] for plasto-hydrodynamic strip drawing through a stepped parallel bore unit without accounting for the change in the viscosity of the polymer melt. The change in shear stress was not shown in that analysis due to the change in viscosity and reduction of strip.

Here a non-Newtonian hydrodynamic strip drawing solution has been presented in which the change in viscosity has been included with the change in temperature and pressure within plasto-hydrodynamic pressure unit and compared with the experimental results [24]. This strip drawing analysis incorporating change in viscosity was published as reference [62].

The volumetric flow rate and wall shear stress at a longitudinal section of the strip (section A in Figure 4.28) given in section 4.2. The wall shear stress at the rear face of the section B of strip (Figure 4.28) is given by

$$\begin{aligned} \tau_{c31} = & \left(-\frac{\mu(1-1)V}{2Kh_3} + \left(\frac{\mu(1-1)^2V^2}{4K^2h_3^2} + \frac{1}{27} \left(\frac{1}{K} + \right. \right. \right. \\ & \left. \left. \left. \frac{1}{4} P_1 \left(h_3^2 \right)^3 \right)^{1/2} \right)^{1/3} + \left(-\frac{\mu(1-1)V}{2Kh_3} - \left(\frac{\mu(1-1)^2V^2}{4K^2h_3^2} \right. \right. \right. \\ & \left. \left. \left. + \frac{1}{27} \left(\frac{1}{K} + \frac{1}{4} P_1 \left(h_3^2 \right)^3 \right)^{1/2} \right)^{1/3} - \frac{1}{2} P_1 \left(h_3 \right. \right. \right. \end{aligned} \quad (4.62)$$

The yielding position of the strip inside the dieless unit :

Consider a point at a distance x_1 (Figure 4.28) from entry of the unit, where yielding of strip has just commenced. Principal stresses acting on the strip are

$$\sigma_1 = \sigma_{x1} \quad \text{and} \quad \sigma_2 = \sigma_3 = -P_1,$$

where σ_{x1} is the axial stress and P_1 is the radial pressure at point x_1 .

Equilibrium of forces on the strip in x direction gives

$$P_1 = \frac{P_m X_1}{L_1} \quad (4.63)$$

The yield characteristics of the strip are taken of the form

$$Y = Y_0 + K_0 \epsilon^n \quad (4.64)$$

Therefore, yielding occurs as soon as $Y = Y_0$

Substituting equations (4.63)- (4.64) into equation $(P_1 + \sigma_{x1} = Y_0)$ and rearranging, position of yield in the strip may be expressed as

$$x1 = \frac{Y_0}{\frac{2\tau_{c1}}{t_1} + \frac{2\tau_{c3}}{W_1} + \frac{P_m}{L_1}} \quad (4.65)$$

Here W_1 is the width of strip in section B and τ_{c3} is the shear stress at that section according to Figure (4.29)

This equation enables the prediction of the position where the strip starts to yield plastically in the first section of the unit

Deformation zone

Consider a section of the unit within which the strip is plastically deformed as shown in Figure 4.29. Since the variation of strip dimension is to be deformed theoretically, and is not pre-defined as a function of x , the equations containing this variable cannot be solved analytically. Hence a finite difference technique is adopted to solve the equations governing the zone assuming that between any two points of distance dx apart on the deforming strip, the deformation takes place linearly. Therefore,

$$\begin{aligned} \frac{dt}{dx} &= b \\ \frac{dw}{dx} &= b* \end{aligned} \quad (4.66)$$

Expressing this equation in finite-difference form gives,

$$\begin{aligned} t_1 &= t_{1-1} - b\Delta x \\ W_1 &= W_{1-1} - b*\Delta x \end{aligned} \quad (4.67)$$

where Δx is the length increment in the deformation zone. The "*" term refers to

section B and without "*" refers to section A

Similarly, the variation in gap in these sections gives

$$\begin{aligned} h_1 &= h_{1-1} + \frac{1}{2} b \Delta x \\ h_1^* &= h_{1-1} + \frac{1}{2} b^* \Delta x \end{aligned} \quad (4.68)$$

where b and b^* are the deformation profiles within the distance Δx in sections A and B (Figure 4.29 a) respectively

The change in the area of the strip will cause the velocity to change in the deformation zone, hence this should be included in the analysis. Considering the continuity of flow of metal, it can be shown that the current velocity is given by,

$$V_1 = V_{1-1} \left(\frac{W_{1-1} t_{1-1}}{W_1 t_1} \right) \quad (4.69)$$

Considering a small element of the deformed strip (Figure 4.29 b and 4.29 c), the equilibrium of forces in x-direction gives

$$\begin{aligned} \sigma_{x1} W_1 t_1 &= (\sigma_{x1} + d\sigma_{x1}) (W_1 + dW_1) (t_1 + \\ dt_1) &+ 2P_1 \sin\theta \frac{dt_1}{2\sin\theta} W_1 + 2\tau_{c1} \cos\theta \frac{dt_1}{2\sin\theta} W_1 + \\ 2P_1^* \sin\beta \frac{dW_1}{2\sin\beta} t_1 &+ 2\tau_{c1}^* \cos\beta \frac{dW_1}{2\sin\beta} t_1 \end{aligned} \quad (4.70)$$

Equation(4.70) can be simplified to give,

$$\begin{aligned} d\sigma_{x1} &= -\frac{dt_1}{t_1} (P_1 + \sigma_{x1}) - \frac{dW_1}{W_1} (P_1^* + \\ \sigma_{x1}) &- \tau_{c1} \cot\theta \frac{dt_1}{t_1} - \tau_{c1}^* \cot\beta \frac{dW_1}{W_1} \end{aligned} \quad (4.71)$$

Now using the Levy-Mises flow rule, it can be shown that

$$b^* = mb \quad (4.72)$$

where m is constant and is the ratio of the initial width to initial thickness

ie, $m = W_1 / t_1$

Applying the Von-Mises yield criterion

$$P_1 + \sigma_{x1} = Y_1 \quad (4.73)$$

equation (4.71) becomes

$$\sigma_{x1} = Y_1 \left(\frac{t_{1-1}}{t_1} + \frac{W_{1-1}}{W_1} - 2 \right) + \frac{2\tau_{c1}\Delta x}{t_1} + \frac{2\tau_{c1}^*\Delta x}{W_1} + \sigma_{x1-1} \quad (4.74)$$

Equation (4.74) is the governing equation for determining the axial stress in the deformation zone. This equation is a function of shear stresses on the wire and must be determined independent. The wall shear stress at section A can be written as

$$\begin{aligned} \tau_{c1} = & \left(-\frac{\mu(1-1)V_1}{2Kh_1} + \left(\frac{\mu(1-1)^2V_1^2}{4K^2h_1^2} + \frac{1}{27} \left(\frac{1}{K} + \right. \right. \right. \\ & \left. \left. \frac{1}{4} P_1^{-2} h_1^2 \right)^3 \right)^{1/2} \right)^{1/3} + \left(-\frac{\mu(1-1)V_1}{2Kh_1} - \left(\frac{\mu(1-1)^2V_1^2}{4K^2h_1^2} \right. \right. \\ & \left. \left. + \frac{1}{27} \left(\frac{1}{K} + \frac{1}{4} P_1^{-2} h_1^2 \right)^3 \right)^{1/2} \right)^{1/3} - \frac{1}{2} P_1^{-1} h_1 \end{aligned} \quad (4.75)$$

Assuming that the pressure acts equally in section A and B, then for section B the wall shear stress is

$$\begin{aligned} \tau_{c1}^* = & \left(-\frac{\mu(1-1)V_1}{2Kh_1^*} + \left(\frac{\mu(1-1)^2V_1^2}{4K^2h_1^{*2}} + \frac{1}{27} \left(\frac{1}{K} + \right. \right. \right. \\ & \left. \left. \frac{1}{4} P_1^{-2} h_1^{*2} \right)^3 \right)^{1/2} \right)^{1/3} + \left(-\frac{\mu(1-1)V_1}{2Kh_1^*} - \left(\frac{\mu(1-1)^2V_1^2}{4K^2h_1^{*2}} \right. \right. \\ & \left. \left. + \frac{1}{27} \left(\frac{1}{K} + \frac{1}{4} P_1^{-2} h_1^{*2} \right)^3 \right)^{1/2} \right)^{1/3} - \frac{1}{2} P_1^{-1} h_1^* \end{aligned} \quad (4.76)$$

This equation contains the pressure gradient and variation of the strip velocity in the deformation zone and they must be determined separately. Hence the flow of the polymer melt in this region may be expressed as

$$Q_1 = Q_1 = \frac{P_1' h_1^3}{6\mu(1-1)} + \frac{\tau_{c1} h_1^2}{2\mu(1-1)} + \frac{K}{\mu(1-1)} \left(\frac{P_1'^3 h_1^5}{20} + \frac{\tau_{c1}^3 h_1^2}{2} + \frac{P_1'^2 h_1^4 \tau_{c1}}{4} + \frac{\tau_{c1}^2 P_1' h_1^3}{2} \right) + V h_1 \quad (4.77)$$

Equations (4.76) and (4.77) may be solved simultaneously in order to determine P_1' and τ_{c1} by iterating P_1' at point 1 in the deformation zone.

Therefore

$$P_1(1) = P_1(1-1) + P_1' \Delta x \quad (4.78)$$

Equation (4.78) will give the hydrodynamic pressure at any point in the deformation zone. Substituting the value P_1' in equation (4.76), the shear stress τ_{c1} , in section B, in the deformation zone can be calculated.

Percentage reduction in strip

The true strain-stress relationship of the strip in the deformation zone may be shown as

$$Y_1 = Y_0 + K_0 \epsilon_1^n$$

where $\epsilon_1 = 2 \ln(a_1/a_0)$

Therefore,

$$Y_1 = Y_0 + K_0 \left(2 \ln \left(\frac{a_1}{a_0} \right) \right)^n \quad (4.79)$$

This equation represents the yield stress of the strip, incorporating strain hardening effect.

Now the material will continue to deform until the Von-Mises criterion given below

is satisfied,

$$P_1 (1) + \sigma_{x1} \geq Y_1 \quad (4.80)$$

Substituting the pertinent values, equation(4.74) can be iterated until equation (4.80) is satisfied, to evaluate the values of b and b^* . Once the parameters b and b^* are determined the percentage reduction in strip size is given by,

$$PRT = \left(1 - \frac{t_2}{t_1}\right) * 100 \quad (4.81)$$

$$PRW = \left(1 - \frac{W_2}{W_1}\right) * 100 \quad (4.82)$$

The new shear stress within the zone where deformation of strip has been observed is then given by,

$$\tau (1) = P_1' h_1 + \tau_{c1} \quad (4.83)$$

Theoretical results have been calculated on the basis of equations derived as in the theoretical analysis. In order to calculate theoretical results, the following values of the parameters were used based on reference [24]

$B=5.6 \times 10^{-1} \text{ } ^\circ\text{C}/\text{Nmm}^2$, $C=0.1 \text{ } ^\circ\text{C}/\text{mm}$, $\alpha=0.017 \text{ } ^\circ\text{C}$, $DX=1$, mm, $h_1=0.3$ mm, $h_2=0.02$ mm, $h_3=0.13$ mm $K=5.0 \times 10^{11}$ m^4/N^2 , $L_1=150$ mm, $L_2=30$ mm, $t_1=1.59$ mm, $W_1=12.7$ mm, $y_0=75$ MNm^2 , $K_0=600$ MNm^2 , $n=0.6$

The polymer was Alkathane WVG23 at 130°C and the strip material was Copper. Figure 4.30 shows the theoretical change in the viscosity of the polymer from the entrance of the plasto-hydrodynamic unit. In the first part of the unit the viscosity increases up to the step. In the second part, the viscosity decreases up to a certain value. With the increase in strip velocity the viscosity also increases.

Figure 4.31 shows the theoretical magnitude in change in the shear stress within the

unit due to the change in the shear rate and viscosity. In the first part, before the deformation the shear stress remains constant, after the yielding point it increases linearly up to the step where the deformation of strip stops. In the second part there is a large drop in the shear stress and it remains constant up to the exit of the unit. The shear stress within the deformation zone increases with the increase in the strip velocity.

Figures 4.32 and 4.33 illustrate the theoretical hydrodynamic pressure within the unit for a strip velocity of 0.1 m/s and 0.25 m/s respectively. In these Figures the present solution in which the change in viscosity has been included are compared with the pressure profile from experiment [24] and with the theoretical pressure predicted in reference [24]. In the present solution, the theoretical pressure has been generated for each small increment of length in the plasto-hydrodynamic pressure unit. The initial pressure in the first section of the unit and final pressure in the second section of the unit is zero. For the present solution, the pressure in the first section increases linearly before the deformation zone. After that zone, it also increases linearly but at a different rate. In the second section of the unit the pressure decreases linearly but near the end of the second section there is a large drop of pressure. With the increase in strip velocity the pressure also increases. In the theoretical solution of Memon [24] pressure only can be obtained at the step of the unit. From the Figures (4.32 and 4.33) it can be seen that the present theoretical pressure profiles are closer to that of the experimental profiles in the first section of the unit than the theoretical profile by Memon [24]. In the experiment the pressure was not measured in the second section of the unit. The only assumption made was that the pressure decreases in this part linearly from the maximum to zero.

Figures 4.34, 4.35 and 4.36 show comparisons of the percentage reduction in thickness, width and area for different speeds of the strip both theoretically and experimentally. Theoretically, these reductions increase with the increase in velocities. After a strip velocity 0.4 m/s they become almost constant. The reduction obtained by present solution is less than that of Memon's [24] theoretical solution. From the experimental curve it appears that the reductions do not vary much with the strip velocity as predicted by theory. However, the present theoretical prediction of reduction fairly compares with the experimental curve at higher velocity.

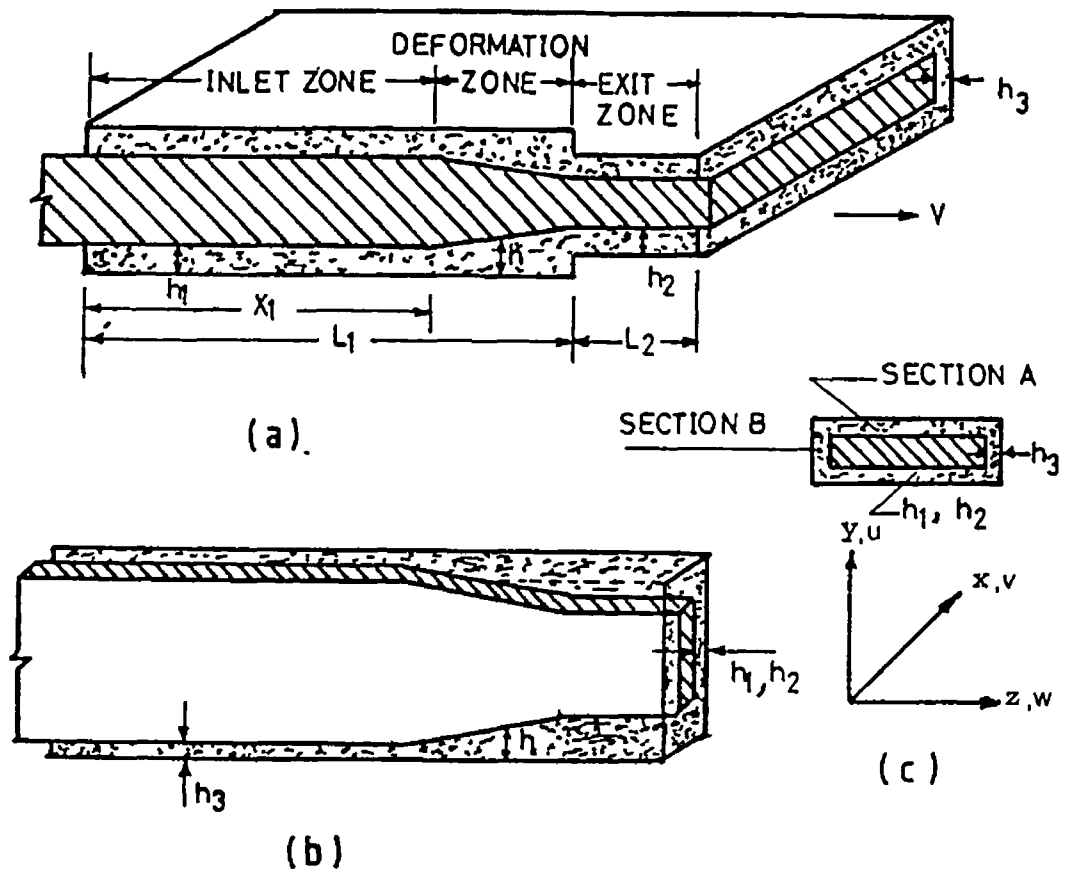


Figure 4.28. Schematic diagram of the process

(a) Zones and deformation profile for thickness

(b) Deformation profile for width

(c) Sections A and B and directions of x, y, z

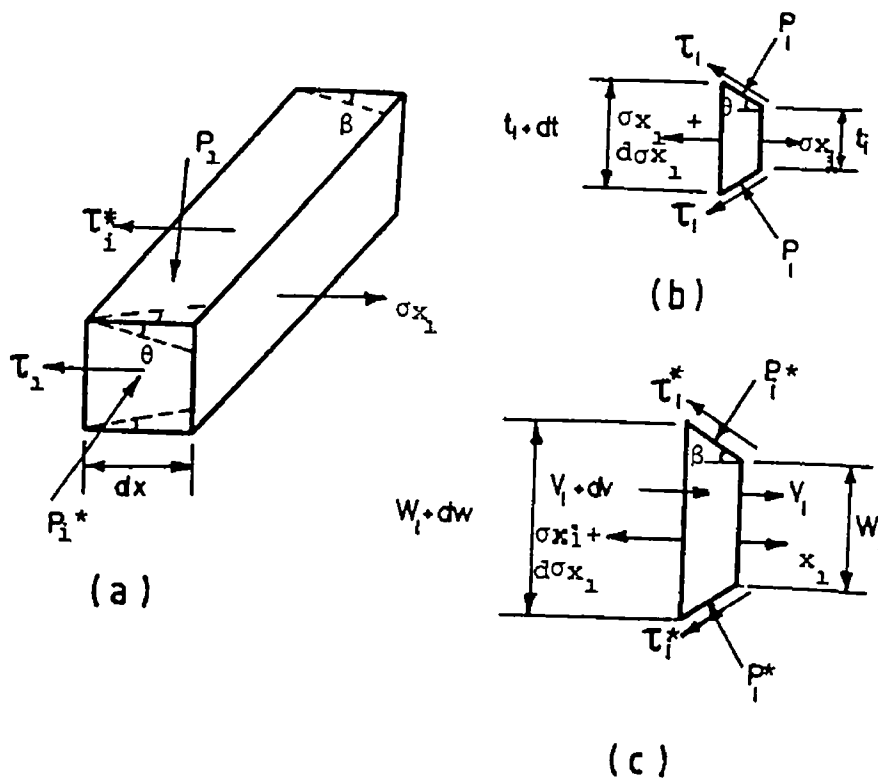


Figure 4.29 Stresses acting on a small element

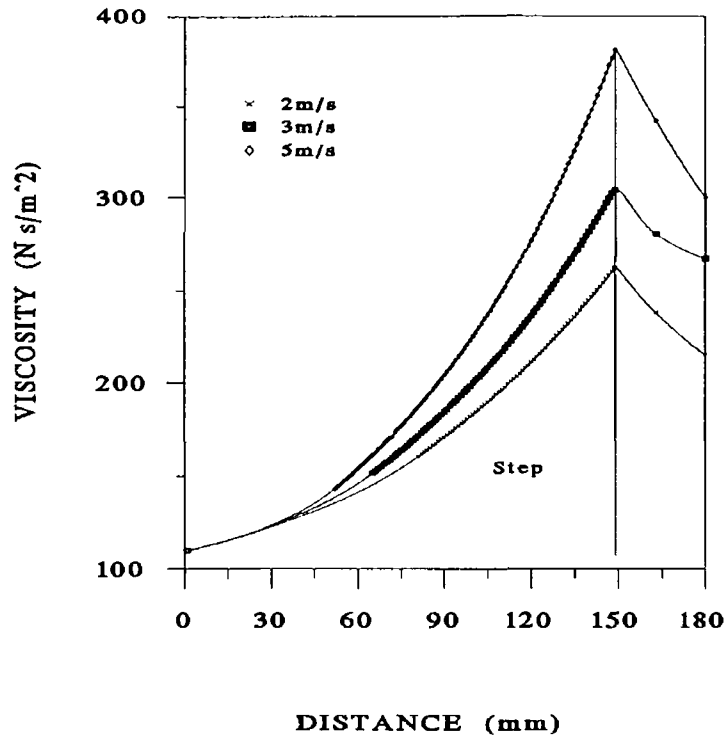


Figure 4 30 Theoretical change in viscosity during strip drawing

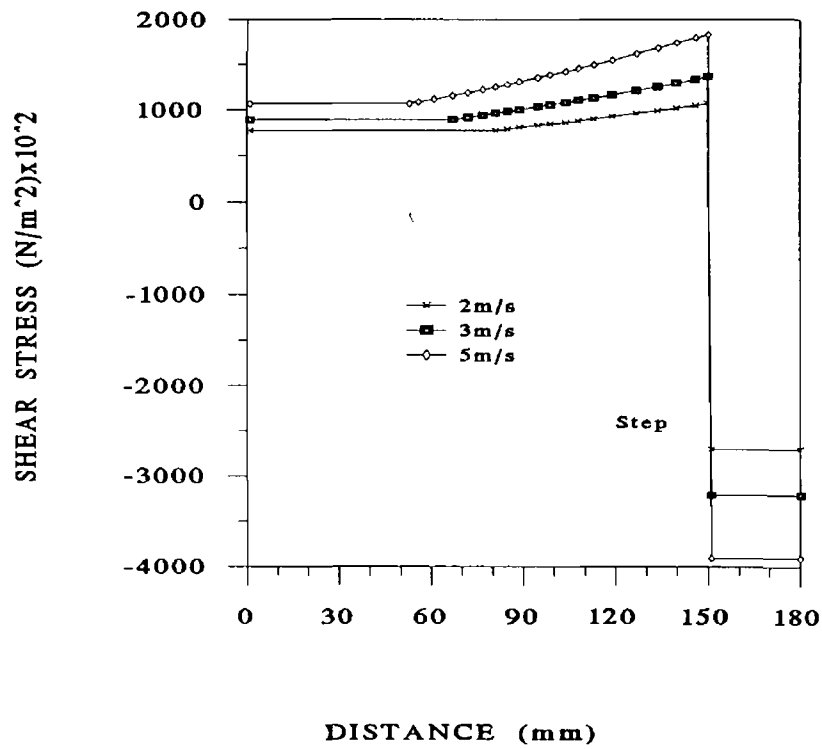


Figure 4 31 Theoretical change in shear stress during strip drawing

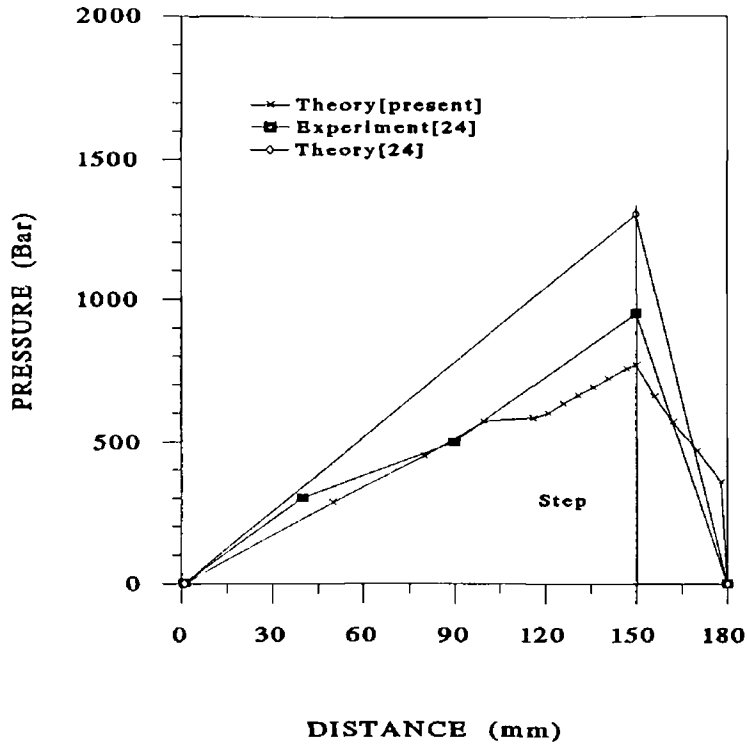


Figure 4 32 Pressure distribution within the unit for strip velocity 0 1m/s

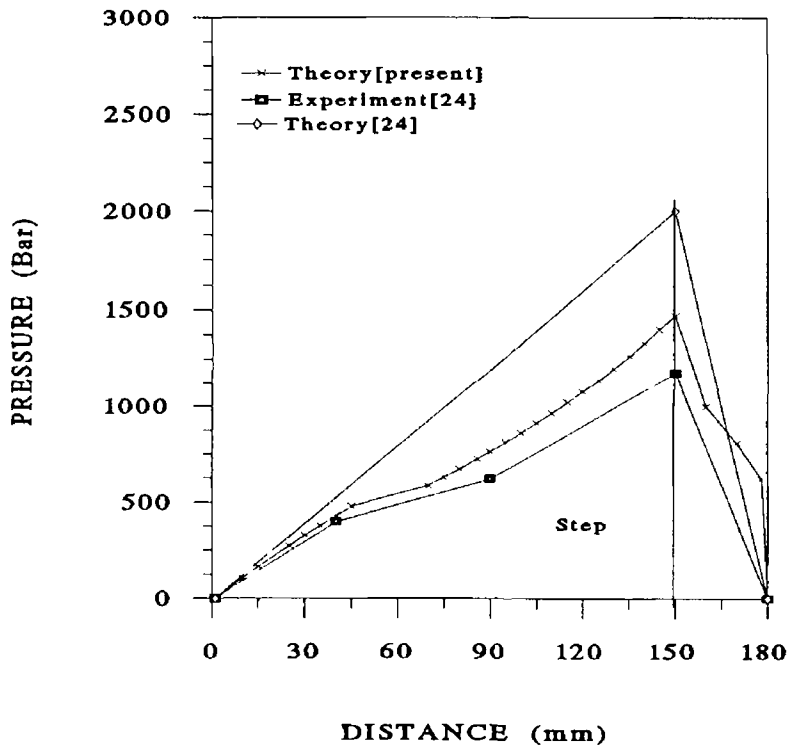


Figure 4 33 Pressure distribution within the unit for strip velocity 0.25 m/s

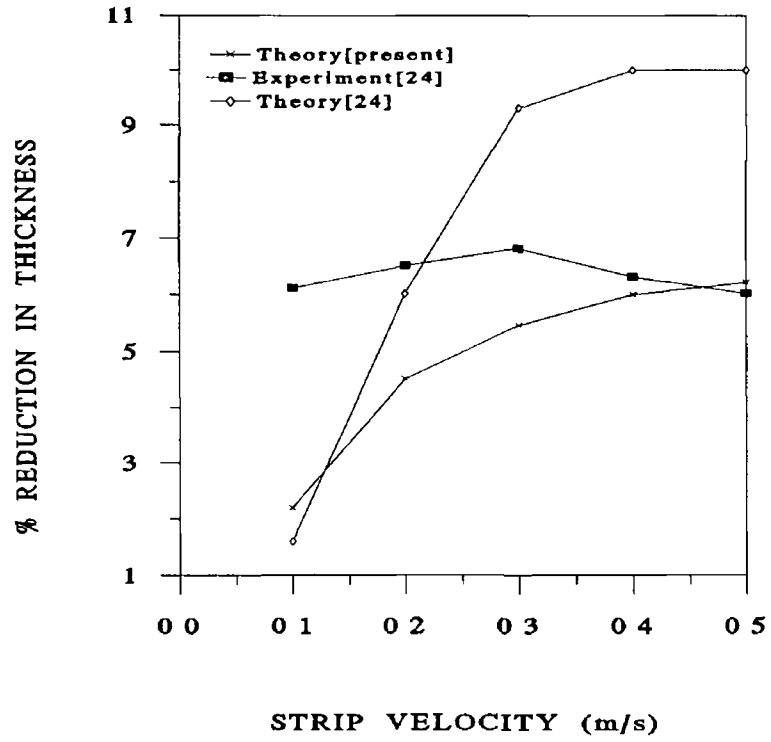


Figure 4 34 Percentage reduction in thickness during strip drawing process

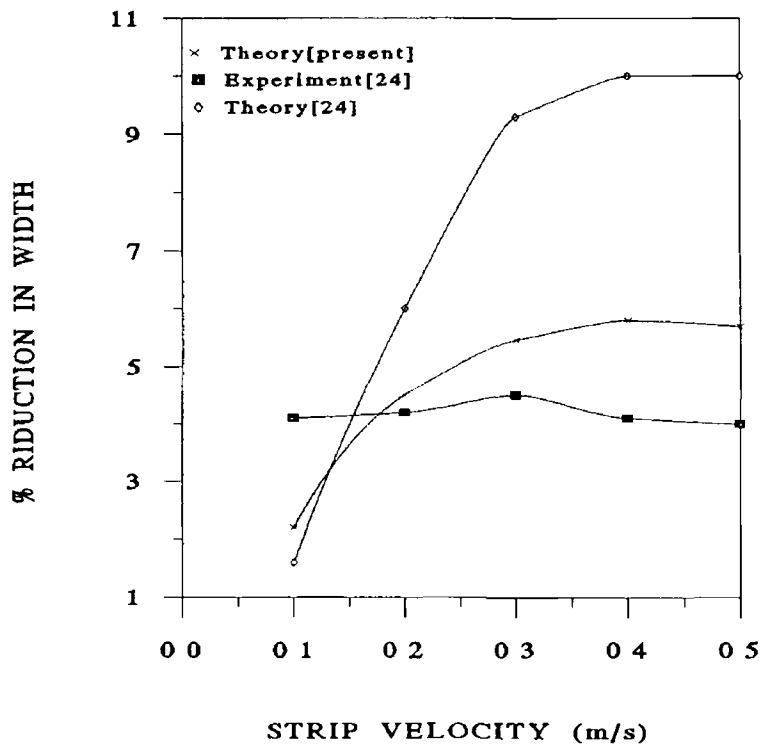


Figure 4 35 Percentage reduction in width during strip drawing process

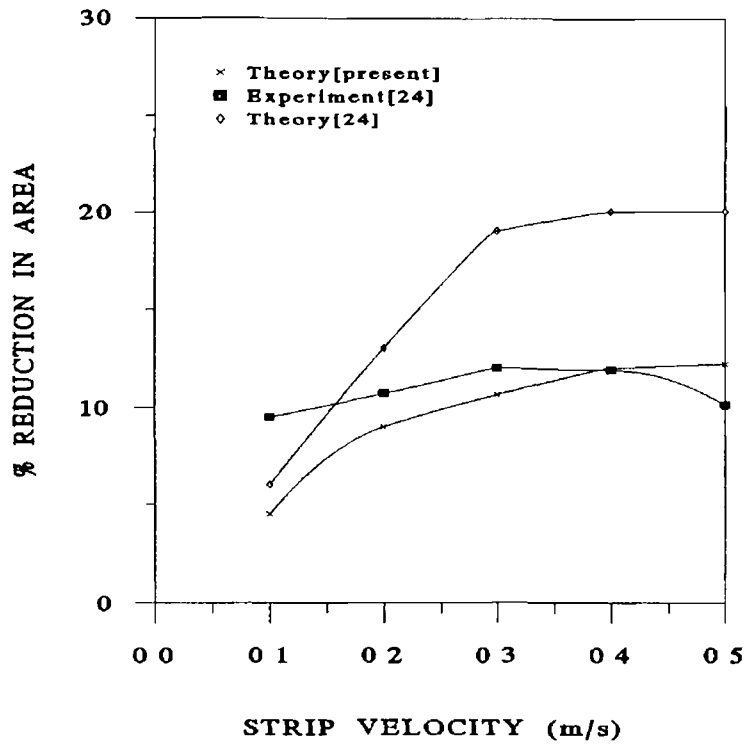


Figure 4 36 Percentage reduction in area during strip drawing process

CHAPTER FIVE

PLASTO-HYDRODYNAMIC ANALYSIS USING CONVERGING TAPERED, PARABOLIC AND EXPONENTIAL GEOMETRY UNIT

5.1 Introduction

For the drawing of a solid continuum pulled through a conical orifice filled with a viscous fluid, Newtonian solution was first published in references [26-27]. Later another model was developed [28-30] for a tapered unit considering the polymer as a non-Newtonian fluid. In those models the viscosity of the fluid and shear stress were considered to remain constant during the drawing process.

Several authors [35,38] were able to show and confirm experimentally that pressure and temperature invariant representation of the viscosity function is possible and reliable. Also the influence of shearing history of the polymer melt is important for the hydrodynamic pressure [34]. Considering these factors in this chapter a different mathematical model has been developed for the pressure distribution within a tapered bore unit. Theoretical results are obtained for different wire speeds in terms of the changes in viscosity, shear stress (due to the change in shear rate and viscosity) and pressure distributions within the unit. These results have been compared with those from experimental and theoretical results presented elsewhere [28-30].

In previous works models for hydrodynamic pressure have been developed for different types of pressure units such as stepped parallel bore, tapered bore and combined parallel-tapered bore. There are other possible units such as converging parabolic and exponential units which were not investigated before. In this chapter, an attempt has been taken to develop analytical models for these types of units.

5.2 Non Newtonian plasto-hydrodynamic pressure analysis for coating process in a tapered unit

Figure 5.1 shows schematic diagram for a tapered bore plasto-hydrodynamic pressure unit. The following analysis is based on the geometrical configuration

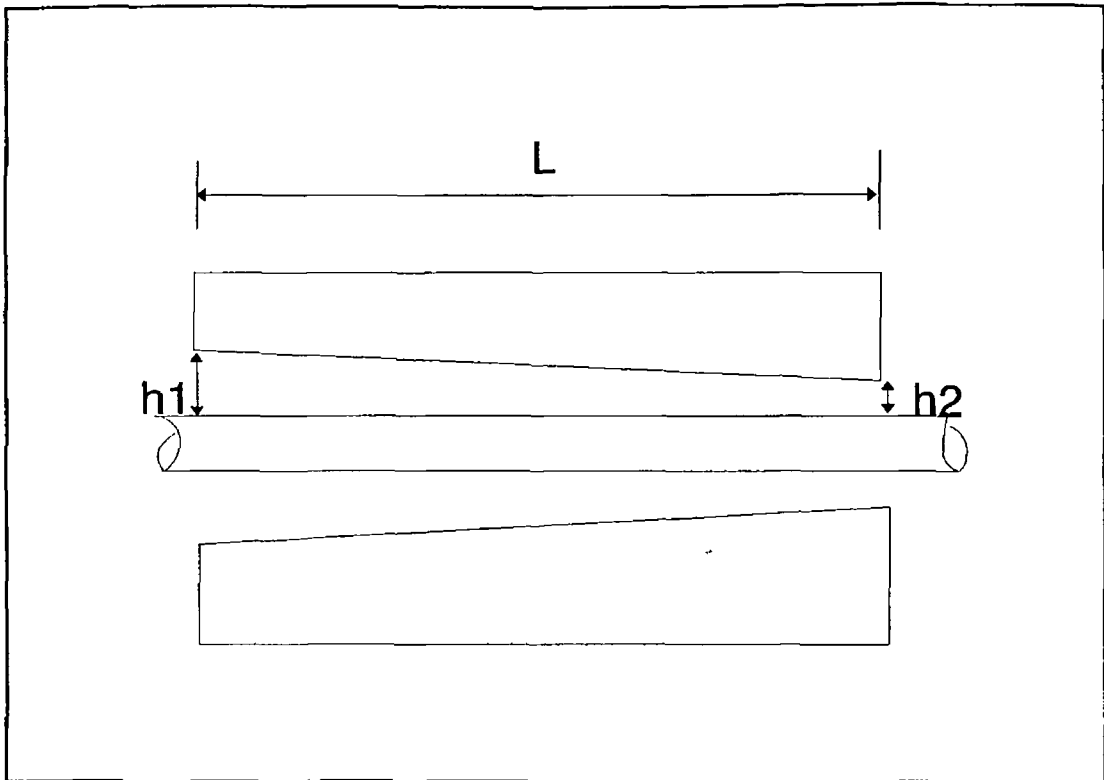


Figure 5 1 Schematic diagram of a tapered bore pressure unit

shown in the figure

To simplify the analysis the following assumptions are made That is to say, the

a)flow of the polymer melt is laminar

b)flow of the polymer melt is axial

c)thickness of the polymer layer is small compared to the dimensions of the unit

The relationship between the pressure and shear stress gradient is given by

$$\left(\frac{dp}{dx}\right) = \left(\frac{d\tau}{dy}\right) \quad (5.1)$$

According to Rabinowitsch[41] the equation for the polymer melt relating shear stress and shear rate is

$$\tau + K\tau^3 = \mu \left(\frac{dU}{dy}\right) = \mu\dot{\gamma} \quad (5.2)$$

Differentiating this equation with respect to y gives

$$\left(\frac{d\tau}{dy}\right) + 3K\tau^2 \frac{d\tau}{dy} = \mu \left(\frac{d^2U}{dy^2}\right)$$

substituting $(d\tau/dy)$ for (dP/dx) from equation (5 1) and integrating it twice w r t y it gives,

$$\left(\frac{dP}{dx}\right) \frac{y^2}{2} + 3K\tau^2 \left(\frac{dP}{dx}\right) \frac{y^2}{2} + C_2y + C_3 = \mu U$$

The boundary conditions are

- (a) at $y = 0$, $U = V$
- (b) at $y = h$, $U = 0$

Using the boundary conditions (a) and (b) the velocity profile becomes

$$U = \frac{P'y^2}{2\mu} + \frac{3KP'}{2\mu} (\tau^2 y^2 - \tau^2 y h) - \frac{P'hy}{2\mu} - \frac{Vy}{h} + V \quad (5 3)$$

The flow of the polymer melt in the unit is ,

$$Q = \int_0^h U dy$$

Substituting the expression for U from equation (5 3) and integrating the flow becomes

$$Q = -\frac{P'h^3}{12\mu} - \frac{K}{\mu} \left(\frac{\tau^2 P'h^3}{4}\right) + \frac{Vh}{2} \quad (5 4)$$

Now, differentiating equation (5 4) with respect to x , integrating it again and noting

that $dQ/dx = 0$ it gives

$$\frac{P'h^3}{6\mu} + \frac{K}{\mu} \left(\frac{\tau^2 P'h^3}{2} \right) = Vh + C4 \quad (5.5)$$

and then integrating this equation it gives

$$P = \frac{6\mu V}{M[1+3K\tau^2]} \left[\frac{V}{h} + \frac{C5}{2h^2} \right] + C6 \quad (5.6)$$

where M can be obtained from the geometry of the unit, $M = (h_1 - h_2)/L$

Also $h = h_1 - Mx$

The boundary conditions are, at $x=0$, $h=h_1$, $P=0$ and $x=L$, $h=h_2$, $P=0$

Substituting these conditions in equation(5.6) it gives,

$$C5 = \frac{2V}{\left(\frac{1}{h_2} - \frac{1}{h_1} \right)}$$

and

$$C6 = -\frac{6\mu V}{M[1+3K\tau^2]} \left[\frac{V}{h_2} + \frac{C5}{2h_2^2} \right]$$

Therefore, the pressure distribution becomes,

$$P = \frac{6\mu V}{M[1+3K\tau^2]} \left[\frac{1}{h} - \frac{1}{h_2} \right] + \frac{3\mu}{M[1+3K\tau^2]} \left[\frac{1}{h^2} - \frac{1}{h_2^2} \right] \frac{2V}{\left(\frac{1}{h_2} - \frac{1}{h_1} \right)} \quad (5.7)$$

If it is considered that the polymer is a Newtonian fluid then the above solution becomes (substituting the value for K equals to zero)

$$P = \frac{6\mu V}{M} \left[\frac{1}{h} - \frac{1}{h_2} \right] + \frac{3\mu}{M} \left[\frac{1}{h^2} - \frac{1}{h_2^2} \right] \frac{2V}{\left(\frac{1}{h_2} - \frac{1}{h_1} \right)} \quad (5.8)$$

Solution procedure.

Introduction of viscosity in pressure distribution:

The viscosity which depends on hydrodynamic pressure and temperature can be expressed as,

$$\mu(j) = \mu(j-1) e^{(-\alpha(T(j) - B DP - T(j-1)))} \quad (5.9)$$

The temperature can be written as

$$T(j) = T(j-1) - C DX \quad (5.10)$$

Introduction of shear rate and viscosity change

Solution of equation (5.2) gives the shear stress where viscosity and shear rate change can be incorporated

$$\tau(j) = \left(\frac{\mu(j-1)\dot{\gamma}(j)}{2k} + \left[\left(\frac{1}{3k} \right)^3 + \left(\frac{\mu(j-1)\dot{\gamma}(j)}{2k} \right)^2 \right]^{\frac{1}{2}} \right)^{\frac{1}{3}} - \left(\frac{-\mu(j-1)\dot{\gamma}(j)}{2k} + \left[\left(\frac{1}{3k} \right)^3 + \left(\frac{\mu(j-1)\dot{\gamma}(j)}{2k} \right)^2 \right]^{\frac{1}{2}} \right)^{\frac{1}{3}} \quad (5.11)$$

In this equation $\dot{\gamma}(j) = V/h(j)$ and $h(j) = h(j-1) - M DX$

Differentiating equation (5.7) with respect to x, the pressure in finite difference form can be written as

$$P(j) = P(j-1) + \left[\frac{6\mu(j-1)V}{M[1+3K\tau(j)^2]} \left[\frac{1}{h(j)^2} \right] + 12\mu(j-1) \frac{V}{M[1+3K\tau(j)^2]} \left[\frac{1}{h(j)^3 \left(\frac{1}{h_2} - \frac{1}{h_1} \right)} \right] \right] dx \quad (5.12)$$

where the magnitude of viscosity and shear stress can be obtained from equations (5.9) and (5.11) respectively.

The initial values are

$P(1)=0, T(1)=$ Polymer melt temperature, $\mu(1)=$ viscosity at $T(1)$.

Theoretical results have been calculated on the basis of equations derived in the theoretical analysis. Two lubricating medium viz. Nylon 6.6 and Borosiloxane were considered for analysis. Different parameter values for Nylon 6.6 are [38,55]:

$B=3.2 \times 10^{-1} \text{ } ^\circ\text{C}/\text{Nmm}^{-2}$, $C=0.03 \text{ } ^\circ\text{C}/\text{mm}$, $\alpha=0.0114 \text{ } ^\circ\text{C}$, $DX=1 \text{ mm}$, $h_1=0.25 \text{ mm}$, $h_2=0.05 \text{ mm}$, $K=10.1 \times 10^{-10} \text{ m}^4/\text{N}^2$, $L=180 \text{ mm}$, initial polymer temperature at the first unit= $280 \text{ } ^\circ\text{C}$, initial polymer viscosity = $63 \text{ N.s}/\text{m}^2$.

Figure 5.2 shows the theoretical change in viscosity of the polymer from the entrance of the plasto-hydrodynamic unit. It can be seen from the figure that the viscosity increases non-linearly and peaks at somewhere along the unit and then decreases gradually to almost its initial value. It is also evident that for higher wire velocity the viscosity maintains higher all along the unit.

Figure 5.3 shows the theoretical change in magnitude of shear stress within the unit due to the change in the shear rate and viscosity. It increases gradually and attains a maximum value at a certain position of the unit and then start decreasing. The shear stress is higher for higher wire velocity.

Figures 5.4, 5.5 and 5.6 illustrates the theoretical hydrodynamic pressure within the unit for wire velocity of 4 m/s, 8 m/s and 12 m/s respectively. In these figures, the results from the present solution have been presented along with the previous solution[28-30]. It may be mentioned that unlike the previous method, the present method considers the change in viscosity and shear stress in the process. The initial pressure at the entry of the unit and final pressure at the exit of the unit are zero. In the previous solution the pressure increases gradually and peaks at a position

determined by h_1 and h_2 [30] and then falls sharply to zero. For the present solution the pressure increases gradually up to certain point (which is variable depending on the wire velocity, viscosity and shear stress) then decreases sharply to zero. The position of maximum pressure is different in the two methods. Also the pressure distribution obtained by the previous model and present model is different. Up to the peak, the pressure is higher by the present method compared to the previous method and the rate of fall is sharper after the peak.

The parameter values for Borosiloxane used for the analysis are [30]

$B=4.2 \times 10^{-1} \text{ } ^\circ\text{C}/\text{Nmm}^2$, $C=0.03 \text{ } ^\circ\text{C}/\text{mm}$, $\alpha=0.016 \text{ } ^\circ\text{C}$, $DX=1 \text{ mm}$, $h_1=0.25 \text{ mm}$, $h_2=0.05 \text{ mm}$, $K=5.6 \times 10^{13} \text{ m}^4/\text{N}^2$, $L=180 \text{ mm}$, Polymer melt temperature 100°C

Figure 5.7 illustrates different theoretical and experimental hydrodynamic pressure within the unit at wire velocity of 0.04 m/s with Borosiloxane as medium. In the figure, the present solution in which the change in viscosity and shear rate have been included are compared with the experimental results from the reference [30]. Also theoretical solution based on non-Newtonian [30] and Newtonian solution has been compared where the viscosity of the polymer and the shear rate are considered to be constant. The initial pressure at the entry of the unit and final pressure at the exit of the unit are zero. From this figure it can be found that the present solution is much closer with the experimental result [30] than the previous [30] theoretical solution as well as the Newtonian solution. Figures 5.8 and 5.9 show these comparisons for wire velocities of 0.08 and 0.16 m/s . The pressure profiles are same as Figure 5.7. From the Figures 5.7 to 5.9 it is clearly evident that the position where peak pressure develops varies for changes in wire velocity. This fact is substantiated by the experimental curves in these figures.

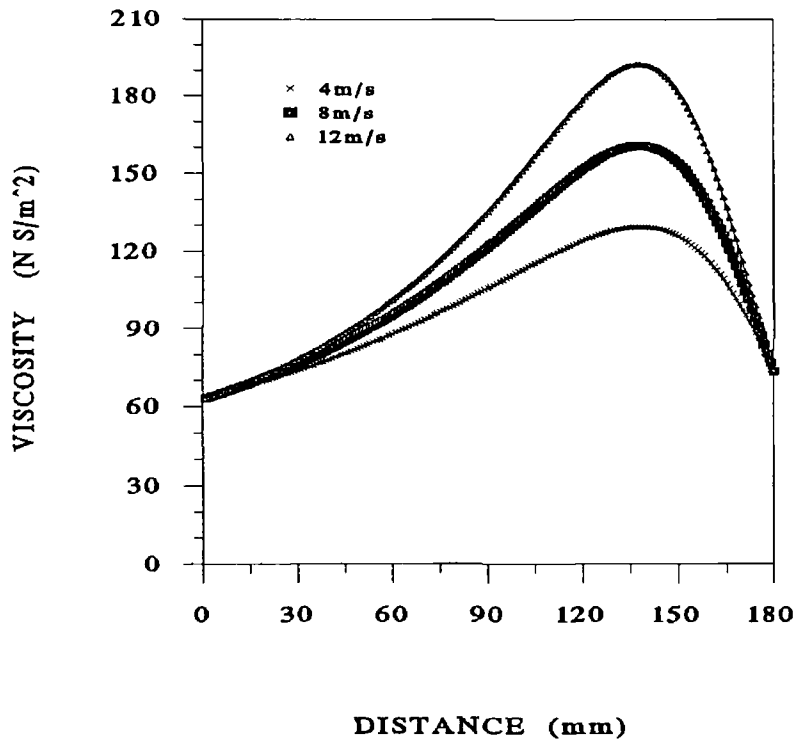


Figure 5.2 Theoretical viscosity distribution within the tapered unit (Polymer-Nylon 6.6)

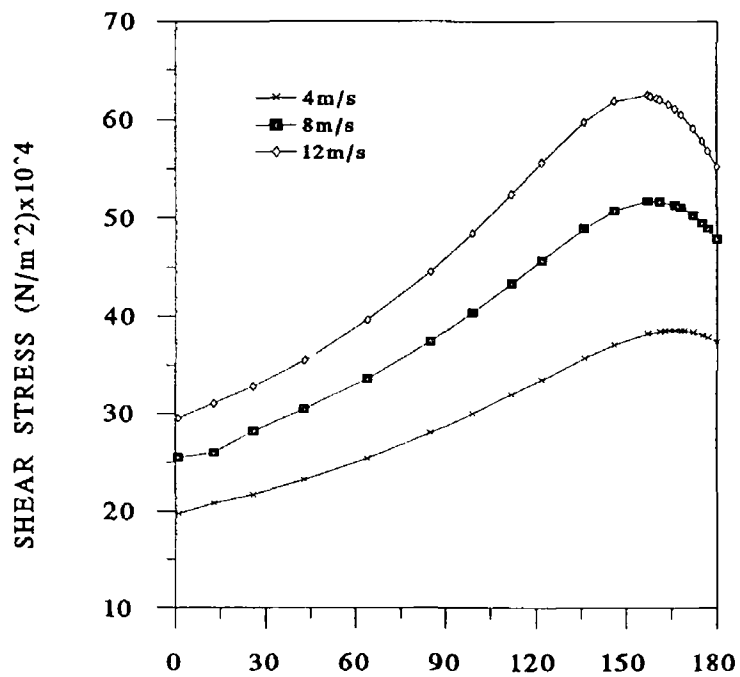


Figure 5.3 Theoretical magnitude in shear stress distribution within the tapered unit (Polymer-Nylon 6.6)

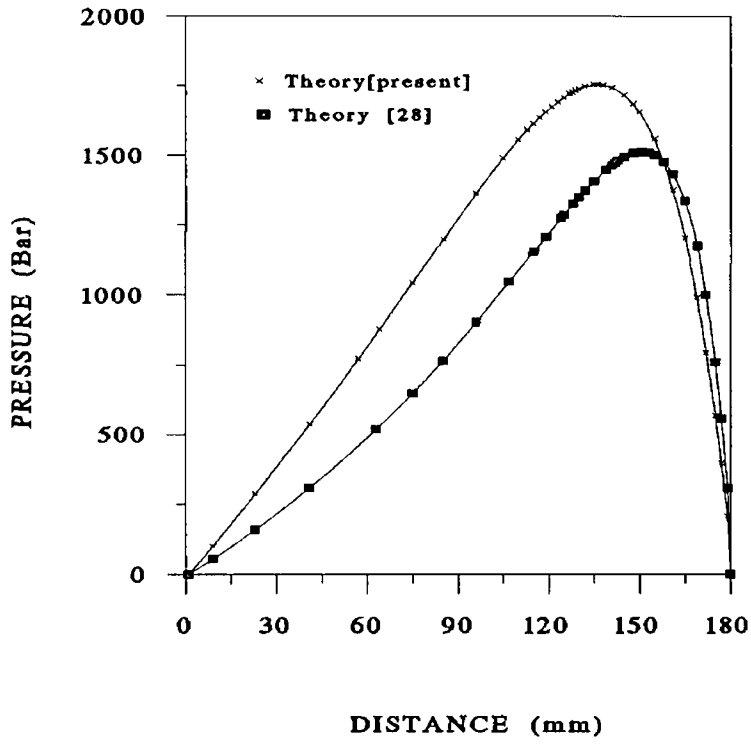


Figure 5 4 Theoretical pressure distribution within the tapered unit for wire velocity of 4m/s (Polymer-Nylon 6 6)

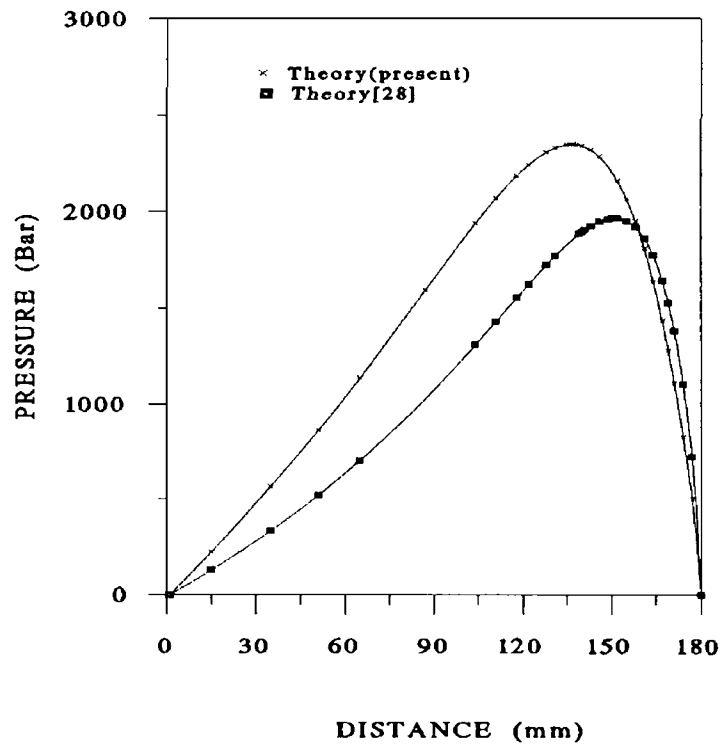


Figure 5 5 Theoretical pressure distribution within the tapered unit for wire velocity of 8m/s (Polymer-Nylon 6 6)

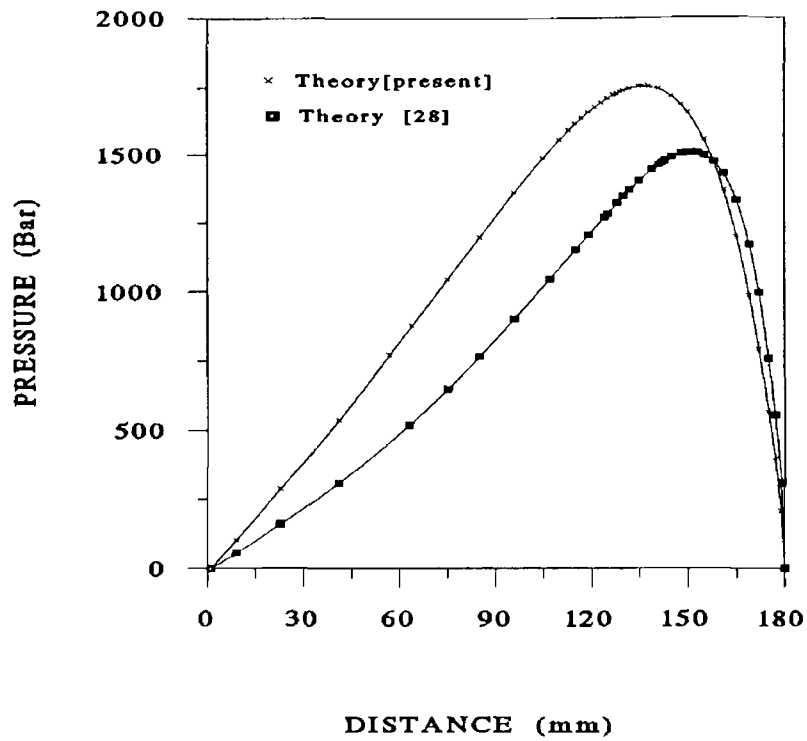


Figure 5.6 Theoretical pressure distribution within the tapered unit for wire velocity of 12m/s (Polymer-Nylon 6.6)

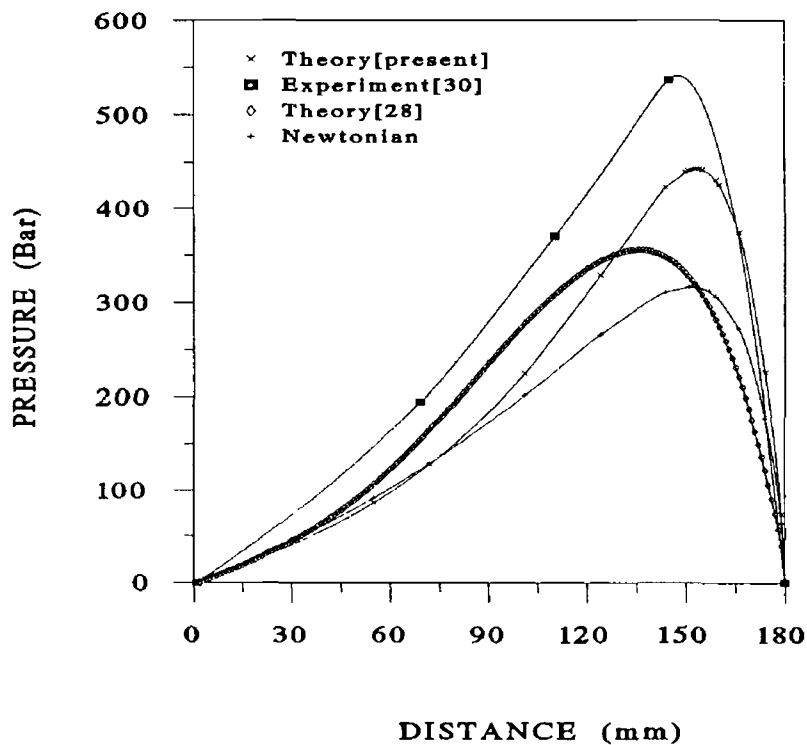


Figure 5.7 Pressure distribution within the tapered unit for wire velocity of 0.04m/s (Polymer-Borosiloxane)

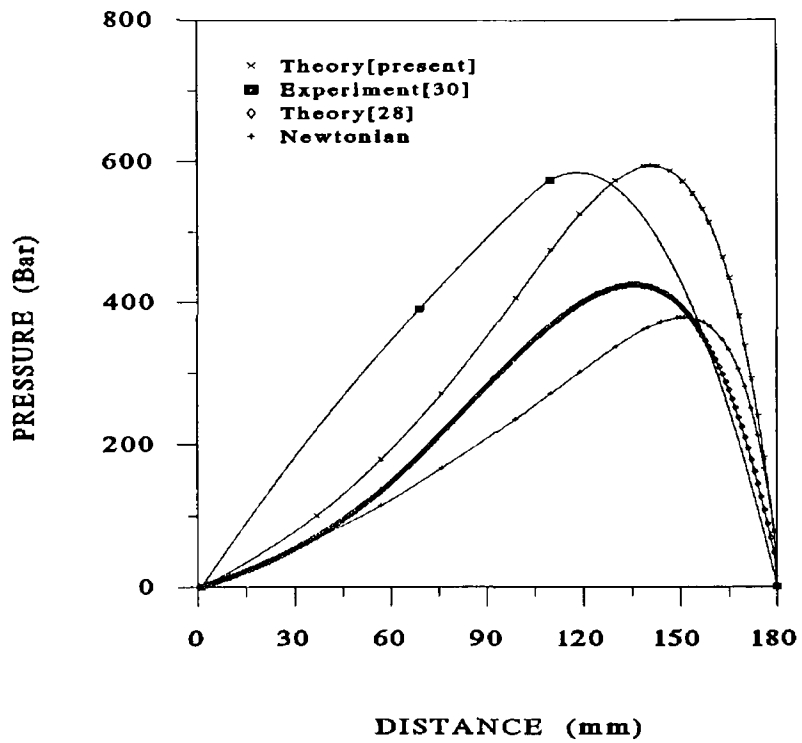


Figure 5 8 Pressure distribution within the tapered unit for wire velocity of 0.08 m/s (Polymer-Borosiloxane)

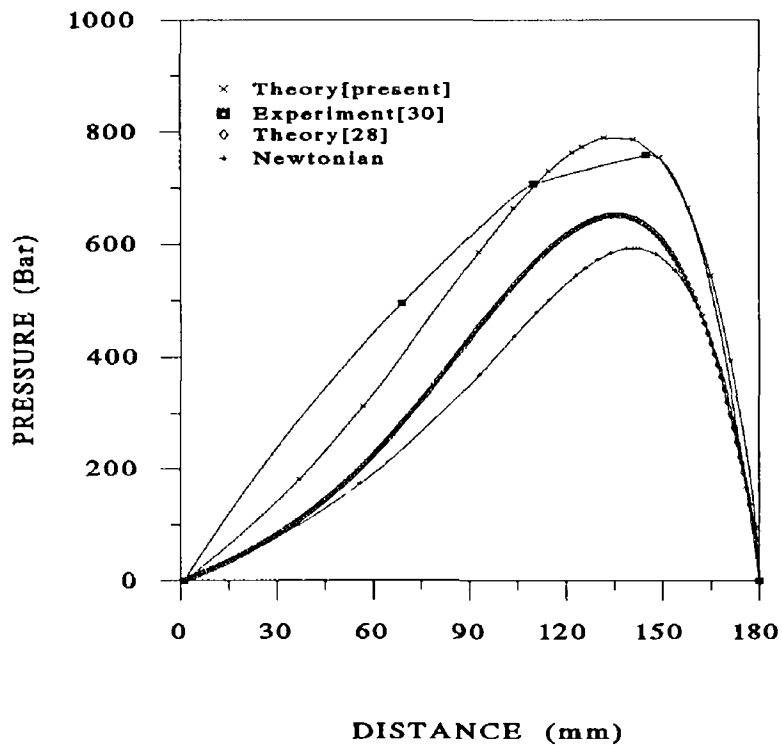


Figure 5 9 Pressure distribution within the tapered unit for wire velocity of 0.16 m/s (Polymer-Borosiloxane)

5.3 Wire drawing in a tapered unit

For the last few years plasto-hydrodynamic wire drawing has been investigated by different researchers. In reference [11] a non-Newtonian analysis for wire drawing was carried out in a stepped parallel bore unit and a Newtonian analysis for wire drawing was carried out in a conical tubular orifice in reference [27].

In this section plasto-hydrodynamic analysis for wire drawing in a tapered bore unit has been developed considering that the polymer is a non-Newtonian fluid. Also the change in viscosity of the polymer and shear stress are included in the analysis.

Plastic yielding

Referring to Figure 5 10(a) the principal stresses acting on the wire are,

$$\sigma_1 = \sigma_{x1} \text{ and } \sigma_2 = \sigma_3 = -P_1 ,$$

where σ_{x1} is the axial stress and P is the radial pressure at point x_1 where the plastic yielding commences. The yield characteristics of the wires are taken as in the form

$$Y = Y_0 + K_0 \epsilon^n \quad (5.13)$$

Therefore yielding occurs as soon as $Y = Y_0$, so that at x_1 according to Tresca yield criterion $P_1 + \sigma_x = Y_0$.

The change in the axial stress in the deformation zone

Referring to Figure 5 10 b and 5 10 c, considering a small section of the wire, the radial equilibrium of forces gives,

$$\sigma_x (\pi D dx) = -P \left(\frac{\pi D dx}{\cos \alpha} \right) \cos \alpha + \tau_c \left(\frac{\pi D dx}{\cos \alpha} \right) \sin \alpha$$

hence

$$\sigma_r = -P \left(1 - \frac{\tau_c}{P} \tan \alpha\right) \quad (5.14)$$

Here α is the semi-angle of the conical deformation profile. The value of τ_c/P has been shown to be very small and since α is also very small, the term $\tau_c \tan \alpha / P$ can be ignored.

Equilibrium of forces in x direction gives

$$-\sigma_x \left(\frac{1}{4} \pi D^2\right) + (\sigma_x + d\sigma_x) \left(\frac{\pi}{4} (D + dD)^2\right) + P \left(\frac{\pi D dx}{\cos \alpha}\right) \sin \alpha + \tau_c \left(\frac{\pi D dx}{\cos \alpha}\right) \cos \alpha = 0$$

Rearranging and ignoring powers of dD

$$2 dD \sigma_x + D d\sigma_x + 4P dx \tan \alpha + 4 dx \tau_c = 0$$

but $\tan \alpha = dD/2dx$, hence

$$2 dD (P + \sigma_x) + D d\sigma_x + 4 dx \tau_c = 0$$

Substituting for $(P + \sigma_x = Y)$ and rearranging gives

$$d\sigma_x = -\frac{2 dDY}{D} - \frac{4 \tau_c dx}{D}$$

This is the governing differential equation in the deformation zone for the axial stress in the wire. Rewriting this equation in finite-difference form gives,

$$\sigma_{x_j} = \frac{2 (D_{j-1} - D_j) Y_j}{D_j} + \frac{4 \tau_{c_j} dx}{D_j} + \sigma_{x_{j-1}} \quad (5.15)$$

The pressure equation in section 5.1 (equation 5.12) in finite difference form is

$$P(J) = P(J-1) + \left[\frac{6\mu(J-1)V}{M[1+3K\tau(J)^2]} \left[\frac{1}{h(J)^2} \right] + 12\mu(J-1) \frac{V}{M[1+3K\tau(J)^2]} \left[\frac{1}{h(J)^3 \left(\frac{1}{h_2} - \frac{1}{h_1} \right)} \right] \right] dx \quad (5.16)$$

The change in shear stress (section 5.1) where viscosity and shear rate change can be incorporated is

$$\tau(J) = \left(\frac{\mu(J-1)\dot{\gamma}(J)}{2k} + \left[\left(\frac{1}{3k} \right)^3 + \left(\frac{\mu(J-1)\gamma(J)}{2k} \right)^2 \right]^{\frac{1}{2}} \right)^{\frac{1}{3}} - \left(\frac{-\mu(J-1)\gamma(J)}{2k} + \left[\left(\frac{1}{3k} \right)^3 + \left(\frac{\mu(J-1)\gamma(J)}{2k} \right)^2 \right]^{\frac{1}{2}} \right)^{\frac{1}{3}} \quad (5.17)$$

where $\gamma(J) = V/h(J)$

As $dP/dx = d\tau/dy$, the wall shear stress within the deformation zone can be obtained from the equation

$$\tau c_J = \tau(J) - P'_J h(J) \quad (5.18)$$

As the deformation is considered to take place linearly, the change in gap between the wire and the unit, velocity and diameter within the deformation zone can be expressed respectively as,

$$\begin{aligned} h(J) &= h(J-1) - (M-k_J) \Delta x \\ V_J &= V_{J-1} \left(\frac{D_{J-1}}{D_J} \right)^2 \\ D_J &= D_{J-1} - 2k_J \Delta x \end{aligned} \quad (5.19)$$

where $\tan \alpha = -k_J$. The velocity profile can be obtained from the continuity of the flow of metal $[(V+dV) \pi/4 (D+dD)^2 = \pi/4 V D^2]$ and ignoring the power of dD . The true strain-stress relationship of the wire in the deformation zone may be shown as

$$Y_j = Y_0 + K_0 \epsilon_j^n$$

where $\epsilon_i = 2 \ln (D_1 / D_j)$

Therefore,

$$Y_j = (Y_0 + K_0 (2 \ln (\frac{D_1}{D_j}))^n) \quad (5.20)$$

Substituting for Y_j in equation (5.15) gives:

$$\sigma_{xj} = 2 \left(\frac{D_{j-1} - D_j}{D_j} \right) (Y_0 + K_0 (2 \ln (\frac{D_1}{D_j}))^n) + \frac{4 \tau_{cj} dx}{D_j} + \sigma_{xj-1} \quad (5.21)$$

Also, the Tresca yield criterion in finite difference form becomes;

$$P(j) + \sigma_{xj} = Y_j \quad (5.22)$$

For plastic yielding

$$P(j) + \sigma_{xj} \geq Y_j \quad (5.23)$$

The plastic deformation is calculated on the basis of equation (5.23) combined with equations (5.16), (5.18), (5.19), (5.20) and (5.21) for a small increment of Δx .

The following values of the parameters were used based on reference [11].

$B = 5.6 \times 10^{-1} \text{ } ^\circ\text{C}/\text{Nmm}^{-2}$, $C = 0.1 \text{ } ^\circ\text{C}/\text{mm}$, $\alpha = 0.017 \text{ } ^\circ\text{C}$, $DX = 1 \text{ mm}$, $h_1 = 0.5 \text{ mm}$, $h_2 = 0.075 \text{ mm}$, $K = 5.0 \times 10^{-11} \text{ m}^4/\text{N}^2$, $L = 57 \text{ mm}$, initial polymer temperature at the first unit = $130 \text{ } ^\circ\text{C}$, initial polymer viscosity = 110 N.s/m^2 , $y_0 = 50 \text{ MNm}^{-2}$, $K_0 = 440 \text{ MNm}^{-2}$, $n = 0.52$, $D_1 = 1.6 \text{ mm}$.

The polymer was Alkathane WVG23 and the wire material was Copper.

Figures 5.11 and 5.12 illustrate the theoretical hydrodynamic pressure within the unit

for wire velocity of 2 m/s and 3 m/s respectively. In these figures the theoretical solution is compared with the pressure profile from experiment[11]. The theoretical pressure solution has been generated for each small increment of length in the hydrodynamic pressure unit. The initial and final pressure in the unit are zero. For the present solution, the pressure in the unit increases gradually at a position up to maximum pressure. After that zone, the pressure decreases gradually. With the increase in the wire velocity the pressure also increases. From these figures it can be seen that the theoretical pressure profiles are closer to the experimental profiles although the peak pressure is significantly different.

Figure 5.13 shows comparisons of the percentage reduction in area for different speeds of the wire by the present analysis and experimental values by Parvinmehr[11]. Theoretically, these reductions increase with the increase in velocities. After wire velocity 3.5 m/s they become almost constant. From the experimental curve it appears that the reduction is higher at lower wire velocity and becomes lower at higher velocity. After wire velocity 3 m/s it becomes almost constant. However, the present theoretical prediction of reduction is comparable with the experimental curve at higher velocity. Figure 5.14 shows comparisons of the coating thickness for different speed of the wire by this analysis and that from experiments by Parvinmehr[11]. The theoretical values of coating thickness is higher than that obtained by experiments for wire velocity of 1 m/s and higher.

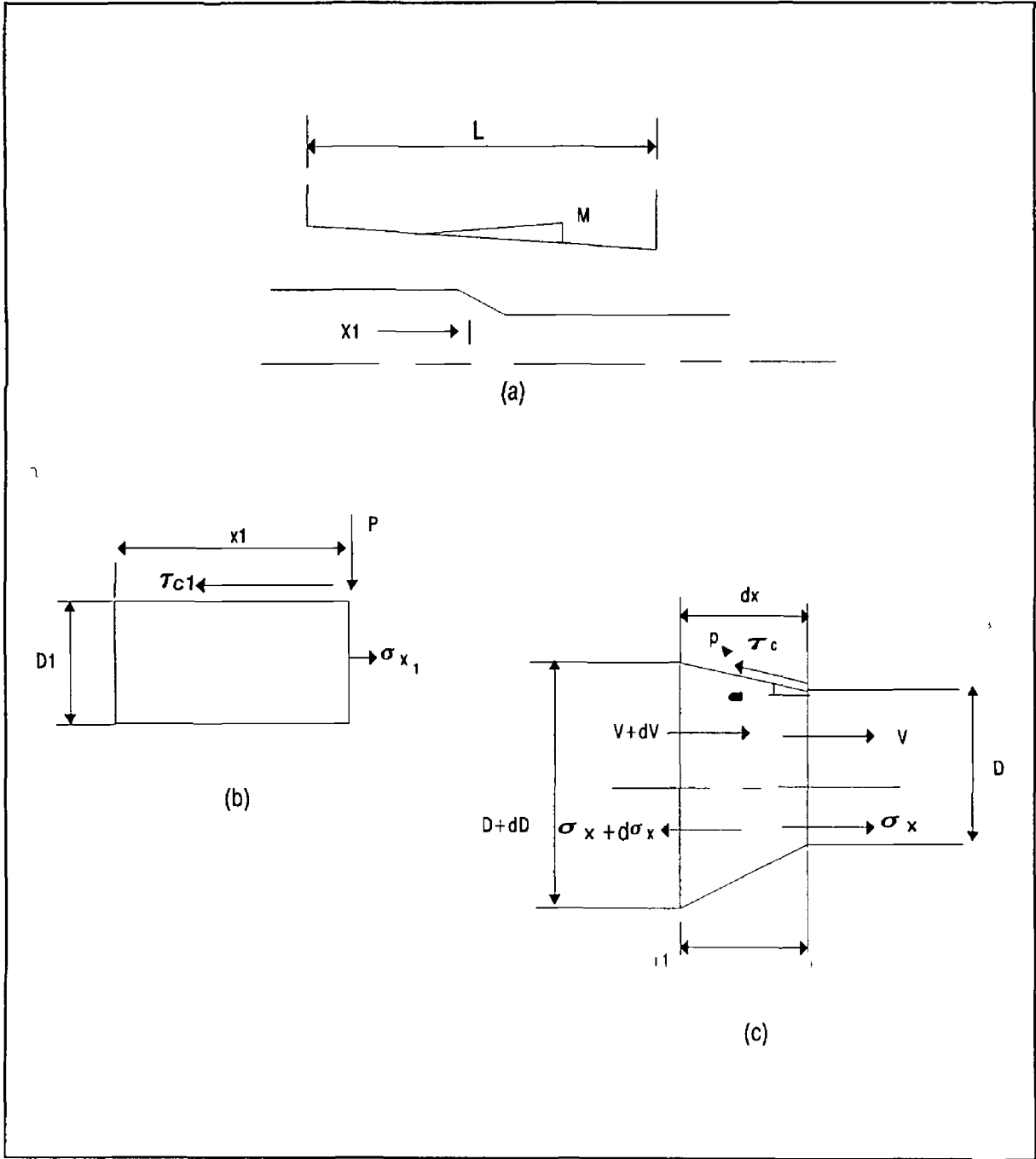


Figure 5 10 Wire drawing analysis in a tapered bore unit

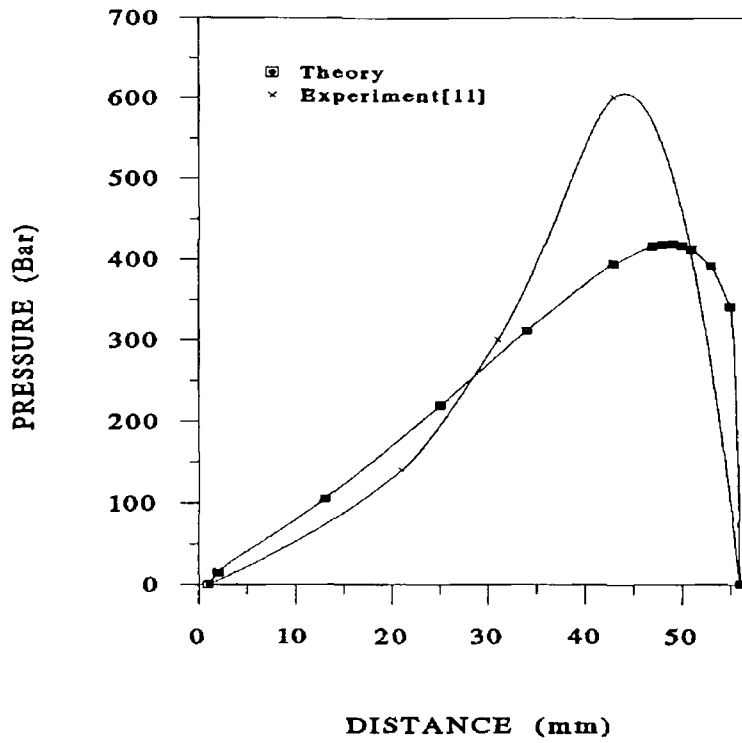


Figure 5 11 Pressure distribution within tapered unit during drawing velocity of 2m/s (Polymer-Alkathane WVG23)

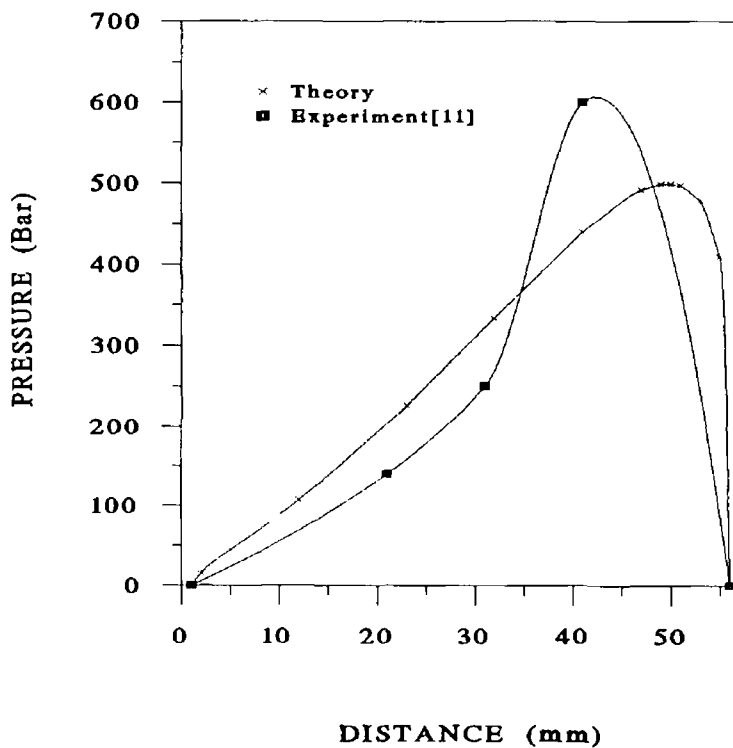


Figure 5 12 Pressure distribution within tapered unit during drawing velocity 3 m/s(Polymer-Alkathane WVG23)

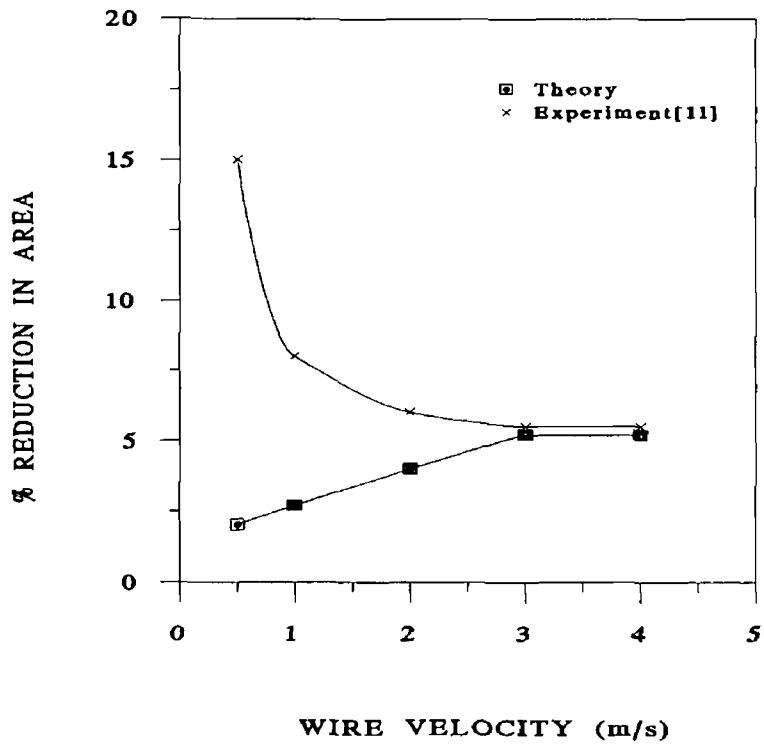


Figure 5 13 Percentage reduction in area in tapered unit during wire drawing (Polymer-Alkathane WVG23)

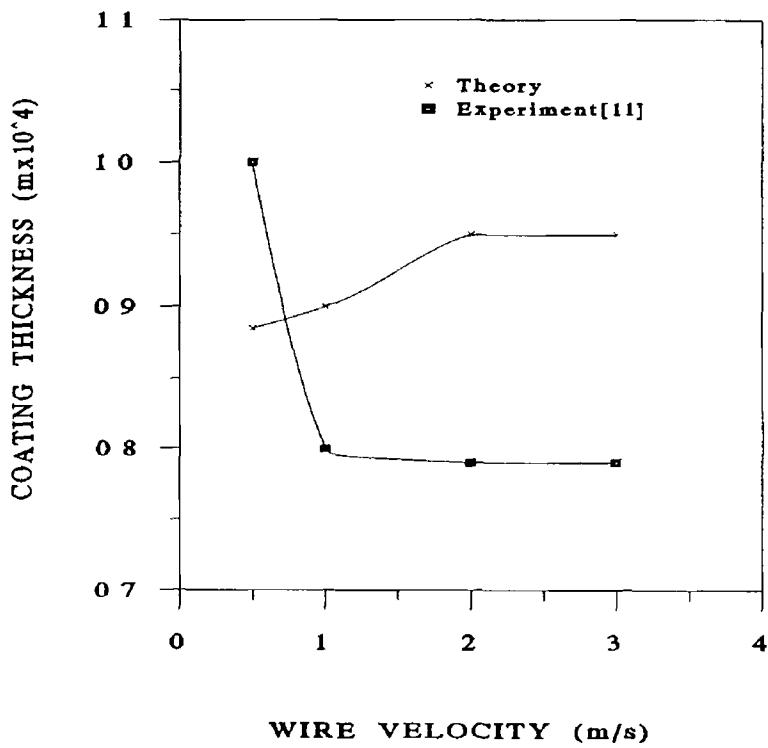


Figure 5 14 Coating thickness formed in tapered unit during wire drawing (Polymer-Alkathane WVG23)

5.4 Finite element temperature and pressure analysis for wire coating in a tapered bore unit

All the previous theoretical models for pressure distribution in plasto-hydrodynamic wire drawing and coating process were developed considering that the hydrodynamic pressure through the polymer film thickness at any point along the length of the unit is constant. In this section a finite element solution has been obtained for the temperature and pressure distributions taking account of their changes both along the direction of the wire velocity and through the thickness of the polymer layer. Pressure distribution within the unit has been obtained for different wire velocities by finite element method. These results are compared with the experimental results reported elsewhere.

Finite element model

Finite element simulation was carried out for a 180 mm long tapered bore unit. The gap between the unit and the wire i.e., lubricant film thickness at the entrance and exit of the unit are 0.25 mm and 0.05 mm respectively. The model was constituted with 20 elements and 103 nodes. Figure 5.15 shows the meshed model for temperature and pressure. The polymer was Borosiloxane melt.

The governing equation

The equation governing the pressure generation in the fluid film is the Reynolds equation[63]

$$\frac{d}{dx} \left(\frac{h^3}{6\mu} \frac{dP}{dx} \right) + \frac{d}{dy} \left(\frac{h^3}{6\mu} \frac{dP}{dy} \right) = 2 \frac{dh}{dt} + U \frac{dh}{dx} \quad (5.24)$$

This equation is valid for a Newtonian fluid. The fluid used in the plasto-hydrodynamic process is polymer melt which is normally a non-Newtonian fluid. But the polymer melt exhibits non-Newtonian behaviour except for very low shear rates[34]. For example Borosiloxane at shear rates between 5×10^2 and 6×10^2 behaves as a Newtonian fluid[42]. Also some polymers, such as Nylon, polyester and polysiloxane act almost like a Newtonian fluid[54]. Therefore, this two dimensional

equation can be employed for plasto-hydrodynamic analysis where the above polymers are used

Also the governing Reynold equation for temperature distribution[63] is

$$\frac{d}{dx} (K_{xx} \frac{dT}{dx}) + \frac{d}{dy} (K_{yy} \frac{dT}{dy}) + \phi = \frac{dT}{dt} + U \frac{dT}{dx} \quad (5.25)$$

The viscosity which is function of temperature and pressure can be expressed arbitrarily as

$$\mu = \mu_0 e^{-\alpha(\Delta T - \beta \Delta P)} \quad (5.26)$$

where μ_0 is the reference viscosity and α and β are the constants

Element characteristics

The lubricant was modelled with two dimensional 8 node quadrilateral elements. The nodes of the elements have two degrees of freedom i.e. in the X direction along the die length and in the Y direction through the polymer melt

Boundary conditions and Solution

Referring to Figure 5.15 the boundary conditions for the elements in the case of pressure are-

along

AB and CD, $P=0$

BD, the wire surface is rigid

AC, the die surface is rigid

Also referring to Figure 5.15 the boundary conditions for the elements in the case of temperature are

along

AB, T is constant for each layer of fluid film (for each element there are two layers)

BD, heat flux through the wire is negligible

CD, T is unknown

AC, temperature at die wall is constant

A Cholesky decomposition matrix technique was used to solve the resulting global sparse matrix and the finite element solution was obtained using the Gauss-Seidel iteration technique [63]

Viscosity for Borosiloxane was taken from Figure 2.5 for different shear rate [42], the value of α is 0.018°C^{-1} and β is $4.2 \times 10^{-1} \text{C}/\text{Nmm}^2$. During the experiment with Borosiloxane, the temperature of the die wall was maintained at 110°C . When the polymer first entered the pressure unit from the melt chamber the polymer melt temperature was about 95°C .

Figure 5.16 shows the simulated temperature profiles in the die flow channel where the wire drawing speed is 0.04 m/s . At the wire surface i.e., $y=0$ pronounced temperature maxima arise when the fluid enters in the die channel. The reason for this maxima is thought to be the high shear heating (high shear rate) at the entry. At the same time negligible heat is transferred to the neighbouring melt layers. At $1/4$ th way through the film thickness, the temperature distribution more or less follows the wire surface temperature profile. The temperature distribution at $3/4$ th way through the film thickness is close to the die wall temperature which was maintained constant by a heater band.

Figure 5.17 illustrates the theoretical hydrodynamic pressure within the unit for wire velocity of 0.04 m/s . In this figure the finite element solution has been compared with the experimental results from references [30]. The initial pressure at the entrance of the unit and the final pressure at the exit of the unit are zero. First the pressure simulation was carried out for a particular viscosity which was obtained from the shear rate and the viscosity relationship. Then the viscosity was modified according to equation (5.26) by incorporating the change in pressure and the change in temperature as obtained from simulation. Using the modified viscosity for each element another simulation was carried out. From the simulations, it was observed that the pressure increases gradually upto 155 mm and then decreases gradually. From the figure it can be seen that the theoretical pressure profile is similar to the experimental pressure profile. The position of the maximum pressure is also almost at the same point as the first simulation (for the second simulation it is at 156 mm).

But the magnitude of the simulated pressure where the modified viscosity was introduced is more closer to the experimental pressure than the simulated pressure where the viscosity was considered to be constant

Similarly, simulation for pressure was carried out for wire velocities of 0.08 m/s and 0.16 m/s. Figures 5.18 and 5.19 show comparisons of pressure profiles from the finite element simulation with those from experiments for wire velocities of 0.08 and 0.16 m/s respectively. It can be seen from these figures that the pressure profiles are reasonably similar to the experimental profiles. The magnitudes of the simulated maximum pressure also agree reasonably well with the experimental ones.

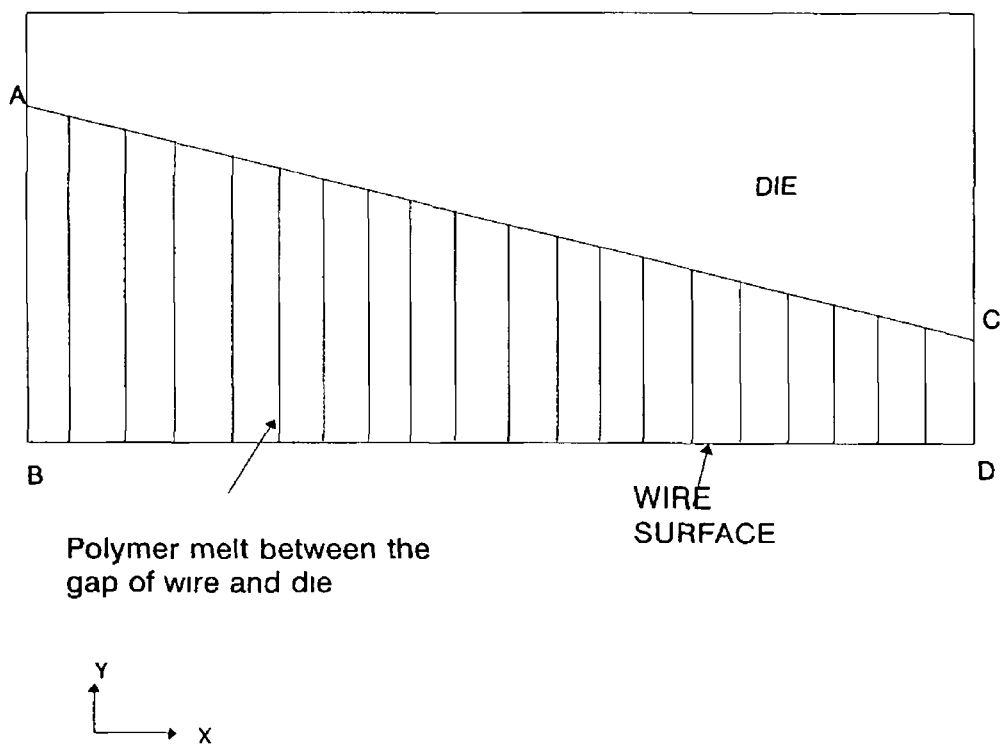


Figure 5.15 Schematic diagram for the meshed model in the tapered unit

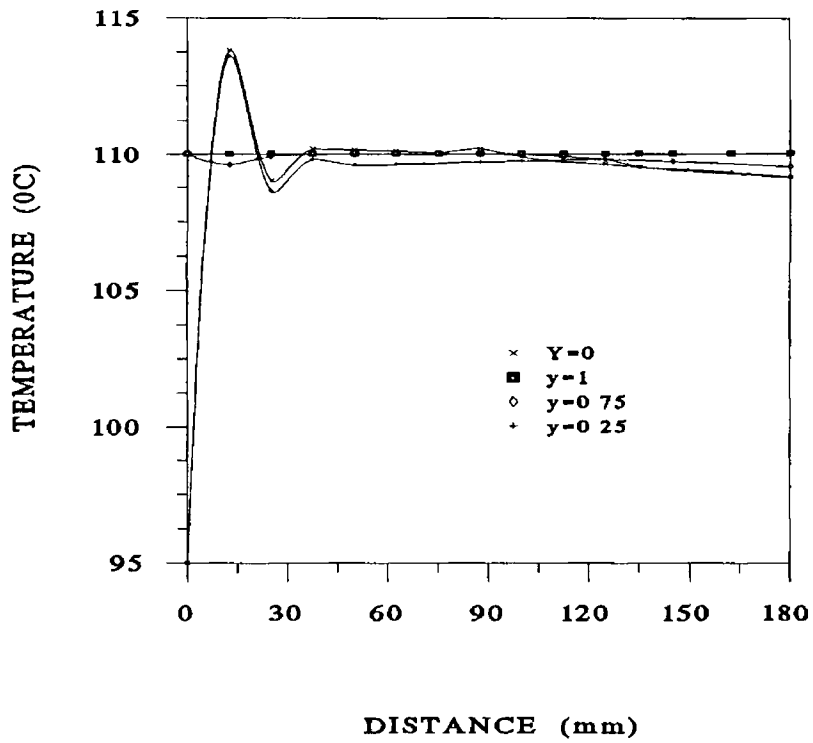


Figure 5 16 Temperature distribution in the tapered unit

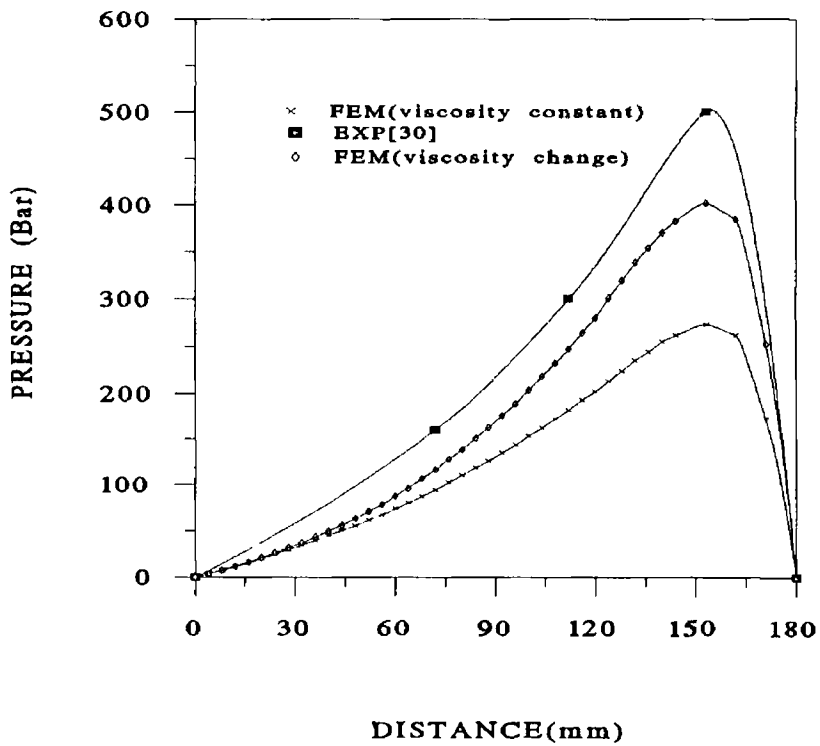


Figure 5 17 Pressure distribution in a tapered unit for wire velocity of 0.04 m/s (Polymer- Borosiloxane)

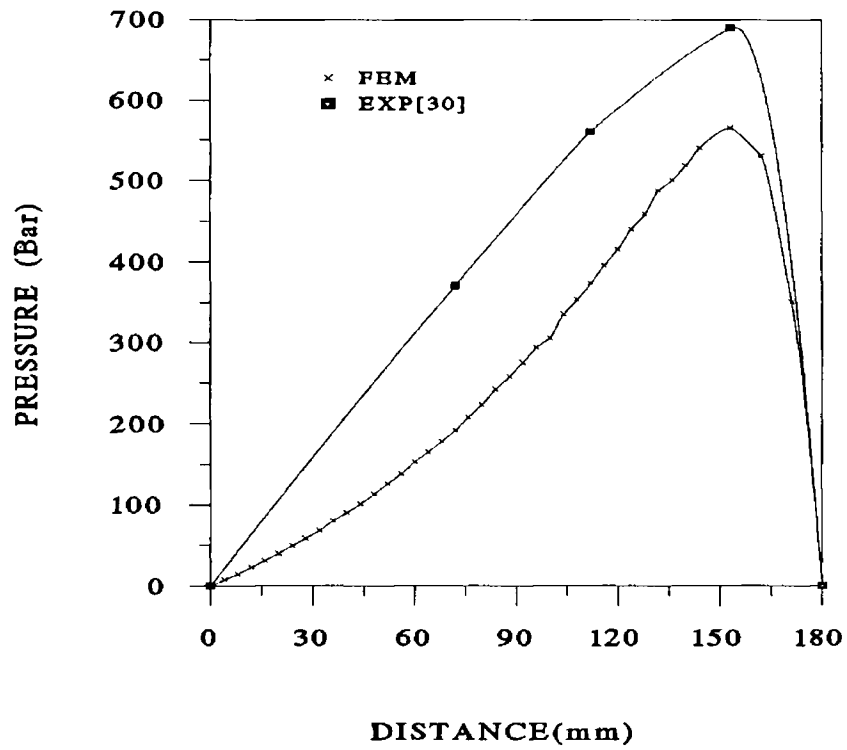


Figure 5 18 Pressure distribution in a tapered unit for wire velocity of 0.08 m/s (Polymer- Borosiloxane)

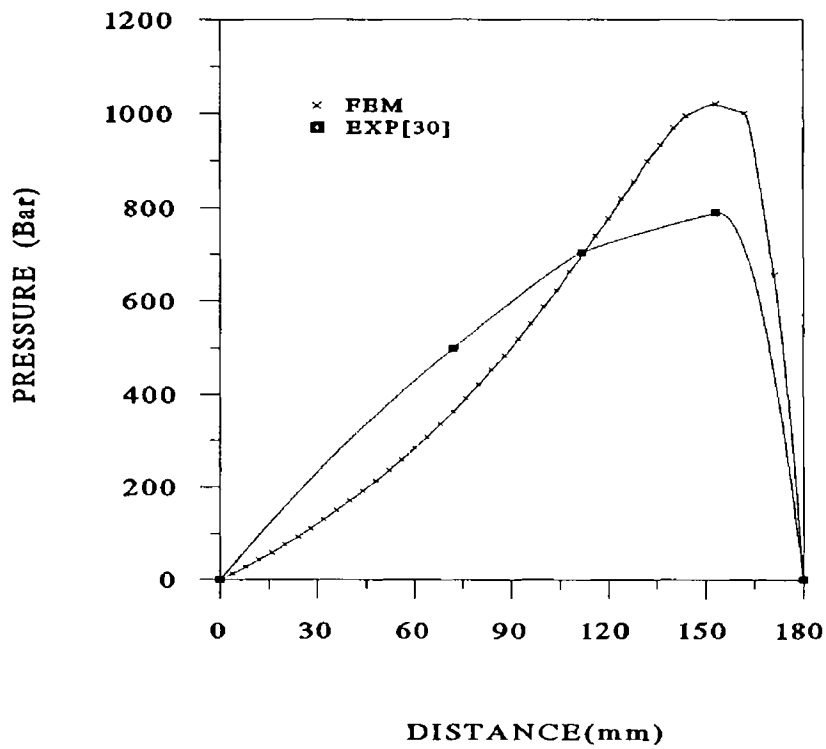


Figure 5 19 Pressure distribution in a tapered unit for wire velocity of 0.16 m/s (Polymer- Borosiloxane)

5.5. Plasto-hydrodynamic pressure analysis in converging parabolic and exponential unit

In this section plasto-hydrodynamic pressure models have been developed for converging parabolic and exponential units (shown in Figures 5 20 and 5 23 respectively)

Equation (5 4) can be written as

$$Q = -\frac{dP}{dx} \frac{h^3}{12\mu} - \frac{K}{\mu} \left(\frac{\tau^2}{4} \frac{dP}{dx} h^3 \right) + \frac{Vh}{2} \quad (5 27)$$

Considering a position where $h = h_b$ ie, the pressure is optimum Therefore in that position $dP/dx = 0$ which gives $Q = Vh_b/2$

Thus,

$$\frac{dP}{dx} = \frac{6\mu V}{[1+3K\tau^2]} \left[\frac{1}{h^2} - \frac{h_b}{h^3} \right] \quad (5 28)$$

Let,

$$H(x) = \int_0^x \frac{1}{h^2} dx, \quad G(x) = \int_0^x \frac{1}{h^3} dx$$

The boundary conditions are

(a) at $x=0$, $P=0$, and (b) at $x=L$, $P=0$

Therefore, with the boundary condition (a) the pressure expression becomes

$$P(x) = \frac{6\mu V}{[1+3K\tau^2]} [H(x) - h_b G(x)]$$

With the boundary condition (b) the position of optimum pressure is

$$h_b = H(L)/G(L)$$

Therefore, the pressure profile in this unit is

$$P(x) = \frac{6\mu V}{[1+3K\tau^2]} \left[H(x) - \frac{H(L)G(x)}{G(L)} \right] \quad (5.29)$$

Now for the converging parabolic unit, the unit geometry can be considered as

$$h(x) = -a^2(x+b)^2 + c^2$$

Substituting $h(x)$ in the expression for $H(x)$, it becomes,

$$H(x) = \int_0^x \frac{1}{(-a^2(x+b)^2 + c^2)^2} dx$$

After integration it becomes,

$$H(x) = \frac{1}{4c^3a} \left[\ln \left[\frac{x+b+d}{x+b-d} \right] - \ln \left[\frac{b+d}{b-d} \right] - d \left[\frac{1}{x+b+d} + \frac{1}{x+b-d} - \frac{1}{b+d} - \frac{1}{b-d} \right] \right] \quad (5.30)$$

and in the same way substituting $h(x)$ in the expression for $G(x)$ for , it gives

$$G(x) = \int_0^x \frac{1}{(-a^2(x+b)^2 + c^2)^3} dx$$

After integration it gives,

$$G(x) = \frac{1}{16d^5a^6} \left[3 \ln \left[\frac{x+b+d}{x+b-d} \right] - 3 \ln \left[\frac{b+d}{b-d} \right] - 3d \left[\frac{1}{x+b+d} + \frac{1}{x+b-d} - \frac{1}{b+d} - \frac{1}{b-d} \right] - d^2 \left[\frac{1}{(x+b+d)^2} - \frac{1}{(x+b-d)^2} - \frac{1}{(b+d)^2} + \frac{1}{(b-d)^2} \right] \right] \quad (5.31)$$

where, $d=c/a$

To obtain the optimum position for pressure it is necessary to calculate $G(L)$ and $H(L)$ For hydrodynamic converging parabolic unit the die geometry can be expressed as $h(x) = - (h_1 - h_2 / L) x^2 + h_1$, therefore in this case the terms a can be substituted for $(h_1 - h_2)^{1/2} / L$, b for 0 and c for $h_1^{1/2}$

Substituting the values for a, b and c at x=L, the expressions for G(L) and H(L) becomes,

$$G(L) = \frac{L}{16h_1^2\sqrt{h_1}\sqrt{h_1-h_2}} \left[3 \ln \frac{\sqrt{h_1-h_2} + \sqrt{h_1}}{\sqrt{h_1-h_2} - \sqrt{h_1}} - 3d \left(\frac{2L}{(L^2-d^2)} + d^2 \left(\frac{4Ld}{(L^2-d^2)^2} \right) \right) \right]$$

Therefore,

$$G(L) = \frac{L}{16h_1^2\sqrt{h_1}\sqrt{h_1-h_2}} \left[3 \ln \frac{\sqrt{h_1-h_2} + \sqrt{h_1}}{\sqrt{h_1-h_2} - \sqrt{h_1}} \right] + \frac{1}{16h_1} \left[\left(\frac{6L}{h_1h_2} + \left(\frac{4L}{h_2^2} \right) \right) \right] \quad (5.32)$$

In the same way,

$$H(L) = \frac{L}{4h_1\sqrt{h_1}\sqrt{h_1-h_2}} \left[\ln \frac{\sqrt{h_1-h_2} + \sqrt{h_1}}{\sqrt{h_1-h_2} - \sqrt{h_1}} \right] + \frac{L}{2h_1h_2} \quad (5.33)$$

For the exponential unit

The geometry defined for converging exponential unit is $h(x) = a^2(x+b)^2 + c^2$

The expressions for H (x) and G(x) in terms of h(x) becomes

$$H(x) = \int_0^x \frac{1}{(a^2(x+b)^2 + c^2)^2} dx$$

and

$$G(x) = \int_0^x \frac{1}{(a^2(x+b)^2 + c^2)^3} dx$$

After integration they give,

$$H(x) = \frac{1}{2c^2} \left[\frac{1}{ac} \left[\arctan\left(\frac{(b+x)a}{c}\right) - \arctan\left(\frac{ab}{c}\right) \right] + \left[\frac{b+x}{a^2(b+x)^2+c^2} - \frac{b}{a^2b^2+c^2} \right] \right] \quad (5.34)$$

and

$$G(x) = \frac{1}{4c^2} \left[\frac{b+x}{(a^2(b+x)^2+c^2)^2} - \frac{b}{(a^2b^2+c^2)^2} \right] + \frac{3}{4c^2} H(x) \quad (5.35)$$

For plasto-hydrodynamic converging exponential unit, the geometry can be presented as $h(x) = ((h_1 - h_2) / L^2) (x-L)^2 + h_2$, therefore in this case the terms a can be substituted for

$(h_1 - h_2)^{1/2} / L$, b for $-L$ and c for $h_2^{1/2}$

Substituting the values for a , b and c at $x=L$, the expressions for $H(L)$ and $G(L)$ becomes,

$$G(L) = \frac{1}{4h_2} \left[\frac{L}{h_1^2} + 3H(L) \right] \quad (5.36)$$

and

$$H(L) = \frac{L}{2h_2} \left[\frac{1}{\sqrt{h_2}\sqrt{h_1-h_2}} \arctan\left(\frac{\sqrt{h_1-h_2}}{\sqrt{h_2}}\right) + \frac{1}{h_1} \right] \quad (5.37)$$

The pressure equation in the finite difference form can be written as

$$P_j = P_{j-1} + \frac{6\mu_{j-1}V}{[1+3K\tau_j^2]} \left[\frac{1}{h_j^2} - \frac{h_b}{h_j^3} \right] \quad (5.38)$$

The shear stress is,

$$\tau(j) = \left(\frac{\mu(j-1)\dot{\gamma}(j)}{2k} + \left[\left(\frac{1}{3k} \right)^3 + \left(\frac{\mu(j-1)\dot{\gamma}(j)}{2k} \right)^2 \right]^{\frac{1}{2}} \right)^{\frac{1}{3}} - \left(\frac{-\mu(j-1)\dot{\gamma}(j)}{2k} + \left[\left(\frac{1}{3k} \right)^3 + \left(\frac{\mu(j-1)\dot{\gamma}(j)}{2k} \right)^2 \right]^{\frac{1}{2}} \right)^{\frac{1}{3}} \quad (5.39)$$

and the viscosity term can be taken from equation (5.9).

From equations(5.37)-(5.39) and (5.9) the hydrodynamic pressure can be calculated for converging parabolic and exponential unit introducing the values of a, b, c, G(L) and H(L).

Results were calculated on the basis of equations derived as above. The polymer melt was taken as Borosiloxane at 100 °C. The geometries of the unit were, h1=0.25 mm, h2= 0.05 mm and L=180 mm.

Figure 5.20 shows a converging parabolic hydrodynamic pressure unit and Figure 5.21 shows the corresponding pressure profile for the unit. The pressure increases gradually up to a certain point (163 to 167 mm depending on different velocities) and then decreases gradually. With the increase in the wire velocity the pressure also increases. Figure 5.22 shows finite element simulation with the same type of unit. The pressure increases gradually up to a certain point (167 mm for wire velocity 0.1 m/s and 163 mm for 0.2 m/s) and then decreases in a linear way. From the two figures it can be seen that the optimum position for pressure in both this method is same but the pressure profile after that position is different. However experimental results in future will justify the profiles.

Figures 5.23 and 5.24 respectively represent the converging exponential pressure unit and the corresponding pressure profile. The pressure increases gradually up to a certain point (133 to 136 mm depending on different velocities) and then decreases gradually. Again the pressure is higher for higher wire velocity. Figure 5.25 shows the finite element pressure profile for the same polymer but with different length of unit. But in this case the pressure profile in both the analytical and finite element method are same. The pressure increases gradually up to a certain point (16 mm for wire velocity 6 m/s and 18 mm for 8 m/s) and then decreases gradually.

The finite element simulation was done in two dimensions ie; along the direction of wire drawing and through the thickness of the fluid film. The pressure difference through the film thickness was found to be negligible by the simulation. Table 5.1 gives values of pressure through the film thickness in a parabolic unit for wire

velocity of 0.2 m/s

Table 5.1 Pressure distribution within a 180 mm converged parabolic unit

Distance along the die (mm)	At wire (Bar) surface	At 1/2 film thickness (Bar)	At full film thickness (Bar)
0	0.0	0.0	0.0
12.2	83.09	83.332	83.57
20.4	139.86	140.01	140.21
28.6	197.5	197.68	197.86
45	316.667	316.51	316.67
53.18	379.15	379.24	379.14
57.2	410.16	410.72	410.16
69.54	512.22	513.57	512.21
77.72	583.84	585.24	583.85
94	741.29	741.76	741.31
102.2	828.43	830.5	829.21
106.3	874.87	875.57	871.42
110.45	923.74	925.21	923.7
118.63	1026.4	1029.2	1026.39
122	1071.76	1081.59	1081.22
143.18	1372.7	1370.8	1372.72
155.45	1501.76	1500.8	1501.78
163.63	1542.55	1542.62	1542.46
171.81	778.37	783.51	781.58
180	0.0	0.0	0.0

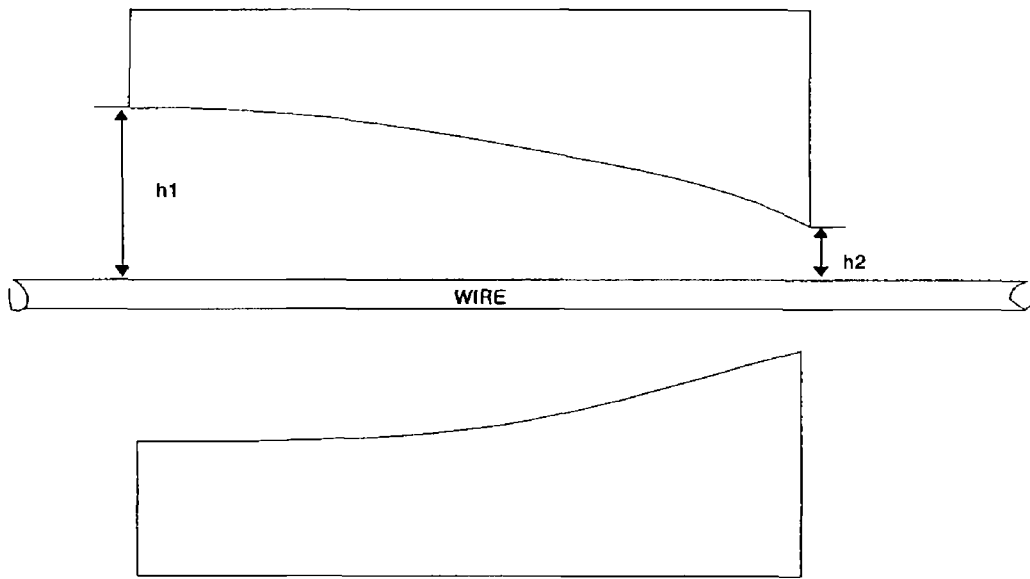


Figure 5 20 Schematic diagram for parabolic hydrodynamic pressure unit

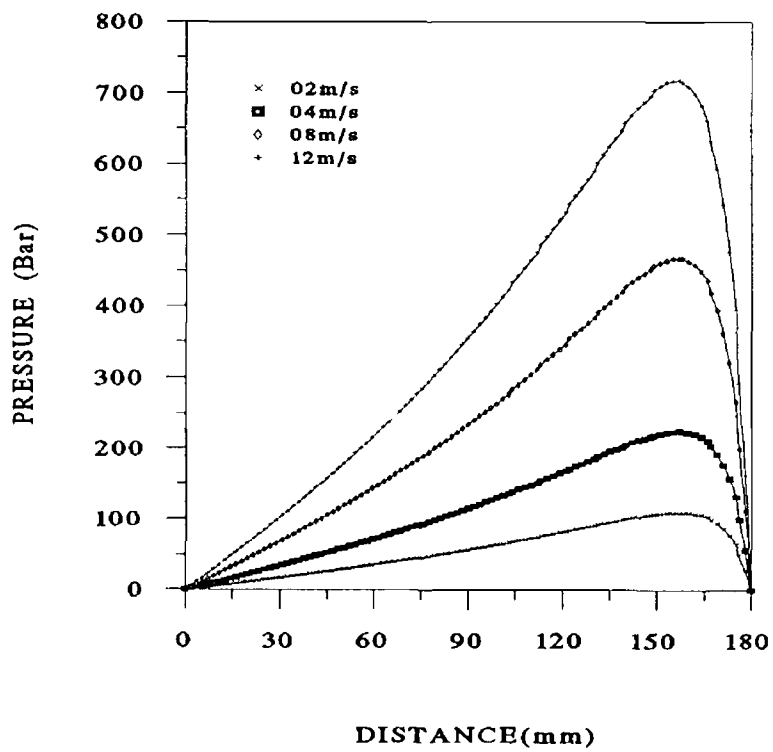


Figure 5 21 Pressure distribution in a parabolic unit (polymer- Borosiloxane)

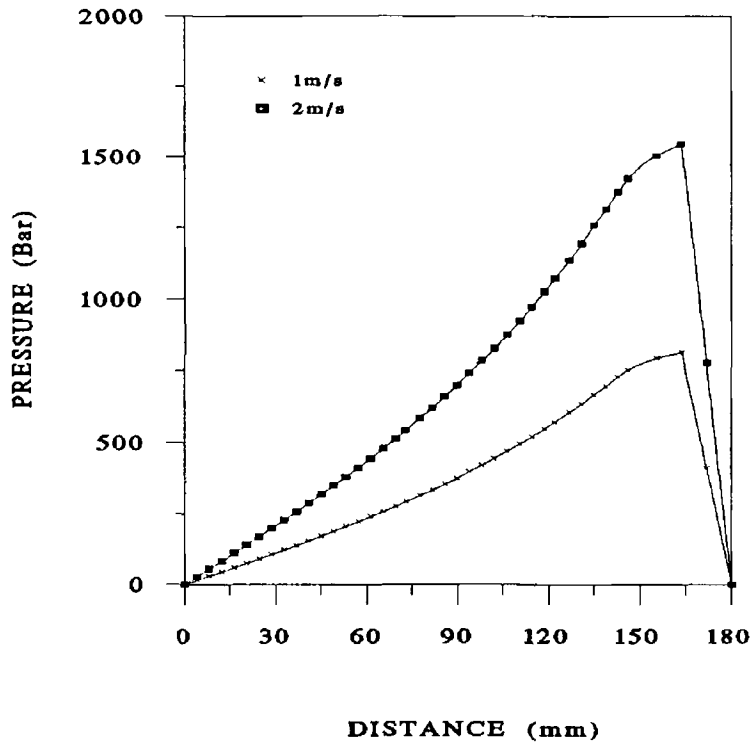


Figure 5 22 Finite element pressure simulation in a parabolic unit (Polymer-Borosiloxane)

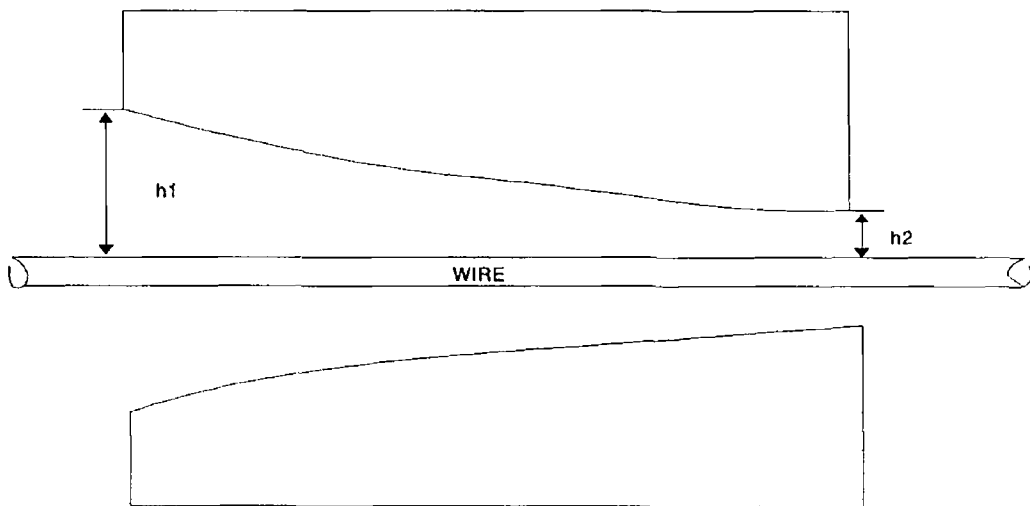


Figure 5 23 Exponential hydrodynamic pressure unit

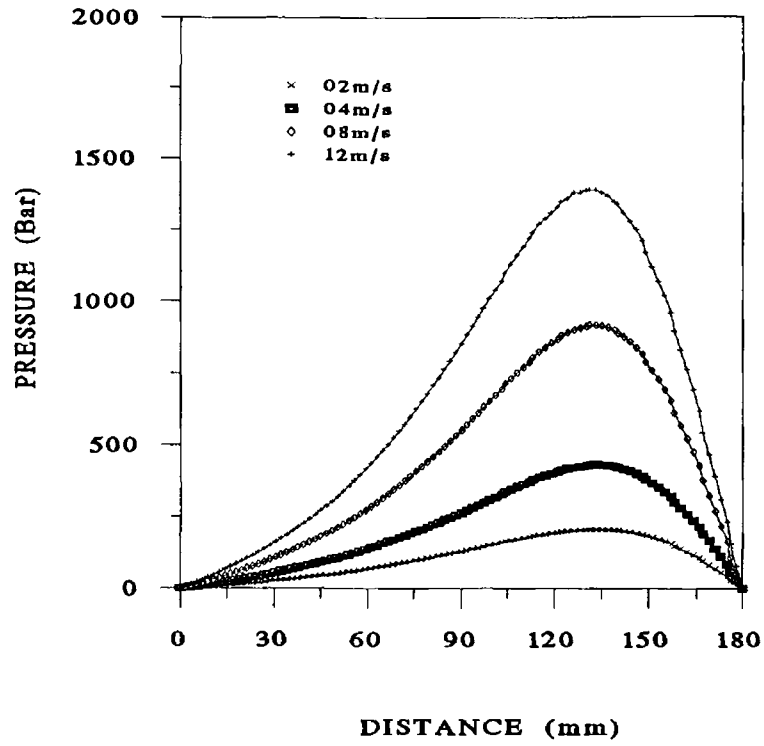


Figure 5 24 Pressure distribution in a exponential converging pressure unit (Polymer-Borosiloxane)

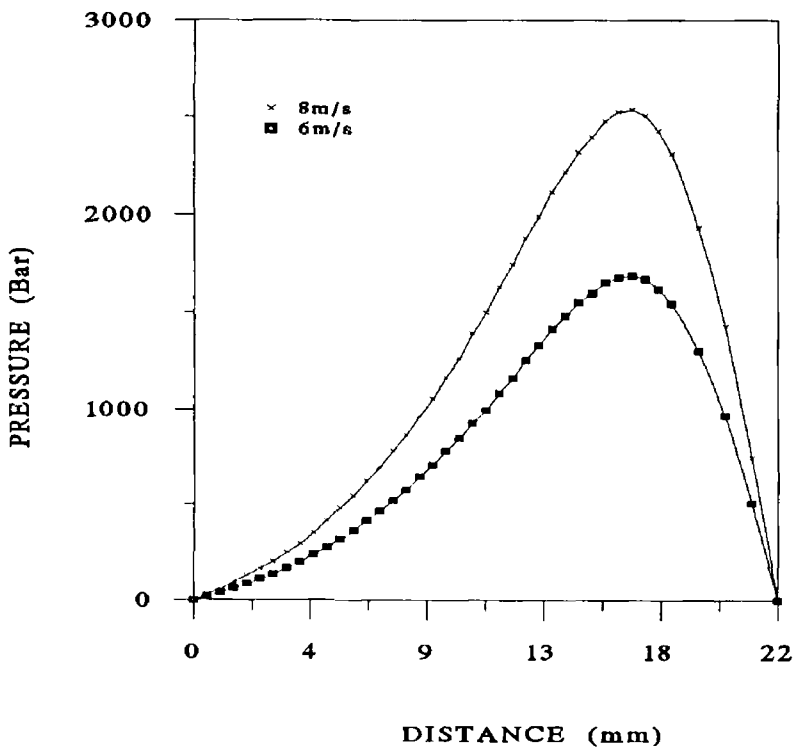


Figure 5 25 Finite element pressure simulation in a hyperbolic unit (Polymer-Borosiloxane)

CHAPTER SIX

ANALYSIS FOR PLASTO-HYDRODYNAMIC WIRE COATING AND DRAWING USING A COMBINED PARALLEL AND TAPERED GEOMETRY UNIT

6.1 Introduction

For plasto-hydrodynamic die-less wire coating using a combined geometry pressure unit, a number of theoretical models for pressure distribution have been presented in previous publications[30,32,33] In reference[32] a Newtonian plasto-hydrodynamic analysis was carried out for a combined hydrodynamic unit While in reference [33] the analysis was carried out considering the polymer melt pressure medium as a non-Newtonian fluid In these models the viscosity of polymer and shear rate was considered to remain unchanged during drawing

In this chapter a new mathematical model has been developed for the pressure distribution within a combined unit taking account of the changes in the viscosity and shear rate of the polymer melt during the drawing process Theoretical results are obtained for different wire speeds in terms of the pressure distributions within the unit These results are compared with those according to the previous theoretical models as well as with experimental pressure distribution results

6.2 Non-Newtonian pressure analysis for coating

This is a non-Newtonian analysis of the coating process which has been reported in[71]

The following analysis is based on the geometrical configuration shown in Figure 6 1 The combined unit consists of two parts The first is a parallel part which is followed by a tapered part

Plasto-hydrodynamic analysis of this unit was done with the following simplifying assumptions,

- a) the flow of the polymer melt is laminar
- b) the flow of the polymer melt is axial

c) the thickness of the polymer layer is small compared to the dimensions of the pressure unit

Analysis for the parallel part of the unit

With reference to figure 6 1, the relationship between the pressure and shear stress

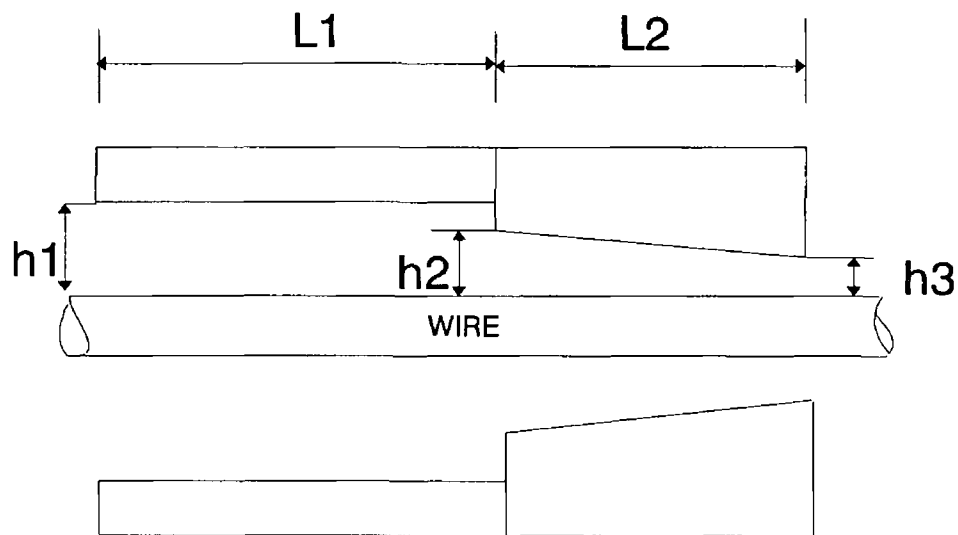


Figure 6 1 Schematic diagram of a combined parallel and tapered bore unit

gradient in the first part of the unit is given by

$$\left(\frac{dp}{dx}\right)_1 = \left(\frac{d\tau}{dy}\right)_1 \quad (6.1)$$

According to Rabinowitsch [41] the equation for the polymer melt relating shear stress and shear rate is

$$\tau + K\tau^3 = \mu \left(\frac{dU}{dy}\right) = \mu\dot{\gamma} \quad (6.2)$$

Integration of equation (6.1) gives

$$\tau_1 = P_1' y + \tau_{c_1}$$

where τ_{c_1} is the shear stress at $y=0$ and $P_1' = (dP/dx)_1$ is assumed to be independent of y

Substituting for τ_1 into equation (6 2) gives

$$\mu \left(\frac{dU}{dy} \right)_1 = P_1' y + \tau_{c_1} + K (P_1'^3 y^3 + \tau_{c_1}^3 + 3 P_1'^2 y^2 \tau_{c_1} + 3 \tau_{c_1}^2 P_1' y)$$

which after integration becomes

$$U_1 = \frac{P_1' y^2}{2\mu} + \frac{\tau_{c_1} y}{\mu} + \frac{K}{\mu} \left(\frac{P_1'^3 y^4}{4} + \tau_{c_1}^3 y + P_1'^2 y^3 \tau_{c_1} + \frac{3}{2} \tau_{c_1}^2 P_1' y^2 \right) + C \quad (6 3)$$

where C is the constant of integration

The boundary conditions are,

(a) at $y = 0$, $U_1 = V$

(b) at $y = h_1$, $U_1 = 0$

Applying condition (a) in equation (6 3), $C=V$ and hence

$$U_1 = \frac{P_1' y^2}{2\mu} + \frac{\tau_{c_1} y}{\mu} + \frac{K}{\mu} \left(\frac{P_1'^3 y^4}{4} + \tau_{c_1}^3 y + P_1'^2 y^3 \tau_{c_1} + \frac{3}{2} \tau_{c_1}^2 P_1' y^2 \right) + V \quad (6 4)$$

Also substituting condition (b) in equation (6 4) and after rearrangement it gives

$$\tau_{c_1}^3 + \frac{3}{2} (P_1' h_1) \tau_{c_1}^2 + \left(\frac{1}{K} + P_1'^2 h_1^2 \right) \tau_{c_1} + \left(\frac{\mu V}{K h_1} + \frac{P_1' h_1}{2K} + \frac{P_1'^3 h_1^3}{4} \right) = 0$$

The real root of this equation is,

$$\tau_{C_1} = \left(-\frac{\mu V}{2Kh_1} + \left(\frac{\mu^2 V^2}{4K^2 h_1^2} + \frac{1}{27} \left(\frac{1}{K} + \frac{1}{4} P_1'^2 h_1^2 \right)^3 \right)^{1/2} \right)^{1/3} + \left(-\frac{\mu V}{2Kh_1} - \left(\frac{\mu^2 V^2}{4K^2 h_1^2} + \frac{1}{27} \left(\frac{1}{K} + \frac{1}{4} P_1'^2 h_1^2 \right)^3 \right)^{1/2} \right)^{1/3} - \frac{1}{2} P_1' h_1 \quad (6.5)$$

The flow of the polymer melt in the first part of the unit is given by,

$$Q_1 = \int_0^{h_1} U_1 dy$$

Substituting for U_1 from equation (6.4) into the above equation and integrating gives,

$$Q_1 = \frac{P_1' h_1^3}{6\mu} + \frac{\tau_{C_1} h_1^2}{2\mu} + \frac{K}{\mu} \left(\frac{P_1'^3 h_1^5}{20} + \frac{\tau_{C_1}^3 h_1^2}{2} + \frac{P_1'^2 h_1^4 \tau_{C_1}}{4} + \frac{\tau_{C_1}^2 P_1' h_1^3}{2} \right) + V h_1 \quad (6.6)$$

For continuous flow operation,

$$Q_1 = Q_2 \quad (6.7)$$

Hence establishment of flow equation in the tapered part is necessary

The pressure gradient in the second part under steady state condition gives,

$$\left(\frac{dp}{dx} \right)_2 = \left(\frac{d\tau}{dy} \right)_2 \quad (6.8)$$

The boundary conditions are

(c) at $y = 0$, $U_2 = V$

(d) at $y = h$, $U_2 = 0$

The shear stress and shear rate is related by

$$\tau_2 + K\tau_2^3 = \mu \left(\frac{dU}{dy} \right) = \mu \gamma \quad (6.9)$$

Differentiating this equation with respect to y gives

$$\left(\frac{d\tau_2}{dy} \right) + 3K\tau_2^2 \frac{d\tau_2}{dy} = \mu \left(\frac{d^2U_2}{dy^2} \right)$$

substituting $(d\tau_2/dy)$ for (dP_2/dx) from equation (6.8) and integrating it twice it gives,

$$\left(\frac{dP_2}{dx} \right) \frac{y^2}{2} + 3K\tau_2^2 \left(\frac{dP_2}{dx} \right) \frac{y^2}{2} + C_2y + C_3 = \mu U_2$$

and then setting the boundary conditions (c) and (d) the velocity profile becomes

$$U_2 = \frac{P_2' y^2}{2\mu} + \frac{3KP_2'}{2\mu} (\tau_2^2 y^2 - \tau_2^2 y h) - \frac{P_2' h y}{2\mu} - \frac{V y}{h} + V \quad (6.10)$$

And the flow of the polymer melt in the tapered part of the unit is,

$$Q_2 = \int_0^h U_2 dy$$

Substituting for U_2 from equation (6.10) the flow becomes

$$Q_2 = -\frac{P_2' h^3}{12\mu} - \frac{K}{\mu} \left(\frac{\tau_2^2 P_2' h^3}{4} \right) + \frac{V h}{2} \quad (6.11)$$

Now differentiating equation (6.11) with respect to x , integrating it again and noting

that $dQ_2/dx = 0$ it gives

$$\frac{P_2' h^3}{6\mu} + \frac{K}{\mu} \left(\frac{\tau_2^2 P_2' h^3}{2} \right) = Vh + C_4$$

and then integrating this equation it gives

$$P_2 = \frac{6\mu V}{M[1+3K\tau_2^2]} \left[\frac{V}{h} + \frac{C_5}{2h^2} \right] + C_6 \quad (6.12)$$

where M can be obtained from the geometry of the unit , $M = (h_2 - h_3)/L_2$

Also $h = h_2 - Mx$

The boundary conditions are at $x=L_1$, $h=h_2$, $P_2=P_1(L_1)$ and $x=L_1+L_2$, $h=h_3$, $P_2=0$ Substituting the conditions in equation(6.12) it gives,

$$C_5 = \frac{2 \left(\frac{P_1(L_1) M [1+3K\tau_2^2]}{6\mu} + V \left[\frac{1}{h_3} - \frac{1}{h_2} \right] \right)}{\left(\frac{1}{h_3^2} - \frac{1}{h_2^2} \right)}$$

and

$$C_6 = - \frac{6\mu V}{M[1+3K\tau_2^2]} \left[\frac{V}{h_3} + \frac{C_5}{2h_3^2} \right]$$

Therefore, the pressure distribution becomes,

$$P_2 = \frac{6\mu V}{M[1+3K\tau_2^2]} \left[\frac{1}{h} - \frac{1}{h_3} \right] + \frac{3\mu}{M[1+3K\tau_2^2]} \left[\frac{1}{h^2} - \frac{1}{h_3^2} \right] \left[\frac{2 \left(\frac{P_1(L_1) M [1+3K\tau_2^2]}{6\mu} + V \left[\frac{1}{h_3} - \frac{1}{h_2} \right] \right)}{\left(\frac{1}{h_3^2} - \frac{1}{h_2^2} \right)} \right] \quad (6.13)$$

Introduction of viscosity in pressure distribution:

The effect of temperature and pressure on the viscosity can be expressed as,

$$\mu (1) = \mu (1-1) e^{(-\alpha(T(1) - B DP - T(1-1)))} \quad (6 14)$$

where the temperature is

$$T(1) = T(1-1) - C DX \quad (6 15)$$

Introduction of shear rate and viscosity change

Solution of equation (6 9) gives the shear stress where viscosity and shear rate change can be incorporated

$$\begin{aligned} \tau_2(j) = & \left(\frac{\mu(j-1)\gamma(j)}{2k} + \left[\left(\frac{1}{3k} \right)^3 + \left(\frac{\mu(j-1)\gamma(j)}{2k} \right)^2 \right]^{\frac{1}{2}} \right)^{\frac{1}{3}} \\ & - \left(\frac{-\mu(j-1)\gamma(j)}{2k} + \left[\left(\frac{1}{3k} \right)^3 + \left(\frac{\mu(j-1)\gamma(j)}{2k} \right)^2 \right]^{\frac{1}{2}} \right)^{\frac{1}{3}} \end{aligned} \quad (6 16)$$

where $\gamma(j) = V/h(j)$ and $h(j) = h(j-1) - M DX$

Solution procedure

Equations(6 5), (6 6), (6 11) and (6 16) may be solved simultaneously Numerical values of P_m (maximum step pressure) and hence P_1' and P_2' may be substituted into above equations, using an iteration technique, until the condition $Q_1 = Q_2$ is satisfied Thus the shear stresses on the wire and volumetric flow rate can be determined To determine the hydrodynamic pressure developed at each small increment of length of the first unit, equation (6 6) can be written in the following way

$$\begin{aligned} Q_1 = Q_2 = & \frac{P_1' h_1^3}{6\mu(1-1)} + \frac{\tau c_1 h_1^2}{2\mu(1-1)} + \frac{K}{\mu(1-1)} \left(\frac{P_1'^3 h_1^5}{20} + \frac{\tau c_1^3 h_1^2}{2} + \right. \\ & \left. \frac{P_1'^2 h_1^4 \tau c_1}{4} + \frac{\tau c_1^2 P_1' h_1^3}{2} \right) + V h_1 \end{aligned} \quad (6 17)$$

This equation is a cubic equation, where each term is known (the viscosity can be determined from equation(5 14)) except P_1' Solution of this equation gives this term But,

$$P_1' = (P_1(i) - P_1(i-1))/DX$$

$$\text{and } P_1(i) = P_1(i-1) + P_1' DX$$

$$\text{also } DP = P_1(i) - P_1(i-1)$$

The initial values are

$$P_1(1)=0, T(1)=\text{Polymer melt temperature, } \mu(1)= \text{viscosity at } T(1)$$

Similarly, the hydrodynamic pressure at the tapered unit can be obtained by differentiating equation (6 20) with respect to x and then written in finite difference form

$$P_2(J) = P_2(J-1) + \left[\frac{6\mu(J-1)V}{M[1+3K\tau_2(J)^2]} \left[\frac{1}{h(J)^2} \right] + \frac{6\mu(J-1)}{M[1+3K\tau_2(J)^2]} \left[\frac{1}{h(J)^3} \right. \right. \\ \left. \left. 2 \left(\frac{P_1(L1)M[1+3K\tau_2(J)^2]}{6\mu(J-1)} + V \left[\frac{1}{h_3} - \frac{1}{h_2} \right] \right) \right. \right. \\ \left. \left. \left[\frac{1}{h_3^2} - \frac{1}{h_2^2} \right] \right] \right] dX \quad (6 18)$$

The viscosity can be determined from equation(6 14) by rearranging as

$$\mu_2(J) = \mu_2(J-1) e^{(-\alpha(T(J) - B DP - T(J-1)))} \quad (6 19)$$

and the

$$T_2(J) = T_2(J-1) - C DX \quad (6 20)$$

where $DP = P_2(J) - P_2(J-1)$ and $h(j) = h(j-1) - M Dx$

The initial values are

$$P_2(1) = P_1(L_1), T_2(1) = T_1(L_1), \mu_2(1) = \text{viscosity at } T_1(L_1), h(1) = h_2$$

$$P_2(L_2) = 0, \text{ at } h(L_1 + L_2) = h_3$$

Results have been calculated on the basis of equations derived in the theoretical analysis. In order to calculate the theoretical results, the following values of the parameters were used

Case-1

Polymer- Nylon 6 6 at 280°C

$h_2=0.5$ mm, $h_3=0.05$ mm, $L_1=135$ mm and $L_2=45$ mm

Figure 6 2 shows the theoretical change in the viscosity of the polymer from the entrance of the plasto-hydrodynamic unit. The viscosity of the polymer increases linearly in the first part. In the tapered part the viscosity gradually gets the maximum value and then it decreases. The viscosity is higher for higher wire velocity.

Figure 6 3 shows the theoretical change in magnitude in shear stress within the tapered part of the unit due to the change in shear rate and viscosity. It increases gradually and becomes maximum near the end of the tapered unit. The shear stress is higher for higher wire velocity.

Figure 6 4 illustrates the theoretical hydrodynamic pressure within the unit for wire velocity of 4 m/s. In this figure the present solution is compared with the results from the previous solution where the viscosity and shear rate of the polymer are assumed to be constant. In the present solution, the theoretical pressure has been generated for every small increment of length in both the parallel and the tapered unit, whereas in the previous method the pressure can be found only in the tapered unit. The initial pressure in the parallel section of the unit and the final pressure in the tapered section of the unit are zero. In the previous solution within the tapered unit the pressure increases gradually, gets a maximum value and then decreases to zero at the exit of the unit. For the present solution the pressure in the parallel section increases linearly, in the tapered section it increases gradually up to a certain point and then decreases. The position of maximum pressure is different in the two methods. Also the pressure distribution obtained by the previous method and present method are different according to this figure. Figures 6 5 and 6 6 show the pressure distribution within the unit for wire velocities of 8 and 12 m/s respectively. They show the same profile as Figure 6 5, but the magnitude of the pressure is higher for higher velocity.

Case-2

Polymer Borosiloxane

$h_1=1$ mm, $h_2=0.5$ mm, $h_3=0.05$ mm, $K=5.6 \times 10^{13}$ m⁴/N², $L_1=135$ mm, $L_2=45$ mm

Figures 6.6, 6.7 and 6.8 illustrate the theoretical hydrodynamic pressure within the unit for wire velocities of 0.04, 0.094 and 0.12 m/s respectively. In these figures the present solution in which the change in viscosity and shear rate has been included are compared with the experimental results [30]. Also the previous non-Newtonian [33] and Newtonian [32] solutions have been compared with these results where viscosity of the polymer and shear rate are assumed to be constant. From these figures it can be found that the present pressure solution is much closer with the experimental result than the previous solutions.

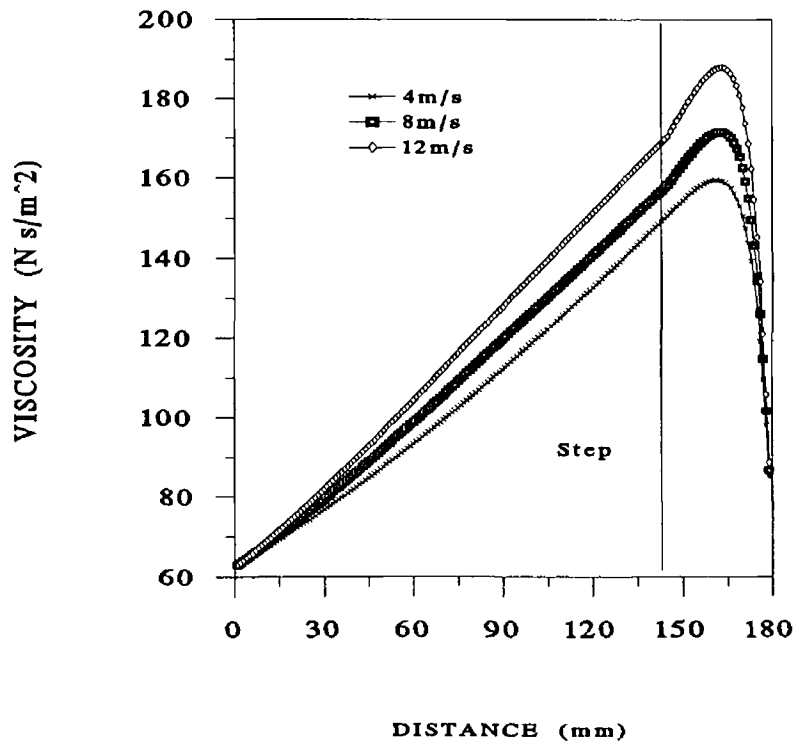


Figure 6 2 Theoretical viscosity distribution within a combined unit (Polymer-Nylon 6 6)

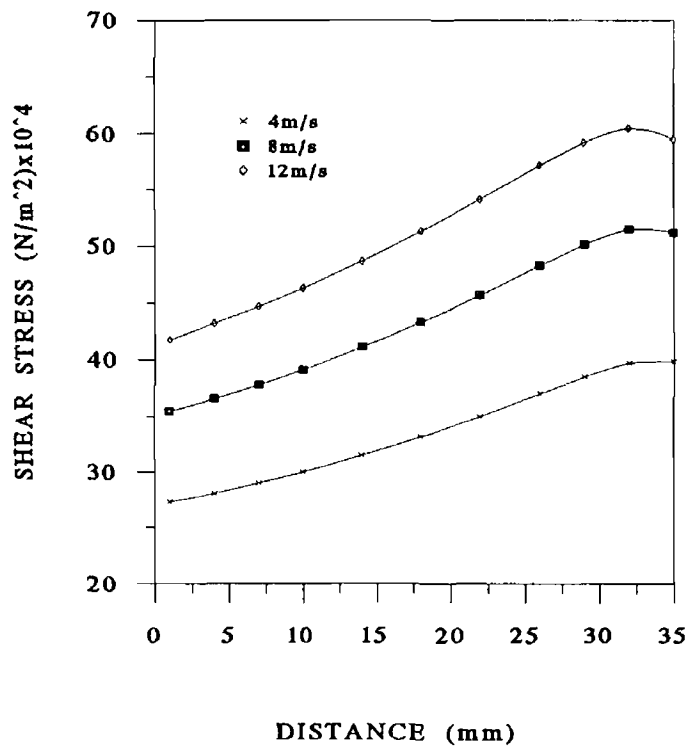


Figure 6 3 Theoretical magnitude of shear stress distribution within a combined unit (Polymer-Nylon 6 6)

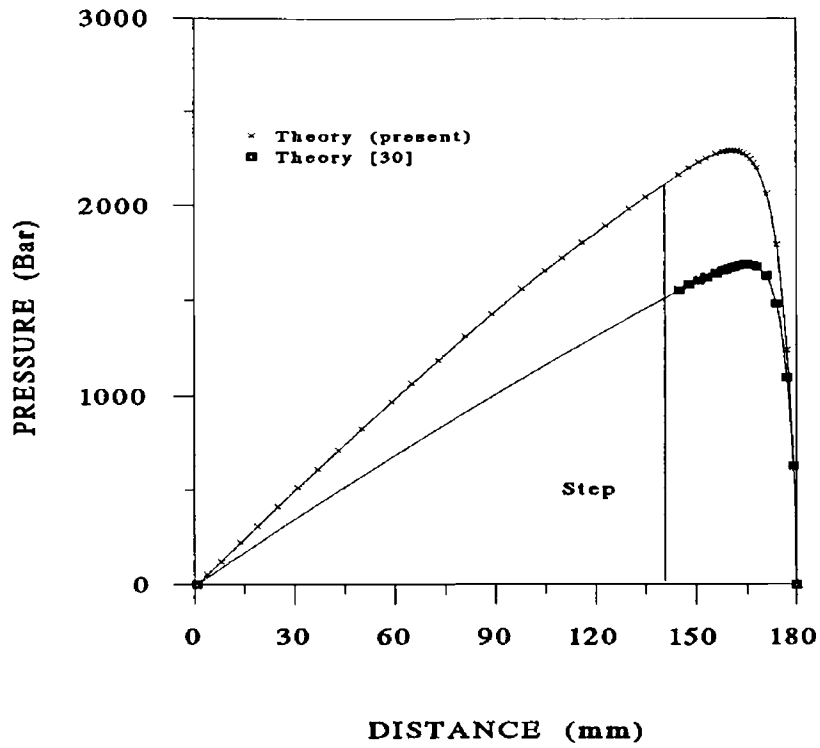


Figure 6 4 Pressure distribution within a combined unit for wire velocity of 4m/s (Polymer-Nylon 6 6)

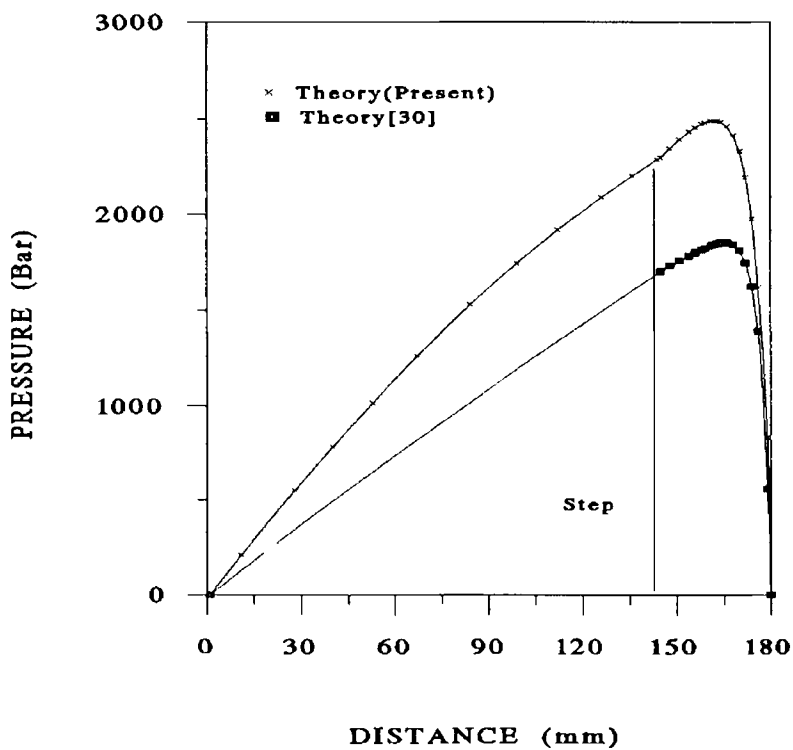


Figure 6 5 Pressure distribution within a combined unit for wire velocity of 8m/s (Polymer-Nylon 6 6)

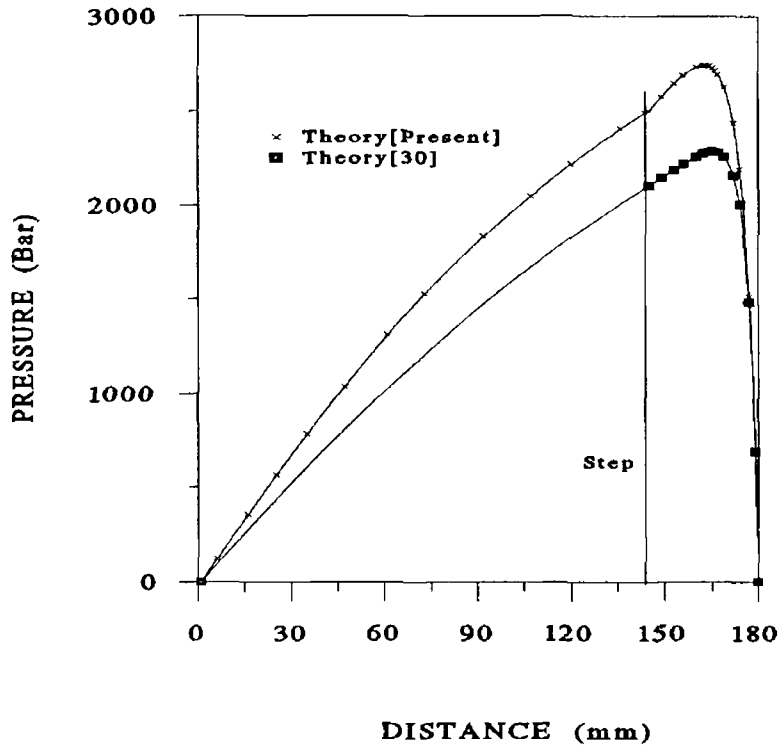


Figure 6 6 Pressure distribution within a combined unit for wire velocity 12m/s (Polymer-Nylon6 6)

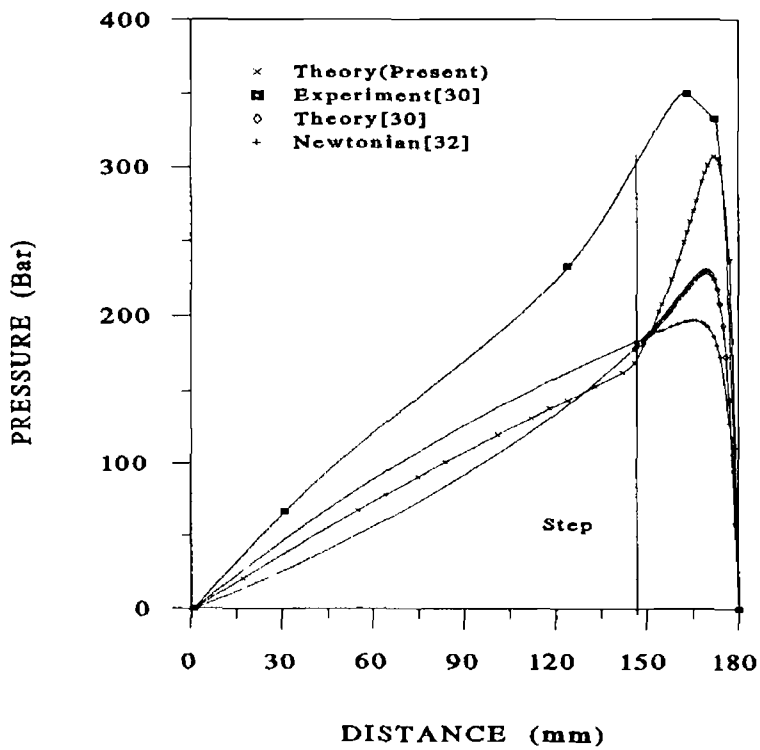


Figure 6 7 Pressure distribution within a combined unit for wire velocity 0.04m/s (Polymer-Borosiloxane)

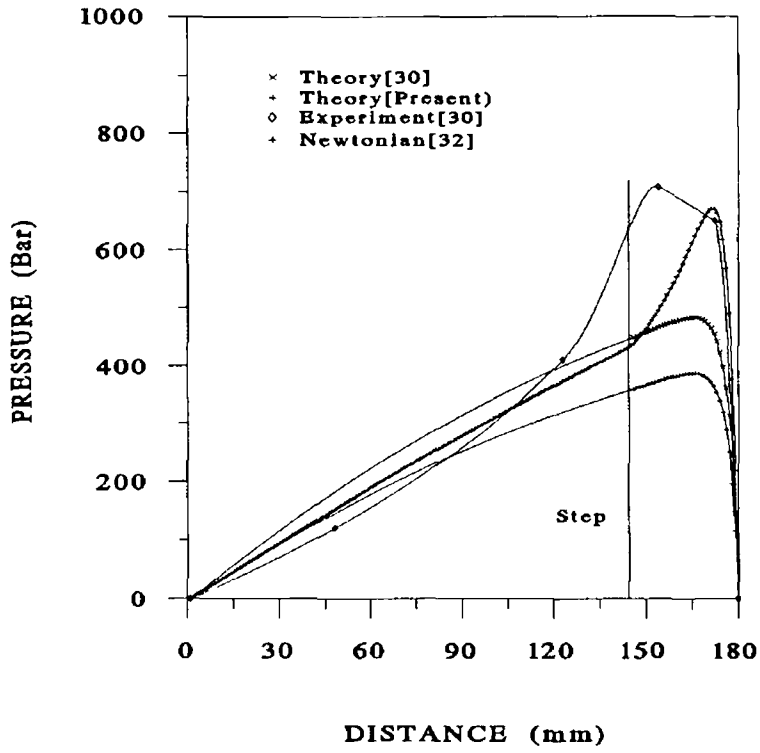


Figure 6 8 Pressure distribution within a combined unit for wire velocity 0.094m/s (Polymer-Borosiloxane)

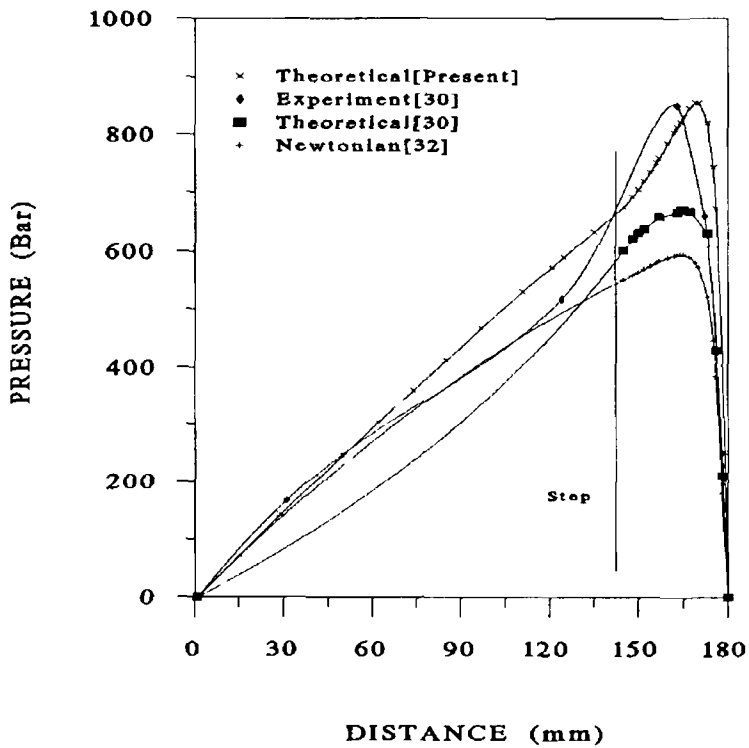


Figure 6 9 Pressure distribution within a combined unit for wire velocity 0.12m/s (Polymer-Borosiloxane)

6.3 Wire drawing in a combined unit

In this section plasto-hydrodynamic wire drawing in a combined parallel and tapered bore unit has been modelled considering that the polymer is a non-Newtonian fluid. Theoretical results are obtained for different wire speeds in terms of the changes in viscosity, shear stress, percentage reduction in area, pressure distribution and coating thickness within the unit.

Deformation analysis for the combined parallel and tapered unit

The yielding position of the wire inside the dieless unit

As the hydrodynamic pressure starts increasing in the first section from zero it is considered that the reduction also starts in the first section.

Consider a distance x_1 from the entry point of the unit where yielding of wire has just commenced [see Figure 6 10 a] The principal stresses acting on the wire are

$$\sigma_1 = \sigma_{x_1} \quad \text{and} \quad \sigma_2 = \sigma_3 = -P_1 ,$$

where σ_{x_1} is the axial stress and P_1 is the radial pressure at point x_1 .

The stress- strain characteristics of the wire are assumed to be of the form

$$Y = Y_0 + K_0 \epsilon^n \tag{6 21}$$

where Y is the flow stress of the wire material and Y_0 is the yield stress.

Therefore, yielding commences when the condition $Y = Y_0$ is satisfied.

Using the Tresca or von-Mises theory of yielding gives,

$$P_1 + \sigma_x = Y \tag{6 22}$$

Equilibrium of forces on the wire in x direction gives

$$\sigma_{x_1} \left(\frac{1}{4} \pi D_1^2 \right) = (\pi D_1 x_1) \tau_{c1}$$

hence,

$$\sigma_{x1} = \frac{4x_1\tau_{c1}}{D_1} \quad (6.23)$$

The pressure at x_1 is given by

$$P_1 = \frac{P_m x_1}{L_1} \quad (6.24)$$

as the pressure in the section builds up linearly along its length. Here P_m is the pressure at the interface of the two unit's step.

Substituting equation (6.23) and (6.24) into equation (6.22) and rearranging, the position of yield in the wire x_1 may be expressed as

$$x_1 = \frac{Y_0}{\frac{4\tau_{c1}}{D_1} + \frac{P_m}{L_1}} \quad (6.25)$$

This equation enables the prediction of the position where the wire starts to yield plastically within the first part of the unit. As soon as yielding occurs, plastic deformation will continue as long as equation (6.22) is satisfied.

Deformation zone

Consider a section of the unit within which the wire is plastically deformed as shown in Figure (6.10 b). Since the deformation of the wire is not pre-defined as a function of x , the equations containing this variable cannot be solved analytically. Hence a finite-difference technique is adopted to solve these equations governing the deformation zone assuming that between any two points of small distance dx apart on the deforming wire, the deformation takes place linearly, therefore,

$$\frac{dD}{2dx} = B$$

Expressing this equation in finite-difference form yields,

$$D_1 = D_{1-1} - 2B_1 \Delta x \quad (6\ 26)$$

and similarly the variation in the gap, dh is given by

$$dh = \frac{dD}{2}$$

hence

$$h_1 = h_{1-1} + B_1 \Delta x \quad (6\ 27)$$

where B_1 is the slope of the deformation profile within distance Δx . Considering a small section of the wire, the radial equilibrium of forces gives,

$$\sigma_r (\pi D dx) = -P \left(\frac{\pi D dx}{\cos \alpha} \right) \cos \alpha + \tau_c \left(\frac{\pi D dx}{\cos \alpha} \right) \sin \alpha$$

hence

$$\sigma_r = -P \left(1 - \frac{\tau_c}{P} \tan \alpha \right) \quad (6\ 28)$$

The value of τ_c/P has been shown to be very small and since α is also very small, the term $\tau_c \tan \alpha / P$ can be ignored.

Equilibrium of forces in x direction gives

$$-\sigma_x \left(\frac{1}{4} \pi D^2 \right) + (\sigma_x + d\sigma_x) \left(\frac{\pi}{4} (D + dD)^2 \right) + P \left(\frac{\pi D dx}{\cos \alpha} \right) \sin \alpha + \tau_c \left(\frac{\pi D dx}{\cos \alpha} \right) \cos \alpha = 0$$

Rearranging and ignoring powers of dD

$$2dD\sigma_x + Dd\sigma_x + 4P dx \tan \alpha + 4dx\tau_c = 0$$

but $\tan\alpha = dD/2dx$ hence

$$2dD(P + \sigma_x) + Dd\sigma_x + 4dx\tau_c = 0$$

Substituting for $(P + \sigma_x = Y)$ and rearranging gives

$$d\sigma_x = -\frac{2dDY}{D} - \frac{4\tau_c dx}{D}$$

This is the governing differential equation in the deformation zone for the axial stress in the wire. Rewriting this equation in finite-difference form gives,

$$\sigma_{x1} = \frac{2(D_{1-1} - D_1)Y_1}{D_1} + \frac{4\tau_{c1}dx}{D_1} + \sigma_{x1-1} \quad (6.29)$$

This equation is a function of shear stress on the wire and it must be determined independently. The equation for the wall shear stress in the first part of the unit may be written as,

$$\begin{aligned} \tau_{c1} = & \left(-\frac{\mu(1-1)V_1}{2Kh_1} + \left(\frac{\mu(1-1)^2V_1^2}{4K^2h_1^2} + \frac{1}{27} \left(\frac{1}{K} + \right. \right. \right. \\ & \left. \left. \frac{1}{4}P_1'^2h_1^2 \right)^{3/2} \right)^{1/3} + \left(-\frac{\mu(1-1)V_1}{2Kh_1} - \left(\frac{\mu(1-1)^2V_1^2}{4K^2h_1^2} \right. \right. \\ & \left. \left. + \frac{1}{27} \left(\frac{1}{K} + \frac{1}{4}P_1'^2h_1^2 \right)^{3/2} \right)^{1/3} - \frac{1}{2}P_1'h_1 \right) \quad (6.30) \end{aligned}$$

This equation contains the pressure gradient and variation of the wire velocity in the deformation zone and they must be determined separately. The flow of the polymer melt in this region may be expressed as,

$$\begin{aligned} Q_1 = Q_1 = & \frac{P_1'h_1^3}{6\mu(1-1)} + \frac{\tau_{c1}h_1^2}{2\mu(1-1)} + \frac{K}{\mu(1-1)} \left(\frac{P_1'^3h_1^5}{20} + \frac{\tau_{c1}^3h_1^2}{2} + \right. \\ & \left. \frac{P_1'^2h_1^4\tau_{c1}}{4} + \frac{\tau_{c1}^2P_1'h_1^3}{2} \right) + Vh_1 \quad (6.31) \end{aligned}$$

Equations (6.30) and (6.31) may be solved simultaneously in order to determine P_1'

and τ_{c1} by iterating P_1' at point 1 in the deformation zone
Therefore,

$$P_1(1) = P_1(1-1) + P_1' \Delta x \quad (6.32)$$

The variation of speed of the wire in the deformation zone may be also included in the analysis. The continuity of flow of metal through the element [Figure 6.10 c] gives

$$(V+dV) \frac{\pi}{4} (D+dD)^2 = \frac{\pi}{4} VD^2$$

Ignoring higher order of dD gives

$$\frac{dV}{V} = - \frac{2dD}{(D+2dD)}$$

Rewriting this equation in finite difference form gives

$$V_1 = \frac{V_{1-1}}{1 - \frac{2(D_{1-1} - D_1)}{2D_{1-1} - D_1}} \quad (6.33)$$

The true strain-stress relationship of the wire in the deformation zone may be shown as

$$Y_1 = Y_0 + K_0 \epsilon_1^n$$

where $\epsilon_1 = 2 \ln (D_1 / D_0)$

Therefore,

$$Y_1 = Y_0 + K_0 \left(2 \ln \left(\frac{D_1}{D_2} \right) \right)^n \quad (6.34)$$

Substituting for Y_1 in equation (6.29) gives

$$\sigma_{x1} = 2 \left(\frac{D_1 - D_2}{D_2} \right) \left(Y_0 + K_0 \left(2 \ln \left(\frac{D_1}{D_2} \right) \right)^n \right) + \frac{4 \tau_{c1} dx}{D_1} + \sigma_{x1-1} \quad (6.35)$$

The new shear stress within the zone where deformation of wire has been observed is then given by,

$$\tau(1) = P'_1 h_1 + \tau_{c1} \quad (6.36)$$

At any point 1 in the deformation zone, D_1 , h_1 , and V_1 may be calculated from equations (6.26), (6.27) and (6.33) respectively for an arbitrary value of B_1 . By substituting the values of D_1 and V_1 into equation (6.34) the yield stress Y_1 may be calculated. Also by substituting for V_1 and h_1 into equations (6.30) and (6.31) gives P'_1 and τ_{c1} and simultaneously iterating for P'_1 until equation (6.31) is satisfied. Hence equation (6.32) gives $P_1(1)$. Similarly τ_{c1} and D_1 may be substituted into equation (6.35) to evaluate σ_{x1} . This $P_1(1)$, τ_{c1} and h_1 gives the shear stress within the deformation zone. Other variables in the above equations are known physical properties. Having calculated σ_{x1} , P_1 and Y_1 , the values of B_1 may be iterated in the above equations until equation $\sigma_{x1} + P_1 = Y_1$ is satisfied.

After the step (in the tapered unit)

Referring to Figure 6.10(c) which shows an element of the wire within a straight conical profile the pressure equation in terms of finite difference term is,

$$P_2(J) = P_2(J-1) + \left[\frac{6\mu(J-1)V}{M[1+3K\tau_2(J)^2]} \left[\frac{1}{h(J)^2} \right] + \frac{6\mu(J-1)}{M[1+3K\tau_2(J)^2]} \left[\frac{1}{h(J)^3} \right] \right. \\ \left. 2 \left(\frac{P_1(L1)M[1+3K\tau_2(J)^2]}{6\mu(J-1)} + V \left[\frac{1}{h_3} - \frac{1}{h_2} \right] \right) \right. \\ \left. \left[\frac{1}{h_3^2} - \frac{1}{h_2^2} \right] \right] dx \quad (6.37)$$

The change in shear stress where viscosity and shear rate change can be incorporated is

$$\tau(J) = \left(\frac{\mu(J-1)\gamma(J)}{2k} + \left[\left(\frac{1}{3k} \right)^3 + \left(\frac{\mu(J-1)\gamma(J)}{2k} \right)^2 \right]^{\frac{1}{2}} \right)^{\frac{1}{3}} - \\ \left(\frac{-\mu(J-1)\gamma(J)}{2k} + \left[\left(\frac{1}{3k} \right)^3 + \left(\frac{\mu(J-1)\gamma(J)}{2k} \right)^2 \right]^{\frac{1}{2}} \right)^{\frac{1}{3}}$$

where $\gamma(J) = V/h(J)$ and

$$\tau_{c_j} = \tau(J) - P'_j h(J) \quad (6.38)$$

The change in gap between the wire and the unit gap, velocity and diameter within the deformation zone can be expressed respectively as,

$$h(J) = h(J-1) - (M-k_j) \Delta x \\ V_j = V_{j-1} \left(\frac{D_{j-1}}{D_j} \right)^2 \\ D_j = D_{j-1} - 2k_j \Delta x \quad (6.39)$$

where $\tan \alpha = -k_j$

The true strain-stress relationship of the wire in the deformation zone may be shown as

$$Y_j = (Y_0 + K_0 (2 \ln \left(\frac{D_1}{D_j} \right))^n) \quad (6.40)$$

The increment in axial stress may be expressed as,

$$\sigma_{xj} = 2 \left(\frac{D_{j-1} - D_j}{D_j} \right) \left(Y_0 + K_0 \left(2 \ln \left(\frac{D_1}{D_j} \right) \right)^n \right) + \frac{4 \tau_{c_j} dx}{D_j} + \sigma_{xj-1} \quad (6.41)$$

The Tresca yield criterion for plastic yielding in finite difference form becomes,

$$P_2(j) + \sigma_{xj} \geq Y_j \quad (6.42)$$

The plastic deformation is calculated on the basis of equation (6.42) combined with equations (6.37) -(6.41) for small increment of Δx

The initial conditions for the deformation of wire in the tapered unit are,

$$P_2(1) = P_1(\text{step}), h_{\text{taper}}(1) = h_{\text{parallel}}(\text{step}), V_{\text{taper}}(1) = V_{\text{parallel}}(\text{step}), Y_{\text{taper}}(1) = Y_{\text{parallel}}(\text{step}), \\ \sigma_{\text{xtaper}}(1) = \sigma_{\text{parallel}}(\text{step}) \text{ and } D_{\text{taper}}(1) = D_{\text{parallel}}(\text{step})$$

Theoretical results have been calculated on the basis of equations derived in the theoretical analysis. In order to calculate theoretical results, the following magnitudes of the parameters were used [11,55]

$B = 5.6 \times 10^{-10} \text{ C/N mm}^{-2}$, $C = 0.1 \text{ }^\circ\text{C/mm}$, $\alpha = 0.017 \text{ }^\circ\text{C}$, $DX = 1 \text{ mm}$, $h_1 = 0.2 \text{ mm}$, $h_2 = 0.1 \text{ mm}$, $h_3 = 0.05 \text{ mm}$, $K = 5.0 \times 10^{11} \text{ m}^4/\text{N}^2$, $L_1 = 50 \text{ mm}$, $L_2 = 30 \text{ mm}$, initial polymer temperature at the first unit = $130 \text{ }^\circ\text{C}$, initial polymer viscosity = 110 N s/m^2 , $y_0 = 50 \text{ MNm}^2$, $K_0 = 440 \text{ MNm}^2$, $n = 0.52$, critical shear stress = 0.5 MNm^2 , $D_1 = 1.6 \text{ mm}$

The polymer was Alkathane WVG23 and the wire material was Copper

Figure 6.11 shows the change in the viscosity of polymer from the entrance of the plasto-hydrodynamic unit. The viscosity is influenced by temperature and pressure. In the parallel part the viscosity of the polymer increases in a non-linear way up to a certain magnitude. In the tapered part, the viscosity increases more non-linearly upto a certain point (different for different velocity) and then decreases gradually. With the increase in the wire velocity the viscosity also increases.

Figure 6.12 shows the theoretical magnitude in change in the shear stress within the unit due to the change in the shear rate and viscosity. In the parallel part, before the deformation the shear stress remains constant, after the yielding point it increases linearly up to the step. At the entrance of the tapered part there is a sudden rise in the shear stress and then it increases gradually up to maximum point. After that, the shear stress decreases near the end of the tapered part. The shear stress increases with

the increase in the wire velocity

Figure 6 13 illustrates the theoretical hydrodynamic pressure within the unit for wire velocity of 1 m/s, 2 m/s and 3 m/s respectively. The initial pressure in the parallel part of the unit and the final pressure in the tapered part of the unit are zero. For the present solution, the pressure in the parallel part increases linearly. In the tapered part it increases gradually up to a maximum pressure then decreases gradually to zero. With the increase in the wire velocity the pressure also increases. The viscosity, shear stress and hydrodynamic pressure profile in drawing and coating process are different from that for the coating process only.

Figure 6 14 shows the theoretical percentage reduction in area for different speeds of the wire. Theoretically, these reductions increase with the increase in velocities. After wire velocity 3 m/s they become almost constant as the wall shear stress reaches the critical shear stress. Figure 6 15 shows the theoretical coating thickness for different speed of the wire. Also in this case it can be found that the theoretical coating thickness increases with velocity at first, then after wire velocity 3m/s it becomes constant.

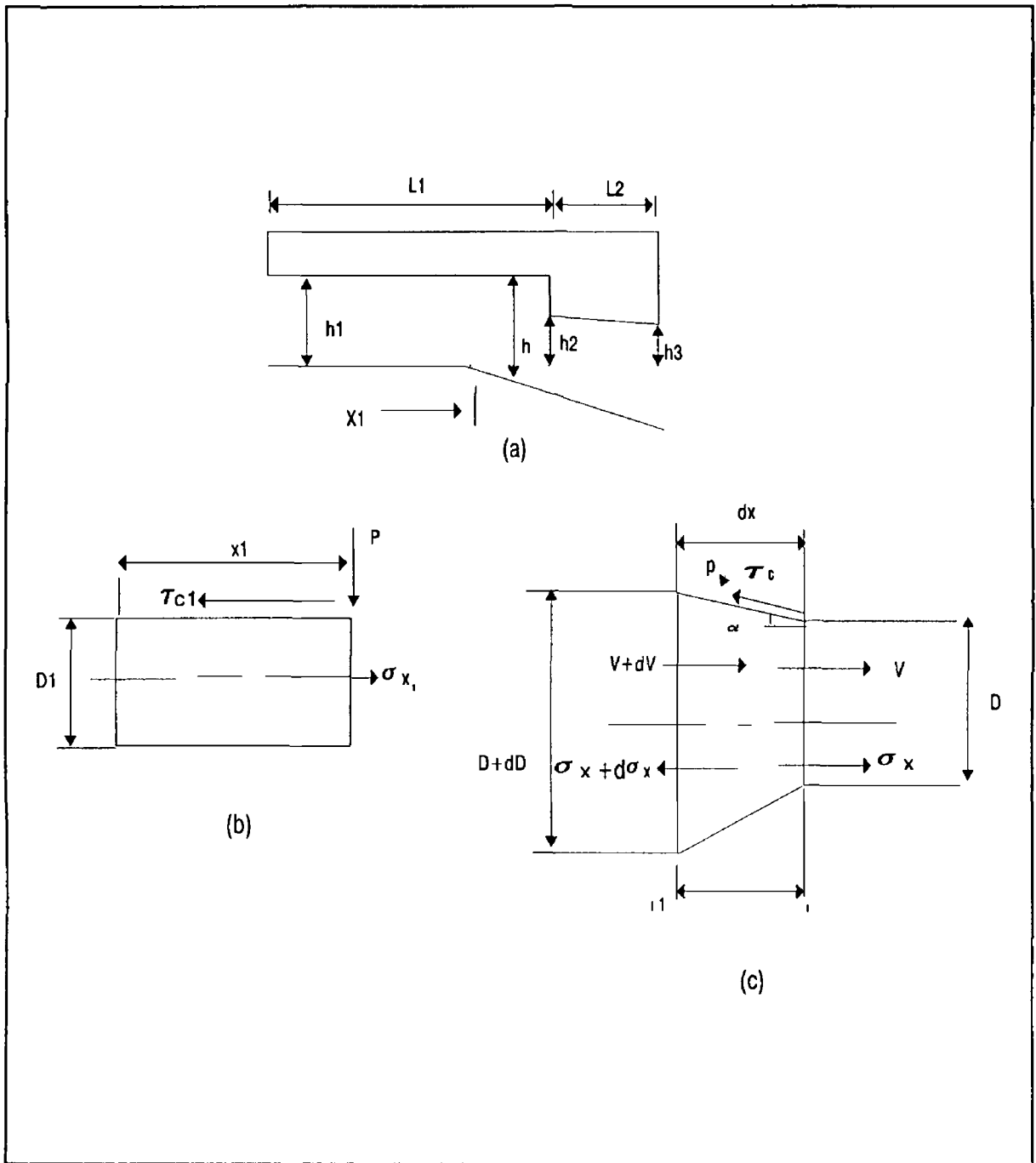


Figure 6 10 Schematic diagram for wire drawing analysis in a combined geometry unit

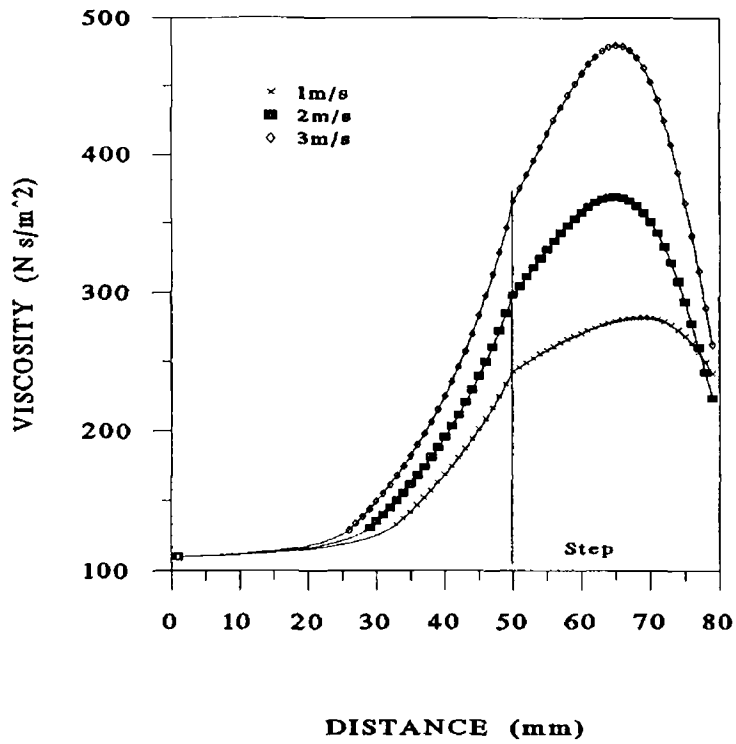


Figure 6 11 Theoretical viscosity distribution for wire drawing in a combined unit (Polymer Alkathane WVG23)

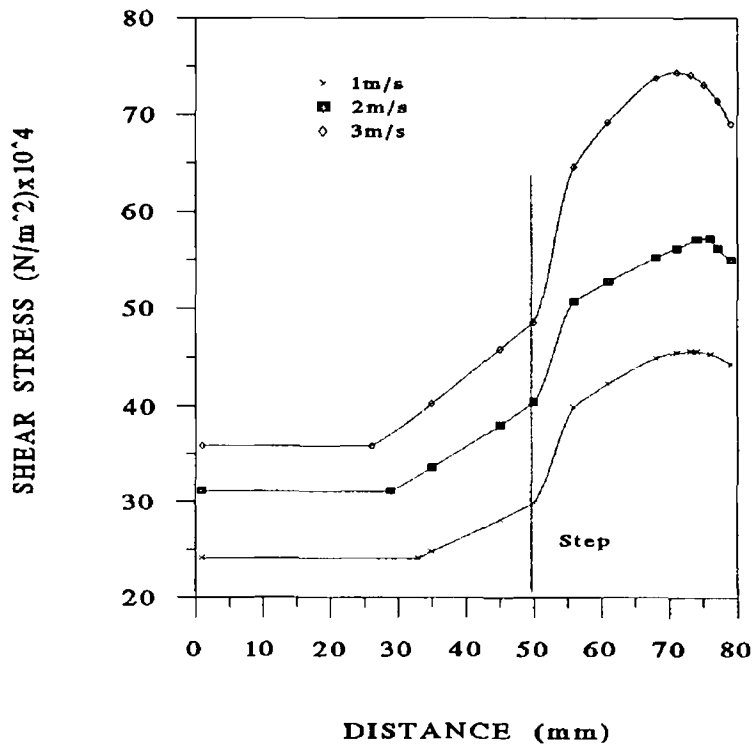


Figure 6 12 Theoretical shear stress distribution for wire drawing in a combined unit (Polymer Alkathane WVG23)

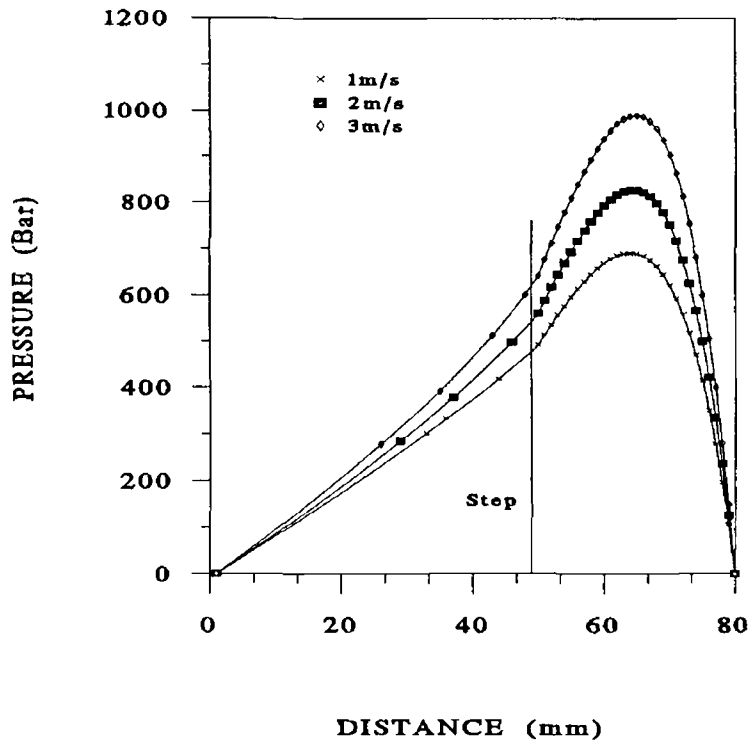


Figure 6 13 Theoretical pressure distribution for wire drawing in a combined unit(Polymer Alkathane WVG23)

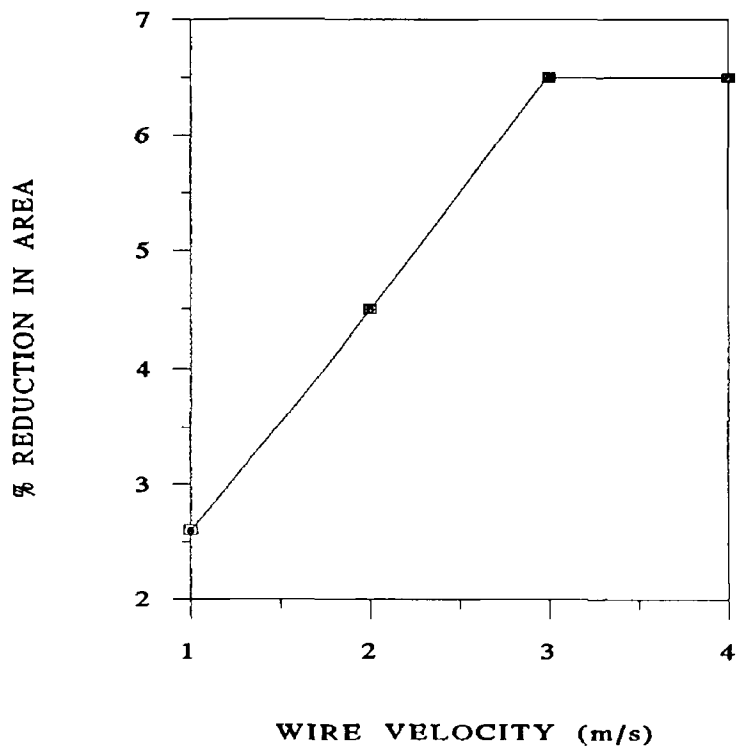


Figure 6 14 Theoretical percentage reduction in area for wire drawing in a combined unit(Polymer Alkathane WVG23)

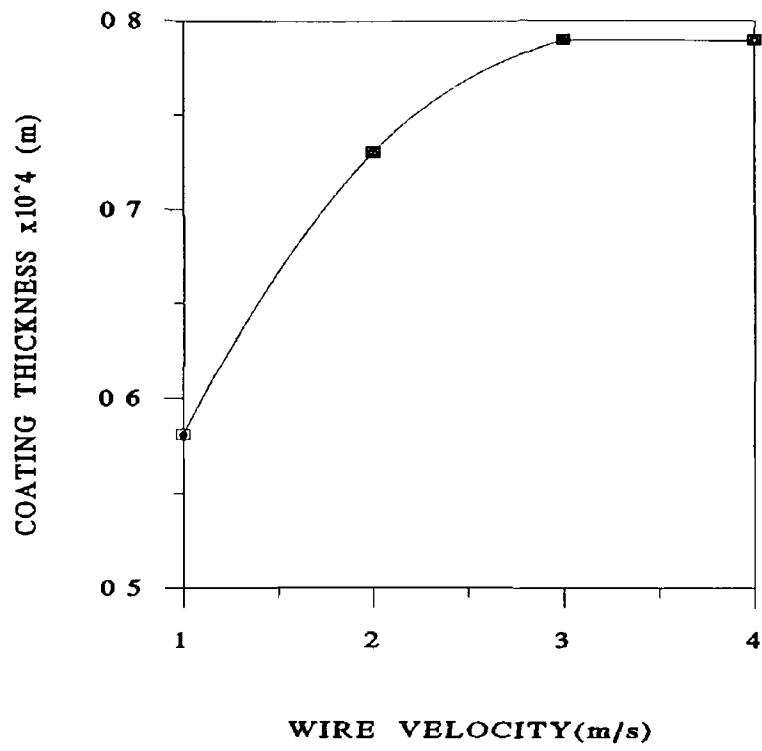


Figure 6 15 Theoretical coating thickness on wire in drawing process in a combined unit(Polymer Alkathane WVG23)

6.4 Finite element temperature and pressure simulation for wire coating in case of combined parallel and tapered unit

In this section a finite element solution has been obtained for the temperature and pressure distributions taking account of their changes along both the direction of the wire velocity and the thickness of the polymer layer. Theoretical results have been obtained for different wire speeds in terms of the pressure distribution within the unit. These results are compared with the experimental results reported elsewhere. This simulation has already been reported as reference [68].

Finite element model

Finite element simulation was carried out for a 180 mm long combined parallel and tapered bore unit. The gap between the unit and the wire i.e., lubricant film thickness at the entrance and exit of the unit are 0.5 mm and 0.05 mm respectively. The gap at the point where there is change of cross section is 0.25 mm. The model was constituted with 20 elements and 87 nodes. Figure 6.16 shows the meshed model for temperature and pressure.

The governing equation

The equation governing the pressure generation in the fluid film is the Reynolds equation [63]

$$\frac{d}{dx} \left(\frac{h^3}{6\mu} \frac{dP}{dx} \right) + \frac{d}{dy} \left(\frac{h^3}{6\mu} \frac{dP}{dy} \right) = 2 \frac{dh}{dt} + U \frac{dh}{dx} \quad (6.43)$$

Also the governing Reynold equation for temperature distribution [63] is

$$\frac{d}{dx} \left(K_{xx} \frac{dT}{dx} \right) + \frac{d}{dy} \left(K_{yy} \frac{dT}{dy} \right) + \phi = \frac{dT}{dt} + U \frac{dT}{dx} \quad (6.44)$$

Element characteristics

The lubricant was modelled with 2 dimensional 8 node quadrilateral elements. The nodes of the elements have two degrees of freedom i.e. in X direction the die length and in Y direction the gap between the wire and the die.

Boundary conditions and Solution

Referring to Figure 6.16 the boundary conditions for the elements in the case of pressure are- along AB and GE, $P=0$

BG, the wire surface is rigid

AC, DE and CD the die surface is rigid

Also referring to Figure 6 16 the boundary conditions for the elements in the case of temperature are-along AB, T is constant for each layer of fluid film

BG, heat flux through the wire is negligible

GE, T is unknown

AC, CD and DE, temperature at the die wall is constant

A Cholesky decomposition matrix technique was used to solve the resulting global sparse matrix and the finite element solution was obtained using the Gauss-Siedal iteration technique [63]

During the experiment with Borosiloxane, the temperature of the die wall was maintained at 110⁰C When the polymer first entered in the pressure unit from the melt chamber the polymer melt temperature was about 95⁰C

Figure 6 17 shows the temperature profiles in the die flow channel when the wire drawing speed is 0 04 m/s The temperature profile is almost the same as for the tapered unit

Figure 6 18 illustrates the theoretical hydrodynamic pressure within the unit for wire velocity of 0 04 m/s In this figure the finite element solution has been compared with the experimental results from reference[33] The initial pressure in the first section of the unit and the final pressure in the second section of the unit is zero In the simulation, it was observed that the pressure increases gradually up to a certain point and then decreases From the figure it can be seen that the theoretical pressure profile is similar to the experimental pressure profile The position of the maximum pressure is also about the same The magnitude of simulated pressure is very close to that of the experimental pressure

Figures 6 19 and 6 20 also show comparisons of pressure profiles from the finite element simulation with those from experiments for wire velocities of 0 094 and 0 12 m/s respectively It can be seen from these figures that the pressure profiles are reasonably similar to the experimental profiles The magnitudes of the simulated maximum pressure are also in reasonable agreement to the experimental ones

The finite element simulation was done in two dimensions ie, along the direction of wire drawing and the direction of the fluid film thickness, but, the pressure difference through the film thickness was predicted to be negligible

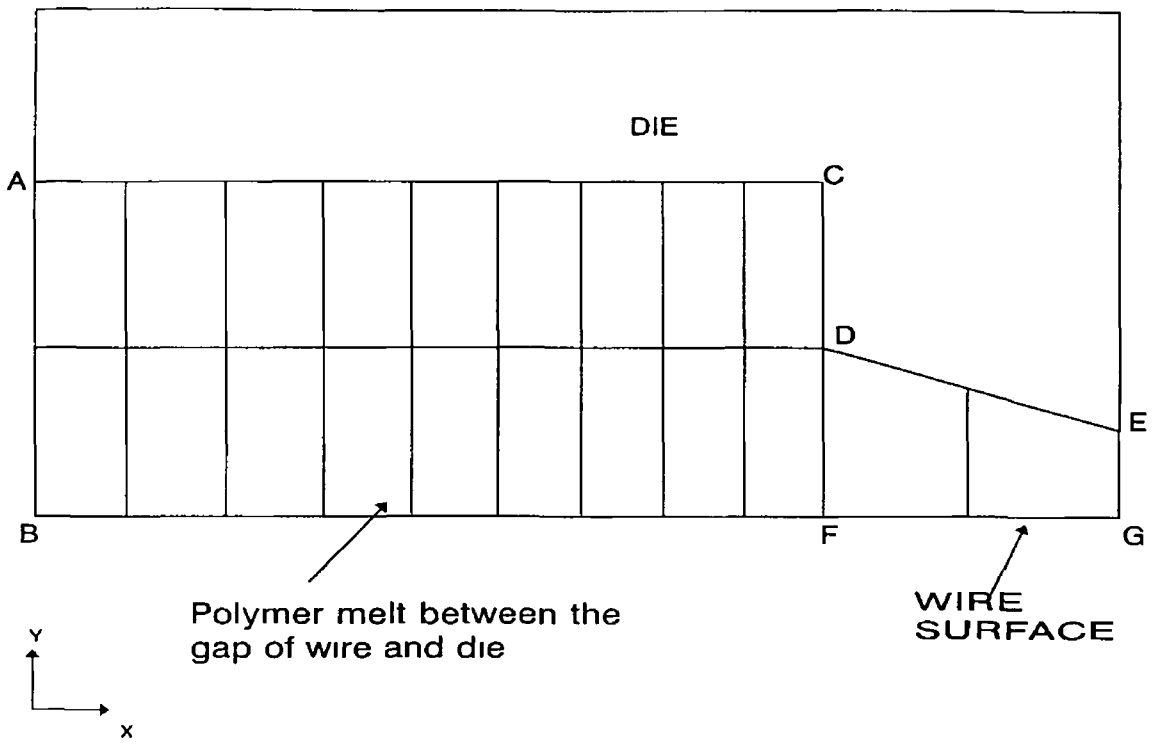


Figure 6 16 Schematic diagram for the meshed model in combined unit

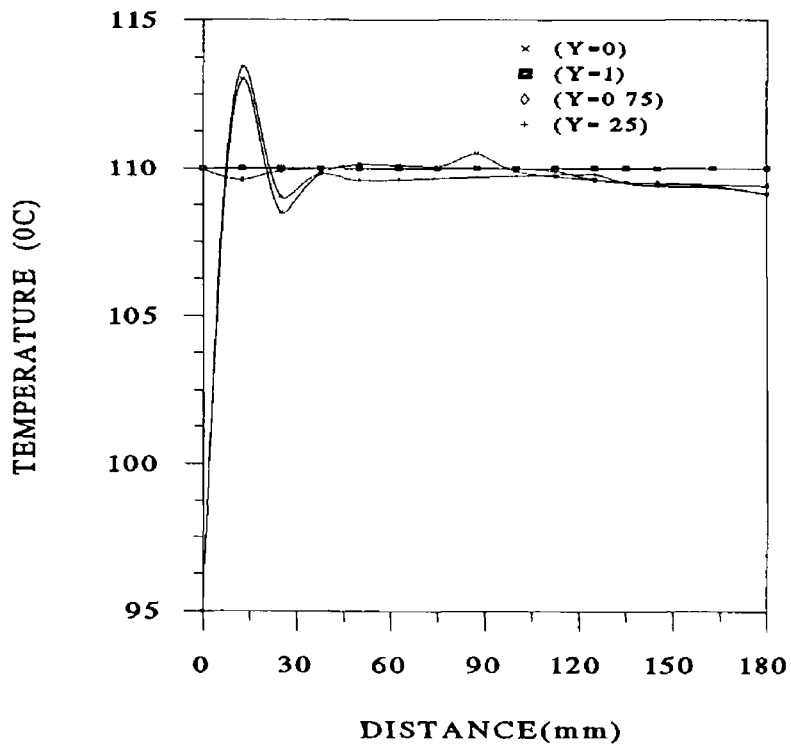


Figure 6 17 Temperature distribution in the combined unit

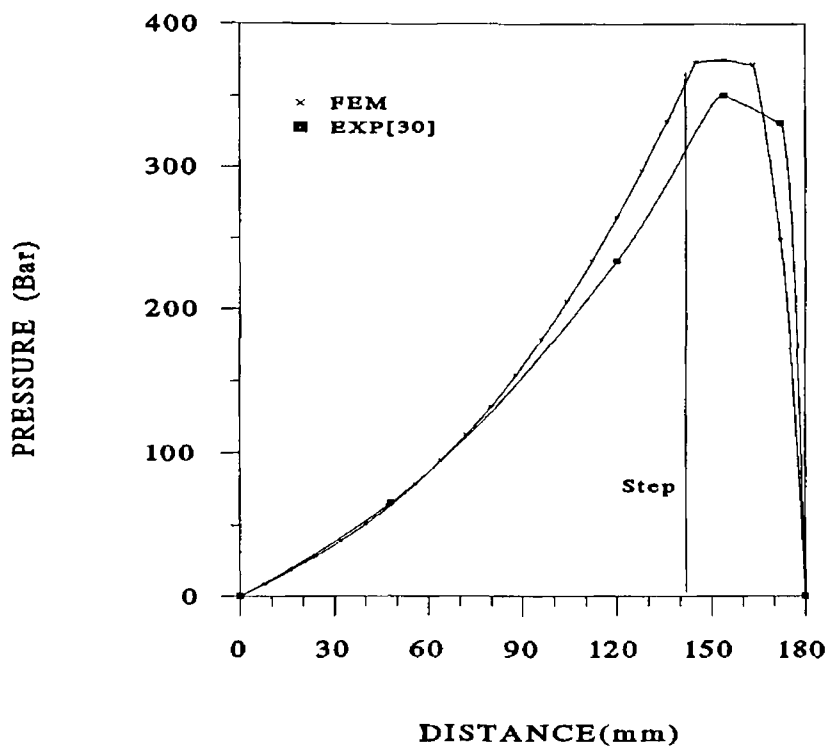


Figure 6 18 Pressure distribution in a combined unit for wire velocity of 0.04 m/s (Polymer-Borosiloxane)

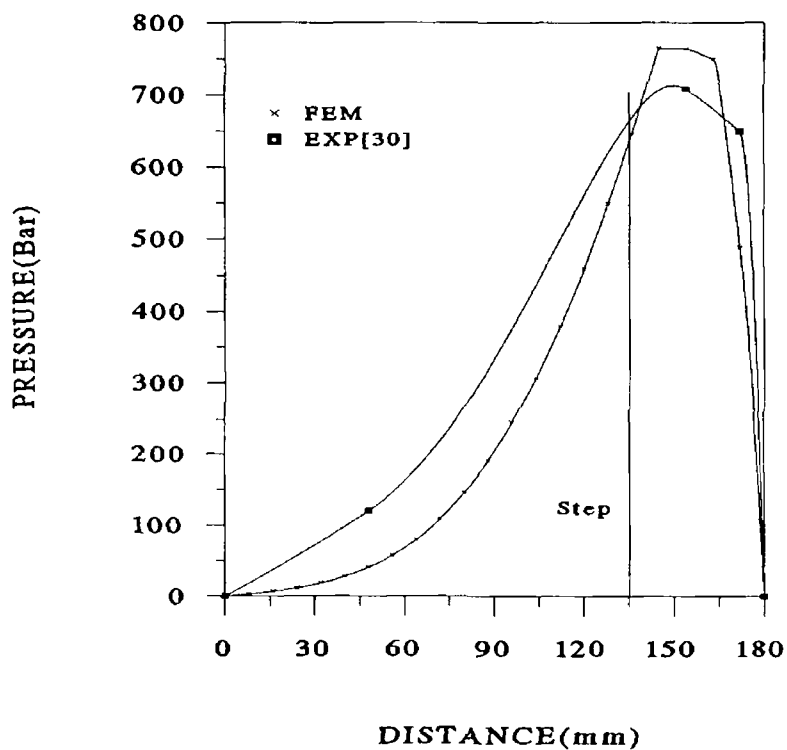


Figure 6 19 Pressure distribution in a combined unit for wire velocity 0.094 m/s (Polymer-Borosiloxane)

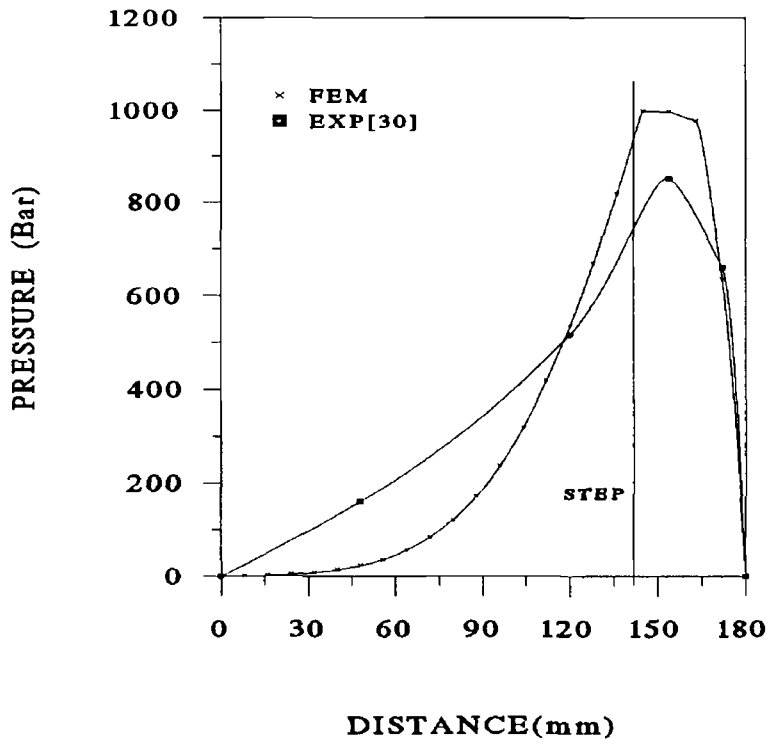


Figure 6 20 Pressure distribution in a combined unit for wire velocity 0 12m/s (Polymer-Borosiloxane)

CHAPTER- SEVEN

EXPERIMENTAL RESULTS FOR THE WIRE COATING PROCESS

7.1 Introduction

In the conventional process of wire coating the wire is either dipped in the coating material or is coextruded along with the coating material. Detail description of such coating processes can be found in references [73-80].

Apart from dipping or coextrusion methods there is another innovative method called hydrodynamic coating described in references [81-92]. A brief review of different experimental works on this new process is presented below. In the next section results from the experiments carried out in the present study are presented.

Hydrodynamic wire coating using a die-less drawing unit was first carried out by Parvinmehr et al [7-11] who used a die-less drawing unit whose smallest bore was slightly greater than the diameter of the undeformed wire. For this work the tests were carried out with wire of 1.6 mm diameter.

Relatively recently Symmons et al [84] reported the results of their works on coating fine wire (diameter 0.45 mm) in relation to plasto-hydrodynamic drawing and coating. The drawing speed range was from 0.05 to 0.8m/s. Also Lamb and Hashmi [86] and Yu and Hashmi [89] carried out their research for polymer coating of fine wires (diameter 0.1-0.4mm). They achieved a fairly constant polymer coating for wire speeds of up to a maximum of 0.6m/s.

In all these works, the wire speed in the process was rather low. Coating at this speed does not promise much for industrial scale production.

One of the main objectives of the present investigation is to achieve and assess the quality of coating at wire velocities of between 1-12 m/s. The effect of the polymer melt temperature and back pressure on the coating process will also be investigated. Results of experimental investigation are presented comparing the coating quality on galvanized mild steel wire when molten Nylon 6 is used as the coating material at

different temperatures and back pressures for different pressure units. The coating thickness and quality and drawing force due to the pulling action of the wire through the pressure media are discussed for different wire speeds of up to 12 m/s.

7.2 Experimental procedure and equipment

Based on the theoretical understanding of the process, design of the rig such as length of melt chamber, wire preheating unit, argon back pressure, different pressure units etc. were done. With this design it was possible to obtain continuous and concentric coating on wire up to wire speed of 12 m/s. The details of the experimental procedure and equipment are described in chapter three. However a brief description of these are repeated here again.

The experimental set up consists of the drawing bench, the electrical installations, the wire feed mechanism, the drive system, the polymer feeding and melting unit and the pressure unit. A Schematic diagram of the process is shown in Figure 2.7. The wire enters the leakage control unit attached to the melt chamber. The leakage control unit also acts as a preheating unit for the wire. The wire then passes through the melt chamber and enters the plasto-hydrodynamic pressure unit. The coated wire is then wound in the bull block which is driven by a continuously changeable speed motor. Polymer granules are poured in the hopper which is fitted with a heater band. The hopper is connected to the melt chamber and a pressurised argon gas bottle is connected through a pressure line into the hopper which provides the back pressure in the polymer melt.

To measure the drawing force during the wire drawing process a piezo-electric load cell is located at the exit end of the die unit. A proportional electric charge corresponding to the force is generated in the load cell during drawing and is converted by the charge amplifier into proportional voltage signal. The analog to digital converter receives the signal from the transducer via the charge amplifier. A computer digitizes the signal through a programme written in basic language and displays the magnitude of the force through a printer output.

For higher wire speeds, the polymer coating has not solidified completely by the time it reaches the bull block and the individual strands stick together and the polymer coating gets deformed. The sample of the coated wire is therefore taken

from the part which does not reach the bull block after the motor is suddenly stopped To measure the coating thickness each sample is measured at 5 different positions along its length by a micrometer and the average diameter of the coated wire is noted A small portion of some of the wire samples were cold mounted and polished An optical microscope was then used to assess the actual coating thickness and the concentricity of the coating on the wire

7.3 Experimental results and discussions

7.3.1 Process parameters

The process parameters for the investigations carried out were as follows

Polymer characteristics

polymer type Durethan B 35F 9000/0 KYY (Nylon 6)

polymer melt temperature 230° C - 270° C

Wire characteristics

wire diameter 0.7mm

wire material galvanized mild steel

Pressure unit characteristics:

Five types of pressure units were used to carry out the experiments These were three stepped parallel bore, one tapered bore and one combined pressure unit The schematic diagram of the pressure units are shown in Figure 4.1 (stepped parallel bore unit), Figure 5.1 (tapered bore unit) and Figure 6.1 (combined unit)

The total length of all the pressure units was 22 mm Other geometric parameters for different units which were different are presented in the following,

For stepped parallel bore unit

length of the first part before step, $L_1 = 17\text{mm}$

length of the second part after step, $L_2 = 5\text{mm}$

radial gap between the wire and the pressure unit in the first part, $h_1 = 0.5\text{mm}$

radial gap between the wire and the pressure unit in the second part, $h_2 = 0.05, 0.12$

and 0.03 mm

For tapered bore unit

length of the unit, $L=22$ mm

radial gap between the wire and the unit in the first part, $h_1 = 0.25$ mm

radial gap between the wire and the unit in the second part, $h_2= 0.0425$ mm

For combined unit

length of the first part before step, $L_1 = 17$ mm

length of the second part after step, $L_2 = 5$ mm

radial gap between the wire and the unit in the first part, $h_1 = 0.7$ mm

radial gap between the wire and the unit in the second part, $h_2 = 0.051$ mm

7.3.2 Experimental works

Experimental work was carried out at polymer melt temperatures of 230°C, 250°C and 270°C. The back pressure of argon applied in each polymer melt were 5 and 10 bar. For different combinations of polymer melt temperature and argon back pressure experiments were carried out for wire velocities of 2, 4, 6, 8, 10 and 12 m/s in all pressure units except stepped parallel bore pressure unit with h_2 equal to 0.05 mm. For this unit wire velocities were 1, 4, 6, 8, 10, 12 and 12.5 m/s and the argon back pressures were 0, 5 and 10 Bar.

The results of these tests are presented in the following figures in terms of the coating thickness, drawing load, melt temperature, back pressure and drawing speed.

Stepped parallel bore pressure unit ($h_2=0.05$ mm)

Figure 7.1 shows the thickness of Nylon 6 coating at the melt temperature of 230°C. From the graph it can be seen that the coating thickness is uniform at about 0.05 mm for velocities of up to 12m/s. Inspection of the coating also showed that the coating was continuous. The coating thickness of 0.05 mm is equal to the radial gap between the wire and the exit pressure unit.

During the experiment it was observed that there was no deformation of the wire. If there is no deformation in the wire then theoretically the coating thickness should

be equal to the gap between the wire and the exit of the pressure unit. The experimental results confirm this. It is also evident from the figure that the thickness and continuity of the polymer coating on the wire are not affected by back pressure of the polymer melt.

The results in Figure 7.2 show the coating thickness and continuity with Nylon 6 at the melt temperature of 250°C. For argon pressures of 0, 5 and 10 bar the test was carried out at up to 12.5 m/s. The coating thickness was 0.05 mm for wire velocities of up to 6 m/s for 0 Bar argon pressure. At wire velocity 12 m/s it was 0.048 mm. At 5 bar back pressure the coating thickness was 0.05 mm up to 12 m/s. However at 12.5 m/s the coating thickness was found to be 0.049 mm. This decrease in coating thickness is thought to be due to the slip that occurred between the layers of polymer and the wire surface. For the argon pressure of 10 bar the coating was continuous within the entire velocity range and the coating thickness was uniform at 0.05 mm. With all these back pressure cases the coating was found to be continuous. But the main problem with zero back pressure was that the Nylon 6 melt burnt as the melt temperature increased beyond 230°C.

Figure 7.3 shows the coating thickness for Nylon 6 at the melt temperature of 270°C. The test was carried out at wire velocities of up to 12.5 m/s for argon pressure of 0, 5 and 10 bar. The coating was continuous and the thickness was uniform at 0.05 mm over the entire range of velocities except for 0 bar.

The coating on the polymer appeared to be concentric. Some samples were prepared and polished for examination using an optical microscope. The cross section of the wire was observed to be circular and the coating was reasonably concentric. Plate 7.1 shows the concentricity of the coating on wire with 5 bar back pressure and wire velocity 4 m/s at 270°C. Plate 7.2 shows the concentricity of coating with zero back pressure at 230°C and wire velocity 10 m/s. They show that the coating is reasonably concentric. Plate 7.3 illustrates the coating concentricity at 250°C for zero bar back pressure and wire velocity 12 m/s which appears to be slightly eccentric.

Figure 7.4 shows the generated drawing force for the polymer melt temperature of 230°C during the coating process. The drawing force generally increases with the increase in the wire velocity. Also it increases with the increase in argon back

pressure For the back pressure of 10 bar the drawing force is on average 25N and 50N greater than those for the back pressure of 5 bar and zero bar respectively Figure 7 5 shows the generated drawing force for polymer melt temperature of 250°C It shows the similar trend as in Figure 7 4 Figure 7 5 shows drawing force for a polymer melt temperature of 270°C The drawing force increases up to 7 m/s after which it decreases This is thought to be due to the critical shear stress that causes slip at the surface of the wire and the polymer melt However, it is evident from the above three figures that the increase in melt temperature in general causes the drawing load to decrease This is because as the temperature increases the viscosity of the polymer melt decreases, which leads to a decrease in the drawing force

The hydrodynamic unit was too small to incorporate pressure transducers at different locations and thus, it was not possible to measure the experimental pressure distribution within the unit Figures 4 2, 4 3 and 4 4(Chapter Four) show the theoretical hydrodynamic pressure within the unit ($h_1/h_2=10$) for polymer melt temperature of 230°C and wire velocities of 4m/s, 8m/s and 12m/s respectively The pressure increases with the increase of wire velocity From this pressure profile it can be seen that the maximum hydrodynamic pressure at wire velocity of 12m/s is about 600 bar According to the Tresca theory of yielding, the deformation of the wire starts when the combined effect of hydrodynamic pressure and axial stress equals or exceeds the elastic limit of the wire material In this case the drawing force at polymer melt temperature 230°C and wire velocity 12 m/s is about 80N (Figure 7 4) The axial stress for this load is 2078 bar The combined effect of hydrodynamic pressure and axial stress is therefore 2678 bar (267 8 MPa) which is still less than the elastic limit of mild steel which is 280 Mpa So in this case the combined effect of the pressure and the drawing load will not be sufficient to cause any plastic deformation in the wire It was also observed in experiments that the wires did not experience any plastic deformation The experimental coating thickness, mentioned hereafter in this chapter should therefore be accurate

Stepped parallel bore pressure unit ($h_2=0$ 12 mm)

The results in Figure 7 7 shows the coating thickness and continuity with Nylon 6

at the melt temperature of 230°C. For argon pressures of 5 and 10 bar the test was carried out at up to 12 m/s. The coating thickness was about 0.09 mm for wire velocities of up to 12 m/s for both back pressure. The coating thickness was smaller than the exit gap between the wire and the unit. As the gap ratio (h_1/h_2 ratio) of the unit was only 4.16, the wall shear stress is higher in this case than other units with higher gap ratio (16.67 and 10). If the wall shear stress reaches the critical shear stress of the polymer melt then slip occurs between the layer of the polymer melt and the wire surface which leads to the decrease in coating thickness. Similarly decrease in the coating thickness is observed in Figures 7.8 and 7.9 for higher polymer melt temperatures viz. 250°C and 270°C respectively. With all these back pressures and all these temperatures the coating was found to be continuous. Plate 7.4 shows the concentricity of coating at 250°C and wire velocity of 12 m/s. The coating thickness is slightly higher in one side. The gap between the wire and the exit of this pressure unit was wide enough to cause inclination of the coating due to gravity.

Figures 7.10, 7.11 and 7.12 show the drawing force generated due to the pulling action of the wire through the pressure medium for polymer melt temperatures 230°C, 250°C and 270°C respectively. With the increase in wire velocity the drawing force also increases except for Figure 7.12 where it decreases after 8 m/s which is also thought to be due to the critical shear stress of the polymer melt. The drawing force increases with the increase in argon back pressure.

Stepped parallel bore pressure unit ($h_2=0.03$ mm)

Tests were also carried out with a stepped parallel bore pressure unit with a very narrow exit gap ($h_2=0.03$ mm) for both back pressure 5 and 10 bar and for polymer melt temperatures of 230°C, 250°C and 270°C. Although in all these tests the coating was found to be continuous, under the microscope the coating was found to be broken in some edges and was not reasonably concentric. Figure 7.13 shows the coating thickness and continuity with Nylon 6 at the melt temperature of 230°C. The coating thickness was about 0.025 and 0.026 mm for wire velocities of up to 6 m/s for the argon pressure 5 bar and 10 bar respectively. At 12 m/s it was about 0.022 mm for both the back pressures. The coating thickness was smaller than the exit gap.

between the wire and the unit. The exit gap between the wire and the unit was so small that it scratched the coating when it came out through that part. At higher back pressure the coating thickness seems to be slightly thicker. Figure 7 14 shows the coating thickness for different velocities at 250°C. At 5 bar back pressure it is 0.023 mm up to wire velocity 8 m/s and at 12m/s it is 0.021 mm. Also at 10 bar up to velocity of 8 m/s it is 0.024 mm and at 12 m/s wire speed it is 0.022 mm. Figure 7 15 displays the coating thicknesses at polymer melt temperature of 270°C. For both the back pressures the coating thickness at 2 m/s velocity are 0.023 mm and at 12 m/s the thicknesses are 0.022 mm. Plate 7 5 shows the concentricity of coating at 270°C, back pressure 10 bar and wire velocity 12 m/s. The coating is not radially even because of the narrow gap between the wire and the pressure unit.

Figures 7 16, 7 17 and 7 18 show the drawing force generated due to the pulling action of the wire through the pressure medium for polymer melt temperatures of 230°C, 250°C and 270°C respectively. With the increase in wire velocity the drawing force also increases generally except for Figure 7 16 where it decreases after 6 m/s. The drawing force is generally higher for higher argon back pressure.

Tapered bore pressure unit

The coating thickness on the wire in the case of tapered bore pressure unit were observed to be different than the coating formed using other pressure units. The coating thickness was higher than the exit gap between the wire and the pressure unit which was 0.0425 mm. Figure 7 19 shows the coating thickness on the wire for velocities of up to 12 m/s for polymer melt temperature 230 °C. For the back pressure of 5 bar the coating thickness at 2 m/s was 0.045 mm and at 12 m/s it was 0.0425 mm. At 10 bar back pressure, the coating thickness at 2 m/s was 0.053 mm and at 12 m/s it was 0.05 mm. From Figures 7 20 and 7 21 it is apparent that at higher polymer melt temperatures viz 250 °C and 270 °C, the coating thickness decreases as the wire speed increases as in the case in Figure 7 19. However the overall coating thickness is higher for higher polymer melt temperature. At polymer melt temperatures of 250 °C and 270 °C it was observed that higher back pressure gives higher coating thickness (Figure 7 19 and 7 20). As shown in Figure 7 21, for 270 °C temperature of the polymer melt, the back pressure seems to have no

effect on the coating thickness at lower wire speeds

This type of thickening of the coating can be explained by the phenomena called die swelling. At the time of melt flow the molecules slide past each other. The forces of attraction between the molecules cause a drag force, the magnitude of which is reflected in the viscosity of the melt. The chains of molten polymer with high-molecular weight, tend to uncoil as they are sheared. But when the polymers enter a narrow capillary, because of high shear rate there is considerable uncoiling (orientation) and the oriented molecules then pass down the capillary. Actually two motions work on those molecules. One is the shear stress and the other is the Brownian motion, which tries to slide the molecules past each other.

When the fluid is flowing along a channel which has uniform cross section (like the stepped parallel bore unit) then the fluid is subjected to shear stresses only. If the channel section changes (like the tapered bore unit) then tensile stresses will also be set up in the fluid. Therefore the equivalent stress acts on the polymer melt in the case of purely tapered unit is higher than any other units. So when the polymer melt comes out from the pressure unit in the form of the coating there is only Brownian motion as the stresses are absent outside the pressure unit. This Brownian motion expands or swells the coating in the radial direction and causes slight shrinkage in the longitudinal direction. The swelling increases with the increase in molecular weight and decreases for longer capillary length. Therefore in this case the swelling of the polymer coating is thought to be the combination of the following factors

- (i) the hydrodynamic pressure unit is purely tapered
- (ii) the molecular weight of Nylon 6 $\sim [\text{NH}(\text{CH}_2)_5 \text{CO}]_n \sim$ is higher than other conventional polymer used for hydrodynamic coating
- (iii) the length of the pressure unit is only 22 mm (the previous hydrodynamic coating researchers used it from 57 to 180 mm)

Plate 7.6 shows the coating on wire in a tapered unit for wire velocity of 8 m/s, back pressure 5 bar and polymer melt temperature 270°C. The coating is reasonably concentric.

Figures 7.22, 7.23 and 7.24 show the drawing force due to the pulling action of the wire through the tapered unit. In all these cases the drawing forces increase with the increase in the wire velocities and increase in the argon back pressure.

Combined pressure unit

Figures 7 25, 7 26 and 7 27 represent the coating thickness on wire formed in a combined parallel and tapered bore unit. The variables were drawing speed (up to 12 m/s), argon back pressure (5 and 10 bar) and polymer melt temperature (230°C, 250°C and 270°C). In all these cases the coating was found to be continuous. The thickness was almost equal to the exit gap between the wire and the unit (0.051 mm). Plate 7 7 shows the concentricity of the coating on wire formed in a combined unit. The wire velocity was 10 m/s, back pressure was 5 bar and the melt temperature was 230°C. Plate 7 8 represents the coating concentricity for wire velocity of 6 m/s, polymer melt temperature of 230°C and back pressure of 10 bar. Both of the plates show a concentric coating.

Figures 7 28, 7 29 and 7 30 show the drawing force generated on the wire in the combined pressure unit. These figures illustrate that with the increase in wire velocity and back pressure the drawing force also generally increases.

It may be mentioned again that no reduction in the cross sectional area of the wire was observed and there was no discontinuity of the coating in any of these cases. For each of the test conditions the adhesion of the coating to the wire was assessed qualitatively by attempting to scratch off the coating using a sharp edged tool. It was quite difficult to debond the coating from the wire unless the tool edge sharpness is like that of a razor blade. As such, the coating applied should be good enough to withstand any subsequent processing steps involving contact with mechanical tools and dies.

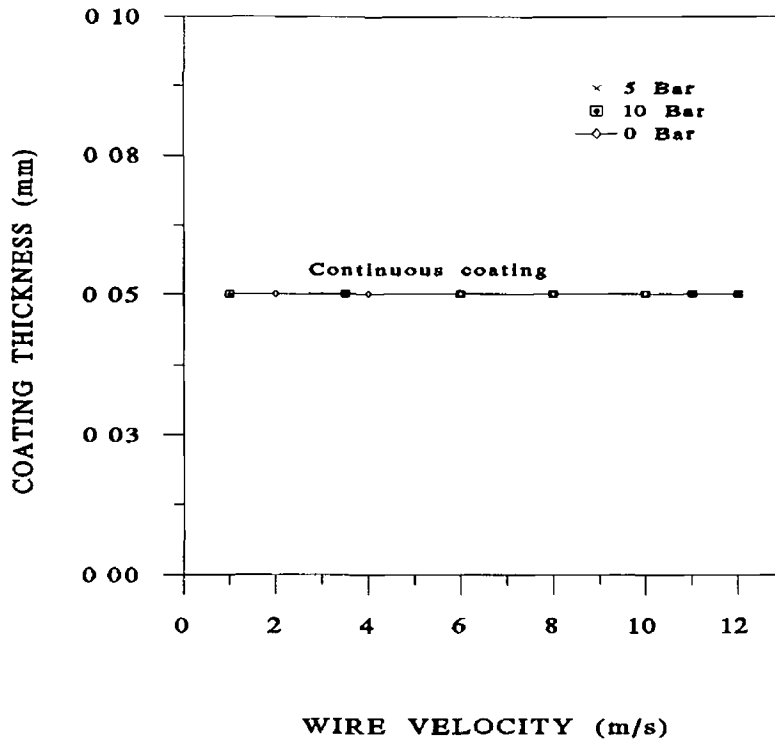


Figure7 1 Coating thickness on wire in stepped parallel bore pressure unit ($h_2=0.05$ mm) for polymer melt temperature 230 °C

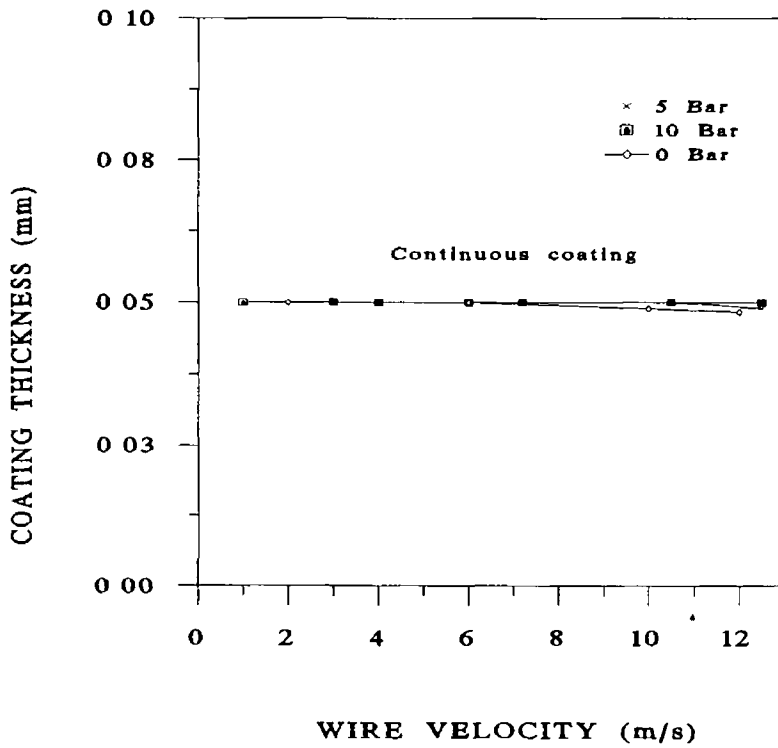


Figure7 2 Coating thickness on wire in stepped parallel bore pressure unit ($h_2=0.05$ mm) for polymer melt temperature 250 °C

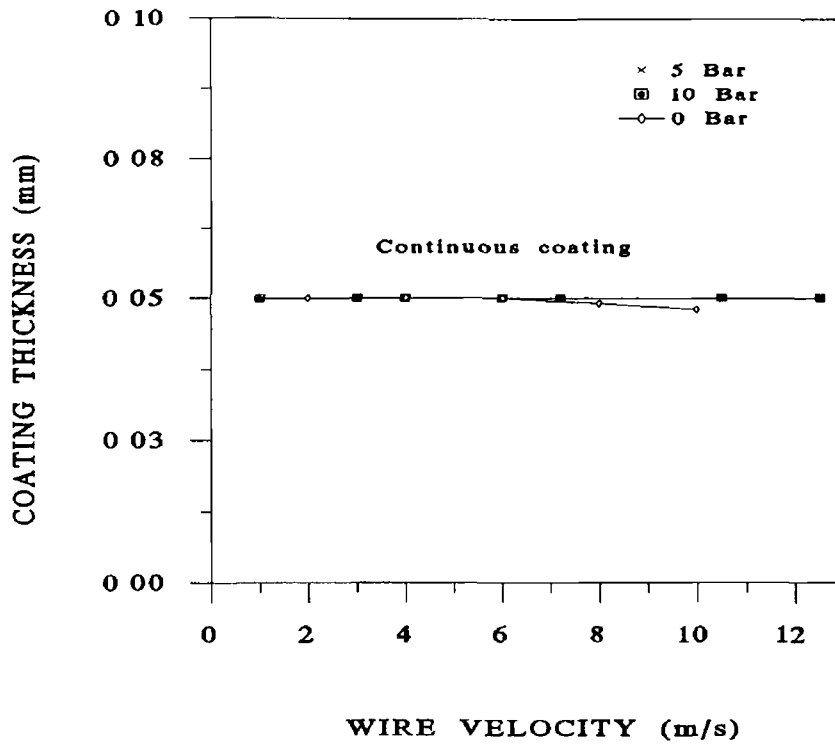


Figure7 3 Coating thickness on wire in stepped parallel bore pressure unit ($h_2=0.05$ mm) for polymer melt temperature 270°C

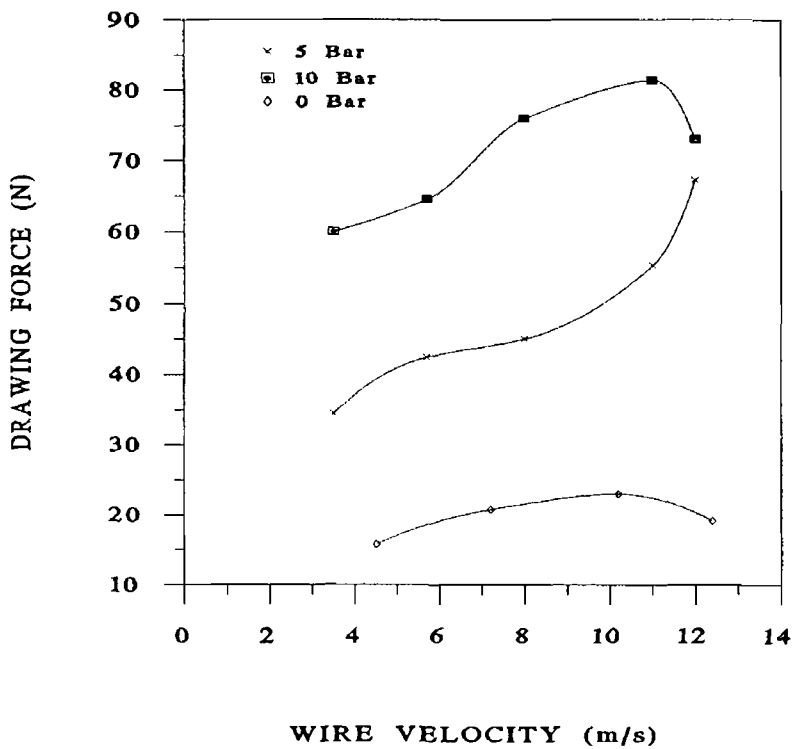


Figure7 4 Drawing force for wire pulling in stepped parallel bore pressure unit ($h_2=0.05$ mm) for polymer melt temperature 230°C

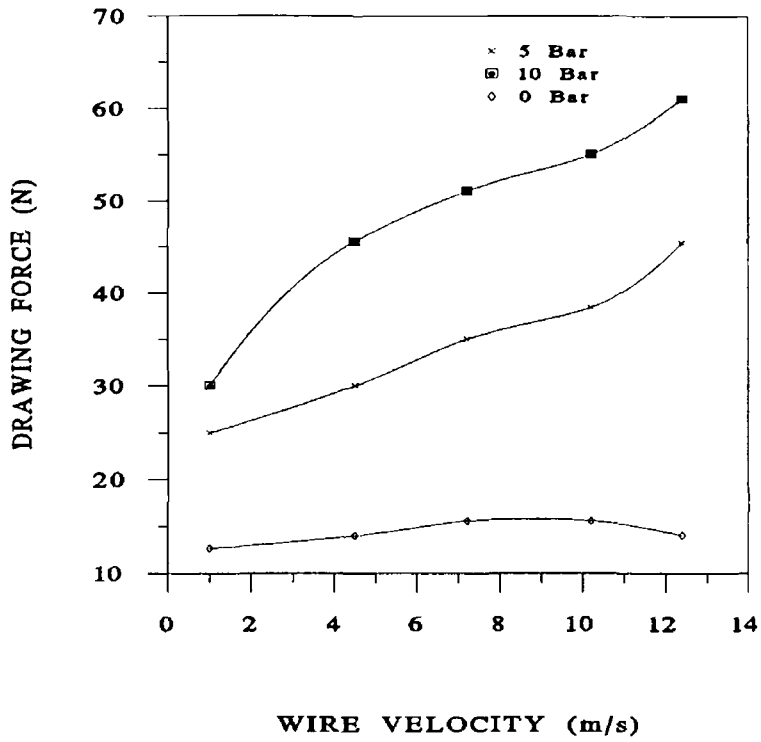


Figure7 5 Drawing force for wire pulling in stepped parallel bore pressure unit ($h_2=0.05$ mm) for polymer melt temperature 250 °C

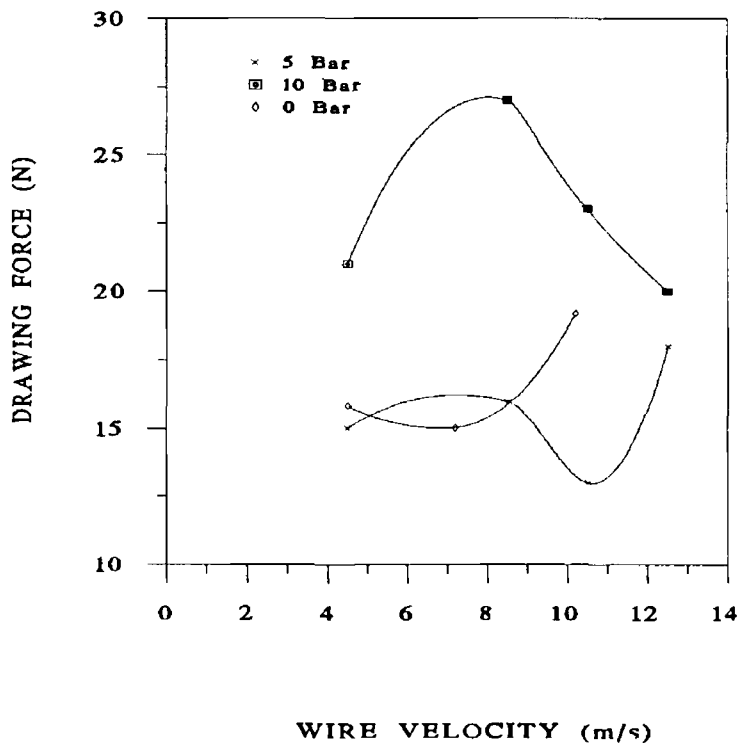


Figure7 6 Drawing force for wire pulling in stepped parallel bore pressure unit ($h_2=0.05$ mm) for polymer melt temperature 270 °C

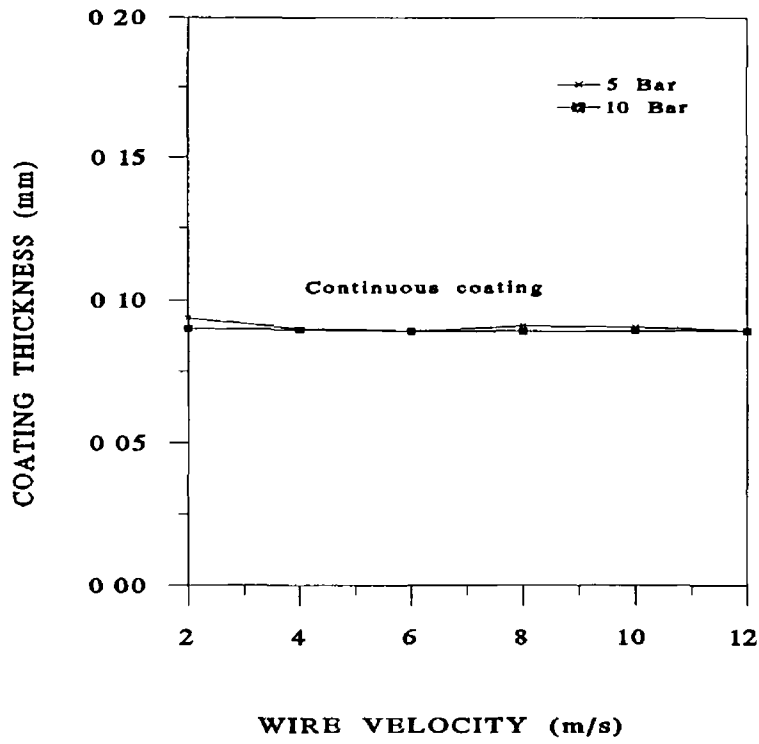


Figure 7.7 Coating thickness on wire in stepped parallel bore pressure unit ($h_2=0.12$ mm) for polymer melt temperature $230\text{ }^\circ\text{C}$

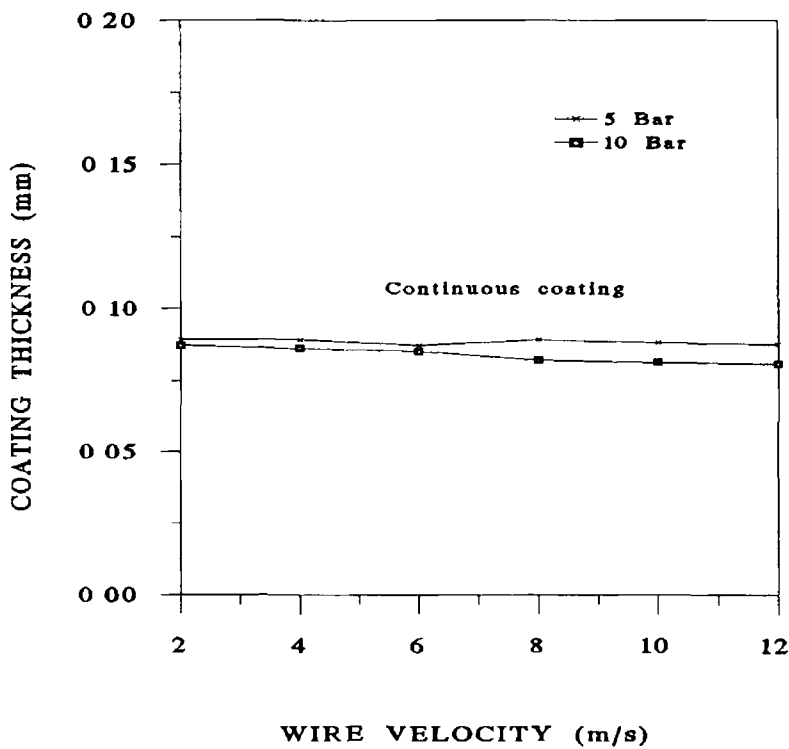


Figure 7.8 Coating thickness on wire in stepped parallel bore pressure unit ($h_2=0.12$ mm) for polymer melt temperature $250\text{ }^\circ\text{C}$

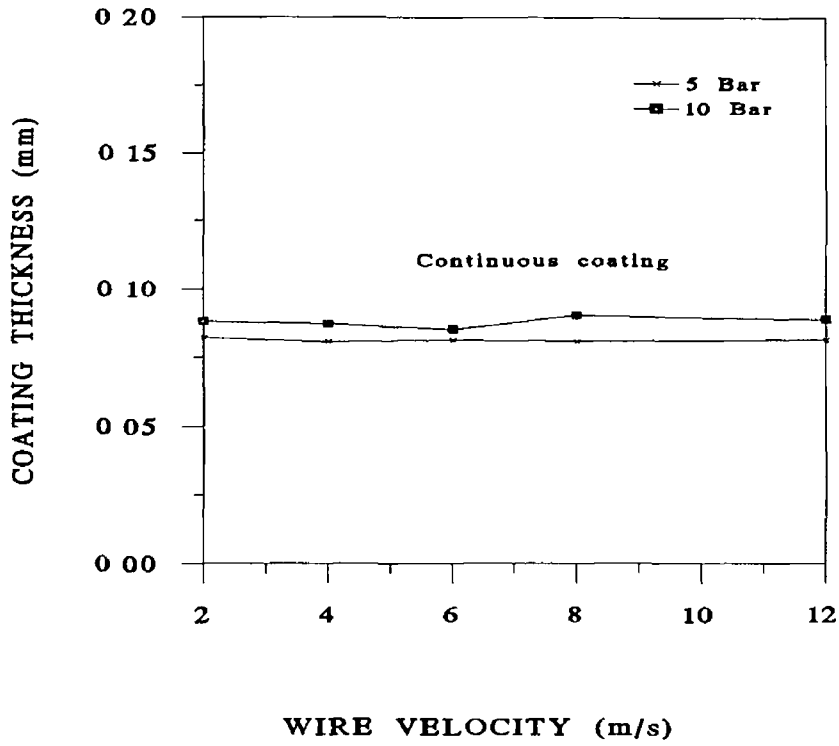


Figure 7.9 Coating thickness on wire in stepped parallel bore pressure unit ($h_2=0.12$ mm) for polymer melt temperature 270°C

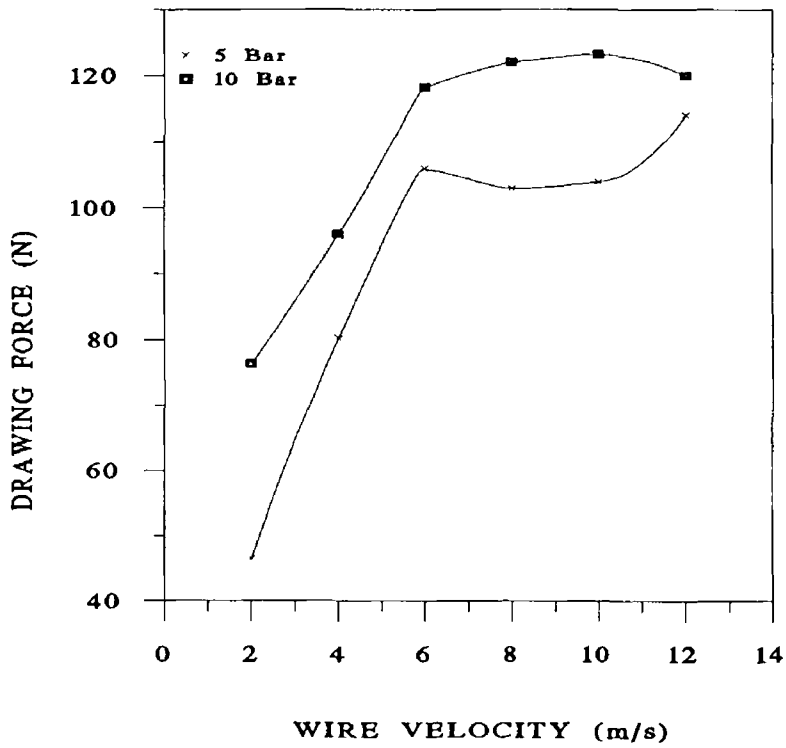


Figure 7.10 Drawing force for wire pulling in stepped parallel bore pressure unit ($h_2=0.12$ mm) for polymer melt temperature 230°C

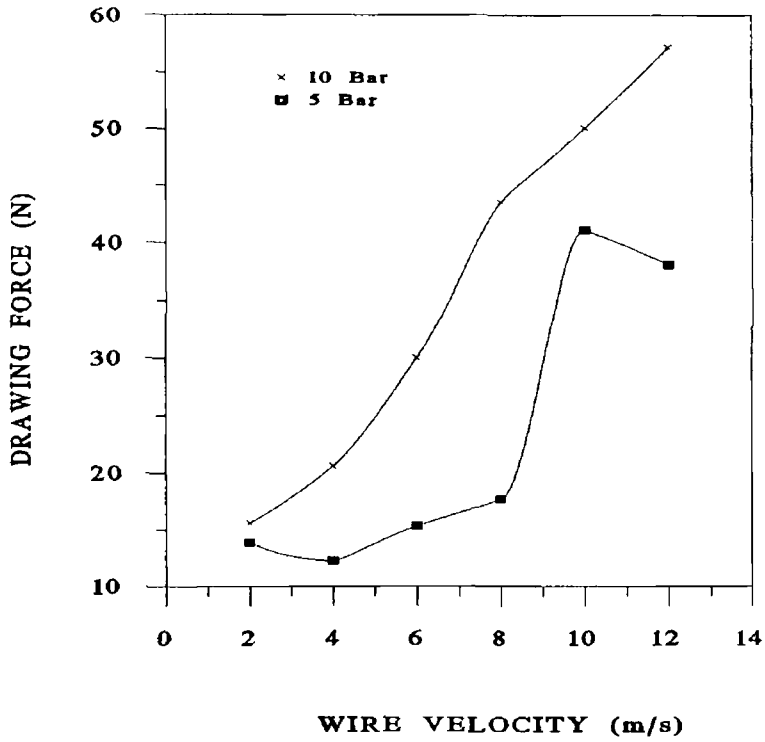


Figure7 11 Drawing force for wire pulling in stepped parallel bore pressure unit (h2=0 12 mm) for polymer melt temperature 250 °C

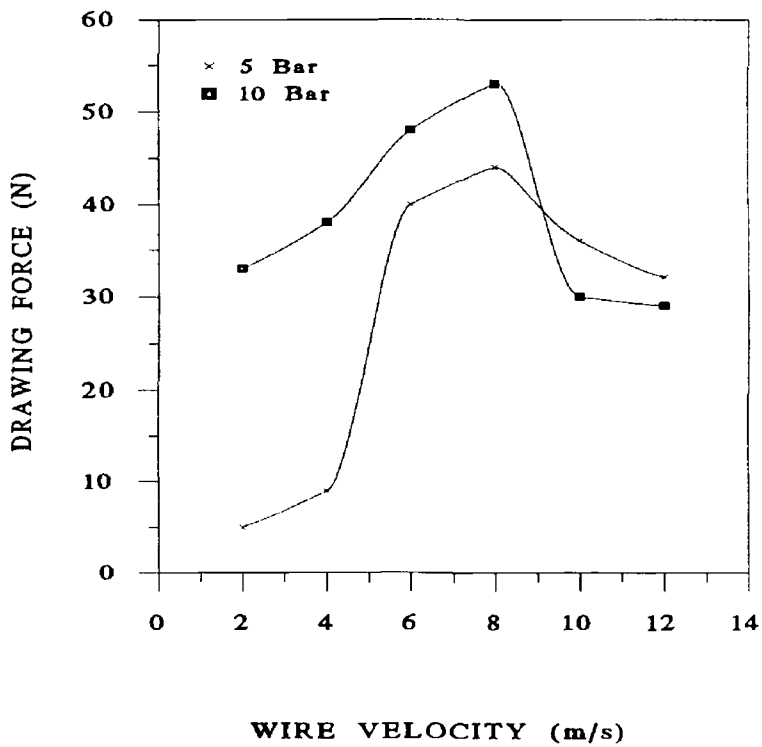


Figure7 12 Drawing force for wire pulling in stepped parallel bore pressure unit (h2=0 12 mm) for polymer melt temperature 270 °C

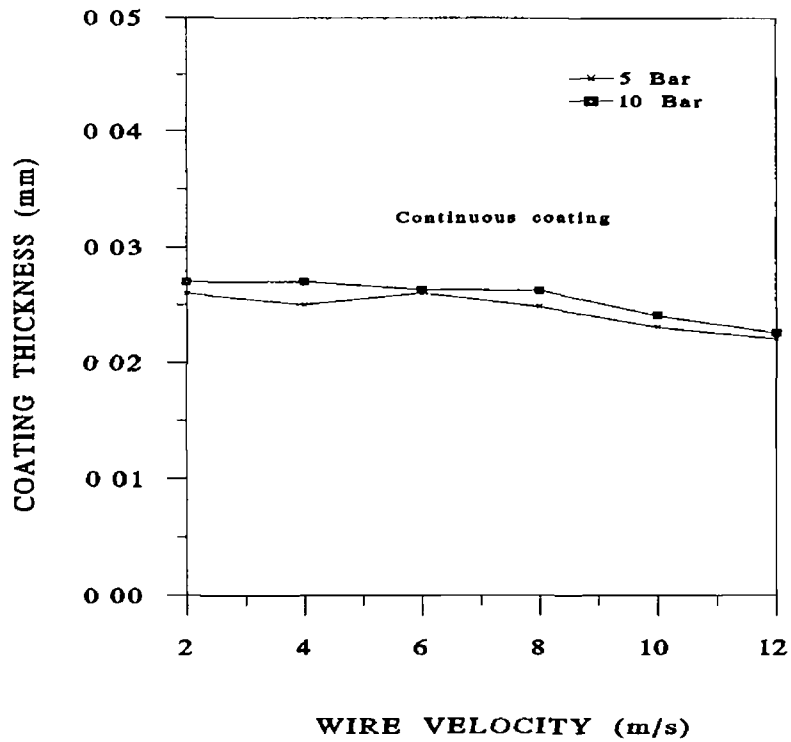


Figure7 13 Coating thickness on wire in stepped parallel bore pressure unit ($h_2=0.03$ mm) for polymer melt temperature $230\text{ }^\circ\text{C}$

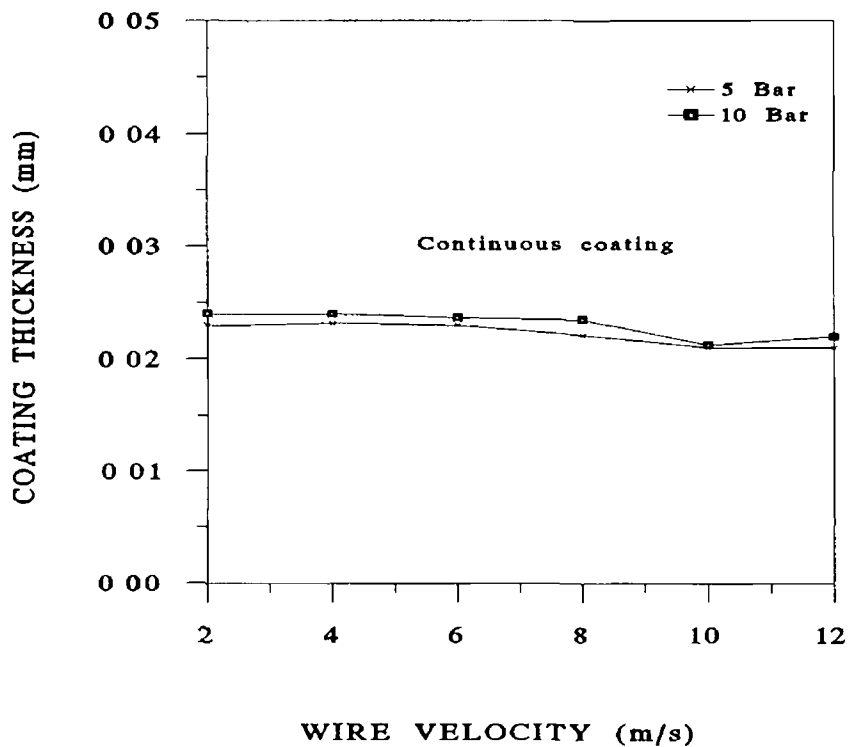


Figure 7 14 Coating thickness on wire in stepped parallel bore pressure unit ($h_2=0.03$ mm) for polymer melt temperature $250\text{ }^\circ\text{C}$

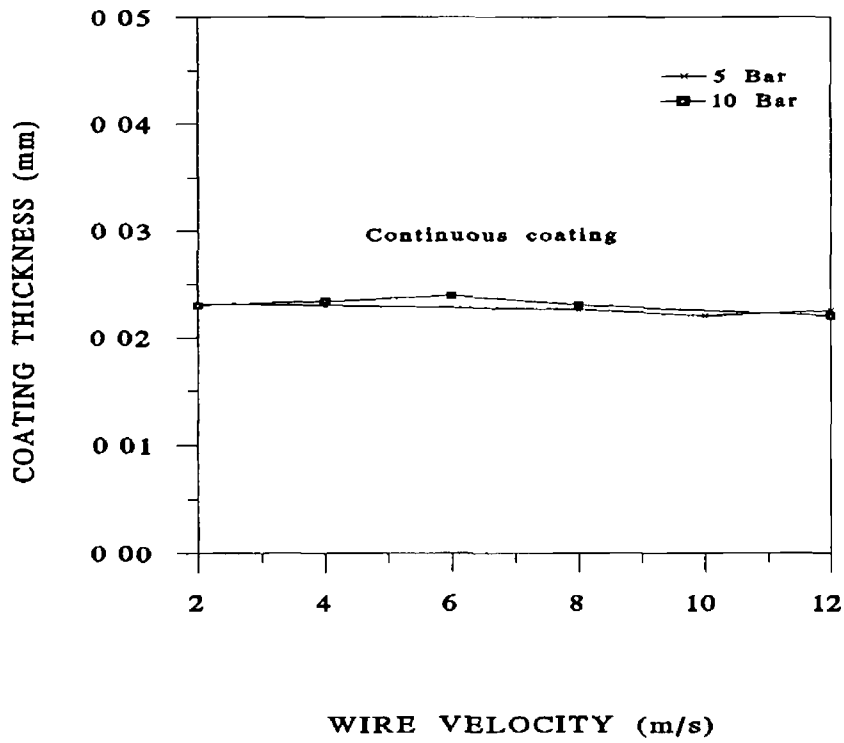


Figure7 15 Coating thickness on wire in stepped parallel bore pressure unit ($h_2=0.03$ mm) for polymer melt temperature 270°C

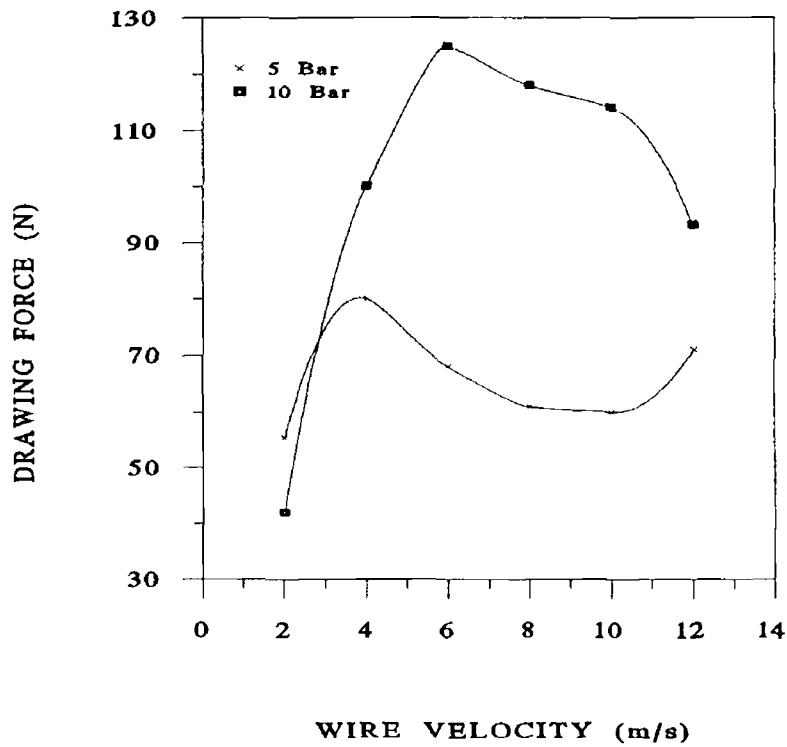


Figure7 16 Drawing force for wire pulling in stepped parallel bore pressure unit ($h_2=0.03$ mm) for polymer melt temperature 230°C

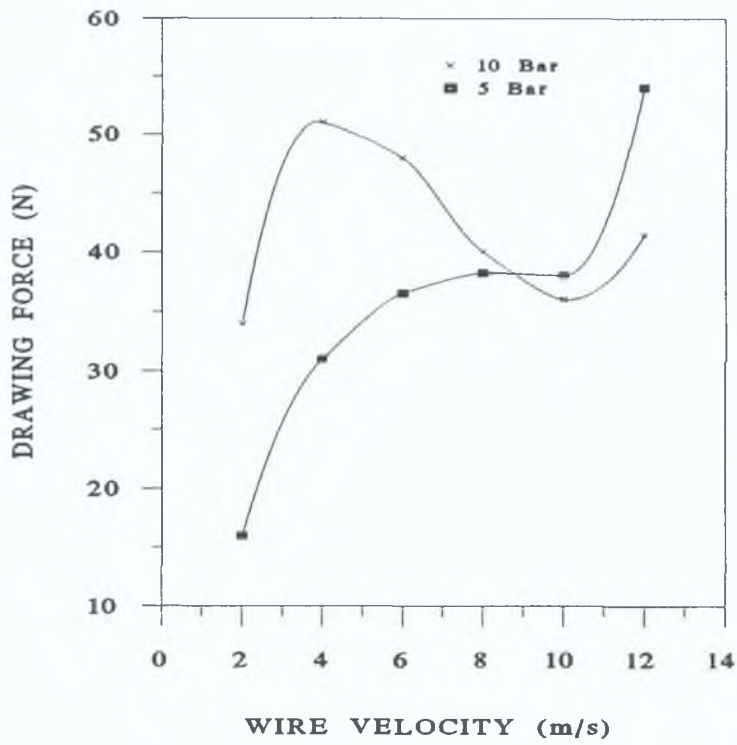


Figure7.17 . Drawing force for wire pulling in stepped parallel bore pressure unit ($h_2=0.03$ mm) for polymer melt temperature 250 °C.

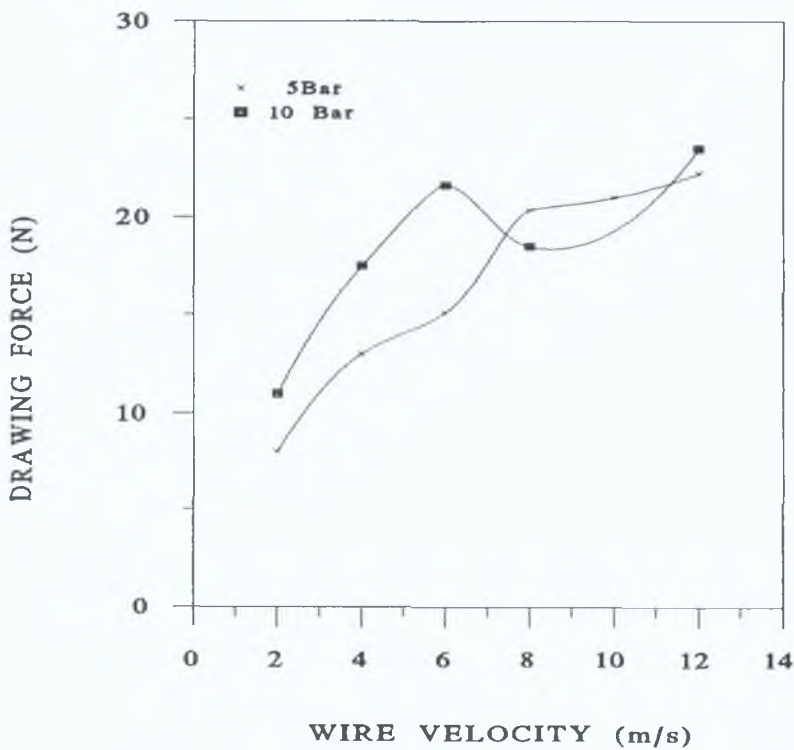


Figure7.18 . Drawing force for wire pulling in stepped parallel bore pressure unit ($h_2=0.03$ mm) for polymer melt temperature 270 °C.

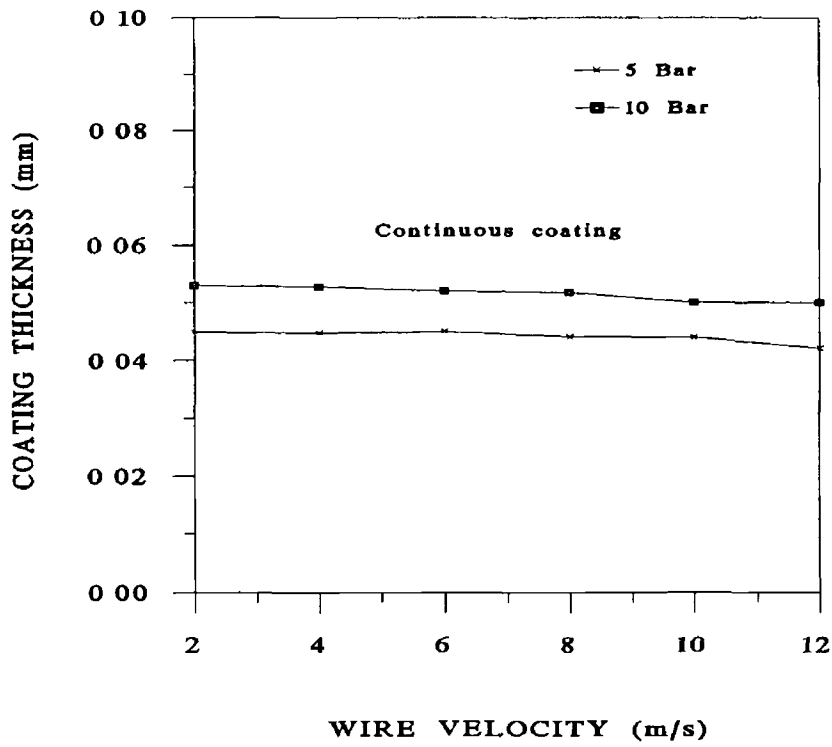


Figure 7 19 Coating thickness on wire in tapered bore pressure unit for polymer melt temperature 230 °C

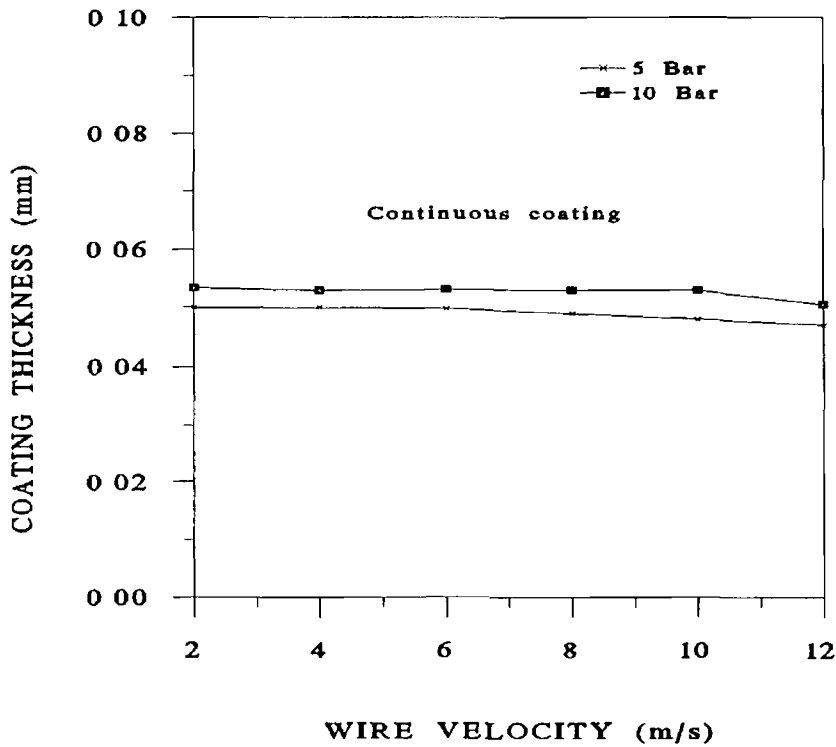


Figure7 20 Coating thickness on wire in tapered bore pressure unit for polymer melt temperature 250 °C

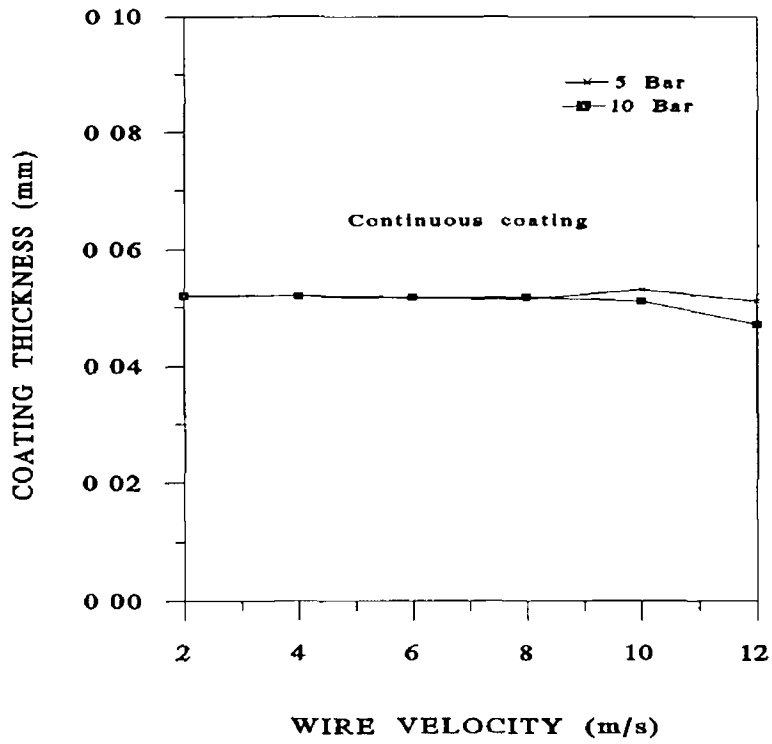


Figure 7 21 Coating thickness on wire in tapered bore pressure unit for polymer melt temperature 270 °C

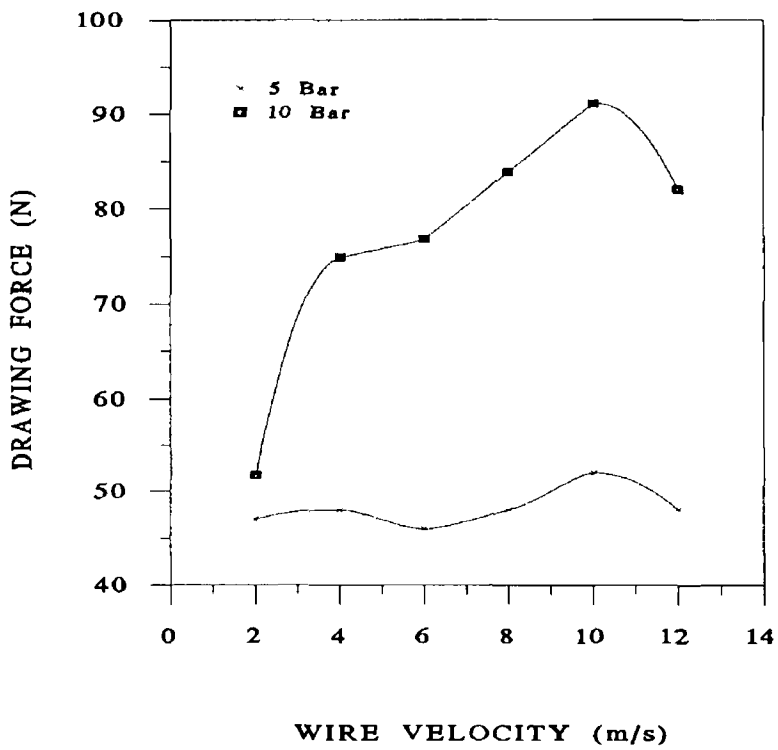


Figure 7 22 Drawing force for wire pulling in tapered bore pressure unit for polymer melt temperature 230 °C

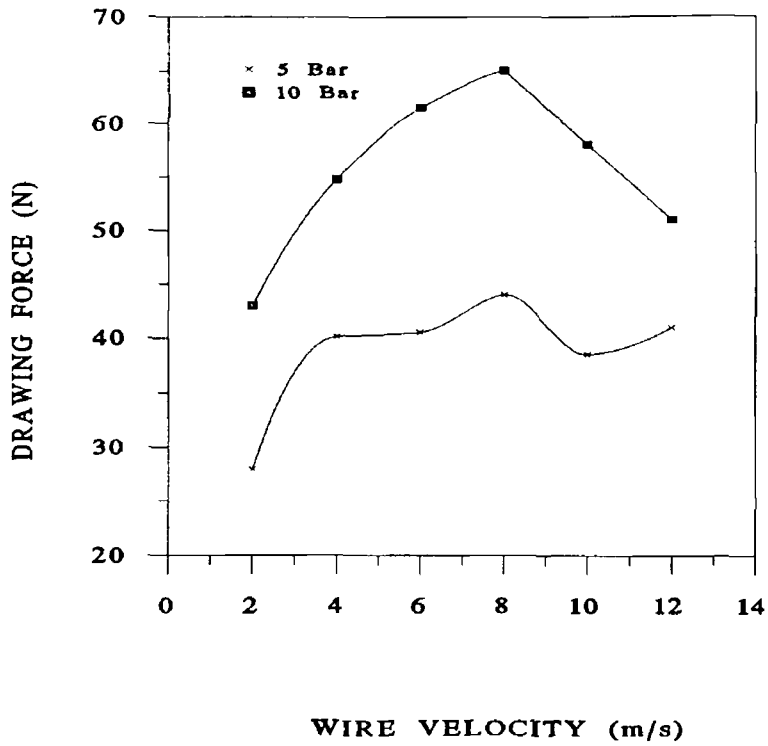


Figure7 23 Drawing force for wire pulling in tapered bore pressure unit for polymer melt temperature 250 °C

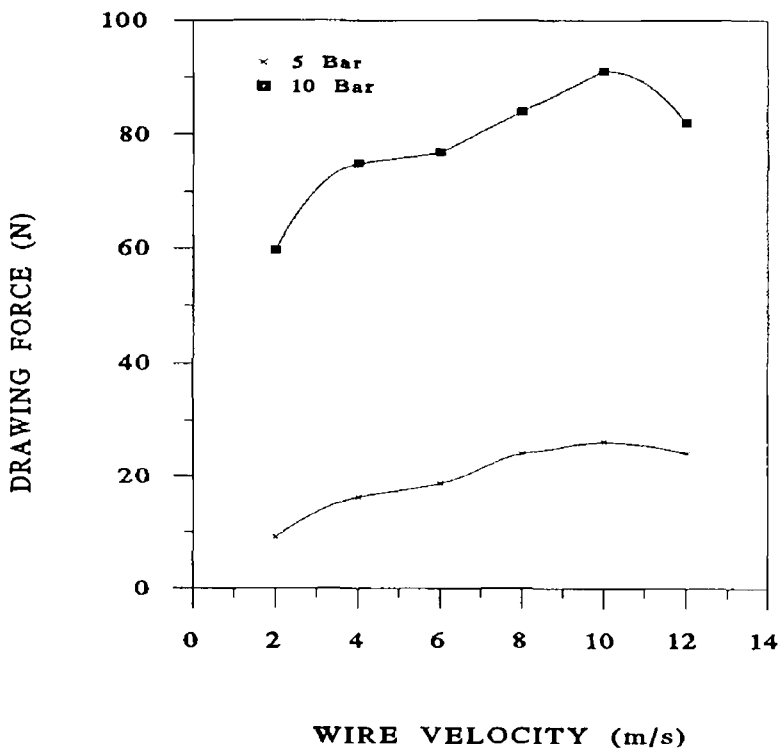


Figure7 24 Drawing force for wire pulling in tapered bore pressure unit for polymer melt temperature 270 °C

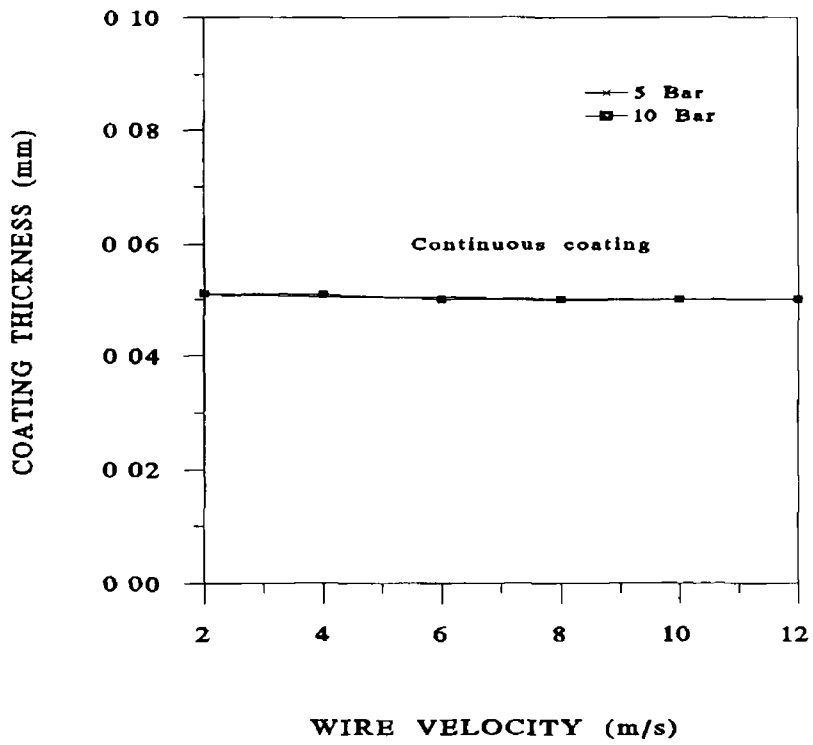


Figure7 25 Coating thickness on wire in combined pressure unit for polymer melt temperature 230 °C

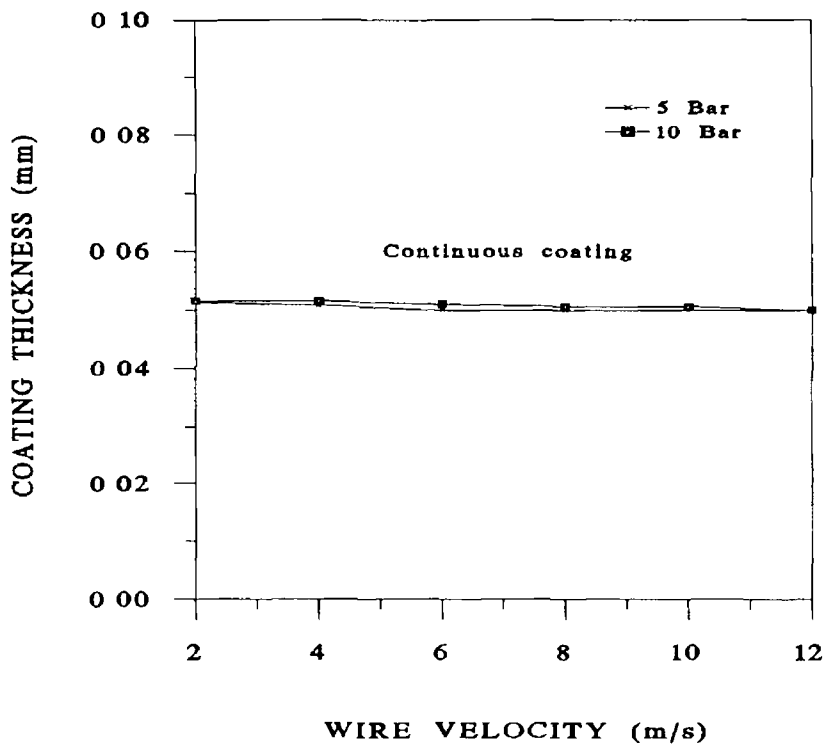


Figure 7 26 Coating thickness on wire in combined pressure unit for polymer melt temperature 250 °C

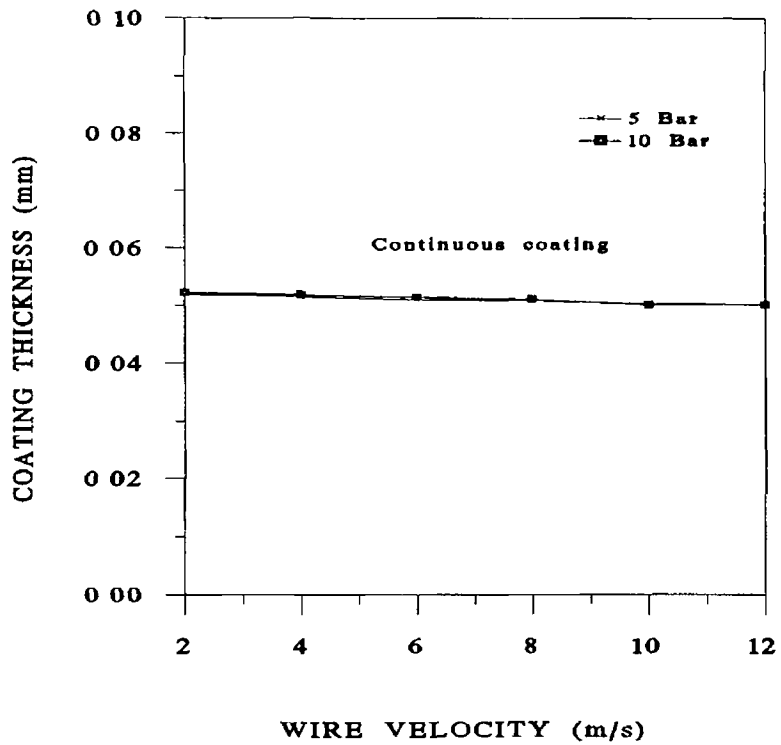


Figure7 27 Coating thickness on wire in combined pressure unit for polymer melt temperature 270 °C

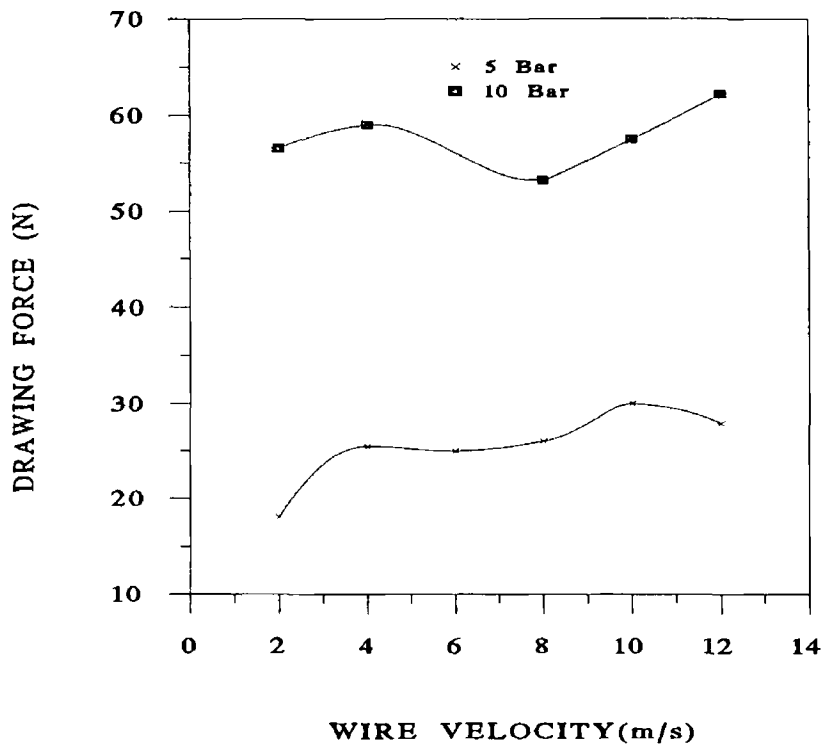


Figure7 28 Drawing force for wire pulling in combined pressure unit for polymer melt temperature 230 °C

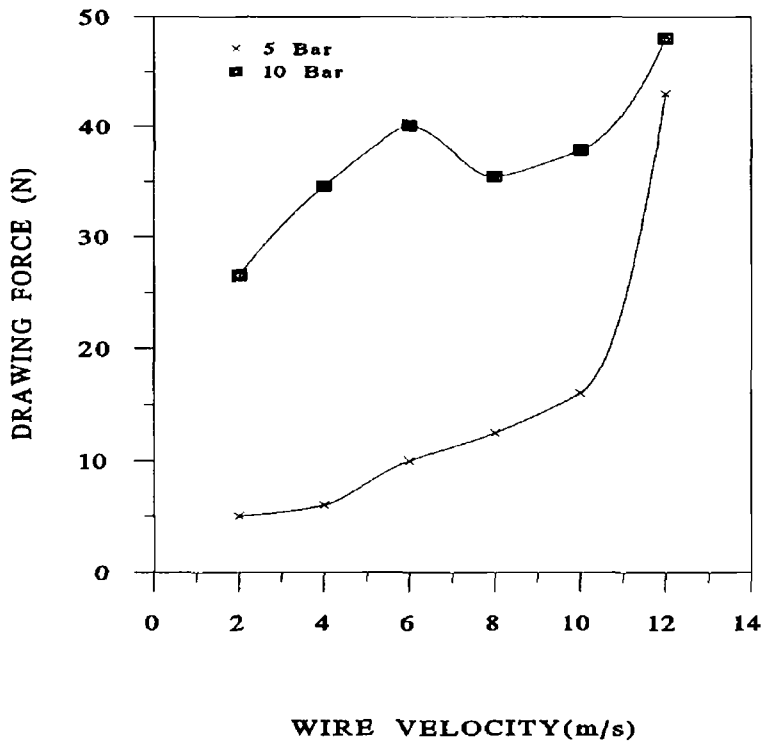


Figure 7 29 Drawing force for wire pulling in combined pressure unit for polymer melt temperature 250 °C

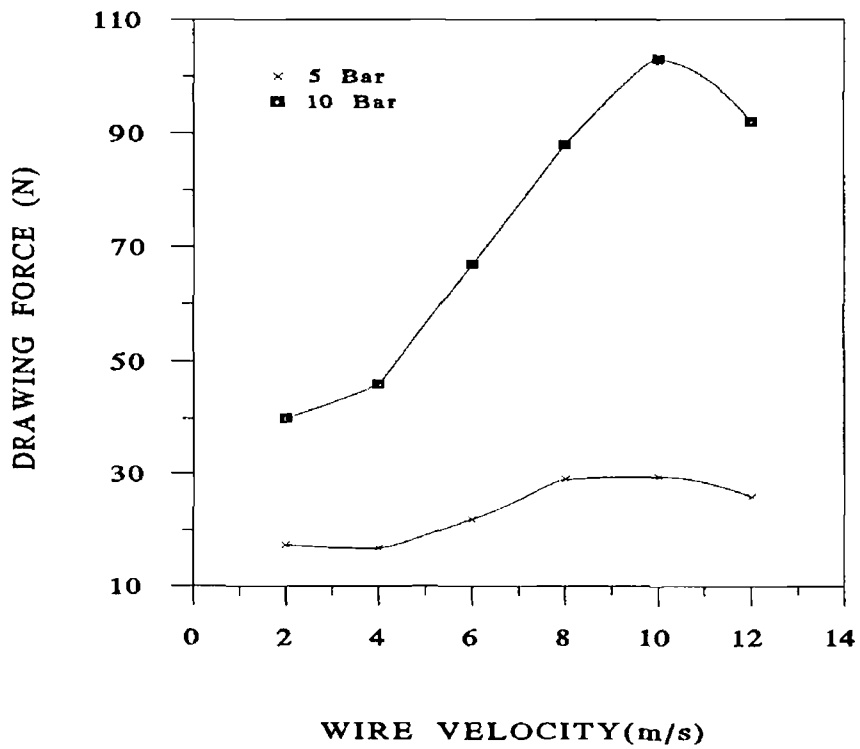


Figure7 30 Drawing force for wire pulling in combined pressure unit for polymer melt temperature 270 °C

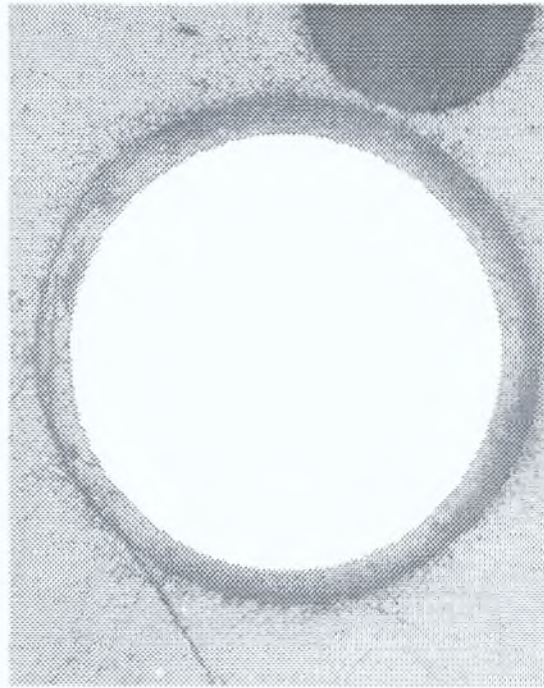


Plate 7.1. Concentricity of coating on wire in a stepped parallel bore unit ($h_2=0.05$ mm, wire velocity 4 m/s, polymer melt temperature 270 °C and back pressure 5 bar)

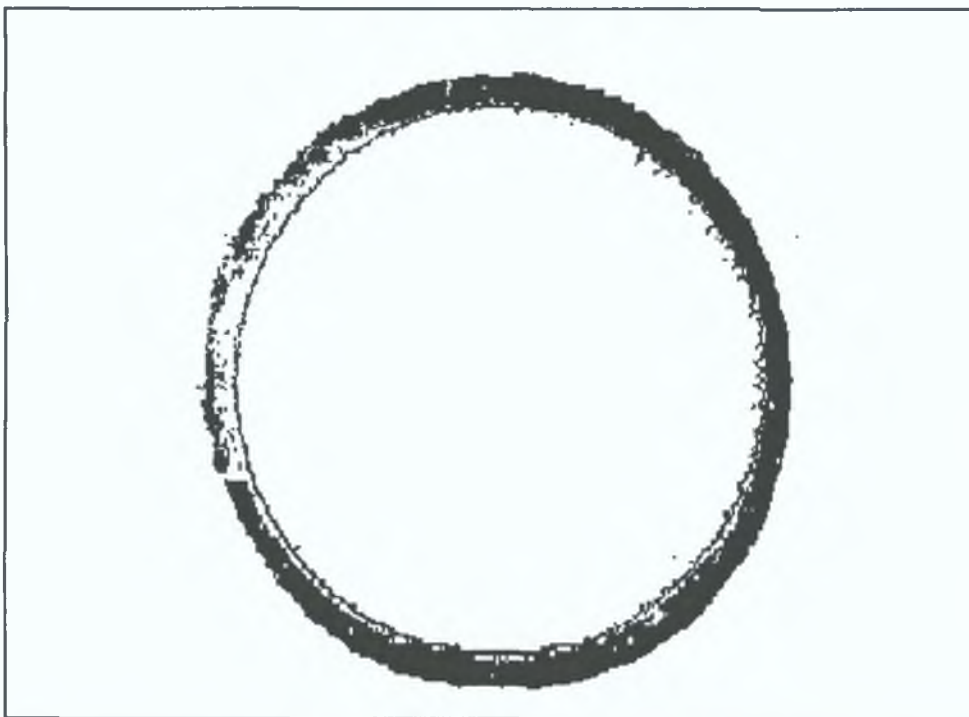


Plate 7.2. Concentricity of coating on wire in a stepped parallel bore unit ($h_2=0.05$ mm, wire velocity 10 m/s, polymer melt temperature 230 °C and back pressure 0)

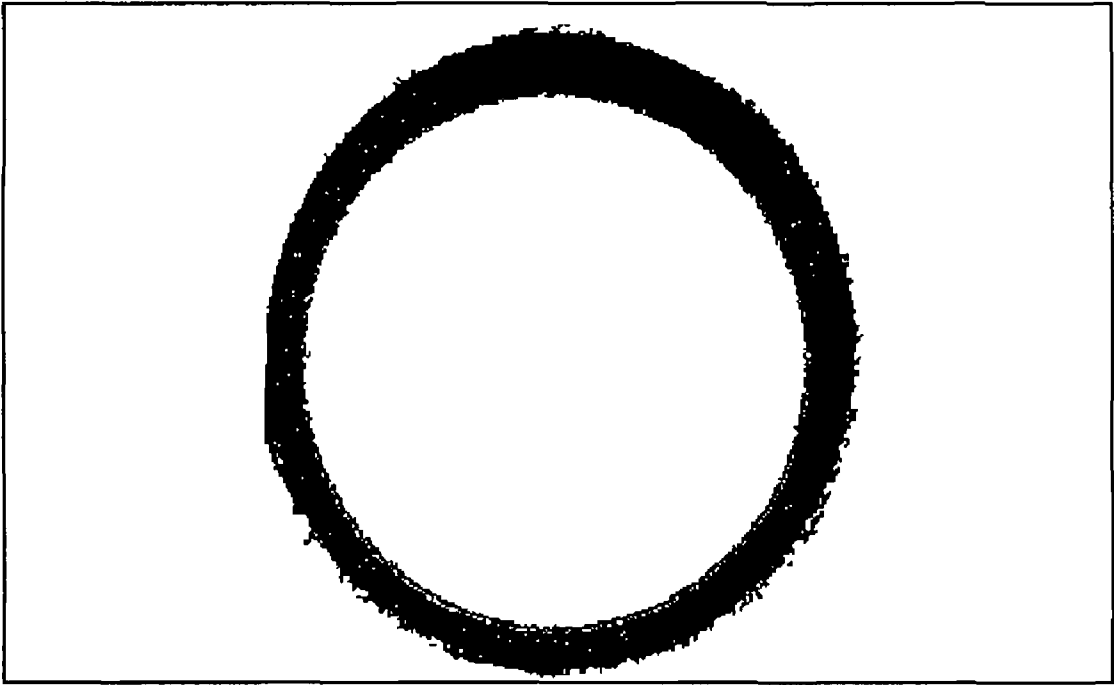


Plate7 3 Concentricity of coating on wire in a stepped bore unit ($h_2=0.05$ mm, wire velocity 12 m/s, polymer melt temperature 250 °C and back pressure 0)

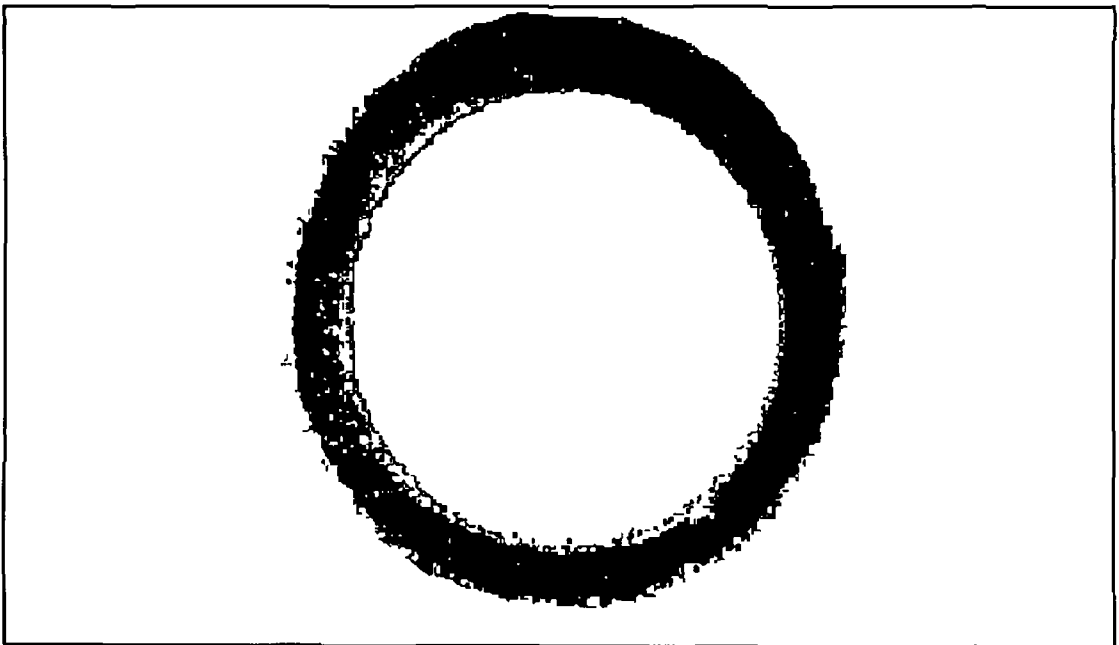


Plate7 4 Concentricity of coating on wire in a stepped bore unit ($h_2=0.12$ mm, wire velocity 12 m/s, polymer temperature 250 °C and back pressure 10 bar)

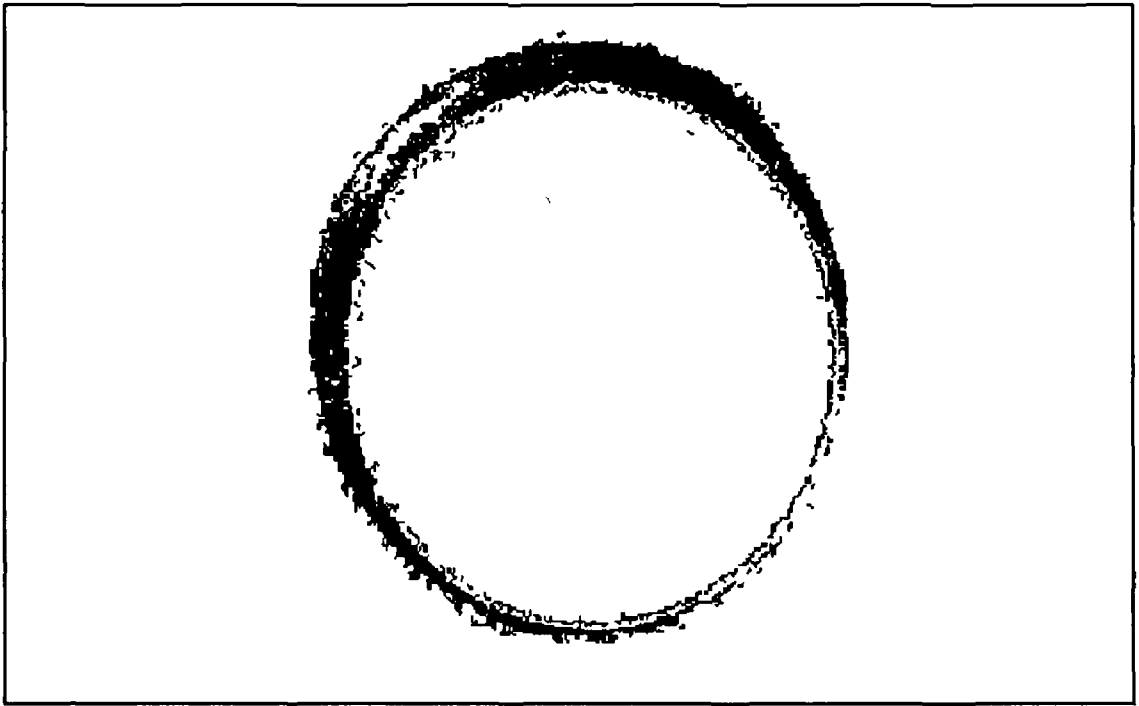


Plate7 5 Concentricity of coating on wire in a stepped bore unit ($h_2=0.03$ mm, wire velocity 12 m/s, polymer temperature 270 °C and back pressure 10 bar)

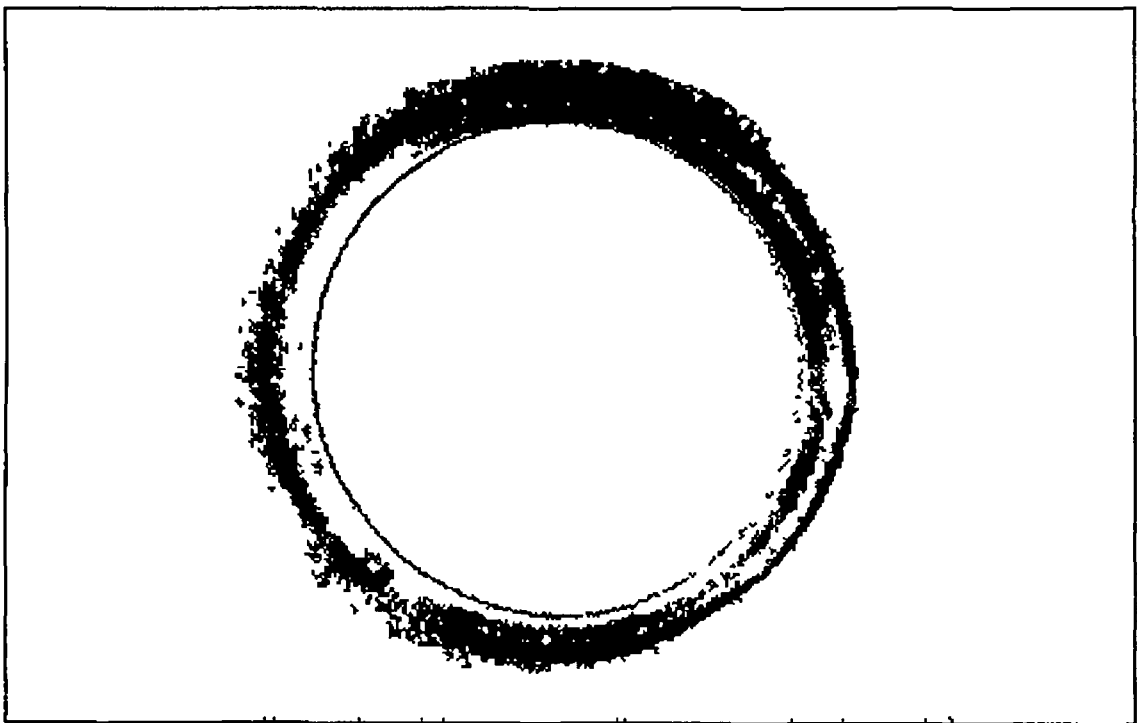


Plate7 6 Concentricity of coating on wire in a tapered unit ($h_2=0.0425$ mm, wire velocity 8 m/s, polymer melt temperature 270 °C and back pressure 5 bar)

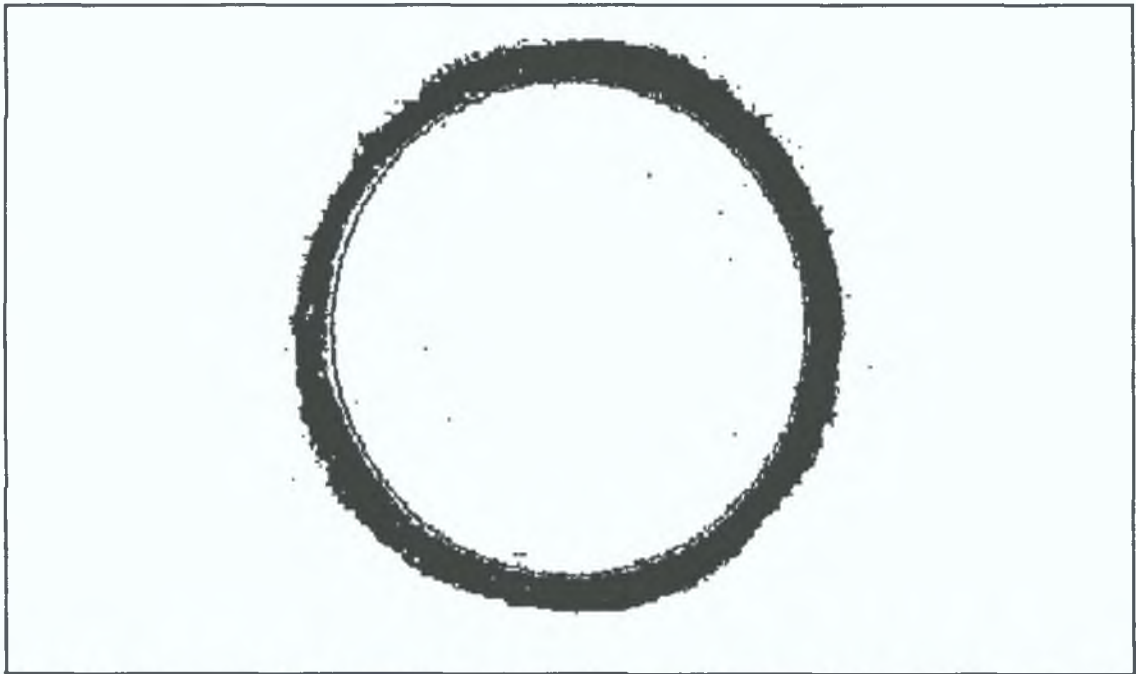


Plate7.7. Concentricity of coating on wire in a combined unit ($h_2=0.051$ mm, wire velocity 10 m/s, polymer temperature 230 °C and back pressure 5 bar)

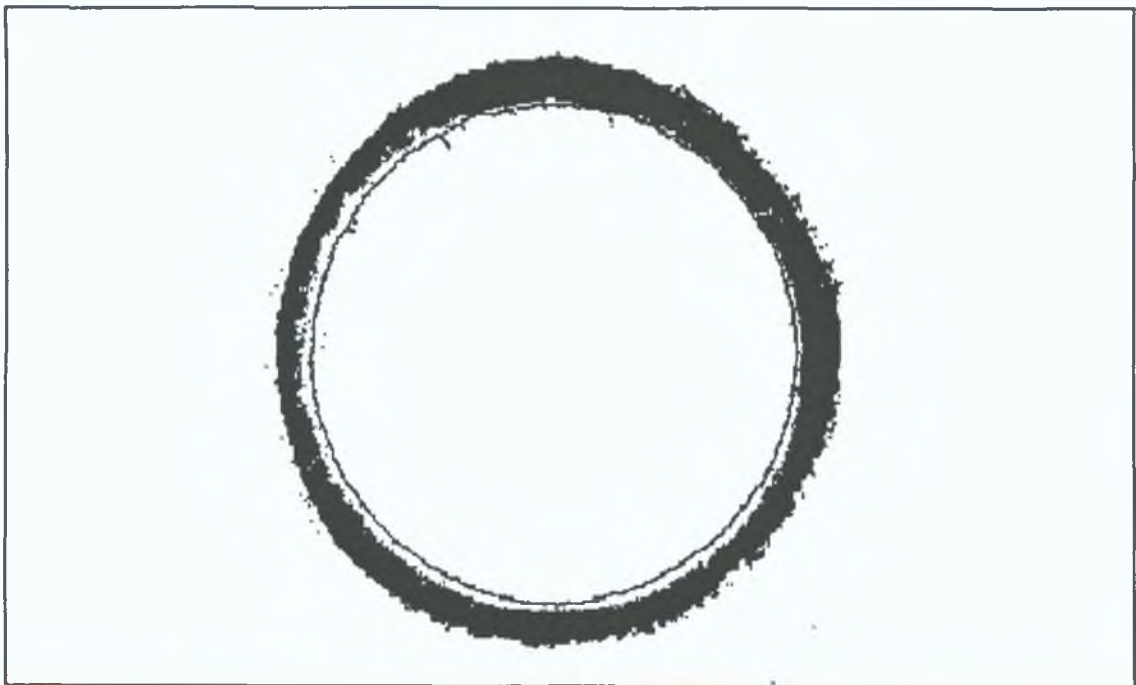


Plate7.8. Concentricity of coating on wire in a combined unit ($h_2=0.051$ mm, wire velocity 6 m/s, polymer temperature 230 °C and back pressure 10 bar)

CHAPTER - EIGHT

CONCLUSIONS AND SUGGESTIONS FOR FUTURE WORK

8.1 Introduction

This chapter presents a summary of the current thesis. It is divided into four sections. The first represents the investigation under consideration, the second identifies the techniques to carry out this task, the third gives a brief summary of the conclusions and the fourth identifies further studies that can be pursued in future works.

8.2 Statement of the tasks

In the plasto-hydrodynamic drawing and coating process, the solid continuum (wire, tube or strip) is first pulled through the polymer melt chamber before the plasto-hydrodynamic die-less unit. Therefore, the melt chamber plays an important role for the drawing and coating of the wire. In previous studies, the fluid flow and temperature characteristics in the melt chamber were not investigated.

Different types of pressure units (stepped parallel, tapered and combined parallel and tapered) have been used by a number of researchers to explore and study the die-less drawing and coating process. However, some limitations were observed in those studies. The viscosity of the polymer melt was considered to remain unchanged during the drawing and coating process. Also, the change in the shear stress was not incorporated in any of the previous analyses of the process. In the stepped parallel bore unit, the pressure could be found only in the step of the unit. In the combined parallel and tapered bore unit, the pressure could be calculated only in the tapered part of the unit. No attempt was made to predict the pressure through the fluid film thickness, which was considered to be constant. Also, some more types of hydrodynamic units such as the converging exponential and the converging parabolic unit were never considered before for analysis.

The previous researchers achieved a fairly constant polymer coating for wire speeds of only up to a maximum of 0.6 m/s. This speed of coating is rather slow for

industrial scale application

8.3 Summary of theoretical and experimental investigations

Both theoretical and experimental investigations were conducted in this study. For the solution of boundary layer problems both the analytical and numerical methods were used. Finite difference technique was used for the pressure and deformation solutions in continuum drawing and coating processes. Also, finite element simulation was carried out to obtain temperature and pressure solutions for different types of pressure units. To obtain a concentric and continuous coating at a high wire velocity Nylon 6 was used as the coating material which gives a good bonding with the wire. Also argon back pressure, a leakage control unit (which also acts as a preheating unit) certain length of melt chamber and proper polymer melt temperatures were used to obtain good quality coating up to wire velocity of 12 m/s.

8.4 General conclusions

The conclusions from the current study are summarised below under main headings.

Velocity and temperature gradient boundary layer in the melt chamber

- (i) With the increase in continuum velocity, the velocity and temperature gradient thickness of the layer decreases.
- (ii) As the temperature gradient thickness of the layer decreases, the solid layer within the boundary melts quickly and leads to good coating.

Hydrodynamic pressure and reduction in continuum in different types of pressure units

- (i) For hydrodynamic pressure in stepped parallel, tapered and combined parallel and tapered unit, the present theoretical pressure profiles are closer to the experimental results than the previous theoretical profiles.
- (ii) Also the present theoretical reduction for different continuums are closer to the experimental results than the previous theoretical reductions.
- (iii) The finite element simulation for pressure is reasonably closer to the experimental pressure.

8.4.3 Wire coating at high velocity of up to 12 m/s

- (i) With the stepped parallel bore unit ($h_2=0.05$ mm) the coating was concentric and the thickness was equal to h_2
- (ii) For the stepped parallel bore unit ($h_2=0.12$ mm) the coating was concentric but thickness was less than h_2
- (iii) The coating with the stepped parallel bore unit ($h_2=0.03$ mm) was not concentric enough
- (iv) For the tapered unit the coating was concentric but the thickness was slightly higher than h_2
- (v) With the combined unit the coating was concentric and the thickness was equal to h_2
- (vi) In all these cases the coating was continuous
- (vii) The coating is more constant at higher back pressure
- (viii) At 230° C, the coating is better than at other temperatures

8.5 Thesis contribution

The main contribution of the current thesis are

- (i) Modelling of velocity and temperature gradient boundary layer thickness for the drawing of a continuous wire through a polymer melt chamber (solution by both analytical and finite difference technique)
- (ii) Modelling of the melting profile of solid polymer layer produced on the wire due to the introduction of cold wire in the polymer melt chamber
- (iii) Modelling of the pressure distribution within a hydrodynamic pressure unit (for five different types of pressure units viz stepped parallel bore, tapered bore, combined geometry, converging exponential and parabolic)
- (iv) Finite element temperature and pressure simulations for different types of pressure units
- (v) Modified deformation solutions for wire, strip and tube in the stepped parallel bore pressure unit
- (vi) Deformation model for wire in the tapered and the combined unit
- (vii) To achieve continuous and concentric coating on wire up to wire speed 12 m/s using different types of pressure units

Main conclusion

Continuous and concentric coating of thickness 30 to 50 μm in Nylon 6 is possible at maximum of 12 m/s velocity on 0.5 to 1.0 mm diameter of mild steel wire

8.6 Recommendation for future work

Hydrodynamic process of wire coating is an evolving process. Although a considerable amount of work on the process has been done so far, there are more avenues of work on this process in the future. Some of them are mentioned below:

- (i) To use different types of polymer melts other than Nylon 6 with different melt temperatures and back pressures for this wire coating process
- (ii) To change the geometries of the different pressure units
- (iii) Carry out the coating process with different new types of pressure units such as a combined tapered and parallel unit, converging exponential and converging parabolic units
- (iv) Using preheating temperature as a variable in the coating process
- (v) To modify the rig so that tests can be carried out at more than 12 m/s (say up to 20 m/s)
- (vi) For a high speed coating process a chilled air cooling device will be needed for rapid solidification of the coating when it was applied at more than about 2 m/s, unless the distance between the coating unit and the winding drum can be increased to more than 20 meters to allow air cooling
- (vii) The effect of process parameters on die swelling can also be considered for further study
- (viii) Other wire diameters and materials could be used as the test material

REFERENCES

- 1 D G CHRISTOPHERSON and P B NAYLOR,
Promotion of fluid lubrication in wire drawing" *Proceeding of Institute of Mechanical Engineering*, (1955), 169,643
- 2 J G WISTRICH,
"Lubrication in wire drawing" *Wear*, March 1957, PP 505-511
- 3 S I ORLOV, V L KOLMOGROV, V I URALSKLL and V T STUKALOV,
"Integrated development and introduction of new high speed mills and hydrodynamic lubrication system for drawing wires", *Steel in the USSR* , Vol 10, PP 953-956, 1974
- 4 P J THOMPSON and G R SYMMONS,
"A Plasto-hydrodynamic Analysis Of The Lubrication And Coating Of Wire Using Polymer Melt During Drawing", *Proceeding of Institute of Mechanical Engineering*, vol 191, 13/77, 1977
- 5 A J STEVENS,
"A Plasto-hydrodynamic investigation of the lubrication and coating of the wire using a polymer melt during drawing process", *M Phil Thesis*, Sheffield City Polytechnic, 1979
- 6 R CRAMPTON,
"Hydrodynamic lubrication and coating of wire using a polymer melt during drawing process", *Ph D Thesis*, Sheffield City Polytechnic, 1980
- 7 H PARVINMEHR, G R SYMMONS and M S J HASHMI
"A non-Newtonian plasto-hydrodynamic analysis of dieless wire-drawing process using a stepped bore unit" *International Journal of Mecanical Science* Vol 29, No 4, PP 239-257, 1987
- 8 M S J HASHMI, G R SYMMONS and H PARVINMEHR
"A Novel technique of wire drawing", *Journal of Mechanical Engineering Sci Inst Mech Engrs* 24, 1982
- 9 G R SYMMONS, M S J HASHMI, and H PARVINMEHR
"Plasto-hydrodynamic dieless wire drawing theoretical treatment and experimental results", *Proceeding of International Conference on Developments in Drawing Metals*, Metals Society, PP 54-62, London, May 1983
- 10 G R SYMMONS, M S J HASHMI, and H PARVINMEHR
"Aspects of product quality and process control in plasto-hydrodynamic dieless wire drawing", *Proceeding of 1st Conference on Manufacturing Technology*, Irish Manufacturing Committee, PP 153-172, Dublin, March 1984
- 11 H PARVINMEHR,
"Optimisation Of Plastohydrodynamic System Of Wire Drawing Using Polymer Melts" *Ph D Thesis*, Sheffield City Polytechnic, 1983
- 12 M I PANWHAR, R CRAMPTON and M S J HASHMI
"Die-less tube sinking A plasto-hydrodynamic analysis based on Newtonian fluid characteristics" *Proceeding of 5th Polytechnic Symposum on Manufacturing Engineering*, PP 40-58, Brighton, May 1986
- 13 M S J HASHMI , R CRAMPTON and M I PANWHER

- "Plasto-hydrodynamic tube sinking Experimental evidence and numerical solution" *Proceeding of 3rd International Conference on Numerical methods for non-linear problems*", PP 115-129, Dubrovnik, Yugoslavia, September 1986
- 14 M S J HASHMI, R CRAMPTON and M I PANWHER
 "Mathematical modelling of die-less tube sinking based on non-linear deformation profile", *Proceeding of 6th Conference of the Irish Manufacturing Committee*, PP 248-254, Dublin, August 1989
- 15 M I PANWHER, R CRAMPTON and M S J HASHMI
 "Analysis of the die-less tube-sinking process based on non-Newtonian characteristics of the fluid medium", *Journal of Material Processing Technology*, Vol 21, PP 155-175, 1990
- 16 M I PANWHER
 "A Novel Technique For Tube Drawing", *Ph D Thesis*, Sheffield City Polytechnic, 1986
- 17 Y D XIE
 "Modelling and control of dieless wire drawing", *Ph D Thesis*, Sheffield City Polytechnic, 1987
- 18 G R SYMMONS, M S J HASHMI and Y D XIE
 "The optimisation of a plasto-hydrodynamic wire drawing process", *Proceeding of 6th International Conference on Modelling*, PP 362-366, Paris, France, June 1987
- 19 G R SYMMONS, Y D XIE and M S J HASHMI
 "Thermal effect on a plasto-hydrodynamic wire drawing process using a polymer melt", *Proceeding of Xth International Conference on Rheology*, Vol 2, PP 295-297, Sydney, Australia, August 1988
- 20 G R SYMMONS, A H MEMON and M S J HASHMI
 "A mathematical model for plasto-hydrodynamic drawing of narrow strip" *Mathematical computation modelling*, Vol 11 PP 926-931, 1988
- 21 G R SYMMONS, A H MEMON and M S J HASHMI
 "A Newtonian model of a plasto-hydrodynamic drawing process of a rectangular cross sectional continuum", *Proceeding of 7th international conference on modelling identification and control*, PP 67-70, Grindlewald, Switzerland, February 1988
- 22 G R SYMMONS, A H MEMON, R CRAMPTON and M S J HASHMI
 "Thermal effect on a plasto-hydrodynamic strip drawing process using a polymer melt", *Proceeding of 5th Conference of the Irish Manufacturing Committee*, PP 248-265, Queens University, Belfast, September 1988
- 23 G R SYMMONS, A H MEMON, R CRAMPTON and M S J HASHMI
 "An experimental study of a plasto-hydrodynamic strip drawing process of rigid non-linearly strain hardening strips through a stepped rectangular slot", *Journal of process mechanical engineering, Proceeding of IMechE*, Part E, Vol 203, PP 57-65, 1989
- 24 A H MEMON
 "Plasto-hydrodynamic Die-less Strip Drawing", *Ph D Thesis*, Sheffield City Polytechnic, 1988
- 25 G R SYMMONS, A H MEMON, R CRAMPTON and M S J HASHMI

- "A numerical solution for plasto-hydrodynamic drawing of rigid non-linearly strain hardening strips through a stepped rectangular slot", *Proceeding of 3rd International Conference on Numerical methods in Ind Forming Process*, PP 575-580, Colorado, U S A , June, 1989
- 26 M S J HASHMI and G R SYMMONS
 "A mathematical model for the drawing of solid continuum through Newtonian fluid filled tubular orifice", *Proceeding of 4th International Conference on Mathematical Modelling*, PP 627-633, Zurich, June 1983
- 27 M S J HASHMI and G R SYMMONS
 "A numerical solution for the plasto-hydrodynamic drawing of a rigid non-linearly strain hardening continuum through a conical orifice", *Proceeding of 2nd International Conference on Numerical Methods for Non-linear problems*, PP 1048-1059, BARCELONA, Spain, April 1984
- 28 M A NWIR and M S J HASHMI
 "Optimization of pressure and drawing stress in a simple tapered pressure unit using Borosiloxane as a pressure fluid, *Proceedings of Twelfth conference of the Irish Manufacturing Committee*, PP 253-258, 1995
- 29 M A NWIR and M S J HASHMI
 "Hydro-dynamic pressure distribution in a tapered, stepped parallel bore and complex geometry pressure units experimental results" *Proceedings of Advances in Materials and Processing Technologies*, PP 1431-1437, 1995
- 30 M A NWIR,
 "Plastohydrodynamic pressure in a simple tapered and combined geometry unit or drawing and coating of wires", *Ph D Thesis*, Dublin City University, 1994
- 31 I AL-NATOUR and M S J HASHMI
 "Development of a complex geometry pressure unit for hydrodynamic coating applications", *Proceeding of 6th Conference of the Irish Manufacturing Committee*, Dublin City University, PP 280-297, August 1989
- 32 I AL-NATOUR
 "Plasto-hydrodynamic pressure due to the flow of viscous fluid through a confined passage", M Eng Thesis, Dublin City University, 1989
- 33 M A NWIR and M S J HASHMI
 "Plasto-hydrodynamic pressure distribution in a complex geometry pressure unit Experimental results using Borosiloxane as a pressure fluid" *Proceedings of Eleventh conference of the Irish Manufacturing Committee*, PP 117-125, 1994
- 34 J A BRYDSON,
 "Flow properties of polymer melts", *Published By Plastic Institute*, London, Illiffe Books, 1970
- 35 M L WILLIAMS, R F LANDEL and J D FERRY,
 "The temperature dependence of relaxation mechanisms in amorphous polymers & other glass-forming liquids", *Journal of the American Chemical Society*, 77, 3701
- 36 R F WESTOVER,
 "Effect of hydrostatic pressure on polyethylene melt rheology", *Society of Plastics Engineers Transactions*, 1,14

- 37 B MAXWELL and A JUNG,
"Hydrostatic pressure effect on polymer melt viscosity", *Modern Plastics*, 35,
November, 174
- 38 F N COGSWELL,
"The influence of pressure on the viscosity of polymer melts", *Plastics &
Polymers*, 41, 39
- 39 S Y CHOI,
"Determination of melt viscosity as a function of hydrostatic pressure in a
melt viscometer ", *Journal Of Polymer Science A-2*, 6, 2043
- 40 V SEMJONOV,
"Über ein Rotationsviskosimeter zur Messung der Druckabhängigkeit der
Viskostat einiger Polyolefinschmelzen", *Rheologica Acta*, 2, 133
- 41 B RABINOWITSCH,
"Über Die Viskostat und Elastizität Von Solen", *Z Phys Chem A145*, pg
141, 1929
- 42 J B HULL, A R JONES, A R W HEPPEL, A J FLETCHER, and
S TRENGOVE
"The effects of temperature rise on the rheology of carrier media used in
abrasive flow machining, *Surface engineering*, Vol 2, Engineering
applications" Pg 240, 1993
- 43 Bayer, Application technology information, ATI 189e, (1988)
- 44 P L CLEGG,
"Elastic effect in the extrusion of polythene", *Rheology Of Elastomers*,
Pergammon Press, London, 1957
- 45 R S SPENCER and R E DILLON,
"The viscous flow of molten polystyrene", *Journal of Colloidal Science* , vol
3, pg 163, 1948
- 46 E B BAGLEY,
"The separation of elastic and viscous effect in polymer flow",
Trans Of The Society Of Rheology, vol 31, PP 355-368, 1961
- 47 E B BAGLEY and H P SCHRABER,
"Effect of die entry on polymer melt fracture and extrusion distortion",
Trans Of Society Of Rheology ,PP 341-353, 1961
- 48 E R HOWELLS and J J BENBOW,
"Flow defects in polymer melts", *ICI Publication*, August 1962
- 49 A B METZNER,
"Fracture of non-Newtonian fluids at higher shear stresses", *Industrial and
eng chemistry*, vol 50, No 10, 1958
- 50 F TSOU, E M SPARROW and R GOLDSTEN,
"Flow and heat transfer in the boundary layer on a continuous moving
surface, *International Journal of Heat and Mass Transfer*, 10, PP 219-235,
1967
- 51 R S R GORLA and I POP
"Heat transfer from a continuous moving surface in a non-Newtonian fluid
second-order effects", *International Journal of Fluid Mechanics*, 5(2) PP
213-229, 1992
- 52 S AKTER and M S J HASHMI

- Modelling of velocity and temperature gradient boundary layer thickness for the drawing of a continuous wire through a polymer melt chamber", *Proceedings of Twelfth conference of the Irish Manufacturing Commutee*, PP 253-258, 1995
- 53 J P HOLMAN,
"Heat Transfer", Sixth edition, McGraw-Hill Book Company, New York, PP 219-228, 1986
- 54 C RAUWENDAAL
"Polymer extrusion", Hunser publications, pg 218, 1986
- 55 Tony Whelan, John Goff "Injection molding of Thermoplastics Materials", Volume 1, Pg 19, 1990
- 56 S AKTER and M S J HASHMI
"Formation and remelting of a solid polymer layer on wire, in a polymer melt chamber", *Proceeding of the International Conference of Advances in Materials and Processing Technologies*, Vol 3, PP 1462-1469
- 57 E C BERNHARDT
"Computer aided engineering for injection molding", Hanser publishers, pg 105, 1984
- 58 M S J HASHMI, R CRAMPTON and G R SYMMONS
"Effect of strain hardening and strain rate sensitivity of the wire material during drawing under non-Newtonian plasto-hydrodynamic lubrication conditions" *Int J of Machine tools Des Res* Vol 21, No 1, PP 71-86, 1981
- 59 S AKTER and M S J HASHMI
"Modelling for the pressure distribution within a hydrodynamic pressure unit Effect of the change in viscosity during wire coating", *Proceeding of the International Conference of Advances in Materials and Processing Technologies*, Vol 3, PP 959-968
- 60 A CAMERON
"Basic lubrication theory", Longman group limited publishers, pg 57, 1970
- 61 M S J HASHMI
"A note on the prospect of plasto-hydrodynamic die-less tube sinking", *Journal of Mechanical Working Technology*", Vol 11 PP 237-242, 1985
- 62 S AKTER and M S J HASHMI
"Effect of change in viscosity of polymer in plasto-hydrodynamic drawing of strip using a hydrodynamic pressure unit" *Proceedings of the International Conference on Sheet Metal*, Vol 1 , PP 435-445, Netherlands, 1996
- 63 D W PEPPER and J C HEINRICH
"The finite element method, basic concepts and applications", Taylor & Francis, 1992
- 64 A I ISAYEV
"Injection and compression molding fundamentals", Marcel Dekker Inc, New York and Basel, PP 14-15, 1987
- 65 M S J HASHMI and G R SYMMONS
"A numerical solution for the drawing of a solid continuum through a stepped bore hydrodynamic unit", *Journal of Mathematical modelling*, Vol 8, PP 457-462, 1985

- 66 M S J HASHMI
"Strain Rate Sensitivity Of Commercially Pure Copper At Room Temperature And Strain Rate Of Up To 10^6 Per Second", *Sheffield City Polytechnic Technical Report No SCP/MPE/R106*, Oct 1978
- 67 M S J HASHMI
"Plasto-hydrodynamic mandrel drawing of tube using die-less reduction unit", *Proceeding of Xth International Conference on Rheology*, Vol 1, PP 401-403, Sydney, Australia, August 1988
- 68 S AKTER and M S J HASHMI
"Finite element temperature and pressure analysis for pressure distribution in a combined hydrodynamic unit, *accepted for (PEDAC'97)*, Egypt
- 69 J A BRYDSON,
"Plastic materials", Butterworths, pg 463, 1988
- 70 M J CROCHET, A R DAVIES, K WALTERS
"Numerical simulation of non-Newtonian flow, Elsevier, 1984
- 71 S AKTER and M S J HASHMI
"Modelling the pressure distribution within a combined geometry hydrodynamic pressure unit during wire coating process", *Proceedings on the International Congress on Rheology*, PP 689-670, Canada, August, 1996
- 72 M S J HASHMI
"Plasto-hydrodynamic mandrel drawing of tube a Newtonian pressure fluid" *Proceeding of 5th Conference of the Irish Manufacturing Committee*, PP 248-265, Queens University, Belfast, September 1988
- 73 R T FENNER and J G WILLIAMS
"Analytical methods of wire coating die design", *Trans J Plastics Instd* , PP 701-706, October 1967
- 74 H H WINTER
"Thermal capacitance and cooling length in the wire coating process", *SPE Techn Pap* ,PP 462-465, 1978
- 75 C D HAN and D RAO
"Studies on wire coating extrusion 1-the rheology of wire coating extrusion", *Journal of Polymer Engineering and Science*, Vol 18, PP 1019-1029, October, 1978
- 76 H ZHANG, M K MOALLEMI, and S KUMAR
"Thermal analysis of the hot dip-coating process", *Journal of heat transfer in metals and containerless processing and manufacturing*, ASME, P 49 55, 1991
- 77 K FUSE, K ORIMO and K SHIBATA
"Numerical analysis of viscous flow in a wire coating", *Journal of wire industry*, PP 554-562, August 1979
- 78 S BASU
"A theoretical analysis of non-isothermal flow in wire-coating co-extrusion dies", *Journal of Polymer Engineering and Science*, Vol 21, PP 1128-1137, December, 1981
- 79 K T O'BRIEN
"Computer modelling for extrusion and other continuous polymer process applications, Hanser publishers, PP 68-71, 1992

- 80 W MICHAELI
"Extrusion dies, design and engineering computations, Hanser publishers, pg 23, 1984
- 81 R CRAMPTON, G R SYMMONS and M S J HASHMI,
"A non-Newtonian plasto-hydrodynamic analysis of the lubrication and coating of wire using a polymer melt during drawing", Proc Int symposium on metal working lubrication, Sanfransisco, USA, 1980
- 82 R E LAMB
"Plasto-hydrodynamic polymer coating of fine wires", M Eng Thesis, Dublin City University, 1989
- 83 G R SYMMONS and Z MING,
"Die-less wire drawing using Borosiloxane as a pressure medium", *Proceeding of (IMC'7) Dublin*, PP 466-475, August 1990
- 84 G R SYMMONS, A H MEMON, ZHANG MING and M S J HASHMI,
"Polymer coating of wire using a die-less drawing process" *Journal of Material Processing Technology*, Vol 26, PP 173-180, 1991
- 85 M S J HASHMI and G R SYMMONS
"Computer modelling of the die-less wire drawing and coating process", *Proceeding of the International Conference on CAD of Machinery 91*, PP 225-231, Beijing, P R China, September 1991
- 86 R E LAMB and M S J HASHMI,
"Polymer coating of superfine wires a new technique to ensure quality", *Journal of Material Processing Technology*, Vol 26, PP 197-205, 1991
- 87 M A TUNIO and M S J HASHMI
"Feasibility of manufacturing polymer coated composite wire ropes using plasto-hydrodynamic technique", *Journal of Material Processing Technology*, Vol 33, PP 367-374, 1992
- 88 M A TUNIO
"Manufacturing of composite ropes using hydrodynamic technique", *M Eng thesis*, Dublin City University, 1990
- 89 J YU, and M S J HASHMI,
"Experimental results for polymer coating of fine wires", *Key Engineering Materials*, Vol 86-87, PP 163-170, 1993
- 90 S AKTER and M S J HASHMI
"High speed nylon coating of wire using a plasto-hydrodynamic pressure unit, *3rd Asia Pacific conference on Material Processing*, PP 453-457, November, 1996
- 91 S AKTER and M S J HASHMI
"Plasto-hydrodynamic Nylon coating of wire and prediction of pressure inside the stepped parallel bore pressure unit", *Proceedings of 13th Conference of the Irish Manufacturing Committee*, University of Limerick, PP 123-133, September 1996
- 92 S AKTER and M S J HASHMI
"Works on polymer coating and drawing of wires using plasto-hydrodynamic pressure units and the evolution of the design units", *proceeding of the 6th International Conference on Production Engineering Design and Control (PEDAC'97)*, Alexandria, Egypt February 1997

**APPENDIX I PROGRAM TO CALCULATE BOUNDARY LAYER THICKNESS FOR
VELOCITY GRADIENT AND COEFFICIENT OF FRICTION FACTOR CALCULATED
BY ANALYTICAL METHOD**

```

REAL AN(10) VIS(10) RHO(10) DEL1(10 10) V(20) RE(10 10) CFX1(10 10)
OPEN(UNIT=1 FILE='A DT1 DAT' STATUS= UNKNOWN )
OPEN(UNIT=2 FILE="A RESULT1" STATUS="UNKNOWN")
OPEN(UNIT=3 FILE="A RESULT2" STATUS="UNKNOWN")
OPEN(UNIT=4 FILE="A RESULT3 STATUS="UNKNOWN")
DO 10 I=1,6
READ (1 *) AN(I) VIS(I) RHO(I)
X=40 0
JJ=0
DO 20 J=2000 10000 2000
JJ=JJ+1
V(JJ) = J*1 0
RE(I JJ)=RHO(I)*(V(JJ)**(2 0 - AN(I)))*(X**AN(I))/VIS(I)
DEL1(I JJ)=X*(4 242*(AN(I)+1 0)*(1 5**AN(I))/(RE(I JJ))**
*(1 0/(AN(I)+1 0))
CFX1(I JJ)=(2 0*(1 5*X/DEL1(I JJ))**AN(I))/RE(I JJ)
WRITE (2 *) RE(I JJ)
WRITE (3 *) DEL1(I JJ)
WRITE (4 *) CFX1(I JJ)
20 CONTINUE
10 CONTINUE
REWIND 1
STOP
END
C PROGRAM FOR TEMPERATURE BOUNDARY LAYER THICKNESS AND TEMPERATURE DISTRIBUTION
IMPLICIT DOUBLE PRECISION(A H O Z)
DIMENSION AN(6) DELT(6 5) V(6) T(20 10) TM(6) ALP(6)
*Z0(6 5) Z1(5 6) Z(5 6) NUX(5 6) RE(10 10) DEL1(10 10) PR(5 6)
X=40 0
OPEN(UNIT=2 FILE="A RESULT1" STATUS="UNKNOWN")
OPEN(UNIT=3 FILE="A RESULT2 STATUS= UNKNOWN )
OPEN(UNIT=15 FILE= A DT3 DAT STATUS="UNKNOWN")
OPEN(UNIT=16 FILE= A RESULT7 STATUS="UNKNOWN )
OPEN(UNIT=17 FILE="A RESULT8' STATUS="UNKNOWN")
OPEN(UNIT=18 FILE= A RESULT9' STATUS= UNKNOWN )
OPEN(UNIT=19 FILE="A RESULT10" STATUS="UNKNOWN")
OPEN(UNIT=14 FILE= A RESULT14 STATUS= 'UNKNOWN )
DO 5 I=1 6
READ (15 *) AN(I) ALP(I) TM(I)
JJ=0
DO 13 J=2000 10000 2000
JJ=JJ+1
V(JJ)=J*1 0
READ (2 *) RE(I JJ)
READ (3 *) DEL1(I JJ)
PR(I JJ)=(V(JJ)*X/ALP(I))*RE(I JJ)**( 2 0/(AN(I)+1 0))
Z0(I JJ)=((8 0/PR(I JJ))*(4 242*(AN(I)+1 0)*1 5**AN(I))** ( 2 0/
*(AN(I)+1 0))** 5
Z1(I JJ)=(6 0/55 0)*Z0(I JJ)**2 0
Z(I JJ)=Z0(I JJ)+Z1(I JJ)
DELT(I JJ)=DEL1(I JJ)*Z(I JJ)
NUX(I JJ)=1 5*X/DELT(I JJ)
DO 20 TW=20 0 80 0 20 0
DO 22 Y=0 0 DELT(I 1) 01
T(I 1)=TW+1 5*(TM(1)-TW)*Y/DELT(I 1)- 5*(TM(1)-TW)*Y/
*(DELT(I 1))**3 0
WRITE (14 *) AN(I) ALP(I) TM(I)
WRITE (16 *)PR(I JJ)
WRITE (17 *) DELT(I JJ)
WRITE (18 *) NUX(I JJ)
WRITE (19 *) T(I 1)
22 CONTINUE
20 CONTINUE
13 CONTINUE
5 CONTINUE
REWIND 2
RWIND 3
RWIND 15
STOP
END

```

APPENDIX II PROGRAM TO CALCULATE FLOW RATE AND WALL SHEAR STRESS AT CONSTANT VISCOSITY

C THIS PROGRAM IS USED TO OBTAIN THE VALUE OF Q1 Q2 TC1 TC2 FOR A CONSTANT VISCOSITY THIS CVALUES WILL BE USED BY THE NEXT PROGRAM TO
 C OBTAIN THE HYDRODYNAMIC PRESSURE WHERE CHANGE IN VISCOSITY WILL BE
 C INCLUDED

```

DIMENSION E(100)
OPEN (UNIT=40 FILE="A DT20 DAT" STATUS="UNKNOWN")
OPEN (UNIT=44 FILE="A RESULT44" STATUS="UNKNOWN")
OPEN (UNIT=45 FILE="A RESULT45" STATUS="UNKNOWN")
OPEN (UNIT=46 FILE="A RESULT46" STATUS="UNKNOWN")
READ (40 *) V VIS AL1 AL2 H1 H2 AK,H0
WRITE (44 *)V VIS AL1 AL2 H1 H2 AK,H0
PI=3 145926
P1=0 0
STEP1=1 0E08
REM1=1E 10
J1=0
11 P1=P1+STEP1
J1=J1+1
DP1=P1/AL1
POIS1=(4+(AK*(DP1**2 0)*(H1**2 0)))/(12 0*AK)
QUET1=(VIS*V)/(2 0*AK*H1)
T11=-QUET1+(DSQRT((POIS1**3 0)+(QUET1**2 0)))
T12=QUET1+(DSQRT((POIS1**3 0)+(QUET1**2 0)))
PHY1=(T11**0 3333)-(T12**0 3333)
TC1=PHY1-(DP1*H1* 5)
Q1=DP1*H1**3 0/(6 0*VIS)+H1**2 0*TC1/(2 0*VIS)+
1 AK*( 05*(DP1)**3 0*H1**5 0+ 5*H1**2 0*TC1**3 0+ 25*DP1**
12 0*H1**4 0*TC1+ 5*DP1*H1**3 0*TC1**2 0)/VIS+V*H1
DP2=P1/AL2
POIS2=(4+(AK*(DP2**2 0)*(H2**2 0)))/(12 0*AK)
QUET2=(VIS*V)/(2 0*AK*H2)
T21=-QUET2+(DSQRT((POIS2**3 0)+(QUET2**2 0)))
T22=QUET2+(DSQRT((POIS2**3 0)+(QUET2**2 0)))
PHY2=(T21**0 3333)-(T22**0 3333)
TC2=PHY2+DP2*H2* 5
Q2= DP2*H2**3 0/(6 0*VIS)+H2**2 0*TC2/(2 0*VIS)
1 AK*( 05*(DP2)**3 0*H2**5 0+ 5*H2**2 0*TC2**3 0+ 25*DP2**
12 0*H2**4 0*TC2 5*DP2*H2**3 0*TC2**2 0)/VIS+V*H2
RES1=Q1-Q2
E(J1)=ABS(RES1)
FIX=E(J1)-E(J1 1)
IF (ABS(FIX) LE REM1)GO TO 10
IF (RES1)I2 10 11
12 P1=P1 STEP1
STEP1=STEP1/10 0
GO TO 11
10 WRITE (45 *) P1 TC1 TC2 Q1 Q2
FORCE=PI*H0*(AL1*TC1+AL2*TC2)
EST=FORCE/(PI*H0**2 0)
WRITE (46 *) FORCE EST
STOP
END
  
```

C PROGRAM TO CALCULATE THE PRESSURE DISTRIBUTION IN A STEPPED PARALLEL BORE UNIT CWHERE CHANGE IN VISCOSITY HAS BEEEN INCLUDED
 C DISTRIBUTION OF PRESSURURE AT THE FIRST UNIT

```

DIMENSION C1(250) C2(250) C3(250) C4(250) P(250) P1(250) P2(250)
IT1(250) T2(250) PG1(250) PG2(250) VIS1(250) VIS2(250) R(250)
ID(250) PHY(250) P3(250) P4(250)
OPEN (UNIT=50 FILE= A DT50 DAT' STATUS=' UNKNOWN )
OPFN (UNIT=52 FILE= A RESULT52" STATUS= UNKNOWN )
OPFN (UNIT=55 FILE= A RESULT55 STATUS= UNKNOWN )
OPEN (UNIT=53 FILE= A RFSULT53 ' STATUS= UNKNOWN )
OPEN (UNIT=54 FILE= A RFSULT54 STATUS= UNKNOWN )
OPLN (UNIT=56 FILE= A RFSULT56 STATUS= UNKNOWN )
OPFN (UNIT=57 FILE= A RFSULT57 STATUS= UNKNOWN )
OPFN (UNIT=58 FILE="A RESUL158 STATUS= UNKNOWN")
OPFN (UNIT=59 FILE= A RESUL159 STATUS= UNKNOWN )
OPFN (UNIT=60 FILE= A RFSUI 60 STATUS= UNKNOWN )
READ (50 *) ALP B C P0 TO DI IC1 TC2 Q1 Q2 I 1 I 2 AK OVIS V
  
```

```

I H1, H2 DPG
WRITE (60 *) ALP B C P0 T0 DL, TC1 TC2 Q1 Q2 L1 L2 AK, OVIS V
I H1 H2 DPG
PG1(I)=0 0
T1(I)=T0
P1(I)=P0
VIS1(I)=45 0
DO 30 I=2, L1
C1(I)=V*H1 Q1+ 5*H1**2 0*TC1**3 0*AK/VIS1(I 1)+ 5*H1**2 0*
I TC1/VIS1(I 1)
C2(I)=H1**3 0/(6*VIS1(I 1))+ 5*H1**3 0*TC1**2 0*AK/VIS1(I 1)
C3(I)= 25*H1**4 0*TC1*AK/VIS1(I 1)
C4(I)=AK*H1**5 0/(20 0*VIS1(I 1))
CALL COEF(C1 C2 C3 C4 P I DPG)
PG1(I)=P(I)
P1(I)=P1(I-1)+PG1(I)*DL
DP1=P1(I)-P1(I 1)
T1(I)=T1(I-1)-C*DL
VIS1(I)=VIS1(I 1)*EXP( ALP*(T1(I 1)-C*DL-B*DP1- T1(I 1)))
P3(I)=P1(I)/(10 0**5 )
30 CONTINUE
DO 2 I=1 L1
WRITE (52 *)P3(I)
WRITE (53 *)PG1(I)
WRITE (54 *) (VIS1(I))
WRITE (55 *) (T1(I))
2 CONTINUE
C DISTRIBUTION OF PRESSURE IN THE SECOND UNIT
T2(1)=T1(L1)
P2(1)=P1(L1)
VIS2(1)=VIS1(L1)
P2(L2)=0 0
PG2(1)=0 0
L3=L2 1
DO 40 J=2 L3
C4(J)=-AK*H2**5 0/(20 0*VIS2(J-1))
C1(J)=V*H2 Q2+ 5*H2**2 0*TC2**3 0*AK/VIS2(J 1)+ 5*H2**2 0*
I TC2/VIS2(J 1)
C2(J)=-((H2**3 0/(6*VIS2(J 1))+ 5*H2**3 0*TC2**2 0*AK/VIS2(J-1)))
C3(J)= 25*H2**4 0*TC2*AK/VIS2(J 1)
C4(J)= AK*H2**5 0/(20 0*VIS2(J 1))
CALL COEF(C1 C2 C3 C4 P J DPG)
PG2(J)= P(J)
P2(J)=P2(J 1) PG2(J)*DL
DP2=P2(J 1)-P2(J)
T2(J)=T2(J-1)-C*DL
VIS2(J)=VIS2(J 1)*EXP( ALP*(T2(J-1)-C*DL+B*PG2(J)*DL-T2(J 1)))
P4(J)=P2(J)/(10 0**5 0)
40 CONTINUE
DO 3 J=1 L3
WRITE (56 *) P4(J)
WRITE (57 *) VIS2(J)
WRITE (58 *) T2(J)
WRITE (59 *) PG2(J)
3 CONTINUE
STOP
END

SUBROUTINE COEF(C1 C2 C3 C4 P II DPG)
DIMENSION P(50) C1(50) C2(50) C3(50) C4(50)
C CALCULATION OF COEFFICIENTS USING NUMERICAL METHOD C THIS IS CALLED TWICE TO OBTAIN PG1
C AND PG2 THIS SUBROUTINE IS USED TO SOLVE NONLINEAR THIRD ORDER POWER LAW EQUATIONS
C C1+C2*X+C3*X**2 0+C4*X**3 0=0
X1=P(II)
DX=DPG
EPS= 0000001
F1=C1(II)+C2(II)*X1+C3(II)*X1**2 0+C4(II)*X1**3 0
IF(F1) 2 3 2
2 X2=X1+DX
F2=C1(II)+C2(II)*X2+C3(II)*X2**2 0+C4(II)*X2**3 0
IF(F2) 4 5 4
4 II (ABS(X1 X2) EPS) 5 5 8
8 A=\ 1 1*(X2 \ 1)/(1 2 1 1)
FA=C1(II)+C2(II)*A+C3(II)*A**2 0+C4(II)*A**3 0
II (1 A) 1 3 1 1 3
13 \ 1=\ 2

```

```
F1=F2
X2=A
F2=FA
GO TO 4
3 X2=X1
1 X2=A
5 P(II)=X1
RETURN
IF (RES1)12 10 11
12 P1=P1 STEP1
STEP1=STEP1/10 0
GO TO 11
10 WRITE (46,*) P1 TC1 TC2 Q1 Q2
FORCE=PI*H0*(AL1*TC1+AL2*TC2)
EST=FORCE/(PI*H0**2 0)
WRITE (45 *) FORCE EST
STOP
END
```

APPENDIX III PROGRAM TO CALCULATE PERCENTAGE REDUCTION IN DIAMETER IN A TUBE

```

DIMENSION E3(10000) P(500) H(500) Y(500) S(500) VIS(500)
IPS(300) X(500),R(500) V(500) E2(10000) E(10000) HS(500)
OPEN (UNIT=40 FILE="A DT40 DAT" STATUS="UNKNOWN")
OPEN (UNIT=45 FILE="A RESULT45" STATUS="UNKNOWN")
OPEN (UNIT=46 FILE="A RESULT46" STATUS="UNKNOWN")
OPEN (UNIT=5 FILE="A RESULT5" STATUS="UNKNOWN")
OPEN (UNIT=6 FILE="A RESULT6" STATUS="UNKNOWN")
OPEN (UNIT=7,FILE="A RESULT7" STATUS="UNKNOWN")
OPEN (UNIT=8 FILE="A RESULT8" STATUS="UNKNOWN")
OPEN (UNIT=9 FILE="A RESULT9" STATUS="UNKNOWN")
OPEN (UNIT=10 FILE="A RESULT10" STATUS="UNKNOWN")
READ (40 *)V1 AL1 AL2 H1 H2 R1 TW Y0 TER,F TU BA,OVIS AK,
1G C AA,DR
TC1=0 0
P1=0 0
STEP1=1 0E07
REM1=1 E 10
J1=0
11 P1=P1+STEP1
J1=J1+1
DP1=P1/AL1
POIS1=(4+(AK*(DP1**2 0)*(H1**2 0)))/(12 0*AK)
QUET1=(OVIS*V1)/(2 0*AK*H1)
T11=-QUET1+(DSQRT((POIS1**3 0)+(QUET1**2 0)))
T12=QUET1+(DSQRT((POIS1**3 0)+(QUET1**2 0)))
PHY1=(T11**0 3333)-(T12**0 3333)
TC1=PHY1-(DP1*H1* 5)
Q1=DP1*H1**3 0/(6 0*OVIS)+H1**2 0*TC1/(2 0*OVIS)+
1AK*( 05*(DP1)**3 0*H1**5 0+ 5*H1**2 0*TC1**3 0+ 25*DP1**
12 0*H1**4 0*TC1+ 5*DP1*H1**3 0*TC1**2 0)/OVIS+V1*H1
DP2=P1/AL2
POIS2=(4+(AK*(DP2**2 0)*(H2**2 0)))/(12 0*AK)
QUET2=(OVIS*V1)/(2 0*AK*H2)
T21=-QUET2+(DSQRT((POIS2**3 0)+(QUET2**2 0)))
T22=QUET2+(DSQRT((POIS2**3 0)+(QUET2**2 0)))
PHY2=(T21**0 3333)-(T22**0 3333)
TC2=PHY2+(DP2*H2* 5)
Q2=-DP2*H2**3 0/(6 0*OVIS)+H2**2 0*TC2/(2 0*OVIS)
1 AK*( 05*(DP2)**3 0*H2**5 0+ 5*H2**2 0*TC2**3 0+ 25*DP2**
12 0*H2**4 0*TC2 5*DP2*H2**3 0*TC2**2 0)/OVIS+V1*H2
RES1=Q1 Q2
E(J1)=ABS(RES1)
FIX=E(J1) E(J1 1)
IF (ABS(FIX) LE REM1)GO TO 10
IF (RES1)12 10 11
12 P1=P1-STEP1
STEP1=STEP1/10 0
GO TO 11
10 WRITE (46 *) P1 TC1 TC2 Q1 Q2
X1=Y0/((P1/R1)/(TW*AL1)+(ABS(TC1)/TW))
WRITE (45 *) X1
REP=(INT (X1*1000 0)+1)
N=AL1*1000 0 REP
P(1)=(P1*X1)/AL1
Y(1)=Y0
S(1)=(ABS(TC1)*X1)/TW
HS(1)=(P(1)*R1)/TW
PS(1)=HS(1)+S(1)
R(1)=R1
H(1)=H1
V(1)=V1
X(1)=X1
DX= 001
VIS(1)=(OVIS+ 61*X1*1000 0)
DO 23 J=2 N
STEP4=1E 04
REM4=1E 05
ALP= 026
B=0 0
K=0
16 B=B+VIS I FP4
K=K+1

```

```

X(J)=X(J 1)+DX
R(J)=R(J 1)-(B*DL)
H(J)=H(J 1)+B*DL
V(J)=V(J 1)/(1-(R(J 1) R(J))/R(J 1)))
DP=0 0
REM3=1E 10
STEP3=5E09
K1=0
17 DP=DP+STEP3
K1=K1+1
POIS3=(4+(AK*(DP**2)*(H(J)**2)))/(12*AK)
QUET3=(VIS(J 1)*V(J))/(2*AK*H(J))
T31=-QUET3+(DSQRT(((POIS3)**3 0)+((QUET3)**2 0)))
T32=QUET3+(DSQRT(((POIS3)**3 0)+((QUET3)**2 0)))
PHY3=(T31**0 3333)-(T32**0 3333)
TC=PHY3-(DP*H(J)*0 5)
RES2=DP*H(J)**3 0/(6 0*VIS(J-1))+H(J)**2 0*TC/(2 0*VIS(J 1))+
1AK*((05*(DP)**3 0*H(J)**5 0+5*H(J)**2 0*TC**3 0+25*DP**
12 0*H(J)**4 0*TC+5*DP*H(J)**3 0*TC**2 0)/VIS(J 1)+V(J)*H(J)-Q1
E2(K1)=ABS(RES2)
FIX2=E2(K1)-E2(K-1)
IF (ABS(FIX2) LE REM3) GO TO 19
IF (RES2)18 19 17
18 DP=DP-STEP3
STEP3=STEP3/10 0
GO TO 17
19 P(J)=P(J 1)+DP*DX
VIS(J)=VIS(J 1)*EXP(-ALP*( G*(P(J)-P(J 1))- C*DX))
HS(J)=(P(J)*R(J)*(DSQRT(((X(J)-X(J 1))**2)+(R(J-1)-R(J))**2 ))))
1/(TW*(X(J)-X(J 1)))
STRS=0 0
IF (AA.NE 1 0) GO TO 20
EMB=2 0*V(J)*(DLOG(R(J 1)/R(J)))/DX
STRS=(EMB/TU)**(1/BA)
20 Y(J)=(1 0+STRS)*(Y0+(TER*(DLOG(R(1)/R(J))**F)))
S(J)=(Y(J)*(R(J 1)-R(J))/R(J))+(ABS(TC)*DSQRT(((R(J 1)-R(J))**2)+
1((X(J)-X(J 1))**2 )))/TW+S(J 1)
PS(J)=HS(J)+S(J)
RES3=PS(J)-Y(J)
E3(K)=ABS(RES3)
RES4=E3(K)-E3(K 1)
IF (ABS(RES4) LE REM4) GO TO 22
IF (RES3)21 22 16
21 B=B STEP4
STEP4=STEP4/10 0
GO TO 16
22 CONTINUE
HH=H(J) H1+H2
WRITE (6 *) HH S(J) Y(J)
IF (DR EQ 1 0) GO TO 27
27 WRITE(7 *) P(J)
WRITE(8 *)VIS(J)
DR={DP*HH+TC}
PRA=(1 0 ((R(J)**1 )/(R1**1 )))**100 0
WRITE(5 *) DR
WRITE (10 *) PRD
23 CONTINUE
STOP
END

```

APPENDIX IV PROGRAM TO CALCULATE PRESSURE DISTRIBUTION IN A TAPERED UNIT

```

DIMENSION C1(250) C2(250) C3(250) C4(250) P(250) P1(250)
IP2(250) H2(250) T1(250) T2(250) PGI(250) TA2(250),P3(250)
1VIS1(250) VIS2(250) SR(250) S2(250) C5(250) C6(250) P5(250)
OPEN (UNIT=90 FILE=' A DT50 DAT' STATUS="UNKNOWN")
OPEN (UNIT=52 FILE="A RESULT52" STATUS="UNKNOWN")
OPEN (UNIT=55 FILE="A RESULT55" STATUS="UNKNOWN")
OPEN (UNIT=53 FILE="A RESULT53" STATUS="UNKNOWN")
OPEN (UNIT=54 FILE="A RESULT54" STATUS="UNKNOWN")
OPEN (UNIT=56 FILE="A RESULT56" STATUS="UNKNOWN")
OPEN (UNIT=57 FILE="A.RESULT57" STATUS="UNKNOWN")
OPEN (UNIT=58 FILE="A RESULT58" STATUS="UNKNOWN")
OPEN (UNIT=59 FILE="A RESULT59",STATUS="UNKNOWN")
OPEN (UNIT=61 FILE="A RESULT61" STATUS="UNKNOWN")
OPEN (UNIT=62 FILE="A RESULT62" STATUS="UNKNOWN")
READ (90 *) ALP B C P0 T0 DL,L2 AK,OVIS V,H1 H3 R VISI HB
T2(1)=T0
P2(1)=0 0
VIS2(1)= VISI
DO 40 J=2,L2
H2(1)=H1
SR(1)=V/(H2(1))
H2(J)=H2(J 1)-R*DL
SR(J)=V/H2(J)
S2(J)=VIS2(J-1)*SR(J)/(2 0*AK)
G2=1 0/(3 0*AK)
TA2(J)=(S2(J)+(S2(J)**2 0+G2**3 0)** 5)** 333-(-S2(J)+(S2(J)**2 0
1+ G2**3 0)** 5)** 333
P3(J)= 42*(6 0*VIS2(J-1)*V*(1/H2(J)-1/(H3**1 0))+HB/(2 0*H3**2 0)-
1HB/(2 0*H2(J)**2 0))/(R*(1+3 0*AK*TA2(J)**2 0))/(10 0**5 0)
C5(J)=(((0 0-(6 0*VIS2(J 1)*V*(1/H2(1)-1/H3))/(R*(1+3 0*AK*
1TA2(J)**2 0))))/((( 5*(1/H2(1)**2 0 1/H3**2 0)))*6 0*VIS2(J-1)
1/(R*(1+3 0*AK*TA2(J)**2 0))))
C6(J)=-6 0*VIS2(J 1)*(V/H3+C5(J)/(2 0*H3**2 00))/(R*
1(1+3 0*AK*TA2(J)**2 0))
P2(J)=(6 0*VIS2(J 1)*(V/H2(J)+C5(J)/(2 0*H2(J)**2 00))/
1(R*(1+3 0*AK*TA2(J)**2 0))+C6(J))
DP2=(P2(J)-P2(J 1))
T2(J)=T2(J 1)-C*DL
VIS2(J)=VIS2(J 1)*EXP( ALP*(T2(J-1)-C*DL-B*DP2 T2(J 1)))
P5(J)=P2(J)/(1 0*10 0**5 0)
40 CONTINUE
DO 3 J=1 L2
WRITE (56 *) P5(J)
WRITE (57 *) VIS2(J)
WRITE (58 *) T2(J)
WRITE (59 *) TA2(J)
WRITE (62 *) P3(J)
3 CONTINUE
STOP
END

```

**APPENDIX V PROGRAM TO OBTAIN TC1,Q1 AND Q2 FOR THE CALCULATION
OF PRESSURE IN A COMBINED PARALLEL AND TAPERED UNIT USED BY THE
NEXT PROGRAM**

```

IMPLICIT DOUBLE PRECISION (A H O Z)
DIMENSION E(100)
OPEN (UNIT=40 FILE="A DT20 DAT" STATUS= UNKNOWN )
OPEN (UNIT=41 FILE="A RESULT41" STATUS= UNKNOWN )
OPEN (UNIT=43 FILE="A RESULT43" STATUS= UNKNOWN )
READ (40 *) V VIS AL1 AL2 H1 H2 AK,H0 HA
WRITE (41 *)V VIS AL1 AL2 H1 H2 AK,H0 HA
PI=3.145926
P1=0.0
STEP1=1.0E08
REM1=1E 10
J1=0
11 P1=P1+STEP1
J1=J1+1
DP1=P1/AL1
POIS1=(4+(AK*(DP1**2.0)*(H1**2.0)))/(12.0*AK)
QUET1=(VIS*V)/(2.0*AK*H1)
T11= QUET1+(DSQRT((POIS1**3.0)+(QUET1**2.0)))
T12=QUET1+(DSQRT((POIS1**3.0)+(QUET1**2.0)))
PHY1=(T11**0.3333)-(T12**0.3333)
TC1=PHY1-(DP1*H1*5)
Q1=DP1*H1**3.0/(6.0*VIS)+H1**2.0*TC1/(2.0*VIS)+
IAK*(.05*(DP1)**3.0*H1**5.0+5*H1**2.0*TC1**3.0+25*DP1**
12.0*H1**4.0*TC1+5*DP1*H1**3.0*TC1**2.0)/VIS+V*H1
DP2=P1/AL2
POIS2=(4+(AK*(DP2**2.0)*(H2**2.0)))/(12.0*AK)
QUET2=(VIS*V)/(2.0*AK*H2)
T21= QUET2+(DSQRT((POIS2**3.0)+(QUET2**2.0)))
T22=QUET2+(DSQRT((POIS2**3.0)+(QUET2**2.0)))
PHY2=(T21**0.3333)-(T22**0.3333)
TC2=PHY2+(DP2*H2*5)
H3=HA
SR=V/H3
S2=VIS*SR/(2.0*AK)
T2=1.0/(3.0*AK)
TA2=(S2+(S2**2.0+T2**3.0)**5)**.3333-(S2+(S2**2.0+T2**3.0)**5)**
1.333
Q2= DP2*H3**3.0/(6.0*VIS)-DP2*AK*H3**3.0*TA2**2.0/(4.0*VIS)+V*H3*5
RES1=Q1-Q2
E(J1)=ABS(RES1)
FIX=E(J1)-E(J1-1)
IF (ABS(FIX) LE REM1)GO TO 10
IF (RES1)12 10 11
12 P1=P1 STEP1
STEP1=STEP1/10.0
GO TO 11
10 WRITE (43 *) P1 TC1 TA2 Q1 Q2
STOP
END

```

C THIS PROGRAM IS USED TO CALCULATE THE PRESSURE DISTRIBUTION IN THE COMBINED UNIT
C DISTRIBUTION OF PRESSURE AT THE FIRST PARALLEL UNIT

```

DIMENSION C1(250) C2(250) C3(250) C4(250) P(250) P1(250)
IP2(250) H2(250) T1(250) T2(250) PG1(250) TA2(250) P3(250)
I VIS1(250) VIS2(250) SR(250) S2(250) C5(250) C6(250) P4(250)
IP9(250) P10(250) TA3(250)
OPEN (UNIT=5 FILE= A DT50 DAT' STATUS= UNKNOWN )
OPEN (UNIT=52 FILE= A RESULT52 STATUS= UNKNOWN')
OPEN (UNIT=55 FILE= A RESULT55 STATUS= UNKNOWN )
OPEN (UNIT=53 FILE= 'A RESULT53 STATUS= UNKNOWN )
OPEN (UNIT=54 FILE= 'A RESULT54 STATUS= UNKNOWN )
OPEN (UNIT=56 FILE= A RESULT56 STATUS= UNKNOWN")
OPEN (UNIT=57 FILE= A RESULT57 STATUS= UNKNOWN )
OPEN (UNIT=58 FILE= A RESULT58 STATUS= UNKNOWN )
OPEN (UNIT=59 FILE= A RESULT59 STATUS= UNKNOWN )
OPEN (UNIT=60 FILE= A RESULT60 STATUS= UNKNOWN )
OPEN (UNIT=61 FILE= A RESULT61 STATUS= UNKNOWN )
OPEN (UNIT=62 FILE= A RESULT62 STATUS= UNKNOWN )

```

```

OPEN (UNIT=63 FILE="A RESULT63" STATUS="UNKNOWN ")
READ (5 *) ALP B C P0 T0 DL,TC1 TC2 Q1 Q2 L1 L2 AK,OVIS V
IH1 H3 DPG AR,R,VISA,HE HP
WRITE (60 *) ALP B C P0 T0 DL,TC1 TC2 Q1 Q2 L1 L2 AK,OVIS V
IH1 H3 DPG AR,R,VISA,HE HP
PG1(1)=0 0
T1(1)=T0
P1(1)=P0
VISA(1)=VISA
DO 30 I=2 L1
C1(I)=V*HI-Q1+ 5*HI**2 0*TC1**3 0*AK/VISA(I 1)+ 5*HI**2 0*
ITC1/VISA(I 1)
C2(I)=HI**3 0/(6*VISA(I 1))+ 5*HI**3 0*TC1**2 0*AK/VISA(I 1)
C3(I)= 25*HI**4 0*TC1*AK/VISA(I-1)
C4(I)=AK*HI**5 0/(20 0*VISA(I 1))
CALL COEF (C1 C2 C3 C4 P I DPG)
PG1(I)=P(I)
P1(I)=P1(I 1)+PG1(I)*DL
P9(I)=P1(I)/(10 0**5 0)
DP1=P1(I) P1(I 1)
T1(I)=T1(I 1)-C*DL
VISA(I)=VISA(I-1)*EXP( ALP*(T1(I-1)-C*DL-B*DP1 T1(I 1)))
30 CONTINUE
DO 2 I=1 L1
WRITE (52 *) (P9(I))
WRITE (53 *) (PG1(I))
WRITE (54 *) (VISA(I))
WRITE (55 *) (T1(I))
2 CONTINUE
C DISTRIBUTION OF PRESSURE IN THE SECOND TAPERED UNIT
T2(1)=T1(L1)
P2(1)=P1(L1)
VISA(1)=VISA(L1)
DO 40 J=2 L2
H2(1)=HP
SR(1)=V/(H2(1))
H2(J)=H2(J 1)-R*DL
SR(J)=V/H2(J)
S2(J)=VISA(J-1)*SR(J)/(2 0*AK)
G2=1 0/(3 0*AK)
HB=HE
TA2(J)=(S2(J)+(S2(J)**2 0+G2**3 0)** 5)** 333-( S2(J)+(S2(J)**2 0
1+ G2**3 0)** 5)** 333
P3(J)=( 335*6 0*VISA(J-1)*V*(1/H2(J)-1/(H3**1 0))+HB/(2 0*H3**2 0)-
1HB/(2 0*H2(J)**2 0))/(R*(1+3 0*AK*TA2(J)**2 0))/(2 0*(10 0**5 0))
P4(J)=6 0*92 0*V*(1/H2(J)-1/(H3**1 0))+HB/(2 0*H3**2 0)-
1HB/(2 0*H2(J)**2 0))/(R*(1+3 0*AK*AR**2 0))
C5(J)=((P1(L1)-(6 0*VISA(J 1)*V*(1/H2(1)-1/H3)))/(R*(1+3 0*AK*
1TA2(J)**2 0)))/((( 5*(1/H2(1)**2 0 1/H3**2 0))*6 0*VISA(J 1)
1/(R*(1+3 0*AK*TA2(J)**2 0)))
C6(J)= 6 0*VISA(J 1)*(V/H3+C5(J)/(2 0*H3**2 00))/(R*
1(1+3 0*AK*TA2(J)**2 0))
P2(J)=6 0*VISA(J-1)*(V/H2(J)+C5(J)/(2 0*H2(J)**2 00))/
1(R*(1+3 0*AK*TA2(J)**2 0))+C6(J)
DP2=P2(J)-P2(J 1)
T2(J)=T2(J 1)-C*DL
VISA(J)=VISA(J 1)*EXP( ALP*(T2(J-1)-C*DL-B*DP2 T2(J 1)))
P10(J)=P2(J)/(10 0**5 0)
TA3(J)=TA2(J)/100 0
40 CONTINUE
DO 3 J=1 L2
WRITE (56 *) P10(J)
WRITE (57 *) VISA(J)
WRITE (58 *) T2(J)
WRITE (59 *) TA3(J)
WRITE (62 *) P3(J)
3 CONTINUE
STOP
END

SUBROUTINE COEF (C1 C2 C3 C4 P I DPG)
DIMENSION P(50) C1(50) C2(50) C3(50) C4(50)
C CALCULATION OF COEFFICIENTS USING NUMERICAL METHOD
C THIS SUBROUTINE IS USED TO SOLVE NONLINEAR THIRD ORDER POWER LAW EQUATIONS
C C1+C2*X+C3*X**2 0+C4*X**3 0=0
C THIS IS CALLED TWICE TO OBTAIN PG1 AND PG2

```

```

X1=P(I)
DX=DPG
EPS= 0000001
F1=C1(I)+C2(I)*X1+C3(I)*X1**2 0+C4(I)*X1**3 0
IF (F1) 2 3 2
2 X2=X1+DX
F2=C1(I)+C2(I)*X2+C3(I)*X2**2 0+C4(I)*X2**3 0
IF (F2) 4 5 4
4 IF (ABS(X1 X2)-EPS) 5 5 8
8 A=X1-F1*(X2 X1)/(F2 F1)
FA=C1(I)+C2(I)*A+C3(I)*A**2 0+C4(I)*A**3 0
IF (FA) 13 1 13
13 X1=X2
F1=F2
X2=A
F2=FA
GO TO 4
3 X2=X1
1 X2=A
5 P(I)=X1
RETURN
END

```

APPENDIX VI PROGRAM TO CALCULATE THE MESH GENERATION FOR TEMPERATURE DISTRIBUTION WITHIN THE HYDRODYNAMIC UNIT

```

C  OPEN (UNIT=5 FILE= A INFIL' STATUS='UNKNOWN")
C  OPEN (UNIT=15 FILE= A OUTFIL' STATUS= UNKNOWN')
CALL INFILE
CALL GRID
CALL BANDW
CALL OUTPUT
STOP
END

C -----
C  SUBROUTINE GRID
C  *****
C  *                               *
C  * SUBROUTINE GRID  GENERATES MESH BOUNDARY CONDITIONS  *
C  *   INITIAL CONDITIONS AND PROPERTY DATA  *
C  *   BASED ON LIMITED REGIONAL INPUT  *
C  *                               *
C  *****
C
C ARGUMENT LIST
C   LNODS(I,J) - CONNECTIVITY MATRIX
C   KNODS(L,K) - CONNECTIVITY MATRIX FOR FLUX
C   JNODS(L,K)  CONNECTIVITY MATRIX FOR CONVECTION
C   XCORD(I)   - X CO ORDINATE NODAL ARRAY
C   YCORD(I)   - Y CO ORDINATE NODAL ARRAY
C   VALU(I)    NODAL ARRAY OF DEPENDENT VALUES
C   LNODE      INTEGER NUMBER NODES PER ELEMENT
C   IELEM      - SPECIFIC ELEMMENT OF INTEREST
C   NB         NUMBER OF DOMAIN NODE POINTS
C   NEL        NUMBER OF DOMAIN ELEMENTS
C   KBC1       - NUMBER OF DIRICHLET BOUNDARY POINTS
C   KBC2       - NUMBER OF CHAUCHY BOUNDARY SURFACES
C   KBC3       NUMBER OF CONVECTIVE SURFACES
C   Z          ZETA LOCATION FOR INTERPOLATION
C   E          ETA LOCATION FOR INTERPOLATION
C   I          - I=ELEMENTS
C   J          J=DOMAIN NODE
C   K          K=BOUNDARY NODE
C   L          L=INDEX OF CHAUCHY SURFACES
C
COMMON/A/ XP(501) YP(501) XRG(9) YRG(9) NDN(8)
COMMON/B/ NN(20 20) YC(20 20) XC(20 20) NNRB(20 4 20) JT(20 4)
COMMON/C/ NE(501) NR(9) ICOMP(4 4) SN(8)
COMMON/D/ QQ(501) DX(501) DY(501)
COMMON/E/ XCORD(501) YCORD(501)
COMMON/F/ PHI(501) H(501) TINF(501)
COMMON/G/ FIXED(501) NBA(501)
COMMON/H/ LNODS(501 8) KNODS(501 3) JNODS(501 3)
COMMON/I/ LNODE NPOIN NB NEL NELEM NNODE NUMN JFLAG IFLAG
COMMON/J/ KBC1 KBC2 KBC3
COMMON/P/ NSTOP NTYPE DT AF NVEL,KPRNT IAXI
COMMON/S/ ISI(501) LEM(501) ISIH(501) LME(501)
COMMON/PIC/XMIN XMAX YMIN YMAX
COMMON/NEW/NORDER(501)
C  INITIALIZE COUNTERS
C  OPFN (UNIT=5 FILE=' A FET DAT' STATUS='UNKNOWN')
NB=0
KBC1=0
KBC2=0
KBC3=0
NEL=0
NEI OLD=1
DO 1 I=1 501
NORDER(I)=0
DO 1 J=1 8
1 LNODS(I J)=0
DO 2 I=1 501
DO 2 J=1 3
JNODS(I J)=0
2 KNODS(I J)=0
DO 3 I=1 20
DO 3 J=1 20
3 NN(I I)=0

```

```

C   TINF=0 0
C   PH=0 0
C READ INITIAL DATA
  READ(5 *)NUMN NSTOP NTYPE KPRNT NVEL,DT AF IAXI
  WRITE(* *)NUMN NSTOP NTYPE KPRNT NVEL,DT AF IAXI
C 94 FORMAT(1H1,5I5 2F10 5 I5)
  READ(5 *)XMIN XMAX,YMIN YMAX
  WRITE(* *)XMIN XMAX,YMIN YMAX
C 96 FORMAT(10X,'XMIN=' F6 2 2X,'XMAX=' F6 2 2X,'YMIN=' F6 2 2X,
C   1'YMAX=' F6 2)
C READ #REGIONS #INPUT PTS ELEMENT SHAPE PRINT FLAG
C INPUT POINTS ARE THE REGIONS CORNER AND MID POINTS
C   LNODE   ELEMENT GEOMETRY
C   3     3 NODE TRIANGLE
C   4     4 NODE QUADRILATERAL
C   6     6 NODE TRIANGLE
C   8     8 NODE QUADRILATERAL
C IFLAG = 0 NO ECHO PRINTING
C IFLAG = 1 PRINTS COORDINATES CONNECTIVITY MATRIX, REGIONAL INPUT
C IFLAG = 2 PRINTS INITIAL REGIONAL NODE NUMBERS X,Y VALUES AND
C   CONNECTIVITY MATRIX FOR OUTPUT FILE
  READ(5 *) INRG INBP IFLAG
  LNODE=NUMN
C   SET INDICATOR OF NUMBER OF NODES PER ELEMENT SIDE
  KNODE=2
  IF(LNODE EQ 6 OR LNODE EQ 8)KNODE=3
  IF(LNODE EQ 3 OR LNODE EQ 4 OR LNODE EQ 6 OR LNODE EQ 8) GOTO 15
  WRITE(* *)
C 12 FORMAT(10X, ELEMENT SHAPE NOT PROPERLY DEFINED)
  STOP
C READ X AND Y COORDINATES OF INPUT POINTS
  15 DO 16 K=1 INBP
  16 READ(5 *)I XP(I) YP(I)
C READ CONNECTIVITY MATRIX COMMON SIDES OF ADJACENT REGIONS
  DO 30 I=1 INRG
  30 READ(5 *) NRG (JT(NRG J) J=1 4)
C CHECK PRINT FLAG FOR INPUT ECHO
  IF(IFLAG EQ 0) GOTO 100
C   ECHO INPUT
  WRITE(* *)
C 50 FORMAT(/ 1X 18HGLOBAL COORDINATES // 1X 6HNUMBER,10X,
C   1 7HX-COORD 10X,7HY-COORD)
  WRITE(* *) (I XP(I) YP(I) I=1 INBP)
C 60 FORMAT(3X,14 10X,F7 2 10X,F7 2)
  WRITE(* *)
C 70 FORMAT(/ 1X,17HCONNECTIVITY DATA,/ 1X,6HREGION 5X,1H1
C   1 5X,1H2 5X,1H3 5X,1H4)
  DO 80 I=1 INRG
  80 WRITE(* *) 1 (JT(I J) J=1 4)
C 90 FORMAT(3X,14 2X,4(4X,14))
C LOOP ON REGIONS TO GENERATE THE ELEMFNTS
  100 DO 1000 KK=1 INRG
C READ REGION# NO ROWS OF NODES TO BE IN THE REGION NO COLUMNS
C REGION BOUNDARY POINTS STARTING IN LOWER LEFT CORNER PROGRESSING
C COUNTER CLOCKWISE
  READ(5 *) NRG NROWS NCOL (NDN(I) I=1 8)
  READ(5 *) DXX,DYY HGEN
C REGIONS MUST BE READ IN NUMERICAL ORDER
C
  IF(NRG EQ KK) GOTO 108
C
C PRINT MESSAGE AND TERMINATE PROGRAM IF NOT IN ORDER
C
  WRITE(* *)
C 105 FORMAT(10X, PLACE REGIONS IN NUMERICAL ORDER PROGRAM STOPPED)
  STOP
C
C ECHO INPUT IF DFSIRLD
C
  108 IF(IFLAG NE 0)WRITE(* *) NRG NROWS NCOL (NDN(I) I=1 8)
C 110 FORMAT(/ 1X 6HREGION 13 2X 4HROWS 14 2X 7HCOLUMNS 13 /
C   1 1X 14HBOUNDARY NODES 8I5)
C
C GENERATION OF THE INITIAL NODE COORDINATES
C
  DO 120 I=1 8

```

```

II = NDN(I)
XRG(I) = XP(II)
120 YRG(I) = YP(II)
XRG(9) = XRG(1)
YRG(9) = YRG(1)
C
C IF 6 NODED TRIANGLES OR 8 NODED QUADS ARE DESIRED CHANGE GRID
C TO INCLUDE MID POINTS
C
IF(LNODE LT 5) GOTO 130
NROWS = 2*NROWS - 1
NCOL = 2*NCOL - 1
C
C CALCULATE GRID INCREMENTS DELTA ETA AND DELTA SI
C
130 DETA = 2 0 / (FLOAT(NROWS) - 1 0)
DSI = 2 0 / (FLOAT(NCOL) 1 0)
C
C STEP THRU LOCAL CO-ORDINATES ( ETA & SI ) AND USE SHAPE FUNCTIONS
C (SN(1) SN(8) ) TO CALCULATE GLOBAL COORDINATES ( XC & YC )
C START IN UPPER LEFT CORNER AND PROGRESS LEFT TO RIGHT AND TOP TO BOTTOM
C
DO 140 I=1 NROWS
ETA = 1 0 - DETA*(FLOAT(I) 1 0)
DO 140 J=1 NCOL
SI = 1 0 + DSI*(FLOAT(J) - 1 0)
C
C SHAPE FUNCTIONS
C
SN(1) = -0 25 * (1 0 SI) * (1 0 ETA) * (SI+ETA+1 0)
SN(2) = 0 50 * (1 0-SI*SI) * (1 0-ETA)
SN(3) = 0 25 * (1 0+SI) * (1 0 ETA) * (SI-ETA 1 0)
SN(4) = 0 50 * (1 0+SI) * (1 0 ETA*ETA)
SN(5) = 0 25 * (1 0+SI) * (1 0+ETA) * (SI+ETA-1 0)
SN(6) = 0 50 * (1 0-SI*SI) * (1 0+ETA)
SN(7) = 0 25 * (1 0 SI) * (1 0+ETA) * (ETA SI-1 0)
SN(8) = 0 50 * (1 0 SI) * (1 0 ETA*ETA)
C
C INITIALIZE XC & YC TO ZERO PREVIOUS SUMMATION
C
XC(I J) = 0 0
YC(I J) = 0 0
C
C SUM SHAPE FUNCTIONS
C
DO 140 K=1 8
XC(I J) = XC(I J) + XRG(K)*SN(K)
140 YC(I J) = YC(I J) + YRG(K)*SN(K)
C
C GENERATION OF THE REGION NODE NUMBERS
C
KN1 = 1
KS1 = 1
KN2 = NROWS
KS2 = NCOL
C
C CHECK EACH SIDE OF THE REGION FOR OUTSIDE BOUNDARY OR ANOTHER REGION
C
DO 200 I=1 4
C
C CHECK CONNECTIVITY MATRIX
C
NRT = JT(NRG I)
C
C IF SIDE IS OUTSIDE BOUNDARY OR THIS REGION IS LOWER NUMBERED THAN
C ADJACENT REGION THIS REGION HAS PRIORITY IN NUMBERING THE BOUNDARY
C
IF(NRT LE 0 OR NRT1 GT NRG) GOTO 200
C
C IF SIDE HAS BFEN NUMBERED PREVIOUSLY NUMBER ACCORDING TO PREVIOUS WORK
C DETERMINE WHICH SIDE OF ADJACENT REGION IS COMMON
C
DO 150 J=1 4
150 IF(JT(NRT J) I Q NR(I) NR1S = J
k = NCOL
IF(I I Q 2 OR I I Q 4) k = NROWS

```

```

JL = 1
JK = ICOMP(I NR 15)
IF(JK EQ 1) JL = K
DO 190 J=1 K
GOTO(160 165 170 175) J
160 NN(I J) = NNRB(NRT NRTS JL)
KN1 = 2
GOTO 190
165 NN(J NCOL) = NNRB(NRT NRTS JL)
KS2 = NCOL - 1
GOTO 190
170 NN(NROWS J) = NNRB(NRT NRTS JL)
KN2 = NROWS - 1
GOTO 190
175 NN(J 1) = NNRB(NRT NRTS JL)
KS1 = 2
190 JL = JL + JK
200 CONTINUE
C
C IF ELEMENT = 8 NODDED QUAD BRANCH TO DIFFERENT PART OF PROGRAM
C
IF(LNODE EQ 8) GOTO 800
C
C IF THERE IS ONLY ONE ROW OR ONE COLUMN ALL NODES HAVE BEEN NUMBERED
C SKIP NUMBERING REMAINING NODES
C
IF(KN1 GT KN2) GOTO 270
IF(KS1 GT KS2) GOTO 270
C
C NUMBER NEW NODES RELATING REGIONAL 2 D PLACEMENT WITH GLOBAL NUMBERING
C
DO 210 I=KN1 KN2
DO 210 J=KS1 KS2
C
C FOR MULTIPLY CONNECTED REGIONS
C
C IF(NRG EQ 3) NBOW1=1
C IF(NRG EQ 5 AND I EQ NROWS AND J EQ 1) NN(I J)=NNRB(3 2 NBOW1)
C IF(NRG EQ 5 AND I EQ NROWS AND J EQ 1) GO TO 210
C
C IF(NRG EQ 9) NBOW2=1
C IF(NRG EQ 14 AND I EQ NROWS AND J EQ 1) NN(I J)=NNRB(9 2 NBOW2)
C IF(NRG EQ 14 AND I EQ NROWS AND J EQ 1) GO TO 210
C
C END ALTERATION
C
NB = NB + 1
NN(I J) = NB
210 CONTINUE
C
C STORE BOUNDARY NODE NUMBERS
C
DO 220 I=1 NCOL
NNRB(NRG 3, I) = NN(NROWS I)
220 NNRB(NRG 1 I) = NN(I 1)
DO 230 I=1 NROWS
NNRB(NRG 2 I) = NN(I NCOL)
230 NNRB(NRG 4 I) = NN(I 1)
C
C FLAGGED OUTPUT
C
IF(IFLAG EQ 0) GOTO 270
WRITE(* *)
C 240 FORMAT(/ / 1\ 19HREGION NODE NUMBERS)
DO 250 I=1 NROWS
250 WRITE(* *) (NN(I J) J=1 NCOL)
C 260 FORMAT(1615)
C
C NUMBER NODES CONSECUTIVELY K REGIONAL NO NN GLOBAL NO
C
270 K = 1
DO 280 I=1 NROWS
DO 280 J=1 NCOL
NF(K) = NN(I J)
NI K = NF(K)
NORDI R(NI K)=NI K

```

```

XCORD(NEK) = XC(I J)
YCORD(NEK) = YC(I J)
280 K = K + 1
IF(LNODE EQ 6) GOTO 600
C
C INITIALIZATION FOR 3 NODE TRIANGLES AND 4 NODE QUAD
C
L = NROWS 1
DO 499 I=1 L
DO 499 J=2 NCOL
NR(1) = NCOL*I + J 1
NR(2) = NCOL*I + J
NR(3) = NCOL*(I-1) + J
NR(4) = NCOL*(I-1) + J 1
C
C IF 4 NODE QUAD BRANCH
C
IF(LNODE EQ 4) GOTO 400
C
C 3 NODE TRIANGLE
C
C DETERMINE DIAGONAL LENGTHS
C
DIAG1=(XC(I J)-XC(I+1 J-1))**2+(YC(I J)-YC(I+1 J 1))**2
DIAG2=(XC(I+1 J)-XC(I J-1))**2+(YC(I+1 J)-YC(I J 1))**2
C
C DIVIDE QUADS INTO TRIANGLES
C
DO 399 IJ=1 2
NEL = NEL + 1
DX(NEL)=DXX
DY(NEL)=DYY
QQ(NEL)=HGEN
C
C DIVIDE WITH SHORTEST DIAGONAL
C
IF((DIAG1/DIAG2) GT 1 04) GOTO 350
J1 = NR(1)
J2 = NR(IJ+1)
J3 = NR(IJ+2)
LNODS(NEL,1) = NE(J1)
LNODS(NEL,2) = NE(J2)
LNODS(NEL,3) = NE(J3)
GOTO 399
350 J1 = NR(IJ)
J2 = NR(IJ+1)
J3 = NR(4)
LNODS(NEL,1) = NE(J1)
LNODS(NEL,2) = NE(J2)
LNODS(NEL,3) = NE(J3)
399 CONTINUE
GOTO 499
C
C 4 NODE QUADS
C
400 NEL = NEL + 1
DX(NEL)=DXX
DY(NEL)=DYY
QQ(NEL)=HGEN
J1 = NR(1)
J2 = NR(2)
J3 = NR(3)
J4 = NR(4)
LNODS(NEL,1) = NE(J1)
LNODS(NEL,2) = NE(J2)
LNODS(NEL,3) = NE(J3)
LNODS(NEL,4) = NE(J4)
499 CONTINUE
GOTO 900
C
C 6 NODE TRIANGLES
C
600 L = NROWS 2
DO 699 I=1 L,2
DO 699 J=3 NCOL 2
C

```

```

C CALCULATE DIAGONAL LENGTHS SHORTER DIAGONAL WILL DIVIDE
C
  DIAG1=(XC(I J) XC(I+2 J 2))**2 +(YC(I J)-YC(I+2 J 2))**2
  DIAG2=(XC(I+2 J) XC(I J 2))**2 +(YC(I+2 J)-YC(I J 2))**2
C
C NUMBER NODES ACCORDING TO WHICH DIAGONAL WILL DIVIDE
C
  IF((DIAG1/DIAG2) GT 1 04) GOTO 610
  NR(1) = NCOL*(I+1) + J - 2
  NR(2) = NCOL*(I+1) + J - 1
  NR(3) = NCOL*(I+1) + J
  NR(4) = NCOL*I + J
  NR(5) = NCOL*I + J + 1
  NR(6) = NCOL*(I 1) + J
  NR(7) = NCOL*(I-1) + J - 1
  NR(8) = NCOL*I + J + 2
  NR(9) = NCOL*(I 1) + J + 2
  GOTO 620
610 NR(1) = NCOL*(I 1) + J + 2
  NR(2) = NCOL*I + J - 2
  NR(3) = NCOL*(I+1) + J - 2
  NR(4) = NCOL*(I+1) + J - 1
  NR(5) = NCOL*I + J + 1
  NR(6) = NCOL*(I+1) + J
  NR(7) = NCOL*I + J
  NR(8) = NCOL*(I 1) + J + 1
  NR(9) = NCOL*(I 1) + J
620 DO 640 IJ=1 4 3
  NEL = NEL + 1
  DX(NEL)=DXX
  DY(NEL)=DYY
  QQ(NEL)=HGEN
  J1 = NR(1)
  J2 = NR(1+IJ)
  J3 = NR(2+IJ)
  J4 = NR(3+IJ)
  J5 = NR(5+IJ)
  J6 = NR(4+IJ)
  LNODS(NEL,1) = NE(J1)
  LNODS(NEL,2) = NE(J2)
  LNODS(NEL,3) = NE(J3)
  LNODS(NEL,4) = NE(J4)
  LNODS(NEL,5) = NE(J5)
640 LNODS(NEL,6) = NE(J6)
699 CONTINUE
  GOTO 900
C
C 8 NODED QUADS
C
C NUMBER NODES CONSECUTIVELY GLOBAL# = NN(REGION ROW REGION COL)
C SKIP NUMBERING IF ONLY ONE ROW OR ONE COLUMN PRESENT
C
800 IF(KN1 GT KN2) GOTO 816
  IF(KS1 GT KS2) GOTO 816
  DO 814 I=1 KN2 2
  DO 812 INC=1 2
  I2 = I + INC - 1
  IF(I2 LT KN1) GOTO 812
  IF(I2 GT KN2) GOTO 812
  DO 810 J=1 KS2 INC
  IF(J LT KS1) GOTO 810
  NB = NB + 1
  NN(I2 J) = NB
810 CONTINUE
812 CONTINUE
814 CONTINUE
816 CONTINUE
C
C STORE BOUNDARY NODES
C
  DO 820 I=1 NCOL
  NNRB(NRG,3 I) = NN(NROWS I)
820 NNRB(NRG,1 I) = NN(1 I)
  DO 830 I=1 NROWS
  NNRB(NRG,2 I) = NN(1 NCOL I)
830 NNRB(NRG,4 I) = NN(1 I)

```

```

C
C FLAGGED OUTPUT
C
  IF(IFLAG EQ 0) GOTO 870
  WRITE(* *)
C 840 FORMAT(// 1X,19HREGION NODE NUMBERS)
  DO 850 I=1 NROWS
  850 WRITE(* *) (NN(I J) J=1 NCOL)
C 860 FORMAT(16I5)
C
C NUMBER NODES CONSECUTIVELY K=REGION#, NE(K)=GLOBAL#
C
870 K = 1
  DO 882 I=1 NROWS 2
  DO 882 INC=1 2
  I2 = I + INC 1
  IF(I2 GT NROWS) GOTO 881
  DO 880 J=1 NCOL,INC
  NE(K) = NN(I2 J)
  NEK = NE(K)
  NORDER(NEK)=NEK
  XCORD(NEK) = XC(I2 J)
  YCORD(NEK) = YC(I2 J)
  K = K + 1
880 CONTINUE
881 CONTINUE
882 CONTINUE
  L = (NROWS 1) / 2
  NCOL2 = (NCOL + 1) / 2
  DO 890 I=1 L
  DO 890 J=3 NCOL,2
  NEL = NEL + 1
  DX(NEL)=DXX
  DY(NEL)=DYY
  QQ(NEL)=HGEN
  J1 = (NCOL + NCOL2)*I + J 2
  J2 = (NCOL + NCOL2)*I + J 1
  J3 = (NCOL + NCOL2)*I + J
  J4 = NCOL*I + NCOL2*(I-1) + (J+1)/2
  J5 = (NCOL + NCOL2)*(I 1) + J
  J6 = (NCOL + NCOL2)*(I 1) + J 1
  J7 = (NCOL + NCOL2)*(I 1) + J 2
  J8 = NCOL*I + NCOL2*(I 1) + (J-1)/2
  LNODS(NEL,1) = NE(J1)
  LNODS(NEL,2) = NE(J2)
  LNODS(NEL,3) = NE(J3)
  LNODS(NEL,4) = NE(J4)
  LNODS(NEL,5) = NE(J5)
  LNODS(NEL,6) = NE(J6)
  LNODS(NEL,7) = NE(J7)
  LNODS(NEL,8) = NE(J8)
890 CONTINUE
C
C CHECK EACH SIDE FOR BOUNDARY CONDITIONS
C
900 DO 990 I=1 4
  J = JT(NRG I)
  IF(J GT 0) GOTO 990
  IF(J EQ 1) GOTO 910
  IF(J EQ -2) GOTO 960
  IF(J EQ 3) GOTO 1001
C
C DIRICHLET BOUNDARY CONDITIONS
C
910 READ(5 *) IRG ISIDE TEMP
  IF(IRG NE NRG OR ISIDE NE I) GOTO 2010
  K = NCOL
  IF(I EQ 2 OR I EQ 4) K = NROWS
  DO 950 L=1 K
  KBC1 = KBC1 + 1
  GOTO(920 925 930 935) I
920 NBA(KBC1) = NN(I L)
  C O I O 940
925 NBA(KBC1) = NN(L NCOL)
  GOTO 940
930 NBA(KBC1) = NN(NROWS I)

```

```

GOTO 940
935 NBA(KBC1) = NN(L,1)
940 FIXED(KBC1) = TEMP
C
C   OMIT ANY NODE POINTS PREVIOUSLY SPECIFIED
C
  KM1=KBC1-1
  IF(KM1 EQ 0)GO TO 950
  DO 955 KKBC1=1 KM1
955 IF(NBA(KBC1) EQ NBA(KKBC1))KBC1=KM1
950 CONTINUE
  GO TO 990
C
C   NEUMANN BOUNDARY CONDITIONS
C
960 READ(5 *)IRG ISIDE PH
  IF(IRG NE NRG OR ISIDE NE I)GO TO 2010
  IF(LNODE EQ 6 OR LNODE EQ 8)GO TO 980
  K=NCOL-1
  IF(I EQ 2 OR I EQ 4)K=NROWS 1
  KSTEP=1
  GO TO 985
980 K=NCOL-2
  IF(I EQ 2 OR I EQ 4)K=NROWS 2
  KSTEP=2
985 DO 986 IK=1 K,KSTEP
  KBC2=KBC2+1
  IF(LNODE EQ 3 OR LNODE EQ 6)THEN
  IF(ISIDE EQ 1)JSIDE=2
  IF(ISIDE EQ 2)JSIDE=2
  IF(ISIDE EQ 3)JSIDE=3
  IF(ISIDE EQ 4)JSIDE=1
  ELSE IF(LNODE EQ 4 OR LNODE EQ 8)THEN
  IF(ISIDE EQ 1)JSIDE=2
  IF(ISIDE EQ 2)JSIDE=3
  IF(ISIDE EQ 3)JSIDE=4
  IF(ISIDE EQ 4)JSIDE=1
  ENDIF
  NS1=0
  NS2=0
  NS3=0
  ISI(KBC2)=JSIDE
  PHI(KBC2)=PH
  KNODS(KBC2 1)=NNRB(NRG I IK)
  KNODS(KBC2 2)=NNRB(NRG I IK+1)
  IF(KNODE EQ 3)KNODS(KBC2 3)=NNRB(NRG I IK+2)
  NS1=NNRB(NRG I IK)
  NS2=NNRB(NRG I IK+1)
  IF(KNODE EQ 3)NS3=NNRB(NRG I IK+2)
  DO 987 IEL=NELOLD NEL
  KE1=0
  KE2=0
  KE3=0
  DO 987 ILLN=1 LNODE
  ILL=L.NODS(IEL,ILLN)
  IF(ILL.EQ NS1)KE1=1
  IF(ILL.EQ NS2)KE2=1
  IF(ILL.EQ NS3)KE3=1
  KEALL=KE1+KE2+KE3
  IF(KEALL GE 2)GOTO 988
987 CONTINUE
988 LEM(KBC2)=IEL
986 CONTINUE
  GO TO 990
C
C   CONVECTION BOUNDARY CONDITIONS
C
1001 READ(5 *)IRG LSIDE HH TINFF

  IF(IRG NE NRG OR LSIDE NE I)GO TO 2010
  IF(LNODE EQ 6 OR LNODE EQ 8)GO TO 1002
C   TINFF=0 0
C   HH=0 0
  K=NCOL-1
  IF(I EQ 2 OR I EQ 4)K=NROWS 1
  KSTEP=1

```

```

      GO TO 1003
1002 K=NCOL-2
      IF(1 EQ 2 OR 1 EQ 4)K=NRWS 2
      KSTEP=2
1003 DO 1004 IK=1 K,KSTEP
      KBC3=KBC3+1
      IF(LNODE EQ 3 OR LNODE EQ 6)THEN
      IF(LSIDE EQ 1)JSIDE=2
      IF(LSIDE EQ 2)JSIDE=2
      IF(LSIDE EQ 3)JSIDE=3
      IF(LSIDE EQ 4)JSIDE=1
      ELSE IF(LNODE EQ 4 OR LNODE EQ 8)THEN
      IF(LSIDE EQ 1)JSIDE=2
      IF(LSIDE EQ 2)JSIDE=3
      IF(LSIDE EQ 3)JSIDE=4
      IF(LSIDE EQ 4)JSIDE=1
      ENDIF
      NS1=0
      NS2=0
      NS3=0
      ISIH(KBC3)=JSIDE
      H(KBC3)=HH
      TINF(KBC3)=TINFF
      JNODS(KBC3 1)=NNRB(NRG I IK)
      JNODS(KBC3,2)=NNRB(NRG I IK+1)
      IF(KNODE EQ 3)JNODS(KBC3 3)=NNRB(NRG I IK+2)
      NS1=NNRB(NRG I IK)
      NS2=NNRB(NRG I IK+1)
      IF(KNODE EQ 3)NS3=NNRB(NRG I IK+2)
      DO 1005 IEL=NELOLD NEL
      KE1=0
      KE2=0
      KE3=0
      DO 1005 ILLN=1 LNODE
      ILL=LNODS(IEL,ILLN)
      IF(ILL EQ NS1)KE1=1
      IF(ILL EQ NS2)KE2=1
      IF(ILL EQ NS3)KE3=1
      KEALL=KE1+KE2+KE3
      IF(KEALL GE 2)GOTO 1006
1005 CONTINUE
1006 LME(KBC3)=IEL
1004 CONTINUE
C
990 CONTINUE
      NELOLD=NEL+1
1000 CONTINUE

C  OPTIMIZE MESH NUMBERING BY PASSING HORIZONTAL PLANES
C
      NSTEP=500
      IF(JFLAG EQ 1)THEN
      WRITE(* *)
C 111 FORMAT(/ 10X MESH BEING OPTIMIZED)
      CALL OPTNOD(NSTEP)
      ENDIF
C
C  FLAGGED OUTPUT
C
      IF(IFLAG NE 1) GOTO 2000
      WRITE(* *)
C 1010 FORMAT(// '**** ELEMENTAL DATA ****')
      WRITE(* *)
C 1100 FORMAT(// 1X,4IHNODE 11X 7HX COORD 10X,7HY COORD /)
      DO 1110 I=1 NB
      J=NORDER(I)
      1110 WRITE(* *) J \CORD(I) YCORD(I)
C 1120 FORMAT(1X I4 10X I9 4 8X I9 4)
      WRITE(* *)
C 1130 FORMAT(// 1X 10HTOPOGRAPHY / 1X 10H----- / 1X,
C 1 7IIELEMENT,15\ 5HNODES //)
      DO 1140 I=1 NLL
      1140 WRITE(* *) I (NORDFR(LNODS(I J)) J=1 LNODE)
C 1150 FORMAT(3\ I4 7X 8(I4))
C  WRITE(* 7000)
C 7000 FORMAT (// 25X MATERIAL PROPERTIES ARE //

```

```

C 15X,'ELEMENT THERMAL HEAT'/
C 25X,'NUMBER DIFFUSIVITY GENERATION',/)
C DO 7080 JELEM=1 NEL
C7080 WRITE(* 7085) JELEM QQ(JELEM) DX(JELEM) DY(JELEM)
C7085 FORMAT(5X,I5 5X,F10 5 2X,F10 5,F10 5 3X,F10 5)
WRITE(* *)KBC1
C 1160 FORMAT(// 1X,I6 ' DIRICHLET BOUNDARY CONDITIONS'// 1X,'NODE',
C 1 5X,'VALUE //)
DO 1170 I=1 KBC1
1170 WRITE(* *) NORDER(NBA(I)) FIXED(I)
C 1180 FORMAT(1X,I4 5X,F9 4)
WRITE(* *)KBC2
C 1190 FORMAT(// 1X,I6 ' NEUMANN BOUNDARY CONDITIONS'// 1X,
C * FLUX NODE NUMBERS',/)
DO 1191 I=1,KBC2
1191 WRITE(* *)PHI(I) (NORDER(KNODS(I J)),J=1 KNODE)
C 1192 FORMAT(F10 5 5X,8I6)
WRITE(* *)KBC3
C 1193 FORMAT(// 1X,I6 ' CONVECTION BOUNDARY CONDITIONS'// 1X,
C *H TINF NODE NUMBERS',/)
DO 1195 I=1,KBC3
1195 WRITE(* *)H(I),TINF(I) (NORDER(JNODS(I J)) J=1 KNODE)
C 1196 FORMAT(2F10 5 5X,8I6)
2000 RETURN
2010 WRITE(*,*)
C 2020 FORMAT(10X,'INCOMPATIBLE BOUNDARY CONDITION INPUT')
STOP
END

```

```

C -----
SUBROUTINE OUTPUT
COMMON/VH/NODES4(4 2) NODES8(4 3) NODES3(3 2) NODES6(3 3)
COMMON/LH/NODE(501 8) KNODE(501) Q(501)
COMMON/NEW/NORDER(501)
COMMON/LL/X(501) Y(501)
COMMON/D/ QQ(501) DX(501) DY(501)
COMMON/E/ XCORD(501) YCORD(501)
COMMON/F/ PHI(501) H(501) TINF(501)
COMMON/G/ FIXED(501) NBA(501)
COMMON/H/ LNODS(501 8) KNODS(501 3) JNODS(501 3)
COMMON/I/ LNODE NPOIN NB NEL,NELEM NNODE NUMN JFLAG IFLAG
COMMON/J/ KBC1 KBC2 KBC3
COMMON/P/ NSTOP NTYPE DT AF NVEL,KPRNT IAXI
COMMON/S/ ISI(501) LEM(501) ISIH(501) LME(501)
COMMON/VE/VX(501) VY(501)
COMMON/PIC/XMIN XMAX,YMIN YMAX
CHARACTER*4 STOP(4)
DATA STOP/'DIRC' 'FLUX' 'CONV' 'VELC'/

```

```

C
NNODE=NB
NELEM=NEL
NUM=2
IF(NUMN EQ 6 OR NUMN EQ 8)NUM=3
DO 33 I=1 NNODE
NODPT=NORDER(I)
X(NODPT)=XCORD(I)
33 Y(NODPT)=YCORD(I)
DO 34 J=1 NELEM
DO 34 L=1 NUMN
34 NODE(J L)=NORDER(LNODS(J L))
DO 35 I=1 NNODE
35 Q(I)=PHI(I)
RHO=1 0
CP=1 0

```

```

C
C WRITE XMIN XMAX, YMIN YMAX

```

```

C
C WRITE(* *)XMIN XMAX,YMIN YMAX

```

```

C
C WRITE THE NUMBER OF SYSTEM NODFS AND ELEMENTS

```

```

C
MTYPE=0
NUMDIM=2
WRITE(15 *)M I Y P I NUMDIM NNODE N I I F M NUMN NSTOP KPRN I NVEL
TO=0 0
WRITE(15 *)NTYPL DI AF TO RHO CP IAXI

```

```

C

```

```

C WRITE NODE NUMBERS AND NODAL COORDINATES
C
WRITE(15 *)X(I) Y(I) I=1 NNODE)
C
C WRITE SYSTEM TOPOLOGY(ELEMENT NO AND NODE NUMBERS
C IN COUNTER-CLOCKWISE FASHION STARTING AT ANY NODE)
C AND INPUT SOURCE TERM FOR EACH ELEMENT
C
DO 105 J=1 NELEM
WRITE(15 *)J QQ(J) DX(J) DY(J) (NODE(J MM) MM=1 NUMN)
105 CONTINUE
C
C CYCLE FOR EACH NODE HAVING SPECIFIED VALUE
C
DO 110 I=1 KBC1
WRITE(15 *)NORDER(NBA(I)) FIXED(I)
110 CONTINUE
WRITE(15 (6X,A4))STOP(1)
C
C WRITE ELEMENT SIDE THAT DEFINES BOUNDARY
C SEGMENT WHERE FLUX (GRADIENT) IS SPECIFIED
C
DO 130 I=1 KBC2
WRITE(15 *)Q(I) LEM(I) ISI(I)
130 CONTINUE
WRITE(15 (6X,A4))STOP(2)
C
C WRITE ELEMENT SIDE THAT DEFINES BOUNDARY SEGMENT
C WHERE CONVECTIVE SURFACE IS SPECIFIED
C
DO 140 I=1 KBC3
WRITE(15 *)H(I) TINF(I) LME(I),ISIH(I)
140 CONTINUE
WRITE(15 (6X,A4))STOP(3)
C
C PRINT ALL DATA THAT HAS BEEN READ IN
C
WRITE(* *)NNODE NELEM
WRITE(* *)
DO 150 I=1 NNODE
WRITE(* *)I X(I) Y(I)
150 CONTINUE
WRITE(* *)
DO 155 I=1 NELEM
WRITE(* *)I QQ(I) DX(I) DY(I) (NODE(I MM) MM=1 NUMN)
155 CONTINUE
WRITE(* *)
555 DO 160 I=1,KBC1
WRITE(* *)I NORDER(NBA(I)) FIXED(I)
160 CONTINUE
WRITE(* *)
DO 170 I=1 KBC2
ISI1=ISI(I)
L=LEM(I)
IF(NUMN EQ 3 OR NUMN EQ 6)THEN
IF(NUM EQ 2)WRITE(* *)I Q(I) (NODE(L,NODES3(ISI1 K)) K=1 NUM)
IF(NUM EQ 3)WRITE(* *)I Q(I) (NODE(L,NODES6(ISI1 K)) K=1 NUM)
ELSE
IF(NUM EQ 2)WRITE(* *)I Q(I) (NODE(L,NODES4(ISI1 K)) K=1 NUM)
IF(NUM EQ 3)WRITE(* *)I Q(I) (NODE(L,NODES8(ISI1 K)) K=1 NUM)
ENDIF
170 CONTINUE
WRITE(* *)
WRITE(* *)
DO 180 I=1 KBC3
ISI1=ISIH(I)
L=LME(I)
IF(NUMN EQ 3 OR NUMN EQ 6)THEN
IF(NUM EQ 2)WRITE(* *)I H(I) TINF(I) (NODE(L,NODES3(ISI1 K))
IK=1 NUM)
IF(NUM EQ 3)WRITE(* *)I H(I) TINF(I) (NODE(L,NODES6(ISI1 K))
IK=1 NUM)
ELSE
IF(NUM EQ 2)WRITE(* *)I H(I) TINF(I) (NODE(L,NODES4(ISI1 K))
IK=1 NUM)
IF(NUM EQ 3)WRITE(* *)I H(I) TINF(I) (NODE(L,NODES8(ISI1 K))
IK=1 NUM)

```

```

      IK=1 NUM)
      ENDF
180 CONTINUE
C
C IF NVEL=1 READ SPECIFIED NODE NUMBERS AND NODAL VELOCITIES
C
      IF(NVEL EQ 0)GO TO 28
      DO 26 J=1 NNODE
26 READ(5 *)I VX(I) VY(I)
      WRITE(* *)
      DO 27 I=1 NNODE
      WRITE(* *)I VX(I) VY(I)
27 WRITE(15 *)I VX(I) VY(I)
28 CONTINUE
      WRITE(15 '(6X,A4)')STOP(4)
C
C FORMAT STATEMENTS
C
C 1004 FORMAT(/ / 5X,4F8 3)
C 1005 FORMAT(8I5)
C 1006 FORMAT(14 2X,5F8 4,2X,I4)
C 1007 FORMAT(5X,I5 5X,2F8 3)
C 1010 FORMAT(15 1X,3F8 3 2X,8I5)
C 1015 FORMAT(10X,I5 5X,F10 5)
C 1018 FORMAT(10X,I5 5X,2F10 5)
C 1025 FORMAT(10X,F10 5 2I5)
C 1026 FORMAT(10X,2F10 5 2I5)
C 1035 FORMAT('0' 10X,'NO OF NODES=' I4 5X,'NO OF ELEMENTS=' I4)
C 1040 FORMAT('0' 2X,'SUMMARY OF NODAL COORDINATES')
C 1041 FORMAT('0' 7X,'T' 9X,'X' 11X,'Y')
C 1045 FORMAT(5X,I4 2(4X,F8 4))
C 1050 FORMAT('0 3X,'ELEMENT' 3X,'SOURCE' 4X,'DX' 5X,'DY' 9X,'NODE NUMBE
C 1RS')
C 1055 FORMAT(5X,I4 3X,3F8 3 8(1X,I4))
C 1060 FORMAT('0 7X,'NODES WHERE CNEW IS SPECIFIED )
C 1065 FORMAT(2X,2(4X,I4) 5X,F8 3)
C 1080 FORMAT('0 15X,'NODES WHERE FLUX IS SPECIFIED')
C 1082 FORMAT('0 8X,I 6X,'FLUX' 5X,'NODE NUMBERS')
C 1081 FORMAT('0' 15X,'NODES WHERE CONF IS SPECIFIED')
C 1083 FORMAT('0' 10X,'I' 7X,'H' 7X,'TINF' 7X,'NODE NUMBERS')
C 1085 FORMAT(6X,I4 3X,F8 3 2X,3(1X,I4))
C 1086 FORMAT(8X,I4 2X,2(2X,F8 3) 2X,3(1X,I4))
C 4041 FORMAT('0' 7X,'I' 12X,'VX' 12X,'VY')
      RETURN
      END
C -----
BLOCK DATA
COMMON/VH/NODES4(4 2) NODES8(4 3) NODES3(3 2) NODES6(3 3)
COMMON/XY/X4(4) Y4(4) X8(8) Y8(8)
COMMON/C/NE(501) NR(9) ICOMP(4 4) SN(8)
DATA ICOMP/-1 -1 1 1 1 1 1 1 1 1 1 1 1 1 1 1 1 1 1 1/
DATA NODES3/3 2 1 1 3 2/
DATA NODES6/5 3 1 6 4 2 1 5 3/
DATA NODES4/4 3 2 1 1 4 3 2/
DATA NODES8/7 5 3 1 8 6 4 2 1 7 5 3/
DATA X4/ 1 0 1 0 1 0 1 0/
DATA Y4/-1 0 1 0 1 0 1 0/
DATA X8/ 1 0 0 0 1 0 1 0 1 0 0 0 -1 0 1 0/
DATA Y8/ 1 0 -1 0 1 0 0 0 1 0 1 0 1 0 0 0/
END
C -----
SUBROUTINE BANDW
COMMON/LH/NODE(501 8) KNODE(501) Q(501)
COMMON/I/ LNODE NPOIN NB NEL,NELEM NNODE NUMN JFLAG IFLAG
COMMON/H/ LNODS(501 8) KNODS(501 3) JNODS(501 3)
COMMON/NEW/NORDER(501)
DIMENSION NOD(8)
C
      DO 34 K=1 NEL
      DO 34 I=1 NUMN
34 NODI(K I)=NORDI'R(LNODS(K,I))
C
C CALCULATT BANDWIDTH FOR EACH ELFMFNT
C
      NI3W=0
      DO 1 K=1 NI 1

```

```

DO 2 I=1 NUMN
2 NOD(I)=NOD(K,I)
L=NUMN-1
DO 3 I=1 L
J=I+1
DO 3 KK=J NUMN
NW=IABS(NOD(I)-NOD(KK))
IF(NW EQ 0)WRITE(* *)K
C 100 FORMAT(10X,'ELEMENT' I4 ' HAS TWO IDENTICAL NODE NUMBERS')
IF(NW LE NBW)GO TO 3
INBW=K
NBW=NW
3 CONTINUE
1 CONTINUE
NBW=NBW+1
WRITE(*,*) NBW INBW
C 101 FORMAT(// 5X,'BANDWIDTH IS' I4 ' IN ELEMENT' I4)
RETURN
END
C -----
SUBROUTINE OPTNOD(NSTEP)
C
C *****
C * *
C * SUBROUTINE OPTNOD OPTIMIZES NODE NUMBERING BY PASSING A *
C * SERIES OF HORIZONTAL LINES THROUGH THE *
C * MESH *
C * *
C *****
C
COMMON// LNODE NPOIN NB NEL,NELEM NNODE NUMN JFLAG IFLAG
COMMON/E/ XCORD(501) YCORD(501)
COMMON/PIC/XMIN,XMAX,YMIN YMAX
COMMON/NEW/NORDER(501)
DIMENSION NODX(501) MORDER(501)
C
C INITIALIZE COUNTERS
C
DELT=0.002
YMAX1=YMAX+DELT
YMIN1=YMIN-DELT
NLAST=0
C
C LOOP OVER THE SERIES OF HORIZONTAL LINES
C
STEP=(YMAX1-YMIN1)/FLOAT(NSTEP)
DO 1000 I=1 NSTEP
YDN=STEP*FLOAT(I-1)+YMIN1
YUP=YDN+STEP
C
C LOOP OVER ALL NODES AND LOCATE THOSE WITHIN GIVEN REGION
C
NUM=0
DO 100 IG=1,NB
YPT=YCORD(IG)
C IF(I EQ 1)PRINT * IG YPT
IF(YPT LT YDN OR YPT GE YUP) GO TO 100
NUM=NUM+1
NODX(NUM)=IG
100 CONTINUE
IF(NUM EQ 0) GO TO 1000
C
C SORT THE NUM POINTS INTO ASCENDING ORDER
C
NUM1=NUM+1
DO 300 NSTRT=1, NUM1
XMIN1=XCORD(NODX(NSTRT))
IORDIR=NSTRT
DO 200 J=NSTRT, NUM
JNOD=NODX(J)
YPT=XCORD(JNOD)
IF(YPT GT XMIN1) GO TO 200
XMIN1=YPT
IORDIR=J
200 CONTINUE
N11MP=NODX(IORDIR)

```

```

      NODX(IORDER)=NODX(NSTRT)
      NODX(NSTRT)=NTEMP
300 CONTINUE
C
C   PLACE THIS SWEEP OF NODES INTO LARGE ARRAY
C
      DO 400 J=1 NUM
      NORDER(J+NLAST)=NODX(J)
400 CONTINUE
      NLAST=NLAST+NUM
C   PRINT * NUM NLAST I YDN YUP
1000 CONTINUE
      DO 301 I=1 NB
      DO 201 J=1 NB
      IF(I NE NORDER(J))GO TO 201
      MORDER(I)=J
201 CONTINUE
301 CONTINUE
      DO 302 I=1 NB
      NORDER(I)=MORDER(I)
302 CONTINUE
C
C   PRINT OUT THE ARRAY FOR DEBUGGING
C
      IF(IFLAG EQ 2)THEN
      WRITE(* *)
      DO 1100 I=1 NLAST
      WRITE(* *) I NORDER(I)
1100 CONTINUE
      ENDIF
C 1101 FORMAT(5X,2110)
C 1102 FORMAT(// 5X,'NODE RENUMBERING DEBUG CHECK' //)
      RETURN
      END
C -----
      SUBROUTINE INFIL
      COMMON/ I/ LNODE NPOIN NB NEL,NELEM NNODE NUMN JFLAG IFLAG
      CHARACTER INFIL*12 OUTFIL*12 AJ*1
      DATA INFIL/      / OUTFIL/      / AJ/
      WRITE(* *)
C 105 FORMAT(1X,'IF YOU WANT HARDCOPY OUTPUT PRESS CTL-PRTRSC BEFORE ENT
C   1ERING INPUT FILE NAME)
      WRITE(* (/1X,A))' ENTER INPUT MESH FILE NAME '
      READ(* (BN A))INFIL
      WRITE(* (/1X,A))' ENTER OUTPUT FILE NAME '
      READ(* (BN A))OUTFIL
      WRITE(* (/1X,A))' DO YOU WANT TO OPTIMIZE THE MESH (Y/N)?'
      READ(* (BN A))AJ
      IF(AJ EQ 'N' OR AJ EQ 'n')JFLAG=0
      IF(AJ EQ 'Y' OR AJ EQ 'y')JFLAG=1
      OPEN(5,FILE=INFIL)
C
C   OPEN UNIT 15 FOR OUTPUT
C
      OPEN(15 FILE=OUTFIL,STATUS='NEW')
      WRITE(15 '(A)')OUTFIL
      WRITE(* 104)
104 FORMAT(/ 1X,'PLEASE WAIT GRID IS DEVELOPING' /)
      RETURN
      END

```

APPENDIX VII PROGRAM TO CALCULATE TEMPERATURE DISTRIBUTION IN HYDRODYNAMIC UNIT BY 2 DIMENSIONAL FINITE ELEMENT METHOD

```

COMMON/VA/COLD(601),CNEW(601)
COMMON/VD/AF,AFM,DT,NNQS,NUMN,NUM,NGAUS,NNHC,NNST,NSTOP,KPRNT,IAXI
COMMON/VK/NNODE,NELEM,NTYPE,NTIME,TIME,NFRMAX
C
C  SET UP INITIAL DATA AND BOUNDARY CONDITIONS
C
CALL INIT
CALL GAUSS
KOUNT=0
NTIME=0
TIME=DT
IF(IAXI EQ 0)THEN
CALL MATSET
CALL BNDCON
ELSE
CALL MATAXI
CALL BNDAXI
ENDIF
C
C  STEP THROUGH TIME
C
DO 2 NSTEP=1,NSTOP
CALL ASSEMB
IF(KOUNT EQ KPRNT)THEN
CALL PRINT
KOUNT=0
ENDIF
TIME=TIME+DT
KOUNT=KOUNT+1
NTIME=NTIME+1
CALL RESID
C
C  PUT NEW VALUES INTO OLD ARRAY FOR NEXT TIME STEP
C
DO 3 L=1,NNODE
3 COLD(L)=CNEW(L)
C
2 CONTINUE
WRITE(* 10)
10 FORMAT( 0 ,1X, SOLUTION IS FINISHED )
STOP
END
C
-----
SUBROUTINE INIT
COMMON/VP/P(9901),C(9901),R(9901)
COMMON/VA/COLD(601),CNEW(601)
COMMON/VB/X(601),Y(601),QQ(601)
COMMON/VC/Q(601),F(601),NTS(601),NQS(601),DX(601),DY(601)
COMMON/VEL/VX(601) VY(601)
COMMON/VD/AF,AFM DT,NNQS NUMN,NUM NGAUS NNHC,NNST,NSTOP,KPRNT,IAXI
COMMON/VG/ISI(601),LEM(601),LME(601) ISIH(601)
COMMON/VH/NODES4(4,2),NODES8(4 3) NODES3(3,2) NODES6(3,3)
COMMON/VM/H(601),TINF(601)
COMMON/VK/NNODE NELEM,NTYPE,NTIME,TIME NFRMAX
COMMON/VL/NODE(601,8)
COMMON/SK/NFR(601),JMIN(601) JMAX(601)
COMMON/VT/MTYPE,NUMDIM,TO RHO CP
COMMON/VI/TITLE(18)
CHARACTER*4 STOP(4),WORD
DATA STOP/ DIRC FLUX , CONV VELC /
C
CALL SETPC
C

```

```

    READ(8,100)TITLE
100 FORMAT(18A4)
    WRITE(*,101)TITLE
101 FORMAT( 0 ,5X,18A4)
C
    READ(8 *)MTYPE,NUMDIM NNODE NELEM NUMN NSTOP KPRNT NVEL
    READ(8,*)NTYPE,DT,AF,TO RHO,CP IAXI
    MTYPE=MTYPE+1
    IF(NUMN EQ 3)NGAUS=3
    IF(NUMN EQ 4)NGAUS=4
    IF(NUMN EQ 6)NGAUS=7
    IF(NUMN EQ 8)NGAUS=9
    NUM=2
    IF(NUMN GE 6)NUM=3
    DO 33 I=1,NNODE
    CNEW(I)=0 0
    COLD(I)=TO
    ISI(I)=0
    LEM(I)=0
    LME(I)=0
    ISIH(I)=0
    NTS(I)=0
    NQS(I)=0
    X(I)=0
    Y(I)=0
    QQ(I)=0
    Q(I)=0
    F(I)=0
    H(I)=0
    TINF(I)=0
    DX(I)=0
    DY(I)=0
    VX(I)=0
    VY(I)=0
    DO 34 K=1,NUMN
34 NODE(I,K)=0
33 CONTINUE
C
    READ(8,*)(I,X(I),Y(I),J=1,NNODE)
C
    DO 105 I=1,NELEM
    READ(8,*)J,QQ(J),DX(J),DY(J),(NODE(J,MM) MM=1,NUMN)
    DX(I)=DX(J)/(RHO*CP)
    DY(I)=DY(J)
    QQ(I)=QQ(J)/(RHO*CP)
105 CONTINUE
C
    DO 110 I=1,NNODE
    READ(8 1015)WORD,NT CNT
    IF (WORD EQ STOP(1))GOTO 120
    NTS(I)=NT
    COLD(NTS(I))=CNT
110 CONTINUE
120 NNST=I 1
C
    DO 130 I=1,NNODE
    READ(8,1016)WORD,Q(I) LEM(I) ISI(I)
    IF(WORD EQ STOP(2))GO TO 135
130 CONTINUE
135 NNQS=I-1
C
    DO 140 I=1,NNODE
    READ(8,1017)WORD,H(I),TINF(I) LME(I) ISIH(I)
    IF(WORD EQ STOP(3))GO TO 145
140 CONTINUE
145 NNHC=I 1
C

```

```

DO 146 J=1,NNODE
  READ(8,1018)WORD I VX(I),VY(I)
  IF(WORD EQ STOP(4))GO TO 147
146 CONTINUE
147 CONTINUE
C
  IF(NTYPE EQ 1)WRITE(*,14)NTYPE
  IF(NTYPE EQ 2)WRITE(*,15)NTYPE
  AFM=AF-1 0
  IF(NTYPE EQ 1)GO TO 1
  IF(AF EQ 1 )WRITE(*,10)DT
  IF(AF EQ 0 5)WRITE(*,11)DT
1  WRITE(*,12)NSTOP,KPRNT,TO,IAXI
  WRITE(*,1035)NNODE,NELEM
  WRITE(*,1040)
  WRITE(*,1041)
  DO 150 I=1,NNODE
    WRITE(*,1045)I,X(I),Y(I)
150 CONTINUE
  WRITE(*,1050)
  DO 155 I=1,NELEM
    WRITE(*,1055)I,QQ(I),DX(I),DY(I),(NODE(I MM) MM=1,NUMN)
155 CONTINUE
  WRITE(*,1060)
  WRITE(*,1061)
  DO 160 I=1,NNST
    WRITE(*,1065)I,NTS(I),COLD(NTS(I))
160 CONTINUE
  WRITE(*,1080)
  WRITE(* 1082)
  DO 170 I=1,NNQS
    ISI1=ISI(I)
    IF(NUMN EQ 3 OR NUMN EQ 6)THEN
      IF(NUM EQ 2)WRITE(*,1085)I,Q(I),(NODE(LEM(I),NODES3(ISI1,K)),K=1,N
1UM)
      IF(NUM EQ 3)WRITE(*,1085)I Q(I),(NODE(LEM(I),NODES6(ISI1,K)),K=1,N
1UM)
    ELSE
      IF(NUM EQ 2)WRITE(*,1085)I,Q(I),(NODE(LEM(I) NODES4(ISI1,K)),K=1,N
1UM)
      IF(NUM EQ 3)WRITE(*,1085)I,Q(I),(NODE(LEM(I) NODES8(ISI1,K)),K=1,N
1UM)
    ENDIF
170 CONTINUE
  WRITE(*,1081)
  WRITE(*,1083)
  DO 180 I=1,NNHC
    ISI1=ISIH(I)
    IF(NUMN EQ 3 OR NUMN EQ 6)THEN
      IF(NUM EQ 2)WRITE(*,1086)I,H(I) TINF(I) (NODE(LME(I),NODES3(ISI1,K
1)) K=1,NUM)
      IF(NUM EQ 3)WRITE(* 1086)I H(I) TINF(I) (NODE(LME(I) NODES6(ISI1,K
1)),K=1,NUM)
    ELSE
      IF(NUM EQ 2)WRITE(* 1086)I,H(I) TINF(I) (NODE(LME(I) NODES4(ISI1,K
1)) K=1 NUM)
      IF(NUM EQ 3)WRITE(* 1086)I H(I) TINF(I) (NODE(LME(I) NODES8(ISI1,K
1)) K=1 NUM)
    ENDIF
180 CONTINUE
C
  IF(NVEL EQ 0)GOTO 190
  WRITE(*,4040)
  WRITE(*,4041)
  DO 450 I=1 NNODE
450 WRITE(*,1045)I VX(I) VY(I)
C

```

```

C   CALCULATE BANDWIDTH FOR EACH ROW
C
190 DO 620 I=1,NNODE
    JMIN(I)=NNODE
620 JMAX(I)=1
    DO 630 K=1,NELEM
    DO 630 N=1,NUMN
    DO 630 M=1,NUMN
    I=NODE(K,N)
    J=NODE(K,M)
    IF(J LT JMIN(I))JMIN(I)=J
    IF(J GT JMAX(I))JMAX(I)=J
630 CONTINUE
    NN1=NNODE-1
    DO 635 K=1,NN1
    KP1=K+1
    DO 635 I=KP1,NNODE
    IF(JMAX(I) LT JMAX(K))JMAX(I)=JMAX(K)
635 CONTINUE
C
C   TRANSFORM GLOBAL MATRIX TO A SINGLE INDEX
C
C   NFR(K) INDICATES THE POSITION OF FIRST NONZERO MEMBER IN
C   ROW K OF GLOBAL MATRIX
C
    NFR(1)=JMIN(1)
    DO 700 K=2,NNODE
700 NFR(K)=NFR(K-1)+JMAX(K-1)-JMIN(K-1)+1
    NFRMAX=NFR(NNODE)+JMAX(NNODE)-JMIN(NNODE)
    WRITE(*,29)NFRMAX
    IF(NFRMAX GT 9901)THEN
    WRITE(*,30)
    STOP
    ENDIF
C
    WRITE(*,191)
191 FORMAT(/,5X, PLEASE WAIT SOLUTION IS PROCEEDING )
C
10 FORMAT(/,10X, FULLY IMPLICIT ,2X, DT= F7 4)
11 FORMAT(/,10X, CRANK NICOLSON ,2X, DT= F7 4)
12 FORMAT(/,5X, NSTOP= ,15,2X, KPRNT= ,14,2X, TO= F7 2,2X, AXI= ,14)
14 FORMAT(/,10X, NTYPE= ,12,2X, STEADY STATE CNEW )
15 FORMAT(/,10X, NTYPE= ,12,2X, TIME DEPENDENT CNEW )
29 FORMAT(/,10X, MAXIMUM 1-D ARRAY =',110,/)
30 FORMAT(/,10X, SOLUTION STOPPED MAXIMUM 1 D ARRAY EXCEEDS 9901 )
1015 FORMAT(6X A4,15,5X F10 5)
1016 FORMAT(6X,A4,F10 5,2I5)
1017 FORMAT(6X,A4,2F10 5,2I5)
1018 FORMAT(6X,A4,15,5X,2F10 5)
1035 FORMAT(/,10X, NO OF NODES= ,14,5X, NO OF ELEMENTS= I4)
1040 FORMAT(/,8X, NODAL COORDINATE VALUES )
1041 FORMAT(/,7X I 9X, X 11X Y )
1045 FORMAT(5X,14,2(4X,F8 4))
1050 FORMAT(/,3X, ELEMENT ,3X, SOURCE ,4X DX 6X DY 8X, NODE NUMBE
    IRS )
1055 FORMAT(5X,14,3X,3F8 3,8(1X,I4))
1060 FORMAT(/,7X, NODES WHERE CNEW IS SPECIFIED )
1061 FORMAT(/,8X, I ,5X, NODE ,6X, CNEW )
1065 FORMAT(2X,2(4X,I4),5X,F8 3)
1080 FORMAT(/,15X, NODES WHERE FLUX IS SPECIFIED )
1081 FORMAT(/,15X, NODES WHERE CONV IS SPECIFIED )
1082 FORMAT(/,8X, I 6X, FLUX 5X 'NODE NUMBERS )
1083 FORMAT(/,10X, I ,7X H ,7X, TINF 7X NODE NUMBERS )
1085 FORMAT(6X,14 3X,F8 3,2X,3(1X,I4))
1086 FORMAT(8X,14,2X,2(2X,F8 3),2X,3(1X I4))
4040 FORMAT(/,5X, SUMMARY OF SPECIFIED NODAL VELOCITIES )
4041 FORMAT(/,7X I 12X VX 12X VY )

```

RETURN
END

```
C
-----
SUBROUTINE MATSET
REAL NS NX NY MASS
COMMON/VP/P(9901),C(9901) R(9901)
COMMON/VA/COLD(601),CNEW(601)
COMMON/VB/X(601),Y(601),QQ(601)
COMMON/VC/Q(601),F(601),NTS(601),NQS(601),DX(601),DY(601)
COMMON/VE/NS(8),NX(8),NY(8),NXSI(8),NETA(8)
COMMON/VF/POSG1(9),POSG2(9),W1(9) W2(9)
COMMON/VD/AF AFM,DT,NNQS,NUMN,NUM,NGAUS,NNHC NNST,NSTOP,KPRNT,IAXI
COMMON/VG/ISI(601),LEM(601),LME(601),ISIH(601)
COMMON/VH/NODES4(4,2),NODES8(4,3),NODES3(3,2),NODES6(3,3)
COMMON/VEL/VX(601),VY(601)
COMMON/VM/H(601),TINF(601)
COMMON/VK/NNODE,NELEM,NTYPE NTIME TIME,NFRMAX
COMMON/VL/NODE(601,8)
COMMON/SK/NFR(601),JMIN(601),JMAX(601)

C
CALL CLEAR(R,NFRMAX)
CALL CLEAR(C,NFRMAX)
CALL CLEAR(P NFRMAX)

C
C CONSTRUCT AND STORE MASS MATRIX P
C
DO 1 K=1,NELEM
CALL NODSET(K,I,II,J,JJ,M,MM,N,NN)
DO 1 IQ=1,NGAUS
XSI=POSG1(IQ)
ETA=POSG2(IQ)
CALL SHAPE(K,XSI ETA,I,J,M,N,II JJ,MM NN,DET YETA,XETA,XXSI,YXSI)
DO 1 KK=1 NUMN
L=NODE(K,KK)
F(L)=F(L)+NS(KK)*QQ(K)*DET*W1(IQ)*W2(IQ)
DO 1 KKK=1,NUMN
LL=NODE(K,KKK)
MASS=NS(KKK)*NS(KK)
UPT=NFR(L)+LL-JMIN(L)
1 P(UPT)=P(UPT)+MASS*DET*W1(IQ)*W2(IQ)

C
C CONSTRUCT AND STORE ADVECTION AND DIFFUSION MATRIX C
C
DO 4 K=1,NELEM
CALL NODSET(K,I,II,J,JJ,M,MM,N,NN)
DO 4 IQ=1 NGAUS
XSI=POSG1(IQ)
ETA=POSG2(IQ)
CALL SHAPE(K,XSI,ETA I,J M,N,II JJ MM,NN DET YETA,XETA,XXSI YXSI)
DO 4 KK=1,NUMN
L=NODE(K KK)
DO 4 KKK=1 NUMN
LL=NODE(K KKK)

C
C ADVECTION TERM
C
VELX=VX(L)*NS(KK)*NX(KKK)
VELY=VY(L)*NS(KK)*NY(KKK)
ADVEC=VELX+VELY

C
C DIFFUSION TERM
C
DIFFX=DX(K)*NX(KKK)*NX(KK)
DIFFY=DY(K)*NY(KKK)*NY(KK)
DIFF=DIFFX+DIFFY

C
UPT=NFR(L)+LL JMIN(L)
```

```

4 C(UPT)=C(UPT)+(DIFF+ADVEC)*DET*W1(IQ)*W2(IQ)
C
C CONVECTIVE HEAT FLUX INFLUENCE
C
IF(NNHC EQ 0)GO TO 6
DO 5 K=1,NNHC
NEL=LME(K)
CALL NODSET(NEL,I,II,J,JJ,M,MM,N,NN)
IS11=ISIH(K)
DO 5 IW=1,2
CALL BCSIDE(NEL,IS11,IW,SIDE,COSLX,COSLY,I,II,J,JJ,M,MM,N,NN)
DO 5 JJ=1,NUM
IF(NUMN EQ 3 OR NUMN EQ 6)THEN
IF(NUM EQ 2)KN=NODES3(IS11,JJ)
IF(NUM EQ 3)KN=NODES6(IS11,JJ)
ELSE
IF(NUM EQ 2)KN=NODES4(IS11,JJ)
IF(NUM EQ 3)KN=NODES8(IS11,JJ)
ENDIF
L=NODE(NEL,KN)
DO 5 JJJ=1,NUM
IF(NUMN EQ 3 OR NUMN EQ 6)THEN
IF(NUM EQ 2)KK=NODES3(IS11,JJJ)
IF(NUM EQ 3)KK=NODES6(IS11,JJJ)
ELSE
IF(NUM EQ 2)KK=NODES4(IS11,JJJ)
IF(NUM EQ 3)KK=NODES8(IS11,JJJ)
ENDIF
LL=NODE(NEL,KK)
MASS=NS(KN)*NS(KK)
UPT=NFR(L)+LL-JMIN(L)
5 C(UPT)=C(UPT)+MASS*H(K)*SIDE
6 CONTINUE
C
C FORM LHS
C
DO 7 I=1,NFRMAX
7 R(I)=AF*C(I)+P(I)/DT
C
RETURN
END
C -----
SUBROUTINE ASSEMB
COMMON/VP/P(9901),C(9901),R(9901)
COMMON/VA/COLD(601),CNEW(601)
COMMON/VK/NNODE NELEM,NTYPE NTIME TIME NFRMAX
COMMON/VQ/Q(601),F(601),NTS(601),NQS(601),DX(601),DY(601)
COMMON/VD/AF,AFM,DT,NNQS NUMN,NUM NGAUS NNHC NNST,NSTOP,KPRNT,IAXI
COMMON/SK/NFR(601),JMIN(601),JMAX(601)
DIMENSION B(601),FIXED(601)
C
CALL CLEAR(B NNODE)
C
C CONSTRUCT RHS
C
DO 4 L=1 NNODE
B(L)=F(L)
JSTR=JMIN(L)
JEND=JMAX(L)
DO 4 II=JSTR JEND
NGI=NFR(L)+II-JSTR
RHS=(AFM*C(NGI)+P(NGI)/DT)*COLD(II)
4 B(L)=B(L)+RHS
C
DO 5 I=1,NNST
5 FIXED(I)=COLD(NTS(I))
C

```

```

CALL SKYLIN(B,CNEW,NTS,FIXED,NNST)
C
RETURN
END
C
-----
SUBROUTINE MATAXI
REAL NS,NX,NY,MASS
COMMON/VP/P(9901),C(9901),R(9901)
COMMON/VA/COLD(601),CNEW(601)
COMMON/VB/X(601),Y(601),QQ(601)
COMMON/VC/Q(601),F(601),NTS(601),NQS(601) DX(601),DY(601)
COMMON/VE/NS(8),NX(8),NY(8),NXSI(8),NETA(8)
COMMON/VF/POSG1(9),POSG2(9),W1(9),W2(9)
COMMON/VD/AF,AFM,DT,NNQS,NUMN,NUM NGAUS,NNHC,NNST,NSTOP,KPRNT,IAXI
COMMON/VG/ISI(601),LEM(601),LME(601),ISIH(601)
COMMON/VH/NODES4(4 2),NODES8(4,3),NODES3(3 2) NODES6(3,3)
COMMON/VEL/VX(601),VY(601)
COMMON/VM/H(601) TINF(601)
COMMON/VK/NNODE,NELEM,NTYPE,NTIME,TIME NFRMAX
COMMON/VL/NODE(601,8)
COMMON/SK/NFR(601),JMIN(601),JMAX(601)
C
CALL CLEAR(R,NFRMAX)
CALL CLEAR(C,NFRMAX)
CALL CLEAR(P,NFRMAX)
C
C CONSTRUCT AND STORE MASS MATRIX P
C
DO 1 K=1,NELEM
CALL NODSET(K,I,II,J,II,M,MM,N,NN)
DO 1 IQ=1,NGAUS
XSI=POSG1(IQ)
ETA=POSG2(IQ)
CALL SHAPE(K,XSI,ETA,I,J,M,N,II,JJ,MM,NN DET YETA,XETA XXSI,YXSI)
SUM=0
DO 2 KKKK=1,NUMN
LR=NODE(K,KKKK)
2 SUM=SUM+NS(KKKK)*Y(LR)
DO 1 KK=1,NUMN
L=NODE(K,KK)
F(L)=F(L)+NS(KK)*QQ(K)*SUM*DET*W1(IQ)*W2(IQ)
DO 1 KKK=1,NUMN
LL=NODE(K,KKK)
MASS=NS(KKK)*NS(KK)
UPT=NFR(L)+LL JMIN(L)
1 P(UPT)=P(UPT)+MASS*SUM*DET*W1(IQ)*W2(IQ)
C
C CONSTRUCT AND STORE ADVECTION AND DIFFUSION MATRIX C
C
DO 4 K=1,NELEM
CALL NODSET(K,I,II,J,II,M,MM,N,NN)
DO 4 IQ=1,NGAUS
XSI=POSG1(IQ)
ETA=POSG2(IQ)
CALL SHAPE(K,XSI,ETA,I,J,M,N,II,JJ,MM,NN DET,YETA XETA XXSI,YXSI)
SUM=0
DO 9 KKKK=1,NUMN
LR=NODE(K,KKKK)
9 SUM=SUM+NS(KKKK)*Y(LR)
DO 4 KK=1,NUMN
L=NODE(K,KK)
DO 4 KKK=1,NUMN
LL=NODE(K,KKK)
C
C ADVECTION TERM
C
VELX=VX(L)*NS(KK)*NX(KKK)

```

```

VELY=VY(L)*NS(KK)*NY(KKK)
ADVEC=VELX+VELY
C
C DIFFUSION TERM
C
DIFFX=DX(K)*NX(KKK)*NX(KK)
DIFFY=DY(K)*NY(KKK)*NY(KK)
DIFF=DIFFX+DIFFY
C
UPT=NFR(L)+LL-JMIN(L)
4 C(UPT)=C(UPT)+(DIFF+ADVEC)*SUM*DET*W1(IQ)*W2(IQ)
C
C CONVECTIVE HEAT FLUX INFLUENCE
C
IF(NNHC EQ 0)GO TO 6
DO 5 K=1,NNHC
NEL=LME(K)
CALL NODSET(NEL I,II,J,II,M,MM,N,NN)
ISI1=ISIH(K)
DO 5 IW=1,2
CALL BCSIDE(NEL,ISI1,IW,SIDE COSLX,COSLY,I,II,J,II,M,MM,N,NN)
SUM=0
DO 8 JR=1,NUM
IF(NUMN EQ 3 OR NUMN EQ 6)THEN
IF(NUM EQ 2)KR=NODES3(ISI1,JR)
IF(NUM EQ 3)KR=NODES6(ISI1,JR)
ELSE
IF(NUM EQ 2)KR=NODES4(ISI1 JR)
IF(NUM EQ 3)KR=NODES8(ISI1,JR)
ENDIF
LR=NODE(NEL,KR)
8 SUM=SUM+Y(LR)*NS(KR)
DO 5 JJ=1,NUM
IF(NUMN EQ 3 OR NUMN EQ 6)THEN
IF(NUM EQ 2)KN=NODES3(ISI1,II)
IF(NUM EQ 3)KN=NODES6(ISI1,II)
ELSE
IF(NUM EQ 2)KN=NODES4(ISI1,II)
IF(NUM EQ 3)KN=NODES8(ISI1,II)
ENDIF
L=NODE(NEL,KN)
DO 5 JJJ=1,NUM
IF(NUMN EQ 3 OR NUMN EQ 6)THEN
IF(NUM EQ 2)KK=NODES3(ISI1,III)
IF(NUM EQ 3)KK=NODES6(ISI1,III)
ELSE
IF(NUM EQ 2)KK=NODES4(ISI1,III)
IF(NUM EQ 3)KK=NODES8(ISI1,III)
ENDIF
LL=NODE(NEL,KK)
MASS=NS(KN)*NS(KK)
UPT=NFR(L)+LL-JMIN(L)
5 C(UPT)=C(UPT)+MASS*SUM*H(K)*SIDE
6 CONTINUE
C
C FORM LHS
C
DO 7 I=1 NFRMAX
7 R(I)=AF*C(I)+P(I)/DT
C
RETURN
END
C -----
BLOCK DATA
COMMON/VH/NODES4(4 2),NODES8(4 3) NODES3(3 2) NODES6(3 3)
COMMON/VI/POSG(2) POST(2) WQ(2) WT(2)
COMMON/XY/X4(4) Y4(4) X8(8) Y8(8)

```

```

DATA POSG/0 57735027,-0 57735027/
DATA POST/0 7886751,0 1013249/
DATA WQ/1 0,1 0/
DATA WT/0 5,0 5/
DATA NODES3/3,2,1,1,3,2/
DATA NODES6/5 3 1,6,4,2 1 5 3/
DATA NODES4/4 3,2 1,1 4 3,2/
DATA NODES8/7,5,3,1,8,6,4,2,1,7,5,3/
DATA X4/-1 0,1 0,1 0 -1 0/
DATA Y4/-1 0,-1 0,1 0,1 0/
DATA X8/ 1 0,0 0,1 0,1 0,1 0,0 0,-1 0,-1 0/
DATA Y8/-1 0,-1 0,-1 0,0 0,1 0,1 0,1 0,0 0/
END

```

C

```

SUBROUTINE BNDCON
REAL NS,NX,NY
COMMON/VK/NNODE,NELEM,NTYPE,NTIME,TIME,NFRMAX
COMMON/VC/Q(601),F(601),NTS(601),NQS(601) DX(601),DY(601)
COMMON/VL/NODE(601,8)
COMMON/VD/AF,AFM,DT,NNQS,NUMN,NUM,NGAUS,NNHC,NNST,NSTOP,KPRNT IAXI
COMMON/VE/NS(8),NX(8),NY(8),NXSI(8),NETA(8)
COMMON/VG/ISI(601),LEM(601),LME(601),ISIH(601)
COMMON/VM/H(601),TINF(601)
COMMON/VH/NODES4(4,2),NODES8(4 3) NODES3(3,2) NODES6(3,3)

```

C

C IW=1,2 DENOTES TWO GAUSS POINTS PER SIDE USING GAUSS QUADRATURE

C

```

10 IF(NNQS EQ 0)GO TO 35
DO 3 K=1,NNQS
NEL=LEM(K)
CALL NODSET(NEL,I,II,J,MM,N,NN)
ISII=ISI(K)
DO 3 IW=1,2
CALL BCSIDE(NEL,ISII,IW,SIDE,COSLX,COSLY I,II J,MM,N,NN)
DO 3 L=1,NUM
IF(NUMN EQ 3 OR NUMN EQ 6)THEN
IF(NUM EQ 2)KK=NODES3(ISII,L)
IF(NUM EQ 3)KK=NODES6(ISII,L)
ELSE
IF(NUM EQ 2)KK=NODES4(ISII,L)
IF(NUM EQ 3)KK=NODES8(ISII,L)
ENDIF
KKK=NODE(NEL,KK)
3 F(KKK)=F(KKK)+NS(KK)*SIDE*Q(K)

```

C

```

35 IF(NNHC EQ 0)RETURN
DO 9 K=1,NNHC
NEL=LME(K)
CALL NODSET(NEL,I,II,J,MM,N,NN)
ISII=ISIH(K)
DO 9 IW=1,2
CALL BCSIDE(NEL,ISII,IW,SIDE,COSLX,COSLY I,II J,MM,N,NN)
DO 9 L=1,NUM
IF(NUMN EQ 3 OR NUMN EQ 6)THEN
IF(NUM EQ 2)KK=NODES3(ISII,L)
IF(NUM EQ 3)KK=NODES6(ISII,L)
ELSE
IF(NUM EQ 2)KK=NODES4(ISII,L)
IF(NUM EQ 3)KK=NODES8(ISII,L)
ENDIF
LL=NODE(NEL,KK)
9 F(LL)=F(LL)+NS(KK)*SIDE*H(K)*TINF(K)
RETURN
END

```

C

```

SUBROUTINE BNDAXI
REAL NS NX NY

```

```

COMMON/VK/NNODE,NELEM,NTYPE NTIME,TIME,NFRMAX
COMMON/VC/Q(601) F(601) NTS(601) NQS(601) DX(601) DY(601)
COMMON/VB/X(601),Y(601),QQ(601)
COMMON/VL/NODE(601,8)
COMMON/VD/AF,AFM,DT,NNQS,NUMN,NUM NGAUS NNHC NNST NSTOP KPRNT,IAXI
COMMON/VE/NS(8),NX(8),NY(8),NXSI(8),NETA(8)
COMMON/VG/ISI(601),LEM(601),LME(601),ISIH(601)
COMMON/VM/H(601),TINF(601)
COMMON/VH/NODES4(4,2),NODES8(4,3),NODES3(3,2),NODES6(3 3)
C
C   IW=1 2 DENOTES TWO GAUSS POINTS PER SIDE USING GAUSS QUADRATURE
C
10 IF(NNQS EQ 0)GO TO 35
   DO 3 K=1,NNQS
     NEL=LEM(K)
     CALL NODSET(NEL,I,II,J,J,M,MM,N,NN)
     ISII=ISI(K)
     DO 3 IW=1,2
       CALL BCSIDE(NEL,ISII,IW,SIDE,COSLX,COSLY,I,II,J,J,M,MM,N NN)
       SUM=0
       DO 8 JR=1,NUM
         IF(NUMN EQ 3 OR NUMN EQ 6)THEN
           IF(NUM EQ 2)KR=NODES3(ISII,JR)
           IF(NUM EQ 3)KR=NODES6(ISII,JR)
         ELSE
           IF(NUM EQ 2)KR=NODES4(ISII,JR)
           IF(NUM EQ 3)KR=NODES8(ISII,JR)
         ENDIF
         LR=NODE(NEL,KR)
       8 SUM=SUM+Y(LR)*NS(KR)
       DO 3 L=1,NUM
         IF(NUMN EQ 3 OR NUMN EQ 6)THEN
           IF(NUM EQ 2)KK=NODES3(ISII,L)
           IF(NUM EQ 3)KK=NODES6(ISII,L)
         ELSE
           IF(NUM EQ 2)KK=NODES4(ISII,L)
           IF(NUM EQ 3)KK=NODES8(ISII,L)
         ENDIF
         KKK=NODE(NEL,KK)
       3 F(KKK)=F(KKK)+NS(KK)*SIDE*Q(K)*SUM
C
35 IF(NNHC EQ 0)RETURN
   DO 9 K=1,NNHC
     NEL=LME(K)
     CALL NODSET(NEL,I,II,J,J,M,MM,N,NN)
     ISII=ISIH(K)
     DO 9 IW=1,2
       CALL BCSIDE(NEL,ISII,IW,SIDE,COSLX,COSLY,I,II,J,J,M,MM,N NN)
       SUM=0
       DO 7 JR=1,NUM
         IF(NUMN EQ 3 OR NUMN EQ 6)THEN
           IF(NUM EQ 2)KR=NODES3(ISII,JR)
           IF(NUM EQ 3)KR=NODES6(ISII,JR)
         ELSE
           IF(NUM EQ 2)KR=NODES4(ISII,JR)
           IF(NUM EQ 3)KR=NODES8(ISII,JR)
         ENDIF
         LR=NODE(NEL,KR)
       7 SUM=SUM+Y(LR)*NS(KR)
       DO 9 L=1 NUM
         IF(NUMN EQ 3 OR NUMN EQ 6)THEN
           IF(NUM EQ 2)KK=NODES3(ISII,L)
           IF(NUM EQ 3)KK=NODES6(ISII L)
         ELSE
           IF(NUM EQ 2)KK=NODES4(ISII,L)
           IF(NUM EQ 3)KK=NODES8(ISII L)
         ENDIF

```

```

LL=NODE(NEL, KK)
9 F(LL)=F(LL)+NS(KK)*SIDE*H(K)*TINF(K)*SUM
RETURN
END
C
-----
SUBROUTINE CLEAR(A N)
DIMENSION A(N)
DO 1 I=1, N
1 A(I)=0
RETURN
END
C
-----
SUBROUTINE BCSIDE(K, IS11, IW, SIDE, COSLX, COSLY, I, II, J, JJ, M, MM, N, NN)
COMMON/VD/AF, AFM, DT, NNQS, NUMN, NUM, NGAUS, NNHC, NNST, NSTOP, KPRNT, IAXI
COMMON/VI/POSG(2), POST(2), WQ(2), WT(2)
IF(NUMN EQ 3 OR NUMN EQ 6)GOTO 1
IF(NUMN EQ 4 OR NUMN EQ 8)GOTO 9
C
C 3 OR 6 NODE TRIANGLES
C
1 GO TO (2,3,4), IS11
C
C SIDE 1
C
2 XSI= 0
ETA=POST(IW)
CALL SHAPE(K, XSI, ETA, I, J, M, N, II, JJ, MM, NN, DET, YETA, XETA, XXSI, YXSI)
R=-YETA
S=XETA
GO TO 49
C
C SIDE 2
C
3 XSI=POST(IW)
ETA= 1 -XSI
CALL SHAPE(K, XSI, ETA, I, J, M, N, II, JJ, MM, NN, DET, YETA, XETA, XXSI, YXSI)
R=-YXSI
S=XXSI
GO TO 49
C
C SIDE 3
C
4 XSI=POST(IW)
ETA= 0
CALL SHAPE(K, XSI, ETA, I, J, M, N, II, JJ, MM, NN, DET, YETA, XETA, XXSI, YXSI)
R=YXSI
S= XXSI
49 SIDEL=SQRT(R*R+S*S)
COSLX=R/SIDEL
COSLY=S/SIDEL
SIDE=SIDEL*WT(IW)
RETURN
C
C 4 OR 8 NODE QUADRILATERALS
C
9 GO TO (10 20 30 40) IS11
C
C SIDE 1
C
10 XSI=-1
ETA=POSG(IW)
CALL SHAPE(K, XSI, ETA, I, J, M, N, II, JJ, MM, NN, DET, YETA, XETA, XXSI, YXSI)
R=-YETA
S=XETA
GO TO 50
C
C SIDE 2

```

```

C
20 XSI=POSG(TW)
   ETA=1
   CALL SHAPE(K,XSI,ETA,I,J,M,N,II,JJ,MM,NN,DET,YETA,XETA,XXSI,YXSI)
   R=YXSI
   S=XXSI
   GO TO 50
C
C   SIDE 3
C
30 XSI=1
   ETA=POSG(TW)
   CALL SHAPE(K,XSI,ETA,I,J,M,N,II,JJ,MM,NN,DET,YETA,XETA,XXSI,YXSI)
   R=YETA
   S=-XETA
   GO TO 50
C
C   SIDE 4
C
40 XSI=POSG(TW)
   ETA=-1
   CALL SHAPE(K,XSI,ETA,I,J,M,N,II,JJ,MM,NN,DET,YETA,XETA,XXSI,YXSI)
   R=YXSI
   S=-XXSI
C
50 SIDEL=SQRT(R*R+S*S)
   COSLX=R/SIDEL
   COSLY=S/SIDEL
   SIDE=SIDEL*WQ(TW)
   RETURN
   END
C
-----
SUBROUTINE NODSET(K,I,II,J,JJ,M,MM,N,NN)
COMMON/VL/NODE(601,8)
COMMON/VD/AF,AFM,DT,NNQS,NUMN,NUM,NGAUS,NNHC,NNST,NSTOP,KPRNT,IAXI
IF(NUMN EQ 3)GO TO 1
IF(NUMN EQ 4)GO TO 2
IF(NUMN EQ 6)GO TO 3
IF(NUMN EQ 8)GO TO 4
C
C   3 NODE LINEAR TRIANGULAR ELEMENT
C
1 I=NODE(K,1)
  J=NODE(K,2)
  M=NODE(K,3)
  RETURN
C
C   4-NODE LINEAR QUADRILATERAL ELEMENT
C
2 I=NODE(K,1)
  J=NODE(K,2)
  M=NODE(K,3)
  N=NODE(K,4)
  RETURN
C
C   6 NODE QUADRATIC TRIANGULAR ELEMENT
C
3 I=NODE(K,1)
  II=NODE(K,2)
  J=NODE(K,3)
  JJ=NODE(K,4)
  M=NODE(K,5)
  MM=NODE(K,6)
  RETURN
C
C   8 NODE QUADRATIC QUADRILATERAL ELEMENT
C

```

```

4 I=NODE(K,1)
  II=NODE(K,2)
  J=NODE(K,3)
  JJ=NODE(K,4)
  M=NODE(K,5)
  MM=NODE(K,6)
  N=NODE(K,7)
  NN=NODE(K,8)
  RETURN
  END

```

```

C -----
C SUBROUTINE SHAPE(K,XSI,ETA,I,J,M,N,II,JJ,MM,NN,DET,YETA,XETA,
  1XXSI,YXSI)
  REAL NS,NX,NY,NXSI,NETA
  COMMON/VB/X(601),Y(601),QQ(601)
  COMMON/VL/NODE(601,8)
  COMMON/VD/AF,AFM,DT,NNQS,NUMN,NUM,NGAUS,NNHC,NNST,NSTOP,KPRNT,IAXI
  COMMON/VE/NS(8),NX(8),NY(8),NXSI(8),NETA(8)
  COMMON/XY/X4(4),Y4(4),X8(8),Y8(8)
  D=0.25
  E=0.5
  IF(NUMN EQ 3)GO TO 10
  IF(NUMN EQ 4)GO TO 11
  IF(NUMN EQ 6)GO TO 12
  IF(NUMN EQ 8)GO TO 13

```

```

C
C 3-NODE LINEAR TRIANGULAR ELEMENT

```

```

C
10 NS(1)=1-XSI-ETA
  NS(2)=XSI
  NS(3)=ETA

```

```

C
  NXSI(1)=-1
  NXSI(2)= 1
  NXSI(3)= 0

```

```

C
  NETA(1)=-1
  NETA(2)= 0
  NETA(3)= 1

```

```

C
  XXSI=NXSI(1)*X(I)+NXSI(2)*X(J)+NXSI(3)*X(M)
  XETA=NETA(1)*X(I)+NETA(2)*X(J)+NETA(3)*X(M)
  YXSI=NXSI(1)*Y(I)+NXSI(2)*Y(J)+NXSI(3)*Y(M)
  YETA=NETA(1)*Y(I)+NETA(2)*Y(J)+NETA(3)*Y(M)
  GO TO 7

```

```

C
C 4 NODE LINEAR QUADRILATERAL ELEMENT

```

```

C
11 DO 2 L=1,NUMN
  2 NS(L)=D*(1+XSI*X4(L))*(1+ETA*Y4(L))

```

```

C
  NXSI(1)= D*(1-ETA)
  NXSI(2)= D*(1-ETA)
  NXSI(3)= D*(1+ETA)
  NXSI(4)= D*(1+ETA)

```

```

C
  NETA(1)= D*(1-XSI)
  NETA(2)=-D*(1+XSI)
  NETA(3)= D*(1+XSI)
  NETA(4)= D*(1-XSI)

```

```

C
  XXSI=NXSI(1)*X(I)+NXSI(2)*X(J)+NXSI(3)*X(M)+NXSI(4)*X(N)
  XETA=NETA(1)*X(I)+NETA(2)*X(J)+NETA(3)*X(M)+NETA(4)*X(N)
  YXSI=NXSI(1)*Y(I)+NXSI(2)*Y(J)+NXSI(3)*Y(M)+NXSI(4)*Y(N)
  YETA=NETA(1)*Y(I)+NETA(2)*Y(J)+NETA(3)*Y(M)+NETA(4)*Y(N)
  GO TO 7

```

```

C

```

C 6 NODE QUADRATIC TRIANGULAR ELEMENT

C
 12 NS(1)=(1 -XSI ETA)*(1 -2 *XSI-2 *ETA)
 NS(2)=4 *XSI*(1 XSI ETA)
 NS(3)=XSI*(2 *XSI-1)
 NS(4)=4 *XSI*ETA
 NS(5)=ETA*(2 *ETA-1)
 NS(6)=4 *ETA*(1 -XSI ETA)

C
 NXSI(1)=4 *XSI+4 *ETA-3
 NXSI(2)=4 -8 *XSI-4 *ETA
 NXSI(3)=4 *XSI 1
 NXSI(4)=4 *ETA
 NXSI(5)=0
 NXSI(6)=-4 *ETA

C
 NETA(1)=4 *ETA+4 *XSI-3
 NETA(2)=-4 *XSI
 NETA(3)=0
 NETA(4)=4 *XSI
 NETA(5)=4 *ETA-1
 NETA(6)=4 -4 *XSI 8 *ETA

C
 XXSI=NXSI(1)*X(I)+NXSI(2)*X(II)+NXSI(3)*X(J)+NXSI(4)*X(JJ)+NXSI(5)
 I*X(M)+NXSI(6)*X(MM)
 XETA=NETA(1)*X(I)+NETA(2)*X(II)+NETA(3)*X(J)+NETA(4)*X(JJ)+NETA(5)
 I*X(M)+NETA(6)*X(MM)
 YXSI=NXSI(1)*Y(I)+NXSI(2)*Y(II)+NXSI(3)*Y(J)+NXSI(4)*Y(JJ)+NXSI(5)
 I*Y(M)+NXSI(6)*Y(MM)
 YETA=NETA(1)*Y(I)+NETA(2)*Y(II)+NETA(3)*Y(J)+NETA(4)*Y(JJ)+NETA(5)
 I*Y(M)+NETA(6)*Y(MM)
 GOTO 7

C
 C 8 NODE QUADRATIC QUADRILATERAL ELEMENT

C
 13 DO 5 L=1,NUMN,2
 5 NS(L)=D*(1 +XSI*X8(L))*(1 +ETA*Y8(L))*(X8(L)*XSI+Y8(L)*ETA-1)
 DO 6 L=2,NUMN 2
 6 NS(L)=E*X8(L)*X8(L)*(1 +X8(L)*XSI)*(1 -ETA*ETA)+E*Y8(L)*Y8(L)*(1 +
 1Y8(L)*ETA)*(1 XSI*XSI)

C
 NXSI(1)=D*(ETA+2*XSI 2*XSI*ETA-ETA*ETA)
 NXSI(2)=-XSI+XSI*ETA
 NXSI(3)=D*(ETA+2*XSI-2*XSI*ETA+ETA*ETA)
 NXSI(4)=E*(1 -ETA*ETA)
 NXSI(5)=D*(ETA+2*XSI+2*XSI*ETA+ETA*ETA)
 NXSI(6)= XSI XSI*ETA
 NXSI(7)=D*(ETA+2*XSI+2*XSI*ETA-ETA*ETA)
 NXSI(8)=E*(-1 +ETA*ETA)

C
 NETA(1)=D*(XSI+2*ETA 2*XSI*ETA XSI*XSI)
 NETA(2)=E*(1 +XSI*XSI)
 NETA(3)=D*(XSI+2*ETA XSI*XSI+2*XSI*ETA)
 NETA(4)= ETA XSI*ETA
 NETA(5)=D*(XSI+2*ETA+XSI*XSI+2*XSI*ETA)
 NETA(6)=E*(1 XSI*XSI)
 NETA(7)=D*(-XSI+2*ETA+XSI*XSI 2*XSI*ETA)
 NETA(8)= ETA+XSI*ETA

C
 XXSI=NXSI(1)*X(I)+NXSI(2)*X(II)+NXSI(3)*X(J)+NXSI(4)*X(JJ)+NXSI(5)
 I*X(M)+NXSI(6)*X(MM)+NXSI(7)*X(N)+NXSI(8)*X(NN)
 XETA=NETA(1)*X(I)+NETA(2)*X(II)+NETA(3)*X(J)+NETA(4)*X(JJ)+NETA(5)
 I*X(M)+NETA(6)*X(MM)+NETA(7)*X(N)+NETA(8)*X(NN)
 YXSI=NXSI(1)*Y(I)+NXSI(2)*Y(II)+NXSI(3)*Y(J)+NXSI(4)*Y(JJ)+NXSI(5)
 I*Y(M)+NXSI(6)*Y(MM)+NXSI(7)*Y(N)+NXSI(8)*Y(NN)
 YETA=NETA(1)*Y(I)+NETA(2)*Y(II)+NETA(3)*Y(J)+NETA(4)*Y(JJ)+NETA(5)
 I*Y(M)+NETA(6)*Y(MM)+NETA(7)*Y(N)+NETA(8)*Y(NN)

```

C
7 CONTINUE
  DET=XXSI*YETA YXSI*XETA
  IF(DET EQ 0 0)THEN
    WRITE(*,100)K
100 FORMAT(2X, THE DETERMINANT = 0 0 IN ELEMENT ,I4)
  STOP
  ENDIF
  XSIX = YETA/DET
  XSIY = -XETA/DET
  ETAX = -YXSI/DET
  ETAY = XXSI/DET
  DO 8 KKK=1,NUMN
    NX(KKK)=NXSI(KKK)*XSIX + NETA(KKK)*ETAX
    NY(KKK)=NXSI(KKK)*XSIY + NETA(KKK)*ETAY
8 CONTINUE
  RETURN
  END
C -----
SUBROUTINE GAUSS
COMMON/VD/AF,AFM,DT,NNQS,NUMN,NUM NGAUS NNHC,NNST,NSTOP,KPRNT,IAXI
COMMON/VF/POSG1(9),POSG2(9) W1(9),W2(9)
IF(NUMN EQ 3)GOTO 1
IF(NUMN EQ 4)GOTO 2
IF(NUMN EQ 6)GOTO 3
IF(NUMN EQ 8)GOTO 4
C
C 3 NODE LINEAR TRIANGLE (3 GAUSS POINTS)
C
1 W=0 5
  POSG1(1)=W
  POSG1(2)=W
  POSG1(3)=0
C
  POSG2(1)=0
  POSG2(2)=W
  POSG2(3)=W
C
  W1(1)=1 0/6
  W1(2)=1 0/6
  W1(3)=1 0/6
C
  W2(1)=1 0
  W2(2)=1 0
  W2(3)=1 0
  RETURN
C
C 4 NODE LINEAR QUADRILATERAL (4 GAUSS POINTS)
C
2 W=SQRT(1 0/3 0)
  POSG1(1)= W
  POSG1(2)=W
  POSG1(3)=W
  POSG1(4)= W
C
  POSG2(1)=-W
  POSG2(2)= W
  POSG2(3)=W
  POSG2(4)=W
C
  W1(1)=1 0
  W1(2)=1 0
  W1(3)=1 0
  W1(4)=1 0
C
  W2(1)=1 0
  W2(2)=1 0

```

```
W2(3)=1 0
W2(4)=1 0
RETURN
```

```
C
C 6 NODE QUADRATIC TRIANGLE (7 GAUSS POINTS)
```

```
C
3 POSG1(1)=0
  POSG1(2)=1 /2
  POSG1(3)=1
  POSG1(4)=1 /2
  POSG1(5)=0
  POSG1(6)=0
  POSG1(7)=1 /3
```

```
C
  POSG2(1)=0
  POSG2(2)=0
  POSG2(3)=0
  POSG2(4)=1 /2
  POSG2(5)=1
  POSG2(6)=1 /2
  POSG2(7)=1 /3
```

```
C
  W1(1)=1 /40
  W1(2)=1 /15
  W1(3)=1 /40
  W1(4)=1 /15
  W1(5)=1 /40
  W1(6)=1 /15
  W1(7)=9 /40
```

```
C
  W2(1)=1 0
  W2(2)=1 0
  W2(3)=1 0
  W2(4)=1 0
  W2(5)=1 0
  W2(6)=1 0
  W2(7)=1 0
RETURN
```

```
C
C 8 NODE QUADRATIC QUADRILATERAL (9 GAUSS POINTS)
```

```
C
4 W=SQRT(0.60)
  POSG1(1)=-W
  POSG1(2)=0
  POSG1(3)=W
  POSG1(4)=W
  POSG1(5)=W
  POSG1(6)=0
  POSG1(7)=-W
  POSG1(8)=-W
  POSG1(9)=0
```

```
C
  POSG2(1)=-W
  POSG2(2)=-W
  POSG2(3)=-W
  POSG2(4)=0
  POSG2(5)=W
  POSG2(6)=W
  POSG2(7)=W
  POSG2(8)=0
  POSG2(9)=0
```

```
C
  W1(1)=5 0/9 0
  W1(2)=8 0/9 0
  W1(3)=5 0/9 0
  W1(4)=5 0/9 0
  W1(5)=5 0/9 0
```

```
W1(6)=8 0/9 0
W1(7)=5 0/9 0
W1(8)=5 0/9 0
W1(9)=8 0/9 0
```

C

```
W2(1)=5 0/9 0
W2(2)=5 0/9 0
W2(3)=5 0/9 0
W2(4)=8 0/9 0
W2(5)=5 0/9 0
W2(6)=5 0/9 0
W2(7)=5 0/9 0
W2(8)=8 0/9 0
W2(9)=8 0/9 0
RETURN
END
```

C

```
-----
SUBROUTINE PRINT
COMMON/VA/COLD(601),CNEW(601)
COMMON/VK/NNODE,NELEM,NTYPE,NTIME,TIME,NFRMAX
COMMON/VEL/VX(601),VY(601)
IF(NTYPE EQ 1)THEN
WRITE(*,403)
ELSE
WRITE(*,402)NTIME,TIME
ENDIF
WRITE(*,400)
DO 1 I=1,NNODE
1 WRITE(*,100)I,CNEW(I),VX(I),VY(I)
100 FORMAT(5X,I3,5X,3(F8 3))
402 FORMAT(/,5X, TIME STEPS= ,I3,2X TIME= ,F8 3)
403 FORMAT(/,5X, STEADY STATE')
400 FORMAT(/,5X, NODE ,5X, CNEW ,8X,'VX ,6X, VY )
RETURN
END
```

C

```
-----
SUBROUTINE RESID
COMMON/VD/AF,AFM,DT,NNQS,NUMN,NUM,NGAUS NNHC,NNST,NSTOP KPRNT IAXI
COMMON/VK/NNODE NELEM,NTYPE NTIME,TIME,NFRMAX
COMMON/VA/COLD(601),CNEW(601)
INTEGER ERRPRN
DATA ERRPRN/5/
```

C

```
LOCE=0
RESMAX=0
ERR=0 0001
```

C

```
DO 1 I=1,NNODE
R=ABS(CNEW(I) COLD(I))
IF(R GT RESMAX)THEN
RESMAX=R
LOCE=1
ENDIF
1 CONTINUE
```

C

```
IF(RESMAX GT ERR)THEN
IF(NTIME GE NSTOP)THEN
WRITE(* 101)NTIME RESMAX
CALL PRINT
CALL PRINTF
STOP
END IF
IF(MOD(NTIME ERRPRN) EQ 0)THEN
WRITE(* 102)NTIME RESMAX LOCE
ENDIF
RETURN
ELSE
```

```

WRITE(*,100)NTIME
CALL PRINT
CALL PRINTF
STOP
END IF
100 FORMAT(/ 2X, PROGRAM HAS CONVERGED IN I3 STEPS )
102 FORMAT(/ 2X, TIME STEP = ,I4 RESIDUAL = 1PE10 3,2X, NODE =
1 ,I4)
101 FORMAT(/,2X, PROGRAM HAS NOT CONVERGED IN ,I3, STEPS ,/,3X, TH
IE RESIDUAL VALUE IS ,1PE10 3)
END
C-----
SUBROUTINE PRINTF
COMMON/VK/NNODE,NELEM,NTYPE,NTIME,TIME,NFRMAX
COMMON/VD/AF,AFM,DT,NNQS,NUMN,NUM,NGAUS,NNHC,NNST,NSTOP,KPRNT,IAXI
COMMON/VC/Q(601),F(601),NTS(601),NQS(601),DX(601),DY(601)
COMMON/VA/COLD(601),CNEW(601)
COMMON/VB/X(601),Y(601),QQ(601)
COMMON/VEL/VX(601),VY(601)
COMMON/VL/NODE(601,8)
COMMON/VT/MTYPE,NUMDIM,TO RHO CP
NDUMMY=0
WRITE(9, (8I5) )MTYPE,NUMDIM,NNODE,NELEM,NUMN,NSTOP,KPRNT,NDUMMY
WRITE(9, (I4,2X,5(F8 4,1X)2X,I5) )NTYPE DT,AF,TO RHO CP IAXI
DO 1 I=1,NNODE
1 WRITE(9,101)I,X(I),Y(I)
DO 2 I=1,NELEM
2 WRITE(9,100)I,QQ(I),DX(I),DY(I),(NODE(I,J) J=1,NUMN)
DO 3 I=1,NNODE
3 WRITE(9,102)I CNEW(I),VX(I),VY(I)
100 FORMAT(5X,I4,2X,3(F8 4 1X),8I4)
101 FORMAT(5X,I4,2X,2(F8 3,1X))
102 FORMAT(5X,I4,2X,3(F8 3,1X))
RETURN
END
C-----
SUBROUTINE SETPC
CHARACTER INFIL*12,OUTFIL*12
DATA INFIL/ /,OUTFIL/ /
WRITE(*, (/1X,A\ ) ) ENTER NAME FOR INPUT FILE
READ(*, (BN,A) )INFIL
OPEN(8,FILE=INFIL)
C
WRITE(* (/1X A\ ) ) ENTER NAME FOR OUTPUT FILE
READ(*, (BN,A) )OUTFIL
OPEN(9,FILE=OUTFIL,STATUS= NEW )
WRITE(9, (A) )OUTFIL
RETURN
END
C-----
SUBROUTINE SKYLIN(B,VAR NB FIXED NBOUND)
COMMON/VP/P(9901),C(9901),R(9901)
COMMON/VK/NNODE,NELEM,NTYPE,NTIME,TIME,NFRMAX
COMMON/SK/NFR(601) JMIN(601) JMAX(601)
DIMENSION AG(9901) B(601) VAR(601) NB(601) FIXED(601)
NN1=NNODE-1
DO 1 I=1 NFRMAX
1 AG(I)=R(I)
C
C CHECK FOR DIRICHLET VALUES
C
14 IF(NBOUND EQ 0)GO TO 700
DO 550 K=1 NBOUND
I=NB(K)
NGA=NFR(I)+1 JMIN(I)
AG(NGA)=1 0
J1=JMIN(I)

```

```

J2=JMAX(I)
DO 550 J=J1 J2
IF(J EQ I)GO TO 550
NGA=NFR(I)+J-J1
AG(NGA)=0 0
IF(I LT JMIN(J))GO TO 550
NGA=NFR(J)+I-JMIN(J)
B(J)=B(J)-AG(NGA)*FIXED(K)
AG(NGA)=0 0
550 CONTINUE
DO 600 K=1,NBOUND
I=NB(K)
600 B(I)=FIXED(K)
C
C BACK CALCULATE FOR VARIABLE
C
700 DO 50 K=1,NN1
NGA=NFR(K)+K JMIN(K)
PIVOT=AG(NGA)
JKMAX=JMAX(K)
KP1=K+1
DO 20 I=KP1,JKMAX
IF(K LT JMIN(I))GO TO 20
NGA=NFR(I)+K JMIN(I)
FACTR=AG(NGA)/PIVOT
IF(ABS(FACTR) LT 1 0E-10)GO TO 20
DO 10 J=K,JKMAX
NGE=NFR(I)+J-JMIN(I)
NGI=NFR(K)+J-JMIN(K)
AG(NGE)=AG(NGE)-FACTR*AG(NGI)
10 CONTINUE
B(I)=B(I)-FACTR*B(K)
20 CONTINUE
50 CONTINUE
DO 40 II=1 NN1
I=NNODE+1-II
IM1=I-1
JSTR=JMIN(I)
NGA=NFR(I)+I JSTR
VAR(I)=B(I)/AG(NGA)
DO 30 J=JSTR,IM1
NGI=NFR(I)+I-JMIN(J)
30 B(J)=B(J) VAR(I)*AG(NGI)
40 CONTINUE
NGA=NFR(1)+1 JMIN(1)
VAR(1)=B(1)/AG(NGA)
RETURN
END

```

APPENDIX VIII LIST OF PUBLICATIONS

- 1 S AKTER and M S J HASHMI, "Modelling for the pressure distribution within a hydrodynamic pressure unit effect of the change in viscosity during drawing of wire coating", Proceedings of the International Conference on Advances in Materials and Technologies (AMPT 95), Volume 3, PP 959-968, 8-12 August 1995
- 2 S AKTER and M S J HASHMI, "Formation and remelting of a solid polymer layer on the wire, in a polymer melt chamber", Proceedings of the International Conference on Advances in Materials and Technologies (AMPT 95), Volume 3, PP 1462-1469, 8-12 August 1995
- 3 S AKTER and M S J HASHMI, "Modelling of velocity and temperature gradient boundary layer thickness for the drawing of a continuous wire through a polymer melt chamber ", Proceeding of the Twelfth Conference of the Irish Manufacturing Committee (IMC 12), PP 269-278, 6-8 September
- 4 S AKTER and M S J HASHMI, "Effect of change in viscosity of polymer in plasto-hydrodynamic drawing of strip using a hydro-dynamic pressure unit", Conference of Sheet Metal (She MET 96), The Netherlands, Vol 1, PP 435-445, 1996
- 5 S AKTER and M S J HASHMI "Modelling the pressure distribution within a combined geometry hydrodynamic pressure unit during wire coating process", Proceeding of XIIth International Congress on Rheology, Canada, PP 689-690, August 18-23, 1996
- 6 S AKTER and M S J HASHMI, "High speed Nylon coating of wire using a plasto-hydrodynamic pressure unit, 3rd Asia Pacific conference on Material Processing, Hongkong also published in Journal of Materials processing Technology, PP 453-457, November, 1996
- 7 S AKTER and M S J HASHMI, "Plasto-hydrodynamic Nylon coating of wire and prediction of pressure inside the stepped parallel bore unit", Thirteenth Conference of the Irish Manufacturing Committee, Limerick, PP 123-133, September 1996
- 8 S AKTER and M S J HASHMI, "Finite element temperature and pressure analysis for pressure distribution in a combined hydrodynamic unit, *Design and Control (PEDAC'97)*, Egypt February 1997
- 9 S AKTER and M S J HASHMI, "Works on polymer coating and drawing of wires using plasto-hydrodynamic pressure units and the evolution of the design units", *Proceeding of the 6th International Conference on Production Engineering Design and Control (PEDAC'97)*, Alexandria, Egypt February 1997
- 10 S AKTER and M S J HASHMI, "Theoretical and experimental results in wire drawing using a stepped parallel bore hydrodynamic unit effect of change in viscosity", in international Journal of Science and Engineering, Research and Applications, Editor Prof Bokır S Yılbas(in press)